Scalable Multi-Energy Systems Control: Design and Experimental Validation

Doctoral dissertation of:

Lorenzo Nigro

Advisor: Riccardo Scattolini
Co-advisor: Alessio La Bella



POLITECNICO
MILANO 1863

RSE Ricerca Sistema Energetico | we move rsearch

The real voyage of discovery consists not in seeking new landscapes,
but in having new eyes.

Marcel Proust

Contents

Abstract 1

Sommario 3

1 Introduction 5

Introduction 5

1.1 European Energy Goals . . . 5
1.1.1 European Gas Crisis . . . 5
1.1.2 European Electricity Production . . . 6
1.1.3 District Heating Networks . . . 8
1.1.4 Multi-Energy Systems . . . 9
1.2 State of the Art . . . 10
1.2.1 Simulation of District Heating Networks . . . 10
1.2.2 Control of District Heating Networks . . . 10
1.2.3 Centralized Coordination of Multi-Energy Systems . . . 11
1.2.4 Distributed Coordination of Multi-Energy Systems . . . 11
1.2.5 Game Theory in Multi-Energy Systems . . . 11
1.3 Research Goals and Challenges . . . 12
1.4 Thesis Contributions and Outline . . . 13
1.4.1 Part I: District Heating Networks . . . 13
1.4.2 Part II: Multi-Energy Systems . . . 15
1.5 The RSE Multi-Energy Plant . . . 16
1.6 List of Publications . . . 18

I District Heating Network 19

2 Simulation and control-oriented modelling for control design 21
2.1 Model Development . . . 21

3 Experimental Validation of Simulators for District Heating Network 41
3.1 Simulation of District Heating Network . . . 41

4 Experimental Validation of Optimal Regulators and State Estimation for District Heating Network 49
4.1 District Heating Network Control . . . 49

II Multi-Energy Systems 57

5 Centralized Control for MES Coordination 59
5.1 Centralized Control . . . 59

6 Distributed Control for MES Coordination 79
6.1 Distributed Control . . . 79

7 Design and experimental validation of MES control architectures 87
7.1 Experimental Validation of MES control 87
8 Conclusion 107
Bibliography 111
Acronyms 118
Ringraziamenti 119

Abstract

Climate change and the European Green Deal drive the urgent need to transform how energy is produced, stored, and used. As renewable sources like wind and solar replace fossil fuels, power systems must become more flexible to balance fluctuating supply and demand. This dissertation focuses on Multi-Energy Systems, networks that link electricity, district heating, and other energy carriers to use resources more efficiently and reduce emissions.

The main research goal is to design control architectures that make these interconnected systems operate efficiently, reliably, and sustainably. To achieve this, the work follows three steps. First, it develops accurate yet lightweight models of District Heating Networks (DHNs), a key component of MES, to understand and predict their behavior. Second, it designs a predictive control framework that can coordinate the operation of multiple energy systems, balancing costs and performance. Third, it validates these models and control strategies experimentally on a real test facility, demonstrating their practical effectiveness.

The methodology combines physical modeling, optimization, and control. A detailed DHN simulator is built in Modelica to test and refine control algorithms. A simplified model supports real-time predictive control of interconnected systems. The study then extends to MES coordination, introducing scalable control architectures that can manage several subsystems while preserving privacy and autonomy. Hierarchical and distributed controllers use shared information only when needed, ensuring efficient cooperation among different energy networks.

The results show that the proposed models and control frameworks improve energy efficiency reducing operational costs, preserving privacy, and ensuring profit to subsystems. Academically, this work advances the understanding of control-oriented modeling and coordination in complex energy systems. Practically, it offers tested tools and algorithms that help real-world implementations toward a more flexible, low-carbon energy future. This research demonstrates that scalable and optimal control of multi-energy systems is not only possible, but essential for achieving a sustainable and resilient energy transition.

Sommario

Il cambiamento climatico e il Green Deal europeo rendono urgente una trasformazione profonda nelle modalità di produzione, accumulo e utilizzo dell'energia. Con la progressiva sostituzione dei combustibili fossili da parte delle fonti rinnovabili, quali eolico e fotovoltaico, i sistemi energetici devono diventare più flessibili per bilanciare una disponibilità di energia sempre più variabile. In questo contesto, la presente dissertazione si concentra sui Sistemi Multi-Energia (MES), reti che integrano elettricità, teleriscaldamento e altri vettori energetici, al fine di impiegare le risorse in modo più efficiente e ridurre le emissioni.

L'obiettivo principale della ricerca consiste nel progettare architetture di controllo in grado di rendere questi sistemi interconnessi efficienti, affidabili e sostenibili. A tal fine, il lavoro si articola in tre fasi. In primo luogo, vengono sviluppati modelli accurati ma computazionalmente leggeri delle reti di teleriscaldamento (District Heating Networks, DHN), elemento chiave dei MES, utili a comprenderne e predirne il comportamento. In secondo luogo, viene definita una struttura di controllo predittivo capace di coordinare il funzionamento di più sistemi energetici, bilanciando costi e prestazioni. In terzo luogo, tali modelli e strategie di controllo vengono validati sperimentalmente su un impianto reale, dimostrandone l'efficacia pratica.

La metodologia adottata combina modellazione fisica, ottimizzazione e controllo. Un simulatore dettagliato di DHN è realizzato in Modelica per testare e affinare gli algoritmi di controllo, mentre un modello semplificato supporta l'implementazione del controllo predittivo in tempo reale di sistemi interconnessi. Successivamente, l'analisi viene estesa al coordinamento dei MES, introducendo architetture di controllo scalabili in grado di gestire più sottosistemi preservandone al contempo privacy e autonomia. Controller gerarchici e distribuiti condividono soltanto le informazioni strettamente necessarie, garantendo una cooperazione efficiente tra le diverse reti energetiche.

I risultati evidenziano come i modelli e le strutture di controllo proposte migliorino l'efficienza energetica, riducano i costi operativi, preservino la privacy e assicurino benefici ai sottosistemi. Dal punto di vista scientifico, il lavoro contribuisce ad avanzare lo stato dell'arte nella modellazione orientata al controllo e nel coordinamento di sistemi energetici complessi. Dal punto di vista applicativo, esso fornisce strumenti e algoritmi validati sperimentalmente per favorire implementazioni reali verso un sistema energetico più flessibile e a basse emissioni. La ricerca dimostra che un controllo scalabile e ottimale dei sistemi multi-energia non solo è possibile, ma rappresenta un elemento essenziale per una transizione energetica sostenibile e resiliente.

1 Introduction

1.1 European Energy Goals

A global commitment to decarbonization and ambitious energy transition targets is currently driving significant changes in energy production and consumption worldwide. Within this context, the European Union (EU) has established two courses of action: the REPowerEU and the European Green Deal. The REPowerEU plan is a strategic initiative designed to eliminate the European Union's dependency on imported fossil fuels and trace its origin in the gas import crisis of 2022. Its primary objectives are to enhance the EU's strategic autonomy in the energy sector and accelerate the clean energy transition, thereby reinforcing the goals of the European Green Deal. To achieve this, the plan aims to enhance energy efficiency, especially in buildings. It also seeks to accelerate the development and deployment of renewable energy sources and improve the interconnection of European energy networks to diversify supply routes [17]. The European Green Deal is a legally binding initiative aiming for greenhouse gas (GHG) emissions reduction by 55% by 2030 compared to 1990 levels and for climate neutrality by 2050. A major contributor to these emissions is the energy sector, accounting for 75% [53] of the total greenhouse gas emissions in Europe, thereby making its transformation imperative [19]. Consequently, various sectors of the European energy market, e.g., energy or building, will undergo substantial modifications in the years to come. These two plans specifically aim to accelerate the transition from fossil fuels to renewable energy, enhance energy efficiency, and interconnect energy networks to build a more robust infrastructure.

1.1.1 European Gas Crisis

The Russian aggression against Ukraine in 2022 precipitated a severe energy crisis across Europe by disrupting natural gas imports from Russia, a nation upon which several European countries were heavily dependent. This disruption led to a sharp increase in natural gas prices, which in turn drove up overall energy costs, resulting in record-high electricity prices in mainland Europe, as shown in Figure 1.1.

In response, the European Union promptly introduced the REPowerEU plan in May 2022. This strategic initiative aims to eliminate the EU's dependence on Russian fossil fuels by accelerating the clean energy transition, thereby reinforcing the objectives of the European Green Deal. The plan aims for greater energy independence by accelerating

1

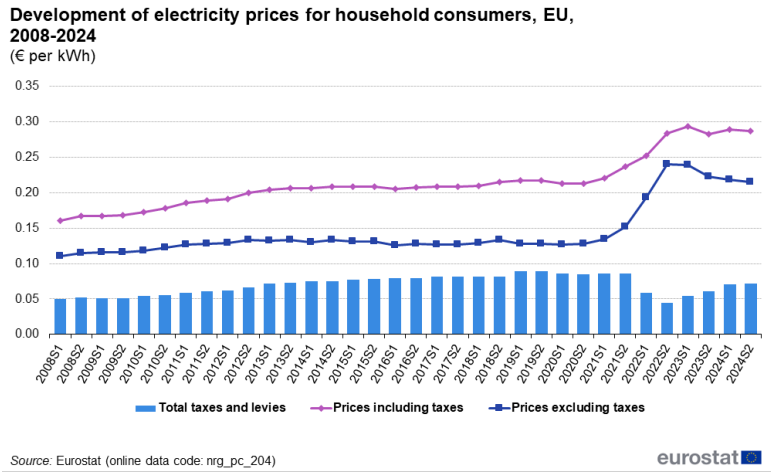


Figure 1.1: Electricity prices in household consumers across EU over the years.

the adoption of renewable energy sources, with the EU increasing its 2030 renewable energy target from 40% to 45%. The effects of the European Union's policies have already impacted the energy sector, as reflected by the European electricity production, where the penetration of renewable resources has drastically accelerated over the last years.

1.1.2 European Electricity Production

The European Union is experiencing consistent growth in renewable electricity production, which, for the first time in 2023, surpassed fossil fuels as the primary source of electricity, see Figure 1.2. This increase is attributed to rising public awareness of climate change, governmental incentives, and a sharp decrease in the cost of renewable technologies. In 2023, the EU produced 2,572 TWh of electricity, with over 45% derived from renewable sources, 31.7% from fossil fuels, and nearly 23% from nuclear power. The share of renewables in electricity generation has more than doubled since 2004, indicating a clear trajectory towards a greener energy mix. Data from Eurostat for 2024 [25] indicate a record high reliance on renewables for electricity generation. In 2024, 47.3% of the electricity in the EU was produced from renewable sources, a notable increase from 44.9% in 2023, while only 29.2% came from fossil fuels. For the second consecutive year, wind generated more electricity than natural gas, reaching 487.6 TWh (18.4%) compared to natural gas at 443.4 TWh (16.0%). Wind and solar power collectively accounted for over 28% of total electricity generation from renewable sources in 2024, see Figure 1.3. Although the environmental benefits, the increasing penetration of intermittent renewable energy sources introduces fundamental challenges to the stability and reliability of traditional electrical grids. The power system needs a supply-demand balance, i.e., production must match consumption at any time. Therefore, the unpredictable and variable nature of renewables places significant stress on the power grid. Additionally, conventional power plants provide robustness to supply-demand variations with rotor inertia. Unfortunately, these power plants are being displaced, and renewables tend to have low to no inertia, sparking the need for new approaches to maintain grid stability [16].

These developments necessitate a fundamental shift towards enhanced network flexi-

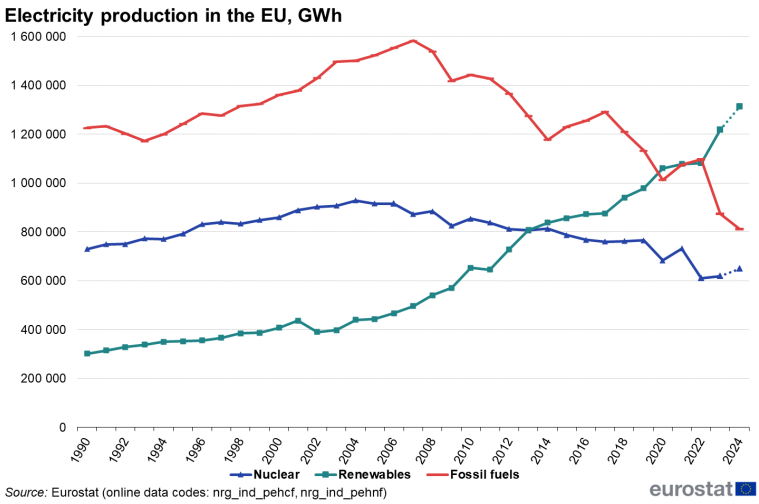


Figure 1.2: European electricity production over time.

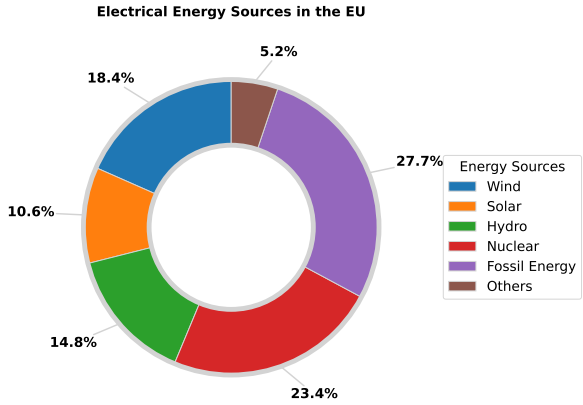


Figure 1.3: EU electricity sources percentages in 2024 [25].

bility, i.e., the ability to manage production and consumption, to maintain a secure and economical supply-demand balance [22].

Among existing solutions to increase network flexibility a cheap source of flexibility is changing the energy carrier, for example, moving energy from electricity to thermal. The change in energy carrier can be achieved by using power to heat devices, e.g., heat pumps, and the resulting energy can be stored in thermal energy storage (TES) systems that can achieve a price per capacity as low as $0.1 - 32$ €/kWh [20]. However, for TESs to provide their flexibility to the power grid, a suitable infrastructure is needed, namely a DHN.

1.1.3 District Heating Networks

District heating networks are systems that produce thermal energy (heat or cold) and distribute it to residential, commercial, and industrial buildings through insulated pipelines.

The European Union promotes DHN as a solution to reduce the carbon footprint of building's heating, offering significant environmental and economic benefits. In fact, DHN facilitate decarbonization by exploiting:

→ Rooftop solar thermal panel, harvesting solar energy for heating applications.

→ Recover waste heat, which is heat generated as collateral by industrial processes.

→ Power to heat devices, such as heat pumps or electrical boilers, converting electricity to thermal energy.

→ thermal energy storage (TES) systems, a cheap alternative to store energy in large quantities.

For this reason, EU aims to substantially increase the role of DHNs, intending to cover at least 50% of the heating demand in most European countries with DHN systems by 2050 [24]. The potential of DHNs can help Europe achieve its climate goals. Specifically, consider the buildings' energy footprint in Europe. Buildings are recognized as the single largest energy consumer in Europe [18]. Heating and cooling demands for residential, commercial, and industrial buildings account for nearly 40% of Europe's total energy demand, with the majority still supplied by fossil fuels, directly contributing to 36% of Europe's energy sector GHG emissions, see Figure 1.4. These numbers are due to a heavy reliance on fossil fuels, particularly natural gas, for space and water heating, which collectively accounts for roughly 80% of the overall energy consumption in EU homes.

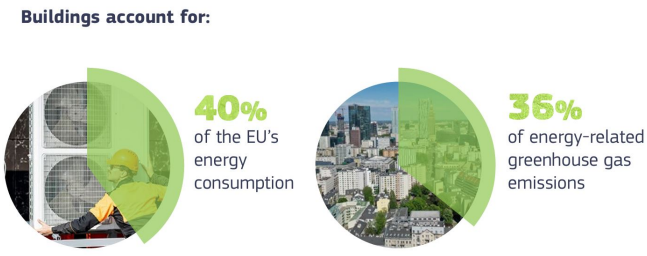


Figure 1.4: Buildings energy consumption and equivalent green house gas emissions [19].

As DHN are expanding in the EU, it is important to recognize their role as flexibility providers for the power grid. The increasing penetration of intermittent renewable energy sources (RES) into the electricity mix necessitates enhanced flexibility across the entire energy system. In this context, the efficient integration of RES is intrinsically linked to the flexibility offered by DHNs. District heating networks can provide flexibility to electrical grids through power-to-heat converters, such as electric boilers and heat pumps. This mechanism allows DHNs to accommodate peaks in renewable electricity production, thereby increasing overall energy efficiency and supporting grid stability [16]. The synergetic operation of different energy vectors, e.g., electrical and thermal, is called Multi-Energy System (MES).

1.1.4 Multi-Energy Systems

A MES, shown in Figure 1.5 is fundamentally defined as the synergetic operation of subsystems belonging to different energy domains, such as thermal, electrical, and gas networks, which interact optimally to enhance overall energy efficiency and economic savings. This integrated approach unlocks higher system flexibility and efficiency by leveraging various conversion devices like heat pumps, electric boilers, and combined heat and power (CHP) units [16]. With their capabilities, multi-energy systems emerge as a crucial solution to adapt to the changing needs of the energy sector.

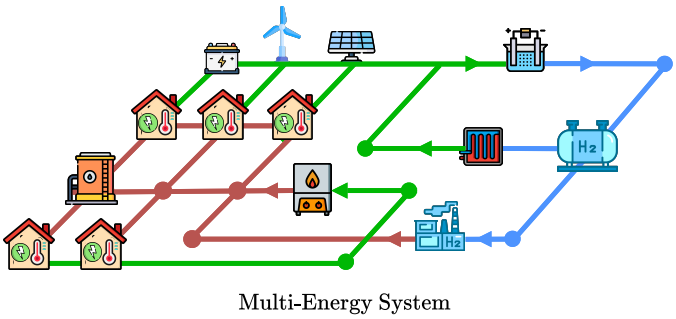


Figure 1.5: A schematic view of a multi-energy system. A power grid in green, a thermal network in red, and a gas network in blue.

A multi-energy system can increase the flexibility of traditional power grids in several key ways:

- MES enable the seamless exchange and optimal coordination of power and energy storage across diverse energy vectors. For instance, surplus renewable electrical energy can be converted into thermal energy via power-to-heat technologies and stored in thermal energy storage units. This effectively provides valuable flexibility to the electrical grid by shifting energy across domains.
- MES facilitate various forms of demand-side flexibility. This allows for the modulation of energy supply across different inputs (e.g., switching between electricity and gas for heating via heat pumps and boilers) or outputs (e.g., Power-to-Heat, Power-to-Gas) to respond to market signals, grid constraints, or demand fluctuations. This

capability is critical for optimizing energy management, reducing peak consumption, and increasing overall system resilience.

These abilities of MESs are fundamental for maintaining a secure and economical supply-demand balance, thereby addressing the challenges posed by the unpredictable and variable nature of intermittent RES. Despite their potential, MES present significant control challenges due to their high model complexity, large-scale dimension, and the diverse dynamical time constants of different energy vectors (e.g., fast electrical versus slow thermal dynamics). Additionally, issues such as privacy concerns arise when different energy domains are managed by separate stakeholders or owners. This intricate landscape directly motivates the core research objective of this doctoral dissertation.

1.2 State of the Art

As discussed, MES have emerged as a pivotal solution in the EU energy market, recognized for their potential to foster affordable, reliable, and low-carbon energy systems. The literature review focuses on district heating networks and multi-energy systems.

1.2.1 Simulation of District Heating Networks

Advanced control strategies must be evaluated in simulation before deployment on physical assets. Simulation models must capture the dominant dynamics of each energy vector while remaining computationally tractable for large-scale scenario analysis and control design. Accordingly, this dissertation first examines suitable modelling approaches for power, gas, and thermal networks.

For power grids, mature modelling frameworks already exist. The optimal power flow, the branch flow model, or the power balance [23, 29, 44] provide reliable approximations for operational planning and control. These models achieve an acceptable balance between accuracy and computational efficiency and are therefore adopted directly from the literature. A similar rationale applies to gas networks: established dynamic models have demonstrated satisfactory performance in optimal control applications and are used here without modification [31].

In constrast, despite DHN importance for decarbonization, their modells span a wide spectrum: high-fidelity PDE formulations [36] or port-Hamiltonian representations [33]. However, these works either oversimplify essential physics or adopt excessively detailed formulations. Similarly, existing modelling libraries, such as ThermoPower [12, 28] or Simscape [21, 43], provide general-purpose capabilities but often include dynamics irrelevant to DHNs resulting in unnecessary computational burden.

1.2.2 Control of District Heating Networks

The complexity of large-scale networks, combined with the nonlinear behavior of detailed DHN models makes large-scale optimal control formulations computationally challenging; therefore, many existing DHN controllers are rule-based, often failing to exploit the system's flexibility [37]. Nonetheless, some optimization schemes tailored to DHNs exists, but are constrained to single-step horizons due computational issues [36].

Most MPC strategies reduce computational burden through model simplifications. Several studies approximate DHN behaviour using steady-state thermal power-balance equations [27, 45, 56, 57], thereby neglecting temperature transport phenomena or pipeline

inertia. However, explicit modelling of temperature dynamics is essential: load supply temperatures must satisfy strict operational limits [36, 46] and its dynamic strongly influences heat losses and production scheduling. Alternative MPC formulations attempt to retain temperature dynamics but introduce simplifying assumptions, such as fixed flow rates and transport delays [55], linearized return temperatures [54], or uniform supply temperatures across all loads [59].

Despite these efforts, none of these strategies can simultaneously capture the network thermal inertia and satisfy all operational constraints.

1.2.3 Centralized Coordination of Multi-Energy Systems

Once defined suitable models for individual energy carrier, e.g., power, gas, and district heating, the next step is their coordinated operation within a multi-energy system. Centralized coordination therefore emerges as possible solution, enabling joint optimization and improved overall efficiency.

A foundational concept in MES control is the energy hub, introduced as a representation of MES. This framework supports model-predictive formulations [2]. Other works propose a mixed-integer linear modelling methodology that facilitates MPC control [45], or employ linear state-space models to implement economic MPC [7]. Related optimization strategies further explore centralized coordination with robust formulations [10, 13] or data-driven approaches [6, 14, 39].

Nonetheless, centralized coordination may be hindered by computational complexity and by issues related to information sharing and privacy. Answering these issues, hierarchical architectures offer improved scalability and faster system response [8, 38, 60]. Nonetheless, the scope of this approach remains confined to the electrical energy domain, without extensions to the broader multi-energy setting.

1.2.4 Distributed Coordination of Multi-Energy Systems

Centralized optimization may require agents to disclose detailed operational data, raising privacy concerns for stakeholders managing proprietary assets.

Distributed control offers a remedy by limiting information exchange. However, strong guarantees on optimality, convergence, and feasibility typically hold only for convex formulations [15], condition rarely satisfied in MES applications. Consequently, many distributed approaches rely on linearized or mixed-integer linear models [3, 40], improving tractability but potentially compromising optimality.

Beyond scalable and privacy-preserving coordination, MES control practical deployment requires guarantees on the profits for the participating stakeholders. Without profits, stakeholders may lack motivation to contribute resources to system-level optimization MES coordination frameworks.

1.2.5 Game Theory in Multi-Energy Systems

To ensure profits to the agents, the literature refere to game theory. Games are primarely classified between cooperative and non-cooperative, depending on whether agents commit to collective optimisation or act in their own interest [34].

Cooperative game theory assumes agents form a coalition to maximize a shared objective. Standard practice involves a two-step workflow: (i) solve a system-wide optimal control problem to obtain the collective optimum, and (ii) apply a benefit-sharing mechanism, commonly the Shapley value [48] or Nash bargaining [5].

However, dividing the problem into an energetic and an economic optimization complicates the control architecture and may introduce computational challenges [3]. Furthermore, cooperative game theory assumes collaboration. This assumption overlooks the competitive nature of agents, who may prioritize their own profit maximization.

Hence, non-cooperative games provide a more suitable framework [35]. Among possible game formulations, Stackelberg games are widespread [34]. While effective, convergence to a unique Stackelberg equilibrium is not always guaranteed [32].

An alternative is to formulate the problem as a Generalized Nash equilibrium problem (GNEP). GNEPs are well-suited for multi-energy system, as they model agents with coupled objective functions and operational constraints. Equilibria of GNEPs are retrieved using distributed algorithms with convergence guarantees, ensuring scalability and preserving agent privacy [4].

1.3 Research Goals and Challenges

The core objectives of this doctoral dissertation are:

The design of control architectures for Multi-Energy Systems to enable their implementation, for the decarbonization of the European Union energy sector.

The experimental validation of said controls on physical plants, assessing their cost reduction and regulation capabilities.

To reach these goals, the following challanges are addressed:

District Heating Networks Model Development

The development of a MES control framework begins with accurate modeling and control of its primary subsystem: the DHN. Their modeling, however, remains challenging as DHNs exhibit large scale, nonlinear thermo-hydraulic dynamics. These characteristics hinder the construction of models that are simultaneously accurate, tractable, and suitable for real-time control.

District Heating Networks Control Design

For the same reasons, optimal control is challenging in DHNs. Moreover, the implementation of optimal controllers, such as MPC, typically requires the entire state as feedback, which is rarely available in practice due to the limited number of sensors and to the spatial distribution of district heating networks.

Multi-Energy Systems Coordination

With the subsystem models in place, the next challange is to establish a systematic strategy for their coordinated operation within a MES. Multi-energy systems combine heterogeneous energy systems whose dynamics are strongly coupled, nonlinear, and distributed. Their scale and interdependencies significantly increase model complexity, creating computational challenges.

A central difficulty lies in the coexistence of widely separated time constants. Fast electrical dynamics must be reconciled with the slow thermal dynamics of district heating networks, making a single monolithic controller impractical. Designing coordination

schemes that preserve stability and performance across these disparate timescales remains a core challenge.

Multi-Energy Systems Privacy and Rationality

As said above, MES subsystems are often operated by independent stakeholders. These agents may be unwilling to disclose detailed plant models, operational constraints, or cost structures, which limits the feasibility of centralized coordination. Moreover, participants typically require profit guarantees, and their strategic behaviour may prioritize individual revenue over system-level efficiency.

Tests on Physical System

Finally, experimental validation on physical energy systems remains a challenging step to assess advanced control strategies. Unlike simulation environments, real systems exhibit uncertainties, unmodeled dynamics, and operational constraints that can compromise controller performance and safety.

Moreover, testing on district heating networks or multi-energy infrastructures typically impose strict limits on test duration, permissible operating ranges, and risk tolerance. As a result, experimental campaigns must be carefully planned.

1.4 Thesis Contributions and Outline

The dissertation is split into two main parts: Part I researches on district heating network, modelling, simulation, control, and validation, while Part II focuses on the design and validation of regulators for the coordination of MES. Below, the reader can find a synthetic overview of each chapter. The work is structured as shown in Figure 1.6.

1.4.1 Part I: District Heating Networks

The first part studies district heating networks, including their modelling, simulation, control, and experimental validation.

Chapter 2, Simulation and control-oriented modelling for control design: This chapter contributions are the development of two complementary thermo-hydraulic models of DHNs:

- **A simulation model and library**, implemented as open-source in Modelica, capable of accurately reproducing thermo-hydraulic transients while retaining computational efficiency. The model captures essential phenomena, including pipe-wall inertia and storage dynamics [49].
- **A control-oriented model**, explicitly designed for real-time Nonlinear MPC regulators. The model preserves the dominant thermal–hydraulic dynamics relevant for decision-making and enables predictive regulators to operate at practical computation times [49].
- **Nonlinear MPC** design for economical management of district heating networks with simulation results [49].

These modelling advancements fill a methodological gap between simplified steady-state representations and computationally prohibitive simulators.

1

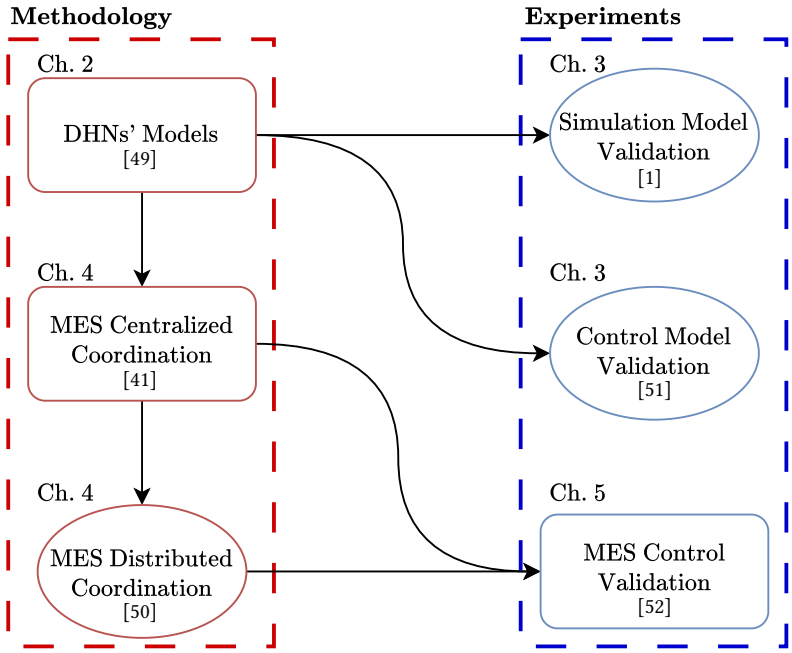


Figure 1.6: Thesis outline. Each shape is a contribution, with related Chapter (Ch.) and artcile.

Chapter 3, Experimental Validation of Simulation Library for DHN: The chapter introduce the validation of the simulation library:

- Section 3.1 details the experimental validation of **simulation library validation**, carried out on the test plant at RSE. The validation assessed the simulation ability to represent dynamical transients with quantified KPIs [1].

The simulation demonstrated accurate representation of the main dynamical behavior of the real plant.

Chapter 4, Experimental Validation of Optimal Regulators and State Estimation for District Heating Network: The chapter research on the experimental validation of the control oriented model and its application as a NMPC:

- Section 4.1 presents the experimental assessment of the **control-oriented model validation**, a nonlinear MPC and a Moving Horizon Estimation (MHE) where tested on the plant for cost-optimal DHN operation, and unmeasured states reconstruction from sparse and noisy measurements [51].

The control-oriented model provided cost saving management and reliable state estimation compared to rule-based baselines.

1.4.2 Part II: Multi-Energy Systems

Part two investigates the control of multi-energy systems and their validation, focusing on optimal coordination strategies and addressing scalability and privacy challenges.

Chapter 5, Centralized Control for MES Coordination: This chapter presents the design of a centralized coordination architectures for multi-energy systems.

- The first Section 5.1 introduces a **hierarchical MPC framework** with a high-level controller based on reduced-order energy models and local MPC regulators governing detailed subsystem dynamics. This approach reconciles multi-timescale behaviours, ensuring tractable coordination across electrical, thermal, and gas domains [41].
- This formulation is used in a **centralized coordination scheme** and leverages the high-level energetic formulation to coordinate energy vectors. A cooperative bargaining mechanism is integrated to ensure fair benefit allocation [41].

These architectures provide a unified control methodology applicable across heterogeneous energy vectors within MES control.

Chapter 5, Distributed Control for MES Coordination: This chapter presents the design of a distributed coordination architectures for multi-energy systems.

- Section 6.1 presents a **distributed coordination** based on a ADMM algorithm. By leveraging an energy-based convex abstraction, the method allows subsystems to coordinate without sharing proprietary models or operational data, thereby addressing both scalability and privacy concerns [50].

This architectures provide a solution to privacy concerns regarding the use of centralized architectures, addressing a critical barrier to real-world deployment.

Chapter 7, Design and experimental validation of MES control architectures: This chapter:

- propose an additional **Game-Theoretic coordination strategy**, that is a non-cooperative game which enables agents to reach equilibrium through distributed algorithms with provable convergence guarantees [52].
- reports the **experimental assessment** of the proposed MES control frameworks on a physical test facility composed of a thermal network, an electrical grid, and an energy hub. The experiments demonstrated that [52] coordination strategies satisfy operational constraints, controllers remain robust to unmodelled dynamics and communication limitations, significant cost reductions are achieved relative to conventional operation.

This validation confirms the practical feasibility of the proposed regulators and their suitability for real-world MES deployment and represents one of the few experimental demonstrations of MES coordination in the literature.

The author's peer-reviewed articles on the topic are attached to each chapter with a summary. The summary captures the motivation behind the work, the applied methodology, and the results achieved in the article to facilitate access to the material included in the dissertation.

1

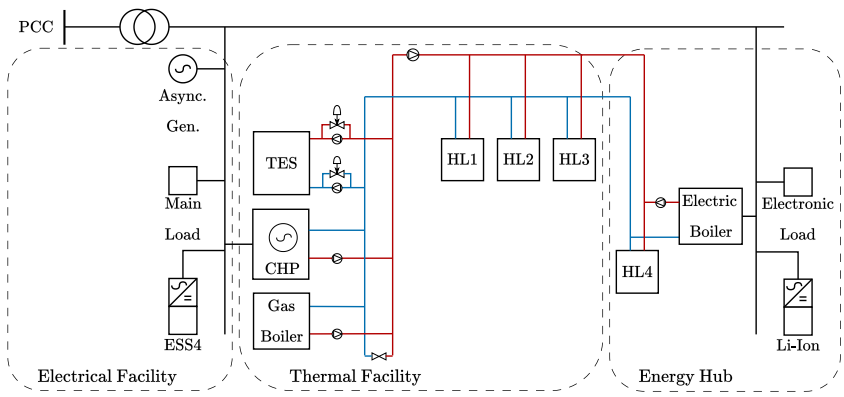


Figure 1.7: Physical plant DER-TF Topology comprising the Electrical Facility, the Thermal Facility, and the Energy Hub.



Figure 1.8: Photo of the thermal facility in Milan.

1.5 The RSE Multi-Energy Plant

The experimental activities were conducted at the Distributed Energy Resources Test Facility (DER-TF) operated by RSE [30] and shown in Figure 1.7. The platform integrates three interacting subsystems: a electrical microgrid (Electric Facility), a district heating network (Thermal Facility), and an Energy Hub (EH), allowing validation of multi-energy control architectures. A picture of the plant in Figure 1.8.

Thermal Facility

The Thermal Facility (TF) consists of multiple heat generation units connected to a set of thermal loads through an insulated pipeline network. Table 1.1 summarizes the components data. As shown in Figure 1.7, the generation section comprises three parallel units: a gas boiler (GB), a combined heat and power (CHP) system, and a thermal energy storage (TES) unit. These supply three primary loads (HL1–HL3) via dedicated pipelines. A fourth load

(HL4) is connected to the DHN but belongs to the energy hub.

The TF has a maximum thermal load capacity of 200 kW_{th}, whereas the generation units provide up to 365 kW_{th}, requiring coordinated operation. The system is rated for 5.5 bar, with nominal operating pressures in the 2–4 bar range. Typical supply and return temperatures vary between 60–80°C, with an upper limit of 95°C.

Component	Data
Gas Boiler	147 kW_{th}
Electric Boiler	50 kW_{th}
Combined Heat and Power	50 kW_e, 81 kW_{th}
Thermal Energy Storage	10 m^3
Gas Boiler	147 kWth

Table 1.1: Data of the thermal facility's components

Electrical Facility

The Electrical Facility (EF) is a low-voltage AC microgrid comprising dispatchable generators, storage units, and flexible loads. The main elements are listed in Table 1.2 and described in detail in [42]. As shown in Figure 1.7, the EF operates as a single-bus network. The controllable resources are an asynchronous generator and a battery energy storage emulator (ESS4). ESS4 emulates a 57 kWh lithium-ion battery, tracks its state of charge via an internal controller, and can deliver up to 15 kW. A fixed "Main Load" provides a baseline demand. All devices are connected to the same bus and can exchange electrical energy bidirectionally.

Component	Data
Asynch. Generator	[0, 6] kW_e
ESS4	57 kWh_e×15kW_e
Main Load	[0, 60] kW_e

Table 1.2: Data of the thermal facility's components

Energy Hub

The Energy Hub couples the thermal and electrical facilities and draws energy from both. Its interdependence with the DHN and EF arises from two components:

1. the fourth heat load (HL4), which consumes thermal energy, and
2. the electronic load, which consumes electrical power.

The EH can meet its internal demand through multiple pathways: by importing energy from the DHN, the electrical microgrid, or via its own local resources, which include an electric boiler and an internal lithium-ion storage unit. The EH components and their specifications are listed in Table 1.3 and depicted on the right side of Figure 1.7.

1

Component	Data
Electric Boiler	45 kW_e
Li-Ion	30 kWh_e×25kW_e
Electronic Load	[0, 10.5] kW_e
Heat Load 4	[0, 50] kW_{th}

Table 1.3: Data of the thermal facility's components

1.6 List of Publications

The dissertation features articles produced during the three-year Ph.D. research conducted between 2022 and 2025. Two articles were published in peer-reviewed journals, and three articles in peer-reviewed international conference proceedings. One is awaiting submission at the time of writing.

1. La Bella, A., *Nigro, L.*, & Scattolini, R. (2023). Predictive control and benefit sharing in multi-energy systems. IEEE Transactions on Control Systems Technology, 32(2), 368-383. DOI: https://doi.org/10.1109/TCST.2023.3310891

2. *Nigro, L.*, La Bella, A., Casella, F., & Scattolini, R. (2024). Control-oriented modelling, simulation, and predictive control of district heating networks. IEEE Transactions on Automation Science and Engineering. DOI: https://doi.org/10.1109/TASE.2024.3460173

3. Alvarado, M. A. M., Anderis, C., Lazzari, R., *Nigro, L.*, & La Bella, A. (2024, September). Development and Experimental Validation of an Open-Source Model Library for District Heating Network Simulation. In 2024 Open Source Modelling and Simulation of Energy Systems (OSMSES) (pp. 1-6). IEEE. DOI: https://doi.org/10.1109/OSMSES62085.2024.10668994

4. *Nigro, L.*, La Bella, A., & Scattolini, R. (2024, June). Distributed two-layer predictive control of multi-energy systems. In 2024 European Control Conference (ECC) (pp. 2429-2434). IEEE. DOI: https://doi.org/10.23919/ECC64448.2024.10590760

5. *Nigro, L.*, Polimeni, S., Anderis, C., Muro, M., & La Bella, A. (2025). Experimental validation and design of nonlinear predictive control and moving horizon estimation for district heating. IFAC-PapersOnLine, 59(9), 157-162. DOI: https://doi.org/10.1016/j.ifacol.2025.08.129

6. *Nigro, L.*, Polimeni, S., & La Bella, A. (2025). Experimental Assessment of Multi-Layer Control Framework for Multi-Energy Systems control with Multiple Coordination Mechanics. To Be Submitted.

Included in this thesis.

Part I
District Heating Network

I - 2

Simulation and control-oriented modelling for control design

District heating networks enables energy sector decarbonization, yet their inherently nonlinear thermo-hydraulic dynamics, large spatial scale, and diverse time constants make their modelling and control challenging. Optimization-based controllers require models that are simultaneously accurate and computationally tractable. This chapter develops two such models to support simulation and control. First, a dynamic simulation model is formulated as a nonlinear differential–algebraic system that captures thermo-hydraulic behaviours at reduced computational cost, forming the basis of a dedicated Modelica library for DHN analysis.

Second, a control-oriented model is derived by model simplifications yielding an order-of-magnitude reduction in state dimension while preserving the key system characteristics required for model predictive control. The resulting framework enables real-time feasible MPC and demonstrates operational improvements over conventional policies in simulated networks and experimental facilities, thereby providing the modelling foundation for the control algorithms developed in this dissertation.

- **Journal Article**: *Nigro, L.*, La Bella, A., Casella, F., & Scattolini, R. (2024). Control-oriented modelling, simulation, and predictive control of district heating networks. IEEE Transactions on Automation Science and Engineering [49].

2.1 Model Development

Introduction

To reduce the carbon footprint of space and water heating, the European Union aims to meet at least 50% of this demand through DHN systems by 2050. As shown in Figure 2.1, DHNs consist of generation, distribution, and consumption units for indoor heating and domestic hot water, integrating thermal generators, storage systems, and loads. Given the complexity of DHNs, simulating tools are essential for analyzing their behavior and supporting the design of effective operational solutions.

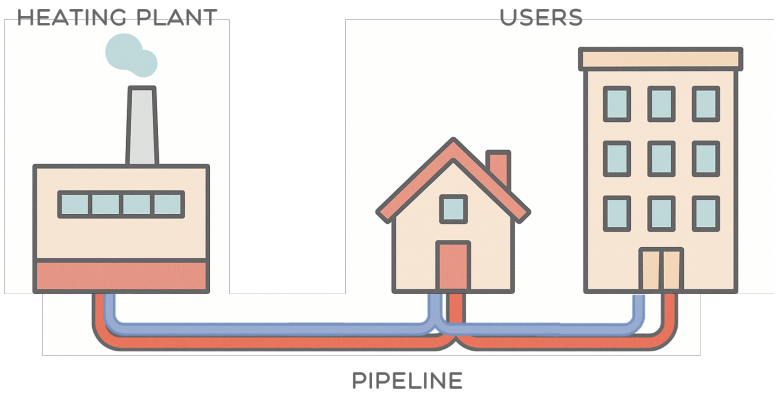


Figure 2.1: Representative image of a DHN. Generation (e.g., heating plant), distribution (pipeline) and consumption (users).

Accurate simulators are needed to reproduce the dynamics of DHNs. However, their large scale and nonlinear behavior present serious challenges in designing dynamic models suitable for control testing and optimal operation computation. Traditionally, district heating networks employ rule-based control strategies that are suboptimal, leading to higher thermal losses and operational costs.

This limitation motivates the adoption of optimization-based control approaches. Although the benefits are significant, computational complexity is challenging in DHN optimal control due to their spatial extension. Balancing accuracy and complexity is essential for effective regulation.

Simulation and Control Models

The author's work [49] proposes two dynamic DHN modeling frameworks: a detailed simulation model and a control-oriented model. The simulation model provides computationally lightweight yet accurate dynamic DHN simulators suitable for testing online control algorithms. It represents the main DHN components while omitting less relevant phenomena, such as fluid phase transitions.

In parallel, a methodology is introduced for deriving a control-oriented DHN model tailored to the design of a nonlinear model predictive control regulator. Key model simplifications include replacing detailed pressure modeling with algebraic relationships for each network loop and combining pipe wall and fluid thermal dynamics into a single reduced-order pipe model. While this approach maintains adequate accuracy, it achieves approximately a 90% reduction of variables compared to the detailed model.

Remark 2.1.1 *The proposed models employ a nonlinear model with real valued states. While the choice allows for the use of efficient optimization solvers, the reduction in modelling accuracy under specific operating conditions can lead to suboptimal or infeasible control decisions. In particular, the proposed models does not account for changes in plant topology, flow direction, start up/shutdown times, minimum generation and piece-wise components efficiencies. It is possible to address these limitations by using integer variables and a mixed-integer nonlinear programming (MINLP) approach. The inclusion of integer variables in the control model would allow lower level controllers to make accurate decisions at the cost of increased computational complexity.*

Contributions: Simulation Library and Optimal Control

The authors' simulation model [49] resulted in the development of a Modelica-based open source simulation library. The library was later expanded and validated on a physical plant, Chapter 3. Modelica is an object-oriented programming language particularly suitable for modeling physical systems. Modelica facilitates the creation of reusable, interpretable code by describing basic components through implicit DAEs consistent with physical laws, thus simplifying the modeling process.

Additionally, the work introduced a NMPC regulator designed using the control-oriented model. This control minimizes generation costs and enhances system efficiency, ensuring optimal performance under the imposed operational constraints. The case study comprises two networks: the *Test Facility* network, serving as a digital twin of an existing system at Ricerca sul Sistema Energetico s.p.a., and the larger AROMA network [36]. The optimal controller is experimentally validated in Chapter 3.

Case Study	Control Strategy	Energy Generation	Operating Cost
Test Facility	Rule Based	1959.5 kWh	898.3$
Test Facility	NMPC	(−14%) 1690.6 kWh	(−15%) 763.2$
AROMA	Rule Based	4494.7 kWh	2100.6$
AROMA	NMPC	(−7%) 4183.7 kWh	(−10%) 1897.4$

Table 2.1: Numerical results comparison for the different case study and control strategies applied [49]

The control-oriented model applied within a nonlinear MPC framework demonstrated significant economic benefits, see Table 2.1, achieving up to 15% cost reduction compared to standard rule-based control strategies in the RSE Thermal Test Facility case study. The regulator also achieved a 10% cost reduction on the larger AROMA network. Notably, the NMPC achieved an average computation time of only 5 seconds for the RSE Test Facility, compared to 1000 seconds for the complete simulation model, and 30 seconds for the AROMA network, indicating its practical feasibility for real-time applications.

The author's work established a mathematical procedure for modelling DHNs for simulation and control, providing simulation results to assess performance. In the next chapter, the models are tested against experimental results to prove their modelling capabilities.

Control-oriented Modelling, Simulation, and Predictive Control of District Heating Networks

Lorenzo Nigro, Alessio La Bella, Francesco Casella, Riccardo Scattolini

***Abstract*—District heating networks (DHNs) are recognized as pivotal infrastructures to reduce the carbon footprint of the heating sector. However, their large-scale dimension and the involved nonlinear dynamics lead to significant issues regarding their modeling and optimal control. Tackling these challenges, two dynamic DHN modeling frameworks are presented: a detailed simulation model and a control-oriented one. The simulation model allows the development of lightweight dynamic DHN simulators, accurately represents the main system dynamics in reduced computational time, and is well-suited for testing online control algorithms. This model is leveraged to develop a simulation library for DHN systems in the Modelica environment, named *DHN4Control*, freely distributed with this article in [1]. Then, a methodology for deriving a control-oriented DHN model is presented, suitable for designing a nonlinear model predictive control (NMPC) regulator, ensuring computationally efficient and cost-effective regulation while respecting operative constraints. The developed modeling and control methods are tested in simulation considering as benchmark a Test Facility district heating plant located at Ricerca sul Sistema Energetico - RSE S.p.A. in Milan (Italy), showing promising results in terms of modelling accuracy, computational efficiency and energy savings.**

***Note to Practitioners* - The dimension and complexity of multi-producer district heating networks (DHN) make their modeling, simulation, and online optimization challenging tasks. This work proposes a solution for district heating networks efficient simulation and optimal control design. The detailed explanations of the modelling equations and the use of open source software increase results replicability for practitioners. The simulation-oriented model comes with a lightweight simulation library, readily available at [1]. The control-oriented model is reusable on generic multi-producer district heating networks, for computationally efficient optimization-based control design. The optimal control is able to manage thermal generators and storages to minimize DHN operational costs while respecting operational constraints over the whole thermal network. The proposed solution is tested in simulation considering a real-world DHN plant currently under construction at Ricerca sul Sistema Energetico - RSE S.p.A in Milan (Italy). The simulation results show the cost saving performances of optimal controllers developed with the proposed model. Overall, by using the proposed solution, one can achieve faster simulation times and ease the burden of optimal control modelling for the development of an optimal-based control strategy for cost-effective DHN operation.**

***Index Terms*—District heating network, Model predictive control, Control-oriented model, Energy efficiency**

Lorenzo Nigro, Alessio La Bella, Francesco Casella and Riccardo Scattolini are Dipartimento di Elettronica, Informazione e Bioingegneria, Politecnico di Milano, Via Ponzio 34/5, 20133 Milano, Italy, (e-mails: *lorenzo.nigro@polimi.it*, *alessio.labella@polimi.it*, *francesco.casella@polimi.it* and *riccardo.scattolini@polimi.it*). Lorenzo Nigro is also with Ricerca Sistema Energetico - RSE S.p.A., Via R. Rubattino 54, 20134 Milano, Italy, (e-mail: *lorenzo.nigro@rse-web.it*).

I. Introduction

HEATING and cooling requirements for residential, commercial, and industrial buildings in Europe account for nearly 50% of their total energy demand, the majority of which is supplied by fossil fuels [2]. In response to the European 2050 targets for net zero greenhouse gas emissions and the global push towards decarbonization, district heating networks (DHNs) have emerged as a promising solution, given their environmental and economic benefits to society [3], [4]. Consequently, the European Union intends to cover at least 50% of the heating demand of most European countries with DHN systems by 2050 [5].

DHNs are plants for the generation, distribution, and consumption of heat which is usable for indoor heating and domestic hot water. They involve thermal generators (e.g., heat pumps, boilers), storages (e.g., insulated tanks), and loads (e.g., households, buildings). The generated heat transfers to loads through water flowing in the supply pipeline. Then, water flows back to the generators via the return pipeline to reheat. Based on the topology, DHNs' structure can be single producer, i.e., where thermal generators lay in a single heating node, or multi-producer, in the presence of generation distributed over the network [6]. Nowadays, most DHN plants are operated by simple rule-based control strategies, which are unable to exploit networks' full potential and cause increased thermal losses and operational costs. The motivation of this study is to unlock district heating network efficiency through optimization-based control strategies [7], [8]. Nevertheless, modeling complex and large-scale DHNs implies two key challenges: suitable dynamical simulator design, which is a necessary tool for testing control strategies' performances and proper system management, as well as the networks' optimal operation point computation, e.g., leveraging Model Predictive Control (MPC) strategies. Two models shall be developed to answer this needs.

A. Related work

Concerning the simulation of DHN, the mathematical modeling describing single-producer DHN in [9] is accomplished using partial differential equations, whereas in [10] is done through a port-Hamiltonian approach. Multi-producer DHN models stability and passivity properties are analyzed in [11] [12]. Nonetheless, some modeling aspects are omitted in the mentioned references, e.g., pipeline metal walls' thermal inertia, pipe sections' variation, or thermal storage dynamics.

A precise DHN model is pivotal to accurately simulate thermo-hydraulic dynamical behavior [13]. DHN simulators

can be based on detailed modeling libraries for thermo-hydraulic systems, for example, the *ThermoPower* library developed in Modelica [14], [15] or the MATLAB toolbox *Simscape* [16], [17]. Nevertheless, these simulation environments require numerous physical parameters that may be unavailable. Moreover, they model dynamics that are less relevant for DHNs (e.g., fluid phase transition, pressure-varying, or temperature-varying heat coefficients) leading to additional computational effort and slower simulations, often without useful information return. Consequently, testing and tuning optimization-based regulators through the mentioned simulation environments becomes increasingly intensive and not practical.

Concerning the design of MPC regulators for DHN systems, some works have been proposed in the literature. For instance, a stabilizing MPC approach is proposed in [18], however not considering the cost-effective DHN management and applied to a small-size exemplary benchmark. In fact, the large-scale dimension and nonlinear dynamics of highly detailed DHN models affect the optimal control problem design and lead to computational issues from the optimization perspective. In this context, [9] describes an optimization scheme for DHNs; nonetheless, it suffers from large-scale nonlinearities and is solvable only using a single-step prediction horizon. On the other hand, in [19], a particle swarm optimization algorithm is employed to solve the DHN control problem, however, the authors states that the resulting computational burden is not admissible for practical implementation.

Most of the exiting solutions to decrease the computational complexity of MPC regulators for DHN systems, most of them rely on simplified models. For instance, in [20]–[23], the MPC regulator employs models based on thermal static power balances, i.e., they neglect temperature dynamics over network pipelines. In fact, temperature dynamics are essential in DHN control design for two main reasons. First, the water temperature must respect different operative constraints over the network (e.g., the supply temperature of all loads must exceed a threshold for proper operation [9], [11]). Second, the generation costs and heat loss minimization require temperature dynamics knowledge to account for the intrinsic water pipelines' thermal inertia. Thus, temperature modelling appear in other MPC solutions, leveraging different simplifying assumptions to reduce complexity. For instance, in [24], authors assume fixed transport delays and water flow over the network. In [25], solely the return network temperature is considered using a linear model, whereas, in [26], water supply temperature is the same across all loads, i.e., neglecting network thermal losses. In [27], bi-directional power flows are also considered, and the complexity is reduced by neglecting delays, heat losses, and the thermal inertia of the pipeline network. Nevertheless, none of these solutions enable to properly consider heating network inertia and constraints.

On the other hand, data-driven models have been also proposed in the literature for DHN systems, as in [8], [28]–[31]. In this context, Gaussian data-based models are employed in [32] for modelling thermal dynamics in DHN systems, whereas data-driven linear models are exploited in [33]. The drawback of these data-based approaches is that they neglect any available physical knowledge of the DHN. This last aspect has been addressed in [34], where a physics-informed data-based model is proposed for DHN systems, combining data and the available physical knowledge, i.e., the network topology. Nevertheless, data-based modelling methods rely on large operational datasets highly exciting system dynamics, which are hardly available in real DHN applications.

B. Main contribution

The above discussion motivates the necessity of developing novel control-oriented DHN models, which must be computationally-efficient and accurate enough to properly represent network thermal dynamics. This control-oriented modelling must enable the design of predictive control strategies capable of effectively optimizing DHN operations, and guaranteeing to respect all required network constraints. On the other hand, lightweight and DHN-oriented simulation environments are also required, for testing and tuning the designed optimization-based controllers. These challenges are solved through the following main contributions of this work.

- *DHN modeling for computationally-efficient and accurate simulators:* As discussed, existing works on detailed DHN models neglect fundamental elements, e.g., [9]-[12], whereas other frameworks involve demanding and slow simulations being not focused on DHN systems, e.g., [14], [15]. Thus, this paper formulates a complete multi-producer DHN model, featuring all main elements (e.g, generators, loads, storages, pipes, pipe fitting, etc.). The model considers the typical DHN operation to capture its relevant dynamics and neglects less relevant phenomena in DHN systems (e.g., fluid phase transition), enabling the design of a fast and accurate dynamic simulation environment, suited for testing online optimization-based controllers. The resulting simulation library, called *DHN4Control*, is developed in Modelica and freely distributed with this work [1]. The *DHN4Control* library can be used for any DHN configuration and it is tested both with experimental data and against other simulation libraries, e.g., [15], showing to be accurate and computationally lighter.
- *DHN control-oriented model and nonlinear predictive control design:* Existing control strategies for DHN systems rely on highly complex models unsuitable for optimal predictive control, e.g., [9] - [12]. Because of this, other control approaches have relied on oversimplifying assumptions, but these are incapable of exploiting DHN thermal inertia, e.g., [20] - [27]. Some data-based controllers for DHN also exists, however they necessitate large amount of exciting operational data, which is not always feasible in practice, e.g., [28] - [34]. In view of this, another contribution of the work consists in developing a novel DHN control-oriented modelling with enhanced dynamical accuracy and computational efficiency, recovered from the detailed simulation one through new model reduction methods. Among these, we here mention: the substitution of pressure modeling with

equivalent, but light-way, algebraic relationships enforced at each network closed path, and the reduced pipe modelling combining pipe wall and flow thermal dynamics. The presented control-oriented model achieves enhanced modeling accuracy when compared with the detailed DHN simulation model, but with a significant lower number of variables (around 90% reduction), paving the way for the design of a computationally-efficient Nonlinear Model Predictive Control (NMPC) regulator, optimizing large-scale DHN plants in few seconds. The designed NMPC regulator enables to minimize generation costs and to increase system efficiency by properly exploiting DHN thermal inertia, while ensuring constraints respect over the whole thermal network.

The developed methods are tested through detailed simulators considering a real DHN benchmark, hereafter named: "Thermal Test Facility", which is currently under construction at the research center Ricerca sul Sistema Energetico - RSE SpA, Milan, Italy. For the sake of completeness, the obtained performances are also evaluated on a larger benchmark taken from the literature, i.e., the AROMA district heating network [9]. The solution obtains high modelling accuracy, reduced computational complexity, and the resulting NMPC regulators achieve up to 15% of cost reduction compared to standard rule-based control strategies.

C. Paper Outline

The paper is organized as follows. In Section II, the DHN modeling is described in detail together with the developed simulation library. In Section III, the DHN control-oriented model, the reduction procedure to obtain it, and the NMPC regulator design are discussed. Additionally, Section IV displays the numerical results regarding the developed modeling and control methods applied to the Thermal Test Facility. The conclusions are in Section V.

D. Notation

Let $\mathbb{R}$ denote the set of real numbers, $\mathbb{R}_{\geq 0}$ the set of positive or null real numbers including zero, and $\mathbb{R}_{>0}$ the set of strictly positive real numbers. Moreover, let $\mathbb{N}$ denote the set of natural numbers. Given a matrix A, $A \in \mathbb{R}^{n,m}$ indicates that it has n rows and m columns and all its entries are real numbers. Given a vector a, $a \in \mathbb{R}^n$ indicates that it has n rows and one column, and all its entries are real numbers. Given a matrix A and a vector a, their transpose are denoted with A' and a', respectively. Given two vectors of variables $x, y \in \mathbb{R}^n$, the inequalities among the two, e.g., $x > y$, are intended element-wise. For a vector $x \in \mathbb{R}^n$, the vectors of the corresponding upper and lower bounds are $\overline{x} \in \mathbb{R}^n$ and $\underline{x} \in \mathbb{R}^n$, respectively, with $\overline{x} > \underline{x}$.

II. Modelling of district heating networks

DHNs are large-scale systems governed by nonlinear Partial Differential Equations (PDE). These PDE describes the dynamical relationships among water mass flows, pressures, and temperatures [9]. A typical DHN is composed of the following main elements, also depicted in Figure 1(a):

- a supply network, where water at high temperature flows from thermal generators to loads;
- a return network, where water flows back to thermal generators after having transferred heat to loads;
- thermal generation, which heat the water supplied by the return network through local units (e.g., boilers) and then pump it back into the supply distribution network;
- thermal loads, which absorb heat from the water in the supply distribution network through a local heat exchanger and then inject it back into the return distribution network;
- thermal energy storages (TESs), which are insulated water tanks with constant mass connected to the supply and return distribution network. TESs typically store high-temperature water and deliver it when convenient.

In addition to these main elements, a DHN comprises valves, pumps, and pipes, which will be modeled in the following relying on their physical equations. Before formulating the DHN model, we state a few assumptions leading to a physical model with reasonable complexity and accuracy for the design and test of control systems. Specifically, the stated assumptions are valid in a typical operating range for high-temperature DHNs, i.e., with water pressure between 2 and 10 bar and water temperatures between 60 and $90°$C, [35].

Assumption 2.1: Water is assumed incompressible and with constant specific heat. The water density and specific heat values derive from IAPWS-IF97 standard[1] and are equal to their average value in the considered operating range. Specifically, the following values are considered $\rho = 998\,\mathrm{kg/m^3}$ and $c = 4185\,\mathrm{J/kg\ K}$.

Assumption 2.2: Each pipe is assumed to have rigid metal walls and a constant circular section. Cross-sectional area variations among pipes are modeled as lumped in specific points of the DHN, commonly named pipe fittings.

Assumption 2.3: Pressure transients are assumed instantaneous, as pressure waves travel in the fluid with the speed of sound, whereas temperature variations travel with the flow velocity [36]. Hence, inertial and compressibility effects in momentum balance equations are neglected, reducing pressure modeling to algebraic nonlinear equations.

Assumption 2.4: For notational simplicity, the supply and return distribution networks are assumed to have the same topology, as typical in DHNs [11], [37].

Consider the DHN reported in Figure 1(a). Given Assumption 2.4, a DHN can be represented with a single undirected, connected, and planar graph $G = (\mathcal{N}, \mathcal{E})$, as shown in Figure 1(b), where $\mathcal{N}$ is the set of nodes of the DHN and $\mathcal{E}$ the set of edges, representing physical interconnections among nodes.

Each node $i \in \mathcal{N}$ represents a significant element in the DHN, e.g., a thermal generator, a storage, a load, or a junction among multiple pipes. Specifically, the set of generation nodes

[1] http://www.iapws.org/relguide/IF97-Rev.html

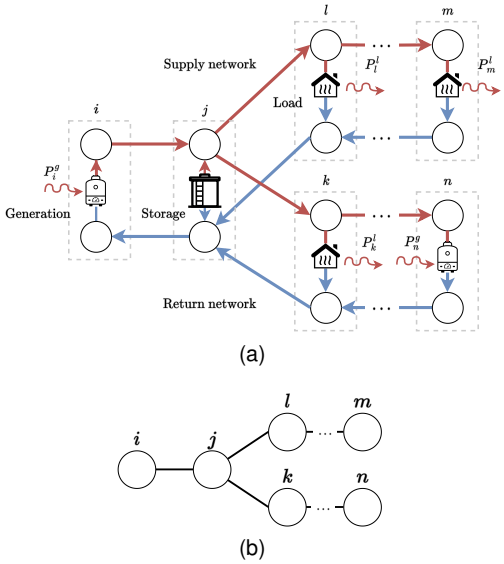


Fig. 1. (a) Schematic of a DHN with supply and return distribution network, respectively in red and blue, a thermal generator at node i, thermal loads at nodes l and k, and a thermal storage at node j. (b) Equivalent graph representation of the DHN.

is denoted as $\mathcal{G} \subset \mathcal{N}$, the set of load nodes as $\mathcal{L} \subset \mathcal{N}$, the set of thermal storage nodes as $\mathcal{Z} \subset \mathcal{N}$. Note that, for the sake of simplicity, it is here assumed that these sets do not have common nodes, i.e., $\mathcal{G} \cap \mathcal{L} \cap \mathcal{Z} = \emptyset$, meaning that if two elements are connected (e.g., a generator and a storage), two fictitious connected nodes are defined. Moreover, specific variables describing the water state are introduced for each node of the DHN: *i)* the water mass flow q [kg/s], *ii)* its pressure p [Pa], and *iii)* its temperature T [°C]. Referring to Figure 1(a), all nodes $i \in \mathcal{N}$ interface with the supply and the return pipelines; hence, they require two sets of variables defined as: (q_i^s, p_i^s, T_i^s) describing the net water flow, pressure, and temperature at the supply distribution network connection, and (q_i^r, p_i^r, T_i^r) describing the same quantities at the return. The superscripts s and r specify if variables and parameters belong to the supply or the return respectively; for the sake of compactness, a generic superscript v with $v \in \{s, r\}$ represents both.

Each edge $(i, j) \in \mathcal{E}$ interconnecting node i and j physically represents either a distribution pipe (see Figure 2) or a pipe fitting, i.e., a lumped-element where the pipe section changes (see Figure 3). Thus, define as $\mathcal{E}_P$ the set of edges representing distribution pipes, and as $\mathcal{E}_F$ the set of edges representing pipe fitting, where $\mathcal{E} = \mathcal{E}_P \cup \mathcal{E}_F$. Moreover, $\forall (i, j) \in \mathcal{E}$, q_{ij}^v and q_{ji}^v describe the water flow where $q_{ij}^v \geq 0$ and $q_{ji}^v \leq 0$ if the water flows from node i to j, whereas $q_{ji}^v > 0$ and $q_{ij}^v < 0$ if the water flows from node j to i; the same holds at the supply $(v = s)$ and the return $(v = r)$ network.

Please refer to Table I for the description of the main variables and parameters used for the DHN model. Note that the superscript v is used for some parameters, which can be referred either to the supply $(v = s)$ or the return $(v = r)$ network. Hereafter, DHN edges modeling is first described, then DHN nodes are modeled.

TABLE I
MAIN VARIABLES AND PARAMETERS

Name	Description	Unit
c	Water specific heat	[J/kg/K]
g	Gravitational acceleration	[m/s^2]
p	Water pressure	[bar]
q	Water mass flow rate	[kg/s]
ρ	Water density	[kg/m^3]
c_f	Pipe fanning coefficient	[-]
c_m	Pipe metal specific heat	[J/m$^3\cdot$ s]
L_{ij}^v	Pipe ij length	[m]
n_{ij}^v	Pipe ij number of sections	[-]
q_{ij}^v	Pipe ij mass flow rate	[kg/s]
r_{ij}^v	Pipe ij internal radius	[m]
r_{ij}^{vm}	Pipe ij external radius	[m]
$T_{ij,k}^v$	Pipe ij kth section water temperature	[°C]
$T_{ij,k}^{vm}$	Pipe ij kth section metal temperature	[°C]
T_{ij}^e	Pipe ij external temperature	[°C]
U_{ij}^{vm}	Pipe ij heat transfer coefficient water-metal	[W/K·m^2]
U_{ij}^{ve}	Pipe ij heat transfer coefficient metal-ambient	[W/K$\cdot$ m^2]
y_{ij}^v	Pipe ij vertical displacement	[m]
k_1^v, k_2^v	Pipe fitting ij friction coefficients	[-]
A_i^l	Load i Valve opening area	[m^2]
θ_i^l	Load i valve opening	[-]
P_i^l	Load i thermal power	[W]
q_i^l	Load i mass flow rate	[kg/s]
T_i^l	Load i output temperature	[°C]
P_i^g	Generator i thermal power	[W]
H_i^z	TES i height	[m]
n_i^z	TES i number of sections	[-]
q_i^z	TES i mass flow rate	[kg/s]
r_i^z	TES i base radius	[m]
$T_{i,k}^z$	TES i kth section water temperature	[°C]
T_i^{ze}	TES i external temperature	[°C]
α	TES i dispersion coefficient	[W/K·m^2]
κ	TES i conduction coefficient	[W/K·m^2]

A. Distribution network model

1) Pipe model:

Pipes are modeled featuring the one-dimensional finite-volume method [9]. This model consists of the spatial discretization in mono-dimensional sections with boundaries orthogonal to the water flow direction, as reported in Figure 2. The pipe's sections comprise a lumped dynamical temperature model that expresses energy balances and exchanges among adjacent sections and their pipe walls.

Supply and return pipes at the edge $(i, j) \in \mathcal{E}_P$ are characterized by a vertical displacement y_{ij}^v, a total length L_{ij}^v, internal radius r_{ij}^v, and external radius r_{ij}^{vm}, as depicted in Figure 2. Given the finite volume method, each supply and return pipe in the edge (i, j) is divided into n_{ij}^v sections with boundaries orthogonal to the water flow direction, each one of length $l_{ij}^v = L_{ij}^v / n_{ij}^v$ and volume $v_{ij}^v = l_{ij}^v \pi {r_{ij}^v}^2$. The water temperature of the generic kth pipe section is denoted with $T_{ij,k}^v$, whereas the temperature of the pipe wall at that section

is $T^{vm}_{ij,k}$, with $k \in \{1, \dots, n^v_{ij}\}$. Thus, the dynamic model of the water temperature for the kth pipe section is

$$c\,\rho\, v^v_{ij}\,\dot{T}^v_{ij,k}(t) = 2\pi r^v_{ij}\, l^v_{ij}\, U^m_{ij}\,(\,T^{v\,m}_{ij,k}(t) - T^v_{ij,k}(t)\,) + c\, q^v_{ij}(t) \begin{cases} T^v_{ij,k-1}(t) - T^v_{ij,k}(t) & \text{if } q^v_{ij}(t) \geq 0 \\ T^v_{ij,k}(t) - T^v_{ij,k+1}(t) & \text{if } q^v_{ij}(t) < 0 \end{cases} \tag{1}$$

for each $k \in \{1, \dots, n^v_{ij}\}$ and $v \in \{s, r\}$. Moreover, by imposing $T^v_{ij,0}(t) = T^v_i(t)$ and $T^v_{ij,n^v_{ij}+1}(t) = T^v_j(t)$, one can express the interface of each pipe (i, j) to the nodes i and j at its extremes (see Figure 2). The left-hand side of equation (1) corresponds to the derivative of the thermal energy in the kth section, whereas the right-hand side includes the heat transfer towards the pipe metal wall, depending on the conduction area and the heat transfer coefficient U^m_{ij}, and the thermal energy exchanged with the adjacent sections due to transport phenomena. For compactness, introduce the vectors

$$\mathbf{T}^v_{ij} = \left[T^v_{ij,1},\ \dots,\ T^v_{ij,n^v_{ij}}\right]', \quad \mathbf{T}^{vm}_{ij} = \left[T^{vm}_{ij,1},\ \dots,\ T^{vm}_{ij,n^v_{ij}}\right]',$$

and the matrices $\Phi, \Psi \in \mathbb{R}^{n^v_{ij}, n^v_{ij}}$, defined as

$$\Phi_{ij} = \begin{cases} -1 & \text{if } i = j \\ 1 & \text{if } j = i-1 \wedge i > 1 \\ 0 & \text{otherwise} \end{cases}, \tag{2a}$$

$$\Psi_{ij} = \begin{cases} -1 & \text{if } i = j \\ 1 & \text{if } j = i+1 \wedge i < n_{ij} \\ 0 & \text{otherwise} \end{cases}, \tag{2b}$$

and the vectors $\boldsymbol{\delta} = [1, 0, \dots, 0]'$ and $\boldsymbol{\omega} = [0, \dots, 0, 1]'$, with $\boldsymbol{\delta}$, $\boldsymbol{\omega} \in \mathbb{R}^{n^v_{ij}}$. Thus, equation (1) can be rewritten as

$$c\,\rho\, v^v_{ij}\dot{\mathbf{T}}^v_{ij}(t) = 2\pi r^v_{ij}\, l^v_{ij}\, U^m_{ij}(\mathbf{T}^{vm}_{ij}(t) - \mathbf{T}^v_{ij}(t)) + c\, q^v_{ij}(t) \begin{cases} \Phi\,\mathbf{T}^v_{ij}(t) + \boldsymbol{\delta} T^v_i(t) & \text{if } q^v_{ij}(t) \geq 0 \\ \boldsymbol{\omega} T^v_j(t) - \Psi\,\mathbf{T}^v_{ij}(t) & \text{if } q^v_{ij}(t) < 0\,, \end{cases} \tag{3a}$$

for each $v \in \{s, r\}$.

Another crucial factor to consider for DHN analysis is the pipe's metal wall thermal dynamic as it can significantly impact the water temperature dynamical behavior, as discussed in [13]. Consider the pipe external radius r^{vm}_{ij} and wall section volume $v^{vm}_{ij} = l^v_{ij}\pi\big((r^{vm}_{ij})^2 - (r^v_{ij})^2\big)$. Then, the pipe metal wall temperature model is

$$c_m\,\rho_m\, v^{vm}_{ij}\,\dot{\mathbf{T}}^{vm}_{ij}(t) = 2\pi r^v_{ij}\, l^v_{ij}\, U^m_{ij}\,(\,\mathbf{T}^v_{ij}(t) - \mathbf{T}^{vm}_{ij}(t)\,) - 2\pi r^{vm}_{ij}\, l^v_{ij}\, U^e_{ij}\,\big(\mathbf{T}^{vm}_{ij}(t) - \mathbb{1}\,T^{v,e}_{ij}(t)\big)\,, \tag{3b}$$

for each $v \in \{s, r\}$. The left-hand side of the equation expresses the derivative of the pipe wall section thermal energy; instead, the right-hand side includes the energy exchange with the flowing water and with the external environment, supposed to be at temperature $T^{v,e}_{ij}$, which may correspond to the ground temperature as DHN pipes commonly lay underground.

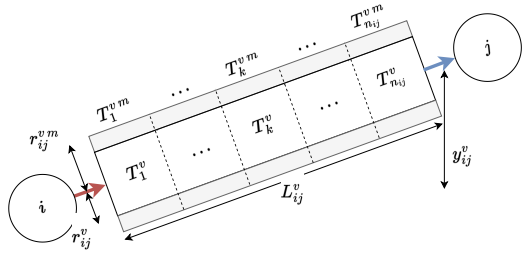


Fig. 2. One-dimensional, finite-volume method, and pipe's parameters and variables.

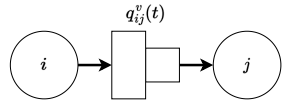


Fig. 3. Pipe fitting for changes in pipe's section.

The pressure drop across pipes is modeled through Fanning's formula [38], which reads as

$$p^v_i(t) - p^v_j(t) = \rho g y^v_{ij} + \rho \begin{cases} c_f \frac{L^v_{ij}}{r^v_{ij}} \left(\frac{q^v_{ij}(t)}{\rho\pi {r^v_{ij}}^2}\right)^2, & \text{if } q^v_{ij}(t) \geq 0, \\ -c_f \frac{L^v_{ij}}{r^v_{ij}} \left(\frac{q^v_{ij}(t)}{\rho\pi {r^v_{ij}}^2}\right)^2, & \text{if } q^v_{ij}(t) < 0, \end{cases} \tag{4}$$

for each $v \in \{s, r\}$, where c_f is the Fanning coefficient, and g is the gravitational acceleration.

2) Pipe fitting model:

As previously discussed, assume lumped cross-section variations and represent them with an edge $(i, j) \in \mathcal{E}_F$ in the supply and return networks, as shown in Figure 3. Exploiting Bernoulli's equation [39], the pressure drop at each pipe fitting edge $(i, j) \in \mathcal{E}_F$ is

$$p^v_i(t) - p^v_j(t) = \frac{q^v_{ij}(t)^2}{2\rho} \begin{cases} k^v_{1,ij} & \text{if } q^v_{ij}(t) \geq 0 \\ -k^v_{2,ij} & \text{if } q^v_{ij}(t) < 0 \end{cases}, \tag{5}$$

where $v \in \{s, r\}$, and $k^v_{1,ij}$ and $k^v_{2,ij}$ are fixed tabulated friction coefficients depending on the pipe fitting geometry (e.g., cross-section variation, contraction angles, etc.). More details on pipe fitting coefficients related to their specific geometry are available in [40]. Moreover, assume no temperature losses occur across pipe fittings, i.e.,

$$T^v_i = T^v_j\,, \tag{6}$$

with $v \in \{s, r\}$, and $(i, j) \in \mathcal{E}_F$.

B. Node models

As anticipated, most DHNs' components belong to one of three node categories: thermal loads, generators, and storages. The first two categories involve static models as their time

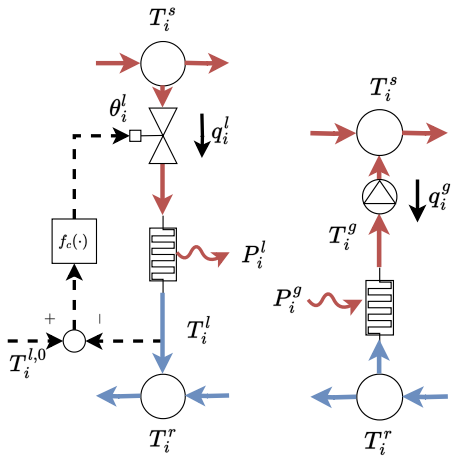


Fig. 4. (a) Generic load structure. (b) Generator node structure.

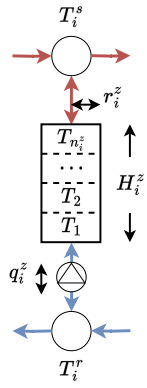


Fig. 5. Schematic of a thermal energy storage.

constants are negligible compared to those of the network transport dynamics. On the other hand, the thermal storage models are dynamic as they show significant thermal inertia.

1) Load model:

Each load node $i \in \mathcal{L}$ connects the supply and the return distribution network, absorbing a water flow $q_i^l \in \mathbb{R}_{\geq 0}$ from the supply network through a locally regulated valve, as depicted in Figure 4(a). The absorbed water goes through the load heat exchanger, which extracts thermal power $P_i^l \geq 0$. Thus, it holds that

$$P_i^l(t) = c\, q_i^l(t)\, (T_i^s(t) - T_i^l(t))\,, \tag{7}$$

where $T_i^l(t)$ is the output water temperature at the load heat exchanger. As proposed in [41], loads are temperature-controlled, implying that the water flow q_i^l is regulated through the local valve to track a reference $T_i^{l,0}$ for the output water temperature. This is modeled as

$$\dot{\theta}_i^l(t) = f_c(\,\theta_i^l(t),\; T_i^{l,0} - T_i^l(t))\,, \tag{8a}$$

$$q_i^l(t) = \theta_i^l(t)\, A_i^l \sqrt{p_i^s(t) - p_i^r(t)}\,, \tag{8b}$$

where $\theta_i^l \in [0,1]$ is the load valve opening, and $f_c(\cdot)$ in (8a) represents a generic valve control law. Additionally, equation (8b) expresses the water flow model dependency on the pressure drop across the valve, and A_i^l is the fully open valve's section [39]. Note that the pressure drop across the load heat exchanger is not modeled as it is negligible compared to the pressure drop across pipes and control valves.

2) Thermal generation model:

Each node $i \in \mathcal{G}$ absorbs a water flow $q_i^g \in \mathbb{R}_{\geq 0}$ at temperature T_i^r from the return distribution network and injects it into the supply network at temperature T_i^g, as in Figure 4(b). It holds that

$$P_i^g(t) = c\, q_i^g(t)\, (T_i^g(t) - T_i^r(t))\,, \quad \forall i \in \mathcal{G}\,, \tag{9}$$

where $P_i^g(t) \geq 0$ is the thermal power transferred by the generator to the absorbed water.

One of the generation nodes is denoted as "slack", and this is indicated with index $h \in \mathcal{G}$. The slack generator accomplishes two tasks: it imposes a reference pressure $p_h^{r,0}$ at the return network layer, thanks to a local expansion vessel, and maintains fixed pressure drop Δp_h^0 between supply and return, using a differential pressure pump [9], [42]. This implies that

$$p_h^s(t) = p_h^{r,0} + \Delta p_h^0\,, \qquad p_h^r(t) = p_h^{r,0}\,. \tag{10}$$

The slack node guarantees a minimum reference pressure in the water circuit and compensates for head losses [43]. Consequently, the slack node water flow can not be externally imposed, as it is regulated locally to keep a constant pressure drop Δp_h^0. Differently, the other generation nodes can directly impose the water flow through local flow-regulated pumps. In particular, if Assumptions 2.1-2.4 hold, then the slack water flow entirely depends on the net water flow circulating in the DHN. In turn, the net flow is determined by the generators' flow-regulated pumps and by the load valve regulations. Finally, note that generation nodes can be either temperature-controlled, i.e., the output temperature T_i^g is externally imposed and tracked by a local controller, or power-controlled, i.e., a specific power P_i^g is requested to be delivered by the generator [8]. Thus, the generators' node set $\mathcal{G}$ includes the set of power-controlled nodes $\mathcal{G}_P$, and the set of temperature-controlled nodes $\mathcal{G}_T$, and it holds $\mathcal{G} = \mathcal{G}_P \cup \mathcal{G}_T$.

3) Storage model:

Thermal energy storage integration considerably increases DHN's flexibility [44]. TES connects the supply and return distribution networks and it can absorb/inject water from/to each network through a local pump, as illustrated in Figure 5.

Consider a generic thermal storage at node $i \in \mathcal{Z}$. Its total height is H_i^z, and its base radius is r_i^z. Concerning TES temperature dynamics, a one-dimensional stratified model is adopted. This modeling approach works similarly to the finite volume method used for pipes, as shown in Figure 5, [45]. Specifically, the storage tank is divided into n_i^z sections; each section has boundaries orthogonal to the water flow direction, height $h_i^z = H_i^z/n_i^z$ and volume $v_i^z = h_i^z\,\pi\,{r_i^z}^2$.

Given that the thermal storage water flow, i.e., q_i^z, is bidirectional, as a convention, it is chosen that $q_i^z \geq 0$ when flowing from the return to the supply distribution network, and $q_i^z < 0$ when flowing in the opposite direction. Thus, for each storage section $k \in \{1, ..., n_i^z\}$, the temperature model is defined as

$$\begin{aligned} c\rho v_i^z\,\dot{T}_{i,k}^z(t) = {} & 2\,\pi\,r_i^z\,h_i^z\,\alpha\,(T_i^{z,e}(t) - T_{i,k}^z(t)) \\ & + \pi\,{r_i^z}^2\,\kappa\,\left((T_{i,k+1}^z(t) - T_{i,k}^z(t)) + (T_{i,k-1}^z(t) - T_{i,k}^z(t))\right) \\ & + c\,q_i^z(t)\begin{cases} T_{i,k-1}^z(t) - T_{i,k}^z(t) & \text{if } q_i^z(t) \geq 0 \\ T_{i,k}^z(t) - T_{i,k+1}^z(t) & \text{if } q_i^z(t) < 0 \end{cases} \end{aligned} \tag{11}$$

where $T_{i,0}^z(t) = T_i^r(t)$ $T_{i,n_i^z+1}^z(t) = T_i^s(t)$ to express the interfacing of the storage tank with the supply and return network. The left-hand side of the above-equation expresses the thermal energy dynamics for the kth section, whereas the right-hand side considers the heat losses towards the external environment at temperature $T_i^{z,e}(t)$, the energy exchange with the adjacent sections due to thermal conduction, and the energy exchange due to mass transport phenomena, depending on the direction of the water flow.

Aiming to write thermal storage dynamics in a compact form, let us introduce the vector $\mathbf{T}_i^z(t) = \left[T_{i,1}^z(t)\ ...\ T_{i,n_i^z}^z(t)\right]'$ and consider again the matrices Φ and Ψ, and the vectors $\boldsymbol{\delta}$ and $\boldsymbol{\omega}$ defined in Section II-A. Thus, for each thermal storage node $i \in \mathcal{Z}$, the following temperature model holds

$$\begin{aligned} c\,\rho\,v_i^z\dot{\mathbf{T}}_i^z(t) = {} & 2\,\pi\,r_i^z\,h_i^z\alpha(\mathbb{1}\ T_i^{z,e}(t) - \mathbf{T}_i^z(t)) \\ & + \pi\,{r_i^z}^2\,\kappa\,(\Psi + \Phi)\,\mathbf{T}_i^z(t) \\ & + c\,q_i^z(t)\begin{cases} \Phi\mathbf{T}_i^z(t) + \boldsymbol{\delta}T_i^r(t) & \text{if } q_i^z(t) \geq 0 \\ \boldsymbol{\omega}T_i^s(t) - \Psi\mathbf{T}_i^z(t) & \text{if } q_i^z(t) < 0 \end{cases}. \end{aligned} \tag{12}$$

C. Node coupling equations

Multiple water flows can converge or split in a single node, implying that node coupling equations must be introduced. Given a generic node $i \in \mathcal{N}$, we introduce the sets $\mathcal{I}_i^s \subset N$ and $\mathcal{I}_i^r \subset N$. These sets include the nodes delivering water to node i respectively at the supply and return distribution network and are defined as

$$\begin{aligned} \mathcal{I}_i^v(t) = {} & \{j \in \mathcal{N} :\ (j,i) \in \mathcal{E} \wedge q_{ji}^v(t)\ \geq 0\} \cup \\ & \{j \in \mathcal{N} :\ (i,j) \in \mathcal{E} \wedge q_{ij}^v(t) < 0\}, \end{aligned} \tag{13}$$

for $v \in \{s, r\}$. Note that the input node sets are time-varying, depending on the current direction of the water flow.

Thus, the overall water flow incoming at each node $i \in \mathcal{N}$ at the supply network is

$$q_i^s(t) = \sum_{\forall j \in \mathcal{I}_i^s(t)} (q_{ji}^s(t) - q_{ij}^s(t)) + \begin{cases} q_i^g(t) & \text{if } i \in \mathcal{G} \\ q_i^z(t) & \text{if } i \in \mathcal{Z} \wedge q_i^z(t) \geq 0 \end{cases}, \tag{14a}$$

whereas the one on the return network is

$$q_i^r(t) = \sum_{\forall j \in \mathcal{I}_i^r(t)} (q_{ji}^r(t) - q_{ij}^r(t)) + \begin{cases} q_i^l(t) & \text{if } i \in \mathcal{L} \\ -q_i^z(t) & \text{if } i \in \mathcal{Z} \wedge q_i^z(t) < 0 \end{cases}. \tag{14b}$$

Furthermore, the average temperatures at node i for the supply and return network are derived from the weighted average of the incoming water flow temperatures and their model are

$$\begin{aligned} q_i^s(t)T_i^s(t) = {} & \sum_{\forall j \in \mathcal{I}_i^s(t)} \left(q_{ji}^s(t)\,T_{ji,n_{ij}^s}^s(t)\ -\ q_{ij}^s(t)\,T_{ij,1}^s(t)\right) \\ & + \begin{cases} q_i^p(t)\,T_i^g(t) & \text{if } i \in \mathcal{G} \\ q_i^z(t)\,T_{i,n_i^z}^z(t) & \text{if } i \in \mathcal{Z} \wedge q_i^z(t) \geq 0 \end{cases}, \end{aligned} \tag{15a}$$

and

$$\begin{aligned} q_i^r(t)T_i^r(t) = {} & \sum_{\forall j \in \mathcal{I}_i^r(t)} \left(q_{ji}^r(t)\,T_{ji,n_{ij}^r}^r(t)\ -\ q_{ij}^r(t)\,T_{ij,1}^r(t)\right) \\ & + \begin{cases} q_i^l(t)\,T_i^l(t) & \text{if } i \in \mathcal{L} \\ -q_i^z(t)\,T_{i,1}^z(t) & \text{if } i \in \mathcal{Z} \wedge q_i^z(t) < 0 \end{cases}, \end{aligned} \tag{15b}$$

where the water temperature either at the first or last section is properly selected for pipes and storages based on the direction of the corresponding water flow.

Finally, considering the mass balance at each node $i \in \mathcal{N}$, the total incoming water flow is equal to the one outgoing from the node. Thus, introduce the set of output nodes $\mathcal{O}_i^s \subset \mathcal{N}$ and $\mathcal{O}_i^r \subset \mathcal{N}$ for the supply and return distribution network, respectively, which are defined as

$$\begin{aligned} \mathcal{O}_i^v(t) = {} & \{j \in \mathcal{N} :\ (i,j) \in \mathcal{E} \wedge q_{ij}^v(t)\ \geq 0\} \cup \\ & \{j \in \mathcal{N} :\ (j,i) \in \mathcal{E} \wedge q_{ji}^v(t) < 0\}, \end{aligned} \tag{16}$$

for $v \in \{s, r\}$. Thus, it holds that

$$q_i^s(t) = \sum_{\forall j \in \mathcal{O}_i^s(t)} (q_{ij}^s(t) - q_{ji}^s(t)) + \begin{cases} q_i^l(t) & \text{if } i \in \mathcal{L} \\ -q_i^z(t) & \text{if } i \in \mathcal{Z} \wedge q_i^z(t) < 0 \end{cases}, \tag{17a}$$

and

$$q_i^r(t) = \sum_{\forall j \in \mathcal{O}_i^r(t)} (q_{ij}^r(t) - q_{ji}^r(t)) + \begin{cases} q_i^g(t) & \text{if } i \in \mathcal{G} \\ q_i^z(t) & \text{if } i \in \mathcal{Z} \wedge q_i^z(t) \geq 0 \end{cases}. \tag{17b}$$

D. Simulation environment and library

The presented DHN model in (3)-(17) is exploited to build a simulation modeling library, named *DHN4Control* library, implemented in the Modelica environment, an object-oriented declarative language suitable for modeling of cyber-physical systems [46]. The developed *DHN4Control* library is available online on GitHub and free to be used [1].

The developed library proves to be flexible and computationally efficient when simulating large-scale DHN systems and it is particularly suited for applications where numerous subsequent simulations are necessary, e.g., during control tuning and testing. The library already includes various default parameters derived from tabulated data, which can be changed based on the user choices. Moreover, the components included in the *DHN4Control* library, whose models are described in previous sections, have been validated against their virtual counterparts from more complex modeling libraries, e.g., the ThermoPower library [14]. As discussed later in Section IV, the formulated DHN models are accurate while enabling the simulation of DHN systems in a shorter time and with fewer parameters with respect to standard simulation libraries, e.g., ThermoPower. The library implementation uses Modelica 4.0.0 on OpenModelica Editor 19.0 [47]. Thanks to Modelica and the OpenModelica environment, it is possible to create portable simulators using the FMU format. This format allows a wide range of software to run Modelica simulations. Among the supported software, but not restricted to, Matlab and Python. More details on these aspects are available in [1].

III. The control problem

In this section, a nonlinear model predictive control (NMPC) regulator is designed, capable of optimally coordinating DHN operations by minimizing operational costs while respecting all necessary constraints. This requires the development of an accurate dynamical system model efficiently solvable from the optimization perspective. In fact, despite the model assumptions introduced in Section II, the simulation-oriented DHN model could be still unpracticable for control purposes due to its dimension and complexity. Thus, model reduction procedures are here presented, enabling to obtain a control-oriented DHN model with enhanced computational efficiency and satisfactory modelling accuracy.

A. Control-oriented modelling

The NMPC control-oriented model derives from equations (3)-(17) by applying the following simplification steps.

1) Fixed flow direction in distribution pipes: Equations (3)-(5) have a switching characteristic related to the direction of the water flow. However, in practice, most supply and distribution network pipes have a fixed flow direction, which can be estimated either from operational data or through preprocessing techniques [9]. Because of this, we here assume that the flow direction in each pipe does not vary over time along the NMPC prediction horizon, avoiding implementing (4)-(5) as Mixed-Logic Dynamical (MLD) constraints [48]. This further implies that the input and output nodes in (14)-(17), i.e., $\mathcal{I}_i^v$ and $\mathcal{O}_i^v$ with $v \in \{s, r\}$, do not vary along the prediction horizon.

2) Storage model reformulation: Contrarily to distribution pipes, thermal storages require reversible flow for their operation as it is related to the charging/discharging modes (see equation (12)). Preserving the aim of mixed-integer variables avoidance in the NMPC problem, we reformulate the storage model similarly to typical battery models [49]. Hence, a charging water flow is introduced, i.e., $q_i^{z,s} \in \mathbb{R}_{\geq 0}$, identifying the water flow injected into the ith thermal storage from the supply distribution network (i.e., hot water), and a discharging water flow is introduced, i.e., $q_i^{z,r} \in \mathbb{R}_{\geq 0}$, identifying the one delivered to the supply network. Given that one single operating mode can be activated at each time instant, it must hold that

$$q_i^{z,s}(t) \cdot q_i^{z,r}(t) = 0. \tag{18}$$

Thus, the storage temperature model (12) is rewritten as

$$\begin{aligned} c\,\rho\, v_i^z \dot{\mathbf{T}}_i^z(t) = {} & 2\,\pi\, r_i^z\, h_i^z \alpha(\mathbb{1} T_i^{z,e}(t) - \mathbf{T}_i^z(t)) \\ & + \pi\, {r_i^z}^2\, \kappa\, (\Psi + \Phi)\, \mathbf{T}_i^z(t) \\ & + c\, q_i^{z,s}(t)\, (\Phi\, \mathbf{T}_i^z(t) + \boldsymbol{\delta} T_i^r(t)) \\ & - c\, q_i^{z,r}(t)\, (\boldsymbol{\omega} T_i^s(t) - \Psi\, \mathbf{T}_i^z(t))\,, \end{aligned} \tag{19}$$

avoiding the explicit use of integer variables to activate the two different models. It is worth noting that one can adopt a similar reformulation for the models of distribution pipes in case the flow direction cannot assumed to be fixed along the prediction horizon.

3) Load model reduction and pressure modeling removal: At the NMPC level, it is possible to assume that the load local control tracks the output load temperature reference, as discussed in [41], implying that

$$T_i^l(t) = T_i^{l,0}\,, \qquad \forall i \in \mathcal{L}. \tag{20}$$

Moreover, pressures are not directly related to the economic management of the DHN; consequently, we may exclude pressure equations from the NMPC problem formulation to reduce its dimension. Nevertheless, even though we neglect pressure equations, the water flows in distribution pipes must respect Kirchhoff's node and loop laws applied to hydraulics networks [50]. The former states that the ingoing and outgoing water flows at each node of $G = (\mathcal{N}, \mathcal{E})$ are balanced, which is guaranteed by (14) and (17). The latter states that the net pressure drop in each closed path of $G = (\mathcal{N}, \mathcal{E})$ must be null, both for the supply and the return distribution network. This property can be imposed without using pressure variables as described in the following.

Consider the DHN graph $G = (\mathcal{N}, \mathcal{E})$, and denote with m the number of its bounded faces, where a bounded face is a closed region of the plane fully delimited by edges and nodes [51]. Each kth graph face, with $k \in \{1, \dots, m\}$, denotes an essential mesh of the graph, i.e., a mesh not containing any other mesh. Thus, denote with $\mathcal{M}_k \subseteq \mathcal{N}$ the set of nodes of each kth mesh and with $\gamma_k \subset \mathcal{M}_k \times \mathcal{M}_k$ a sequence of edges identifying a closed path visiting all nodes in $\mathcal{M}_k$. Moreover,

for the sake of clarity, introduce $\zeta_{ij}^v = \text{sign}(q_{ij}^v(t))$, for each $(i,j) \in \gamma_k$ and $v \in \{s,r\}$, which is a fixed parameter being the water flow direction in pipes assumed to be constant. Hence, to impose that the net pressure drop is null for each closed path, the following equations can be introduced for each kth mesh, with $k \in \{1,\dots,m\}$,

$$\sum_{\forall (i,j)\in\gamma_k} \zeta_{ij}^v \left(a_{ij}^s (q_{ij}^v(t))^2 + b_{ij}^v \right) = 0 \tag{21}$$

with $v \in \{s,r\}$, where a_{ij}^v, b_{ij}^v are defined as

$$a_{ij}^v = \begin{cases} \rho c_f \frac{L_{ij}^v}{r_{ij}^v} \frac{1}{(\rho \pi r_{ij}^{v\,2})^2} & \text{if } (i,j) \vee (j,i) \in \mathcal{E}_P, \\ \frac{k_{1,ij}^v \max(\zeta_{ij}^v,0) + k_{2,ij}^v \min(\zeta_{ij}^v,0)}{2\rho} & \text{if } (i,j) \vee (j,i) \in \mathcal{E}_F, \end{cases} \tag{22}$$

$$b_{ij}^v = \begin{cases} g y_{ij}^v & \text{if } (i,j) \vee (j,i) \in \mathcal{E}_P, \\ 0 & \text{if } (i,j) \vee (j,i) \in \mathcal{E}_F, \end{cases} \tag{23}$$

for each $(i,j) \in \gamma_k$. As evident, (21) exploits (4) and (5) to impose an overall null pressure drop at each kth mesh, without using pressure variables and with a lower number of equations (two equations for each mesh, one for the supply and one for the return network, instead of two equations for each edge).

Now, consider the original DHN model (3)-(17) and note that pressure variables p_i^s, p_i^r and the load valve opening θ_i^l appear solely in (4), (5), (8), (10). If these variables and equations are excluded from the NMPC control-oriented model, whereas (20) and (21) are added, the number of removed equations from the original DHN model is $n_{re} = 2|\mathcal{E}| + 2 + |\mathcal{L}| - 2m$, whereas the net number of removed variables is $n_{rv} = 2|\mathcal{N}| + |\mathcal{L}|$. To ensure that the remaining DHN model is still properly formulated, the number of removed equations and variables must match. This is proved to be true due to Euler's formula in graph theory [51], stating that the number of bounded graph faces is always

$$m = |\mathcal{E}| - |\mathcal{N}| + 1 \,, \tag{24}$$

which, in turns, implies that $n_{re} = n_{rv}$. Note that in case a radial DHN graph is considered, i.e., $m = 0$, equations (21) are not introduced, and the variables p_i^s, p_i^r, and θ_i^l and equations (4), (5), (8), (10) can be removed from the overall model by simply adding (20).

4) Distribution pipes temperature model reduction: Distribution pipe modeling involves separate models for the water and pipe wall temperature dynamics (3). Nevertheless, at the NMPC level, a reasonable modeling reduction is adopted, describing the overall energy exchange in each finite-volume section of distribution pipes.

First of all, consider the pipe wall temperature model (3b) which can be rewritten as

$$\dot{\mathbf{T}}_{ij}^{vm}(t) = \frac{2\pi l_{ij}^v U_{ij}^m}{c_m \rho_m v_{ij}^{vm}} \Bigg(r_{ij}^v \left(\mathbf{T}_{ij}^v(t) - \mathbf{T}_{ij}^{vm}(t) \right) - \frac{U_{ij}^e}{U_{ij}^m} r_{ij}^{vm} \left(\mathbf{T}_{ij}^{vm}(t) - \mathbb{1} T_{ij}^{v,e}(t) \right) \Bigg), \tag{25}$$

for $v \in \{s,r\}$. Considering that pipes are usually insulated and that the heat transfer coefficient between water and the pipe wall is typically high, it follows that $\frac{U_{ij}^e}{U_{ij}^m} \ll 1$ (for the case study in Section IV, $\frac{U_{ij}^e}{U_{ij}^m} \simeq 10^{-5}\ \forall\ (i,j) \in \mathcal{E}$). Hence, the pipe wall temperature model can be approximated as

$$\dot{\mathbf{T}}_{ij}^{vm}(t) = \frac{2\pi r_{ij}^v l_{ij}^v U_{ij}^m}{c_m \rho_m v_{ij}^{vm}} \left(\mathbf{T}_{ij}^v(t) - \mathbf{T}_{ij}^{vm}(t) \right), \tag{26}$$

for $v \in \{s,r\}$. Now, note that the pipe wall thermal dynamic time constant $\tau_{ij}^{vm} = (c_m \rho_m v_{ij}^{vm})/(2\pi r_{ij}^v l_{ij}^v U_{ij}^m)$ is usually relatively small compared to the DHN thermal dynamics (for the case-study in Section IV, $\tau_{ij}^{vm} \simeq 10$s). Therefore, as the usual NMPC sampling time is $\tau_s \gg \tau_{ij}^{vm}$, we can assume that the pipe wall and the water are always at thermal equilibrium, i.e., $\mathbf{T}_{ij}^v(t) = \mathbf{T}_{ij}^{vm}(t)$, at least at the NMPC level. For notational simplicity, the variable $\mathbf{T}_{ij}^v(t)$ will describe the overall temperature of the corresponding distribution pipe, with $v \in \{s,r\}$.

Thus, in the NMPC problem formulation, we substitute the distribution pipe temperature model (3) with the following

$$\begin{aligned} (c\rho v_{ij}^v + c_m \rho_m v_{ij}^{vm}) \dot{\mathbf{T}}_{ij}^v(t) = & c\, q_{ij}^v(t) \left(\Phi \mathbf{T}_{ij}^v(t) + \boldsymbol{\delta} T_i^v(t) \right) \\ & - 2\pi r_{ij}^{vm} l_{ij}^v U_e \left(\mathbf{T}_{ij}^v(t) - \mathbb{1} T_{ij}^{v,e}(t) \right), \end{aligned} \tag{27}$$

for $v \in \{s,r\}$, where the left-hand side describes the stored thermal energy in each pipe section, comprising the pipe wall and water; whereas the right-hand side includes the energy exchanged due to transport phenomena and the heat losses towards the ambient. Note that (27) can be directly obtained by summing (3a) and (3b), assuming the water and pipe wall temperature at equilibrium as described.

It is worth noting that the proposed simplification allows to remove the following number of variables and equations

$$n_r = \sum_{\forall (i,j)\in\mathcal{E}_P} (n_{ij}^s + n_{ij}^r), \tag{28}$$

from the original DHN model (3)-(17), significantly contributing to the reduction of the NMPC problem complexity.

Remark 3.1: The number of sections in pipes and thermal storages is also a tunable parameter, as they can be reduced in the NMPC model based on the desired computational complexity and modeling accuracy.

In conclusion, the reduced DHN control-oriented model for the NMPC design is constituted by (6), (7), (9), (14)-(27). Collecting the states variables in the vector x, the input variables in the vector u, the exogenous signals in d, i.e.,

$$x = [\, (\mathbf{T}_{ij}^{s\,\prime}, \mathbf{T}_{ij}^{r\,\prime})_{ij\in\mathcal{E}_\mathcal{P}}, \mathbf{T}_{i\in\mathcal{Z}}^{z\,\prime} \,]', \tag{29a}$$

$$u = [\, T_{i\in\mathcal{G}_T}^g,\ P_{i\in\mathcal{G}_P}^g,\ q_{i\in\mathcal{G}\setminus h}^g,\ (q_i^{z,s}, q_i^{z,r})_{i\in\mathcal{Z}} \,]', \tag{29b}$$

$$d = [\, (P_i^l, T_i^{l,0})_{i\in\mathcal{L}},\ T_{i\in\mathcal{Z}}^{z,e},\ T_{ij\in\mathcal{E}}^{s,e},\ T_{ij\in\mathcal{E}}^{r,e} \,]', \tag{29c}$$

and the remaining auxiliary variables of the model in the vector w, i.e.,

$$\begin{aligned} w = [\, & (T_i^s, T_i^r)_{i\in\mathcal{N}},\ (q_i^l, T_i^l)_{i\in\mathcal{L}},\ (q_{ij}^s, q_{ij}^r)_{ij\in\mathcal{E}}, \\ & T_{i\in\mathcal{G}_P}^g,\ P_{i\in\mathcal{G}_T}^g,\ q_h^g \,]'. \end{aligned} \tag{29d}$$

It follows that (19) and (27) can be rewritten compactly

$$\dot{x}(t) = f(x(t), u(t), d(t), w(t)) \,, \tag{29e}$$

whereas (6), (7), (9), (14)-(18), (20)-(21) as

$$g(x(t), u(t), d(t), w(t)) = 0 \,, \tag{29f}$$

where $f(\cdot)$ and $g(\cdot)$ are suitable defined nonlinear functions.

B. NMPC optimization problem

The DHN control-oriented model (29) formulation uses discrete time with a sampling time τ_s for the design of the NMPC regulator. We introduce the discrete time index $k_s \in \mathbb{N}$ that defines the time instant $t = \tau_s k_s$ when the NMPC is executed. Therefore, denoting with $k \in \{k_s, \ldots, k_s + N_s - 1\}$ the generic time index along the prediction horizon, with N_s indicating the number of prediction steps, the DHN control-oriented model (29) is formulated in discrete-time as

$$x(k+1) = \tilde{f}(x(k), u(k), d(k), w(k)) \,, \tag{30a}$$

$$g(x(k), u(k), d(k), w(k)) = 0 \,. \tag{30b}$$

In (30a), $\tilde{f}(\cdot)$ derives from $f(\cdot)$ applying a suitable integration method. The control variables are constrained within their physical limits as

$$\underline{u} \leq u(k) \leq \bar{u} \,, \tag{31}$$

whereas state and auxiliary variables are bounded using soft constraints, i.e.,

$$\underline{x} - \sigma_x(k) \leq x(k) \leq \bar{x} + \sigma_x(k) \,, \tag{32}$$

$$\underline{w} - \sigma_w(k) \leq w(k) \leq \bar{w} + \sigma_w(k) \,, \tag{33}$$

where σ_x and σ_w are slack variables such that

$$\sigma_x(k) \geq 0, \quad \sigma_w(k) \geq 0 \,. \tag{34}$$

At this stage, an additional auxiliary variable is introduced, defined as a function of the state variables, i.e., $e = \xi(x(k_s)) \in \mathbb{R}_{\geq 0}$. This variable expresses the total thermal energy stored in the DHN plant when the NMPC is executed and is defined as

$$\begin{aligned} e(k_s) = \xi(x(k_s)) = & \sum_{(i,j)\in\mathcal{E}_P} (c\rho v_{ij}^s + c_m \rho_m v_{ij}^{sm}) \, \mathbb{1}' \, \mathbf{T}_{ij}^s(k_s) \\ & + \sum_{(i,j)\in\mathcal{E}_P} (c\rho v_{ij}^r + c_m \rho_m v_{ij}^{rm}) \, \mathbb{1}' \, \mathbf{T}_{ij}^r(k_s) \\ & + \sum_{i\in\mathcal{Z}} c \, \rho \, v_i^z \, \mathbb{1}' \, \mathbf{T}_i^z(k_s) \,, \end{aligned} \tag{35}$$

where the total thermal energy contained in each water pipe and storage is included. Considering that the NMPC regulator is executed with a prediction horizon of N_s steps, the stored thermal energy of the following constraint is stated

$$e^0 - \sigma_e \leq e(k_s + N_s) \leq e^0 + \sigma_e \,, \tag{36}$$

with e^0 is a nominal thermal energy reference, and σ_e a slack variable such that

$$\sigma_e \geq 0 \,. \tag{37}$$

The idea of (36) is to act as a terminal constraint, imposed as soft for the sake of feasibility so that the NMPC manages the DHN at minimum cost without fully discharging the thermal energy in storages and pipes [52]. The nominal energy reference can be computed using the nominal state values x^0, e.g., $e^0 = \xi(x^0)$. Hence, denoting the vector of slack variables as $\sigma = [\sigma_x', \sigma_w', \sigma_e]'$, the designed NMPC cost function is

$$\begin{aligned} J(k) = & \sum_{i\in\mathcal{G}} \left(c_i^g(k) \frac{P_i^g(k)}{\eta_i^g} + \eta_i^q c_i^q(k) q_i^g(k) \right) \\ & + \sum_{i\in\mathcal{Z}} \eta_i^z c_i^z(k) \big(q_i^{z,s}(k) + q_i^{z,r}(k) \big) + c_\sigma' \sigma(k) \,. \end{aligned} \tag{38}$$

In (38), the main goal is to minimize production costs in generators, considering the efficiency from primary to thermal energy η_i^g and the primary energy cost c_i^g (e.g., in the case of a heat pump, η_i^g would be the pump's coefficient of performance and c_i^g the electrical energy price). The electric consumption of generation pumps is also minimized, modeling it as proportional to the water flow q_i^g through a constant efficiency η_i^q [8]. The same idea applies to thermal storage pumps, recalling that $q_i^{z,s}$ and $q_i^{z,r}$ are not simultaneously different from zero. Finally, slack variables are penalized in (38) through the vector cost c_σ, commonly selected as much higher than the other costs to ensure constraints satisfaction.

Thus, the NMPC problem, solved at each $t = \tau_s k_s$, is

$$\min_{u(\cdot),\, \sigma(\cdot)} \quad \sum_{k=k_s}^{k_s+N_s-1} J(k) \tag{39a}$$

subject to

$$(30) - (37), \; \forall k \in \{k_s, \ldots, k_s + N_s - 1\}, \tag{39b}$$

$$x(k_s) = \tilde{x}_0 \,, \tag{39c}$$

where $\tilde{x}_0$ corresponds to the current system state.

Remark 3.2: It is worth noting that, by adding suitable constraints and cost terms, more advanced energy management strategies can be included in (39), e.g., considering the energy trading with the electrical grid or minimizing the CO_2 emissions in case fossil and renewable primary sources are exploited to generate thermal power [8], [23].

1) State estimation: It is paramount to consider the availability of state variables, given (39c), as not all of them could be measurable in a typical DHN plant. An example of non-measurable state variables is the temperatures of internal sections of pipes, where sensors are typically not placed. Thus, the use of state observers may be necessary. In this context, one effective solution is to employ an Extended Kalman Filter as this is capable of estimating the overall state x by exploiting the knowledge of the input u in (29b), of the DHN model (29), and of an output vector $y = [\,(T_i^s\,, T_i^r)_{\forall i\in\mathcal{N}}\,]$, which can be assumed measurable, since each node $i \in \mathcal{N}$ is a significant DHN component (e.g., a generator, a load, or a thermal storage). The formulation of the implemented Extended Kalman Filter is not reported as this is standard, and the reader can refer to [53] for further details.

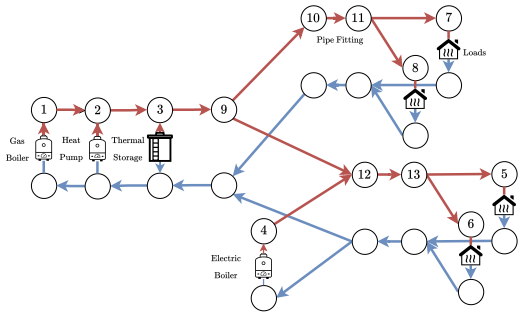


Fig. 6. Schematic of the DHN Thermal Test Facility located at Ricerca sul Sistema Energetico - RSE S.p.A.

IV. Case studies

In this section, we first describe the Thermal Test Facility. It is a district heating network currently under construction at the research center Ricerca sul Sistema Energetico - RSE S.p.A., Milan. Thanks to the Thermal Test Facility, the simulation model, presented in Section II, as well as the control-oriented model, introduced in Section III, can benefit from real-world data to guarantee meaningful outputs. Secondly, the dynamic simulation library and the control-oriented model are validated using experimental data and other simulation libraries. After successful validation, the two models are implemented to test and derive the NMPC regulator, presented in Section III, considering 24h of DHN operations. All test scenarios run on a laptop with processor Intel(R) Core(TM) i7-6700HQ CPU @ 2.60GHz, RAM 16.0 GB.

A. Case study 1: The Thermal Test Facility

The Thermal Test Facility of RSE, when finished, will be an experimental benchmark emulating a real DHN plant and its joint operation with other forms of energy, i.e., hydrogen, natural gas, and electricity. The DHN system, reported in Figure 6, consists of 13 nodes and 2 parallel branches. The main parameters of the Thermal Test Facility are reported in Table II. Being a multi-producer DHN, it comprises 3 thermal generators, i.e., a gas boiler (node 1), a heat pump (node 2), and an electric boiler (node 4). Moreover, the DHN case study features a thermal energy storage unit (node 3) and four thermal loads (nodes 5, 6, 7, 8). Pipes connecting loads to the DHN main pipeline are thinner, implying that pipe fittings are introduced in the edges $(10, 11)$ and $(12, 13)$. The gas boiler at node 1 is temperature-controlled, and it operates as a slack generation node (i.e., $h = 1$), imposing a pressure reference $p_1^{r,0} = 2.5$ bar at the return network and a pressure increase at the supply network equal to $\Delta p_1^0 = 2.5$ bar through the local pump, as discussed in Section II-B2. On the other hand, the heat pump at node 2 and the electric boiler at node 4 are power-controlled and equipped with local pumps regulated to deliver a fixed water flowrate of 0.5 and 0.8 [kg/s] for the electric boiler and the heat-pump respectively.

TABLE II
Main parameters of the Thermal Test Facility at Ricerca sul Sistema Energetico - RSE S.p.A.

Pipes $(i,j) \in \mathcal{E}_P$	L_{ij}^v [m]	r_{ij}^v [cm]	r_{ij}^{vm} [cm]
$(1,2)$	4.5	2.54	2.94
$(2,3)$	1	2.54	2.94
$(3,9)$	17.5	2.54	2.94
$(4,12)$	35	2.54	2.94
$(9,10)$	2.25	2.54	2.94
$(9,12)$	1.51	2.54	2.94
$(11,7)$	8	1.27	2.94
$(11,8)$	15	1.27	2.94
$(13,5)$	13	1.27	2.94
$(13,6)$	10.75	1.27	2.94
Generators $i \in \mathcal{G}$	$(\underline{P}_i^g, \bar{P}_i^g)$ [kW]	$(\underline{T}_i^g, \bar{T}_i^g)$ [°C]	η_i^g [-]
1	$(0, 120)$	$(75, 85)$	0.84
2	$(0, 11)$	$(65, 90)$	5
4	$(0, 50)$	$(65, 90)$	0.92
TES $i \in \mathcal{Z}$	H_i^z [m]	A_i^z [m^2]	(α, κ) [W/K·m^2]
3	5	2.27	$(6.89, 1.62e^{-4})$

In the same way, the thermal energy storage pump is flow-controlled and has a maximum water mass flow of 0.5 kg/s, whereas the TES total volume of 11.35 m^3.

Finally, loads satisfy their thermal demand by absorbing a water flow from the DHN supply network. The flow absorption is regulated to track a return temperature of $T_i^{l,0} = 65$°C through a PI controller. This control acts on an electric valve with a maximum opening area of 67 cm^2. Finally, the supply temperature must be higher than 75°C to ensure the proper functioning of the load heat exchangers.

1) Model validation: The simulation and the control-oriented models, respectively introduced in Section II and III, are hereafter validated before, being exploited for testing the designed control strategy.

a) Simulator model validation: The *DHN4Control* library, exploiting the DHN simulation model, is validated against an existing library, i.e., *ThermoPower* [14]. ThermoPower is a suitable choice as it includes one-dimensional finite-volume pipes with metal wall inertia models similar to those proposed in this paper. We compare the two libraries using real-world experimental data of a 39 m water pipe [54]. The simulated pipes use $n = 25$ sections. The validation test compares the water temperature at the pipe outlets given the same initial conditions, as shown in Figure 7 having on y axis the temperature and on the x axis the time. In particular, the *DHN4Control* library seems accurate, as it matches the experimental data and ThermoPower's output. We employ the root mean square error (RMSE) as the performance index and observe that ThermoPower achieves an RMSE of 0.74, whereas the DHN4Control reaches 0.82. On the other hand, the main difference between the two simulation libraries is computational time. Considering the discussed test,

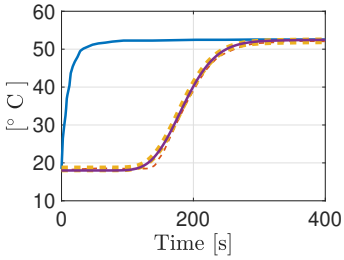


Fig. 7. Validation of the pipe model in [54]. Temperature of the water fed to the pipe (solid blue line). Water temperatures measured at the end of the pipe: (i) experimental (dashed red line), (ii) ThermoPower simulation (solid purple line), (iii) DHN4Control simulation (yellow dotted line).

ThermoPower simulation required 3.47 s; in comparison, the *DHN4Control* library required only 0.03 s. In fact, given the different involved pipe models, the simulator implemented with *DHN4Control* has 179 variables and equations, whereas the ThermoPower simulator has up to 1255 variables and equations. The difference is because the *ThermoPower* model is considerably more complex compared to the one described in Section II, as it accounts for other physical phenomena that are not of interest for DHNs and, especially, for their control testing, e.g., fluid phase-changing or compressibility. Note that the described results are satisfactory even though the experimental data used to validate the models are in the temperature range 18-55 °C, which is outside the one considered in the *DHN4Control* library, where the values of ρ, c reported in Assumption 2.1 are computed.

b) Control-oriented model validation: The control-oriented model derived in Section III is validated against the *DHN4Control* library. Specifically, a 24-hour scenario is considered for both the simulation (3)-(17) and the control-oriented (30) models, the latter using a sampling time of $\tau_s = 1800$ s. The control-oriented model considers two sections for each pipe, whereas, in the simulation model, the pipes' section number vary between 2 to 10 depending on the pipe's length. Regarding the TES, given its reduced dimension, 2 sections are used both for the simulation and the control-oriented model. The control-oriented model has 50 optimization variables for each time step; whereas, the simulation model has 471 variables. To evaluate models performance, the DHN simulation and the control-oriented models are fed with the same known inputs, which are reported in Figure 8. These are: the gas boiler temperature reference (Figure 8(a)), the loads thermal demand (Figure 8(b)), the electric boiler power reference (Figure 8(c)), and the TES mass flow (Figure 8(d)). Figure 9 shows the obtained results for the DHN simulation and the control-oriented model. As shown in Figure 9(a), the thermal energy storage layers' temperature transients almost coincide with the simulated ones. The same holds for the supply temperature at the furthest thermal load, which profile is almost equivalent for the simulation and control-oriented model, as shown in Figure 9(b). To conclude, although pressure variables do not appear in the control-oriented model, the DHN water flow almost coincides for the simulated and control-oriented model,

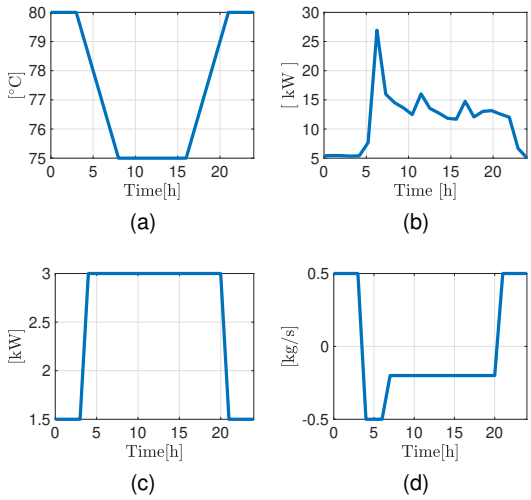


Fig. 8. Inputs and disturbances used for the simulation and control-oriented model comparison: (a) Gas boiler output temperature. (b) Thermal demand of each load. (c) Electric boiler power input. (d) Thermal storage water flow.

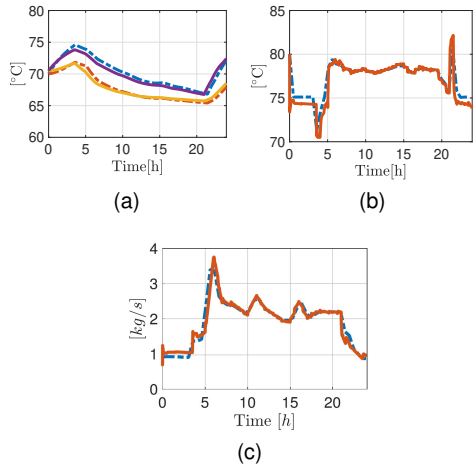


Fig. 9. DHN simulation (solid lines) and control-oriented model (dashed lines) comparison: (a) TES temperatures at layer 2, i.e., the top layer, (solid purple and dashed blue) and at layer 1, i.e., the bottom one, (solid yellow and dashed orange); (b) Load 3 supply temperature; (c) Water flow at the slack generator.

as reported in Figure 9(c).

2) Optimal control results: In this section, we present the NMPC design. The NMPC optimization problem uses the environment CasADi in MATLAB for the implementation of the optimization problem [55] and Ipopt as solver [56]. The NMPC is designed with a prediction horizon of $12h$ and a sample time of $\tau_s = 1800s$ for a total of $N_s = 12/\tau_s = 24$ steps. Since the MPC requires state measurements, an Ex-

tended Kalman Filter is implemented as described in Section III-B1. To test the designed NMPC regulator, it runs for 24 hours, employing the thermal demand profile depicted in Figure 8(a) for each thermal load. Moreover, time-varying costs for the primary energy sources are considered, i.e., for gas and electricity, and these are depicted in Figure 10(a).

Figures 10(b)-(h) report the results of the NMPC regulation applied to a 24 hours scenario. Hereafter, we analyze the results. Given the high cost of gas compared to electricity, the NMPC never uses the gas boiler (node 1) at its maximum power, i.e., $\bar{P}_1 = 120$ kW, as depicted in Figure 10(b). Instead, the heat pump (node 2) runs at max capacity due to its high efficiency, except at night when thermal loads require less power, see Figure 10(c). Additionally, the electric boiler (node 4) turns on only when convenient, e.g., its power generation significantly decreases when the electricity cost reaches peak prices, i.e., at 8:00 and 20:00, as shown in Figure 10(d).

Furthermore, the NMPC exploits the thermal storage to reduce operational costs. As the heat pump is the most convenient component of the network and is saturated almost all day, the TES is precharged during the night, also considering that the electrical price is lower. Then, when thermal load demand peaks (i.e., around 6:00, as depicted in Figure 8(d)), the TES delivers hot water to the supply network. Another shorter cycle of charge/discharge happens in the afternoon, 14:00 - 21:00. Please refer to Figure 10(e) to visualize the temperatures of the TES sections, and to Figure 10(f) for the TES water flow.

Altogether, the joint effects of the generators and TES can be appreciated from 14:00 to 18:00. In this time frame, the electricity energy cost and the thermal demand are lower. Therefore, the TES absorbs hot water from the supply, thus charging. However, the heat pump can divert little energy into the storage, as it already runs at max power output. Therefore, the NMPC, to redirect more energy from the heat pump to the storage, turns the electric boiler on to supply loads 5 and 6, being the closest generator.

Moreover, because of the inclusion of DHN thermal dynamics, the NMPC can pre-charge pipes with hot water when convenient or before load peaks, a strategy known as packing and depicted in Figure 10(g) and (h). The pipe packing starts at 5:00, while the peak of consumption happens at around 6:00. Another effect of including DHN thermal dynamics in the NMPC formulation is the ability to operate the system at the lower supply temperature when the energy costs are higher without violating the constraints on the minimum supply temperature for loads, i.e. 75°C, as illustrated in Figure 10(g)-(h).

The NMPC performances are compared with a rule-based control strategy, similar to the ones applied in real DHNs [8]. The rule-based strategy is simple: *(i)* the gas boiler reference temperature is constant during the day, and between 22:00 and 5:00, it turns off, given lower thermal demand; *(ii)* the electric boiler runs at a fixed power production all day, while the heat pump runs at max power during the day and less during the night, between 22:00 to 5:00; *(iii)* the TES is operated with the same profile of the NMPC optimal management.

For a $24h$ simulation, the obtained results are shown in Table III where it is evident that the management cost of the rule-based strategy is higher than the NMPC one, achieving a net saving of roughly 15%. The total thermal energy produced by the NMPC is also lower because of the optimizer's ability to operate the DHN more efficiently, satisfying network constraints with lower temperatures. Finally, it is worth noting that despite a prediction horizon of 12 hours and considered a nonlinear model, the average NMPC computational time is 5s, mainly due to the control-oriented modeling approach presented in Section III. To better assess the computational performances achieved by the control-oriented model, a NMPC regulator including the DHN simulation model, i.e., the one described in Section II, has been also developed for the RSE Test Facility, maintaining the same cost function, prediction horizon and constraints. It resulted that the computational time becomes on average 1000s, which is much higher with respect to the one achieved with the control-oriented model, witnessing the benefits of the proposed approach. It is worth noting that the computational time of a controller introduces a delay in the control loop, which, if large, can significantly affect control performances and stability.

TABLE III
TOTAL VALUES OF THERMAL POWER GENERATION AND COSTS FOR THE RULE-BASED SIMULATION AGAINST THE NMPC CONTROL.

Control	Generated energy	Operating cost
Test Facility Rule Based	1959.5 kWh	898.3 $
Test Facility NMPC	1690.6 kWh (-14%)	763.2 $ (-15%)
AROMA Rule Based	4494.7 kWh	2100.6 $
AROMA NMPC	4183.7 kWh (-7%)	1897.4 $ (-10%)

B. Case study 2: AROMA Network

The proposed methods are tested in a second case-study, i.e., the AROMA district heating network [9]. The AROMA DHN is a meshed network comprising more than 7 km of pipelines (roughly 20 times larger than the RSE Test Facility), a total of 24 nodes (considering also pipe fitting nodes), a temperature-controlled generator, and five thermal loads. The AROMA network simulation model, defined according to Section II, involves 882 variables for each time step. After the implementation of the model reduction steps described in Section III-A, the control-oriented model consists of just 86 variables per time step. The NMPC regulator is designed considering a sampling time of 30 minutes and a prediction horizon of 48 steps, i.e., $24h$. Also in this case study, the supply temperature of loads is constrained to exceed a lower bound of 75°C. Moreover, the energy prices and the thermal load profiles are reported in Figure 11(a) and (b), respectively. The obtained control results are reported in Figure 11(c) and (d). In particular, during low-price time periods (22:00-6:00, 12:00-16:00), the NMPC increases the temperature in the supply pipelines, acting on the thermal generator. On the opposite, during price peaks the generator temperature is reduced, as evident from Figure 11(c), and the stored thermal energy in pipelines is exploited to satisfy the thermal demand. Moreover, the supply temperature at loads is always maintained higher than $75°C$, as required by operational constraints. Given the computational-efficiency of the control-oriented model, the

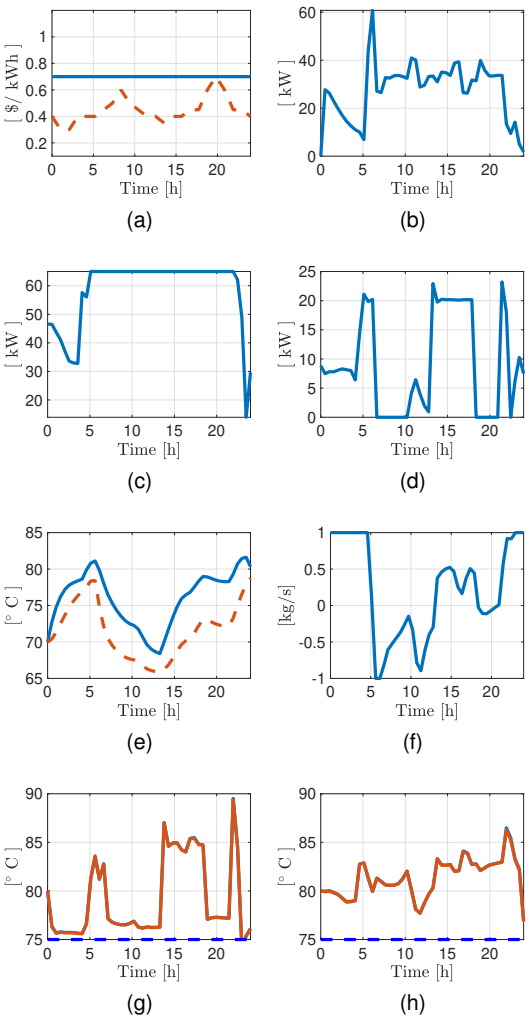


Fig. 10. Case study results: (a) Energy costs: gas (solid line) and electricity (dashed line). (b) Gas boiler power. (c) Heat pump power. (d) Electric boiler power. (e) TES Layers' temperature (solid line - hot layer, dashed line - cold layer). (f) TES Mass flow. (g) Load supply temperature at nodes 7, 8. (h) Load supply temperature at nodes 5, 6.

designed NMPC regulator requires on average 30 seconds to compute its optimal control action. Finally, the performances of the designed NMPC regulator is compared against a rule base-strategy, operating the thermal generator at a constant supply temperature, as done in Section IV-A. The results are reported in Table III, showing that the achieved cost savings are approximately 10%. Note that, differently from the RSE Test Facility described in Section IV-A, here a thermal storage is not available, meaning that just the network thermal inertia is exploited to decrease the costs.

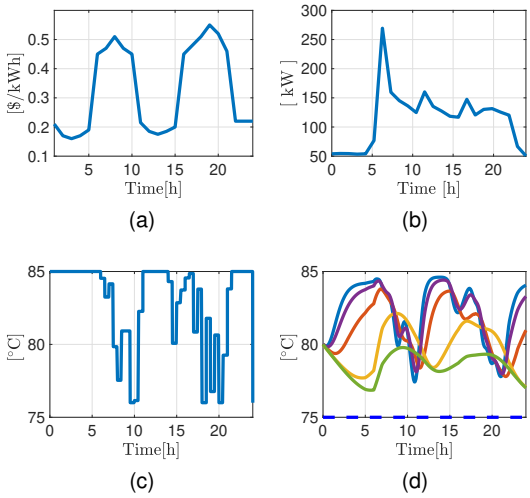


Fig. 11. NMPC results for case-study 2: (a) Electrical Energy prices. (b) Thermal load profile. (c) Generator supply temperature. (d) loads' supply temperatures (dashed line indicating lower bound).

V. Conclusion

In this article, we presented the development of a simulation and a control-oriented district heating network (DHN) model, together with the design of a nonlinear predictive control (NMPC) regulator able to achieve significant energy savings with respect to a rule based strategy. The simulation model performed accurately and efficiently because of carefully chosen assumptions; its implementation led to the development of the *DHN4Control* library, freely available online [1]. Additionally, we proposed a control-oriented optimization model, particularly efficient due to a model reduction procedure. Finally, these two models were validated against experimental and virtual data, showing high accuracy performances despite their reduced complexity. Moreover, the designed NMPC regulator achieves a significant cost reduction (up to 18%) with respect to a benchmark rule-based control strategy, with reduced computational times. The reduction is possible thanks to the control-oriented model capable of leveraging the DHN thermal inertia, i.e., in storages and pipes, minimizing costs, energy production, and satisfying operative constraints over the whole network.

The proposed methodology can be also exploited for thermo-hydraulic applications other than DHN systems, e.g., for cooling systems for industrial processes or for building heating systems. In fact, also in these case, a reduced control-oriented model can be crucial for the design of cost-effective and computationally-efficient NMPC regulators maximizing energy efficiency.

Future work will consider introducing new components for the DHN, which would lead to the investigation of innovative energy management control strategies. Moreover, more structured DHN frameworks can be taken into account, considering the presence of independent energy hubs and prosumers

optimally regulating their thermal power exchange with the DHN system. In this context, future research directions may focus on the design of distributed NMPC architectures, each one regulating a sub-network or an aggregation of thermal prosumers, so as to optimize their internal operation and thermal power exchanges over the DHN. Finally, a further future development will consist in the implementation of the proposed control solution to the real Thermal Test Facility in RSE - Ricerca sul Sistema Energetico S.p.A., as it will be soon available for testing, so as to experimentally assess the achievable performances.

ACKNOWLEDGMENTS

The research activity of Lorenzo Nigro has been financed by the Research Fund for the Italian Electrical System under the Contract Agreement between RSE S.p.A. and the Ministry of Economic Development - General Directorate for the Electricity Market, Renewable Energy and Energy Efficiency, Nuclear Energy in compliance with the Decree of April 16th, 2018. The work of Riccardo Scattolini is carried out within the MICS (Made in Italy – Circular and Sustainable) Extended Partnership and received funding from Next-Generation EU (Italian PNRR – M4 C2, Invest 1.3 – D.D. 1551.11-10-2022, PE00000004). CUP MICS D43C22003120001.

REFERENCES

[1] L. Nigro, *DHN4Control: a Modelica Library for hydro-thermal simulations of district heating systems, Available: https://github.com/Lollo-sk/DHN4Control*. GitHub, 2023.

[2] T. Goodson, "Heating," *IEA*, 2022. [Online]. Available: https://www.iea.org/reports/heating

[3] E. Commission, "Communication from the commission to the european parliament, the council, the european economic and social committee and the committee of the regions — an eu strategy on heating and cooling." *EUR-Lex*, 2016. [Online]. Available: https://eurlex.europa.eu/legal-content/EN/TXT/?uri=CELEX%3A52016DC0051

[4] B. Rezaie and M. A. Rosen, "District heating and cooling: Review of technology and potential enhancements," *Applied energy*, vol. 93, pp. 2–10, 2012.

[5] S. Paardekooper, R. S. Lund, B. V. Mathiesen, M. Chang, U. R. Petersen, L. Grundahl, A. David, J. Dahlbæk, I. A. Kapetanakis, H. Lund *et al.*, "Heat roadmap europe 4: quantifying the impact of low-carbon heating and cooling roadmaps," 2018. [Online]. Available: https://vbn.aau.dk/en/publications/heat-roadmap-europe-4-quantifying-the-impact-of-low-carbon-heatin

[6] S. Werner, "Network configurations for implemented low-temperature district heating," *Energy*, vol. 254, p. 124091, 2022.

[7] S. Buffa, M. H. Fouladfar, G. Franchini, I. Lozano Gabarre, and M. Andrés Chicote, "Advanced control and fault detection strategies for district heating and cooling systems—a review," *Applied Sciences*, vol. 11, no. 1, p. 455, 2021.

[8] A. La Bella and A. Del Corno, "Optimal management and data-based predictive control of district heating systems: The novate milanese experimental case-study," *Control Engineering Practice*, vol. 132, p. 105429, 2023.

[9] R. Krug, V. Mehrmann, and M. Schmidt, "Nonlinear optimization of district heating networks," *Optimization and Engineering*, vol. 22, no. 2, pp. 783–819, 2021.

[10] S.-A. Hauschild, N. Marheineke, V. Mehrmann, J. Mohring, A. M. Badlyan, M. Rein, and M. Schmidt, "Port-hamiltonian modeling of district heating networks," in *Progress in differential-algebraic equations II*. Springer, 2020, pp. 333–355.

[11] J. E. Machado, M. Cucuzzella, and J. M. Scherpen, "Modeling and passivity properties of multi-producer district heating systems," *Automatica*, vol. 142, p. 110397, 2022.

[12] F. Strehle, J. E. Machado, M. Cucuzzella, A. J. Malan, J. M. Scherpen, and S. Hohmann, "Port-hamiltonian modeling of hydraulics in 4th generation district heating networks," in *2022 IEEE 61st Conference on Decision and Control (CDC)*. IEEE, 2022, pp. 1182–1189.

[13] K. Sartor, D. Thomas, and P. Dewallef, "A comparative study for simulating heat transport in large district heating network," in *Ecos2015: 28th International Conference on Efficiency, Cost, Optimization, Simulation and Environmental Impact of Energy Systems*, 2015.

[14] F. Casella and A. Leva, "Modelling of thermo-hydraulic power generation processes using modelica," *Mathematical and Computer Modelling of Dynamical Systems*, vol. 12, no. 1, pp. 19–33, 2006.

[15] "ThermoPower Library," https://github.com/casella/ThermoPower.

[16] A. Dahash, S. Mieck, F. Ochs, and H. J. Krautz, "A comparative study of two simulation tools for the technical feasibility in terms of modeling district heating systems: An optimization case study," *Simulation Modelling Practice and Theory*, vol. 91, pp. 48–68, 2019.

[17] Y. Li, Y. Rezgui, and H. Zhu, "Dynamic simulation of heat losses in a district heating system: A case study in wales," in *2016 IEEE Smart Energy Grid Engineering (SEGE)*. IEEE, 2016, pp. 273–277.

[18] M. Rose, H. Gernandt, J. E. Machado, and J. Schiffer, "Model predictive control of district heating grids using stabilizing terminal ingredients," *arXiv preprint arXiv:2404.01820*, 2024.

[19] X. Zheng, Z. Shi, Y. Wang, H. Zhang, and H. Liu, "Thermo-hydraulic condition optimization of large-scale complex district heating network: a case study of tianjin," *Energy*, vol. 266, p. 126406, 2023.

[20] M. Taylor, S. Long, O. Marjanovic, and A. Parisio, "Model predictive control of smart districts with fifth generation heating and cooling networks," *IEEE Transactions on Energy Conversion*, vol. 36, no. 4, pp. 2659–2669, 2021.

[21] S. S. Farahani, Z. Lukszo, T. Keviczky, B. De Schutter, and R. M. Murray, "Robust model predictive control for an uncertain smart thermal grid," in *2016 European Control Conference (ECC)*. IEEE, 2016, pp. 1195–1200.

[22] S. Long, O. Marjanovic, and A. Parisio, "Generalised control-oriented modelling framework for multi-energy systems," *Applied Energy*, vol. 235, pp. 320–331, 2019.

[23] F. Verrilli, A. Parisio, and L. Glielmo, "Stochastic model predictive control for optimal energy management of district heating power plants," in *2016 IEEE 55th Conference on Decision and Control (CDC)*. IEEE, 2016, pp. 807–812.

[24] G. Sandou, S. Font, S. Tebbani, A. Hiret, C. Mondon, S. Tebbani, A. Hiret, and C. Mondon, "Predictive control of a complex district heating network," in *IEEE conference on decision and control*, vol. 44, no. 8. Citeseer, 2005, p. 7372.

[25] D. Quaggiotto, J. Vivian, and A. Zarrella, "Management of a district heating network using model predictive control with and without thermal storage," *Optimization and Engineering*, vol. 22, no. 3, pp. 1897–1919, 2021.

[26] M. Wirtz, L. Neumaier, P. Remmen, and D. Müller, "Temperature control in 5th generation district heating and cooling networks: An milp-based operation optimization," *Applied Energy*, vol. 288, p. 116608, 2021.

[27] L. Frison, M. Kollmar, A. Oliva, A. Bürger, and M. Diehl, "Model predictive control of bidirectional heat transfer in prosumer-based solar district heating networks," *Applied Energy*, vol. 358, p. 122617, 2024.

[28] A. La Bella, A. Del Corno, and A. Scaburri, "Data-driven modelling and optimal management of district heating networks," in *2021 AEIT International Annual Conference (AEIT)*. IEEE, 2021, pp. 1–6.

[29] S. Buffa, A. Soppelsa, M. Pipiciello, G. Henze, and R. Fedrizzi, "Fifth-generation district heating and cooling substations: Demand response with artificial neural network-based model predictive control," *Energies*, vol. 13, no. 17, p. 4339, 2020.

[30] M. Jiang, M. Speetjens, C. Rindt, and D. Smeulders, "A data-based reduced-order model for dynamic simulation and control of district-heating networks," *Applied Energy*, vol. 340, p. 121038, 2023.

[31] E. Terzi, T. Bonetti, D. Saccani, M. Farina, L. Fagiano, and R. Scattolini, "Learning-based predictive control of the cooling system of a large business centre," *Control Engineering Practice*, vol. 97, p. 104348, 2020.

[32] L. Wang, J. Zhao, Z. Xu, F. Zhao, C. Song, C. Yang, and Z. Shao, "Integrated energy system optimal operation using data-driven district heating network model," *Energy and Buildings*, vol. 291, p. 113100, 2023.

[33] C. M. Jensen, M. C. Frederiksen, C. S. Kallesøe, J. N. Jensen, L. H. Andersen, and R. Izadi-Zamanabadi, "Havok model predictive control for time-delay systems with applications to district heating," *IFAC-PapersOnLine*, vol. 56, no. 2, pp. 2238–2243, 2023.

[34] L. Boca de Giuli, A. La Bella, and R. Scattolini, "Physics-informed neural network modeling and predictive control of district heating systems," *IEEE Transactions on Control Systems Technology*, 2024.

[35] J. Barco-Burgos, J. Bruno, U. Eicker, A. Saldaña-Robles, and V. Alcántar-Camarena, "Review on the integration of high-temperature heat pumps in district heating and cooling networks," *Energy*, vol. 239, p. 122378, 2022.

[36] A. Benonysson, B. Bøhm, and H. F. Ravn, "Operational optimization in a district heating system," *Energy conversion and management*, vol. 36, no. 5, pp. 297–314, 1995.

[37] Y. Wang, S. You, H. Zhang, W. Zheng, X. Zheng, and Q. Miao, "Hydraulic performance optimization of meshed district heating network with multiple heat sources," *Energy*, vol. 126, pp. 603–621, 2017.

[38] M. Stewart, *Surface Production Operations: Volume VI: Fluid flow and pressure drop*. Gulf Professional Publishing, 2015.

[39] P. J. Thomas, *Simulation of industrial processes for control engineers*. Elsevier, 1999.

[40] M. Stewart, *Surface Production Operations: Volume III: Facility Piping and Pipeline Systems*. Gulf Professional Publishing, 2015.

[41] J. E. Machado, J. Ferguson, M. Cucuzzella, and J. M. A. Scherpen, "Decentralized temperature and storage volume control in multiproducer district heating," *IEEE Control Systems Letters*, vol. 7, pp. 413–418, 2023.

[42] L. Saarinen, "Modelling and control of a district heating system," 2008.

[43] T. Nussbaumer, S. Thalmann, A. Jenni, and J. Ködel, "Handbook on planning of district heating networks," *Bern: Swiss Federal Office of Energy*, 2020.

[44] G. Chicco, S. Riaz, A. Mazza, and P. Mancarella, "Flexibility from distributed multienergy systems," *Proceedings of the IEEE*, vol. 108, no. 9, pp. 1496–1517, 2020.

[45] H. Bastida, C. E. Ugalde-Loo, M. Abeysekera, M. Qadrdan, J. Wu, and N. Jenkins, "Dynamic modelling and control of thermal energy storage," *Energy Procedia*, vol. 158, pp. 2890–2895, 2019.

[46] S. E. Mattsson, H. Elmqvist, and M. Otter, "Physical system modeling with modelica," *Control engineering practice*, vol. 6, no. 4, pp. 501–510, 1998.

[47] P. Fritzson, A. Pop, K. Abdelhak, A. Asghar, B. Bachmann, W. Braun, D. Bouskela, R. Braun, L. Buffoni, F. Casella *et al.*, "The openmodelica integrated environment for modeling, simulation, and model-based development," *Modeling, Identification and Control*, vol. 41, no. 4, pp. 241–295, 2020.

[48] A. Bemporad and M. Morari, "Control of systems integrating logic, dynamics, and constraints," *Automatica*, vol. 35, no. 3, pp. 407–427, 1999.

[49] A. La Bella, A. Falsone, D. Ioli, M. Prandini, and R. Scattolini, "A mixed-integer distributed approach to prosumers aggregation for providing balancing services," *International Journal of Electrical Power & Energy Systems*, vol. 133, p. 107228, 2021.

[50] C. De Persis and C. S. Kallesoe, "Pressure regulation in nonlinear hydraulic networks by positive and quantized controls," *IEEE Transactions on Control Systems Technology*, vol. 19, no. 6, pp. 1371–1383, 2011.

[51] D. B. West *et al.*, *Introduction to graph theory*. Prentice hall Upper Saddle River, 2001, vol. 2.

[52] A. La Bella, L. Nigro, and R. Scattolini, "Predictive control and benefit sharing in multi-energy systems," *IEEE Transactions on Control Systems Technology*, 2023.

[53] B. D. Anderson and J. B. Moore, *Optimal filtering*. Courier Corporation, 2012.

[54] K. Sartor and P. Dewalef, "Experimental validation of heat transport modelling in district heating networks," *Energy*, vol. 137, pp. 961–968, 2017.

[55] J. A. Andersson, J. Gillis, G. Horn, J. B. Rawlings, and M. Diehl, "Casadi: a software framework for nonlinear optimization and optimal control," *Mathematical Programming Computation*, vol. 11, pp. 1–36, 2019.

[56] A. Wächter and L. T. Biegler, "On the implementation of an interior-point filter line-search algorithm for large-scale nonlinear programming," *Mathematical programming*, vol. 106, pp. 25–57, 2006.



Lorenzo Nigro received the M.Sc. in Automation and Control Engineering from Politecnico di Milano, Italy, in 2022. In 2021, he was visiting student at RWTH Aachen University in Aachen, Germany. In 2022, he worked as Research Assistant at Politecnico di Milano, collaborating with the research center Ricerca Sul Sistema Energetico - RSE SpA. In 2023, he was assigned the best M.Sc. thesis award in sustainability by the IEEE Italy Section. Currently, he is working towards the Ph.D. Degree in Information Technology at Politecnico di Milano. His research focuses on the areas of model predictive control, optimization, and the modelling of energy systems, with a particular interest in multi-energy systems and district heating networks.



Alessio La Bella received the B.Sc. and M.Sc. in Automation Engineering cum laude from Politecnico di Milano in 2013 and 2015, respectively. In 2016, he received the Alta Scuola Politecnica Diploma, together with the M.Sc. in Mechatronics Engineering cum laude at Politecnico di Torino. He received the Ph.D. Degree cum laude in Information Technology at Politecnico di Milano in 2020. In 2018, he was visiting researcher at the Automatic Control Lab of the École Polytechnique Fédérale de Lausanne, Switzerland. From 2020 to 2022, he worked as Research Engineer at Ricerca sul Sistema Energetico - RSE SpA, designing and implementing advanced predictive control systems for district heating networks and large-scale battery plants, in collaboration with industrial companies and energy utilities. In 2022, he joined Politecnico di Milano as Assistant Professor at Dipartimento di Elettronica, Informazione e Bioingegneria. He is Associate Editor of the International Journal of Adaptive Control and Signal Processing and of EUCA Conference Editorial Board. His research interests concern the theory and design of predictive, multi-agent and learning-based control systems, with particular emphasis on practical challenges arising from the upcoming energy transition. He was recipient of the Dimitris N. Chorafas Prize in 2020.



Francesco Casella got his master's degree cum laude in Electronic Engineering and his PhD in Information and Control Science from Politecnico di Milano, where he is currently associate professor of Control Systems and Advanced Process Control. His main research interests are modelling and control of energy systems and equation-based, object-oriented modelling of engineering systems at large. In recent years he has worked in publicly and privately funded research projects involving innovative thermal generation power plants and gas transportation networks. He has published over 150 journal and conference papers, mostly on these topics. He is the Director of the Open Source Modelica Consortium, which develops the OpenModelica modelling and simulation software, and a member of the Board of the Modelica Association.



Riccardo Scattolini is Full Professor of Automatic Control at Politecnico di Milano, Italy. He was awarded Heaviside Premium of the Institution of Electrical Engineers, United Kingdom, and was Associate Editor of the IFAC journal Automatica. His main research interests include modelling, identification, simulation, diagnosis, and control of industrial plants and energy systems, with emphasis on theory and applications of Model Predictive Control and fault detection methods to large-scale and networked systems.

I - 3

Experimental Validation of Simulators for District Heating Network

This Chapter addresses the experimental validation of the simulation model introduced previously, Chapter 2. The validation aims to assess the model's capability to reproduce transient and steady-state thermal behavior under varied disturbance conditions, ensuring its suitability for simulation design.

- **Conference Article**: Alvarado, M. A. M., Anderis, C., Lazzari, R., *Nigro, L.*, & La Bella, A. (2024, September). Development and Experimental Validation of an Open-Source Model Library for District Heating Network Simulation. In 2024 Open Source Modelling and Simulation of Energy Systems (OSMSES) (pp. 1-6). IEEE [1].

3.1 Simulation of District Heating Network

Library and Experimental Setup

The authors' work [49] led to the development of a simulation model that was extended in subsequent research [1]. To evaluate the proposed model, an experimental validation was performed. Experimental validation is essential for ensuring the accuracy and reliability of DHN models when simulating dynamic behavior. Although several modeling libraries exist, a persistent limitation has been the lack of open-source experimental data under varying operating conditions. To address this issue, Ricerca sul Sistema Energetico s.p.a. designed and implemented a scaled-down District Heating thermal facility (TF) to provide experimental data specifically for DHNs modeling and validation. The network is described in the Introduction 1

Validation Results

The validation process compared simulated results with real measurements obtained from plant sensors monitoring pressure, temperature, and mass flow rates. Quantitative assessment followed the ASHRAE Guideline 14 metrics: the Coefficient of Variation of the Root

Mean Square Error (CVRMSE) and the Normalized Mean Bias Error (NMBE). Models are acceptable if CVRMSE < 30% and NMBE < 10%.

The results reported in the attached work [1] include validation of individual components (e.g., a heat exchanger), subsystems (e.g., a pump and its control valve), and the complete plant simulation, as summarized in Table 3.1.

In the complete plant simulation case, the simulated outlet temperatures exhibited response times closely aligned with the measured data, despite minor deviations. Quantitative validation of this configuration yielded acceptable CVRMSE values from 13.11% to 17.36% and NMBE values ranging from −6.682% to −7.605% across multiple system points.

System	Measured value	CVRMSE	NMBE
Full plant	ΔT_{S900}	13.11%	−7.482%
Full plant	ΔT_{S100}	16.55%	−7.605%
Full plant	ΔT_{S400}	17.36%	−6.682%

Table 3.1: Results of the experimental validation. For the variable definition, please refere to the corresponding work [1]

Overall, the developed Modelica library accurately predicts temperatures, pressures, and mass flow rates across the DHN. This validated simulation tool provides a reliable framework for assessing various operational and control strategies in future DHN applications.

2024 Open Source Modelling and Simulation of Energy Systems (OSMSES) | 979-8-3503-8468-0/24/$31.00 ©2024 IEEE | DOI: 10.1109/OSMSES62085.2024.10668994

Development and Experimental Validation of an Open-Source Model Library for District Heating Network Simulation

Marcelo Andre Muro Alvarado
Materials and Generation Technologies
Ricerca sul Sistema Energetico - RSE
Milan, Italy
marceloandre.muroalvarado@rse-web.it

Claudio Anderis
Materials and Generation Technologies
Ricerca sul Sistema Energetico - RSE
Milan, Italy
claudio.anderis@rse-web.it

Riccardo Lazzari
Materials and Generation Technologies
Ricerca sul Sistema Energetico - RSE
Milan, Italy
riccardo.lazzari@rse-web.it

Lorenzo Nigro
Electronics, Information & Bioengineering
Politecnico di Milano
Milan, Italy
lorenzo.nigro@polimi.it

Alessio La Bella
Electronics, Information & Bioengineering
Politecnico di Milano
Milan, Italy
alessio.labella@polimi.it

***Abstract*—Decarbonization of the energy system requires the widespread use of renewable energy sources, introducing challenges to the stability and reliability of electricity networks. Multi-energy systems (MES) have emerged as a promising approach, integrating various energy vectors and optimizing their interaction through conversion technologies and innovative operating strategies to enhance flexibility. Despite growing interest, the impact of integrating energy systems such as District Heating Networks (DHNs) into modern energy systems is still an open research topic. Modeling and simulation tools play a crucial role in comprehensively studying the complexity of these systems, facilitating the development of effective operational solutions. This paper presents the development of an open-source, object-oriented Modelica library for the study of DHNs, validated using experimental data obtained from a real District Heating Test Facility (DHTF). The construction methodology and modeling equations for the library's main components are outlined, alongside an overview of the DHTF. Three representative validation cases, including a single component, a single subsystem and a centralized configuration of the plant are discussed. This study aims to contribute to the advancement of district heating systems by providing a validated simulation tool for exploring different configurations and operational scenarios.**

***Index Terms*—District Heating Network, Open-Source Library, Experimental Validation, Test Facility, Multi-Energy System, Modeling and Simulation, Modelica.**

I. Introduction

Europe has committed to reducing greenhouse gas emissions by up to 55% by 2030 compared to 1990 levels through initiatives like the European Green Deal [1]. With the energy sector responsible for 75% of these emissions, integrating renewable energy sources (RES) into energy production becomes imperative [2]. However, the intermittent and unpredictable nature of RES such as solar and wind power poses challenges to the stability and reliability of electrical grids.

Multi-energy systems (MES) are emerging as a promising solution by integrating different energy carriers to enhance flexibility. In this context, District Heating Networks (DHNs) have proven their potential to improve energy efficiency and leverage local RES [3]. However, optimizing DHNs requires advanced operating and control strategies tailored to these systems, and, implementing these novel strategies into existing DHNs poses challenges, particularly due to demanding user requirements, complex system dynamics, and the scarcity of daily operating condition data [4].

Addressing these challenges requires the development of simulators that accurately reflect the reality of DHNs. In recent years, the use of Modelica [5] for simulating district energy systems has notably increased, leading to the development of several modeling libraries tailored for this purpose, each with different levels of complexity [6].

One of the earliest libraries, the *ThermoPower* library [7], focuses on dynamic modeling of traditional thermal power plants, incorporating components such as gas boilers, water pumps, and heat exchangers. Subsequently, the *DistrictHeating* library [8] emerged, specializing in accurate and robust simulation of District Heating and Cooling (DHC) systems. Its validation of pipe models using experimental data is noteworthy, as showcased in [9]. The *Buildings* library [10] and the *Modelica Standard* Library (MSL) [11] have also played crucial roles, particularly in supporting the design and operation of building energy systems and control systems. The most recent addition to this landscape is the *AixLib* open-source Modelica library [12], which allows the simulation of large district heating systems and building energy systems.

Despite the availability of these modeling libraries, a significant challenge remains: the lack of open-source experimental data for studying DHNs under diverse operating conditions.

Authorized licensed use limited to: Politecnico di Milano. Downloaded on August 17,2025 at 07:10:26 UTC from IEEE Xplore. Restrictions apply.

In response to this gap, RSE has designed and implemented a scaled-down District Heating Test Facility (DHTF). This facility enables the collection of valuable experimental data for modeling and validating DHNs. Utilizing this data, this paper aims to develop a tailored simulation library for DHNs, providing an additional reliable and specific tool for researchers.

This study introduces the development of an open-source, object-oriented Modelica library, that has been experimentally validated, aimed at studying traditional and modern DHNs. It's important to note that while this library is designed with the intricacies of RSE's DHTF in mind, its modular structure and flexible design could enable its application to a broader range of scenarios.

The paper is structured as follows: Section II outlines the methodology employed in developing the library. In Section III, the authors present a concise overview of the mathematical equations used in the main components of the library. Section IV provides three representative validation cases developed for the library. Finally, Section V provides conclusions from this study and potential future work of the research team.

II. Library Development Approach

Before starting the construction of the library, an analysis of the characteristics of the different components in the DHTF is carried out. Each main component and subsystem underwent analysis during real operation through a series of tests. These tests served two purposes: firstly, to characterize the components under different operating conditions far from the nominal one, and secondly, to evaluate the feasibility of adding ideal low-level controllers into their models, considering the possible presence of internal controllers in some machines. This analysis contributed to simplifying and representing the components more realistically.

Afterward, the library was constructed including all the necessary models for building such systems. The library was developed in Modelica [5], a programming language that allows the creation of reusable and interpretable code, since the basic models are described implicitly through elementary differential-algebraic equations. This feature greatly simplifies the modeling process as the model development of each component is described through conventional physical laws [5]. In this way, the code is reusable and interpretable, since the basic models are described implicitly through elementary differential-algebraic equations.

Later, a validation phase was conducted, starting with the most basic components, and progressing toward a full configuration of the DHTF. The validation process involved utilizing data from the sensors of the plant to ensure that the simulated behavior closely matched real-world observations. Key parameters such as pressure, temperature, and mass flow rates were considered based on the variables measured by existing sensors. Additionally, two metrics were employed for evaluation, aligning with ASHRAE Guideline 14 [13], which are the Coefficient of Variation of the Root Mean Square Error (CVRMSE) and Normalized Mean Bias Error (NMBE).

III. System Model

This section briefly describes the fundamental equations for modeling the main components of the library.

A. General characteristics

For water modeling, which operates within the temperature range of 5°C to 95°C, a constant density assumption was applied, while the specific heat was considered to be temperature-dependent. Equation (1) provides an expression for specific heat derived from data provided by the *Media* package [11].

$$c_p(T) = -7.961e^{-5}T^3 + 0.0903T^2 - 33.187T + 8156.66 \quad (1)$$

where T is the temperature in Kelvin and c_p is the specific heat at constant pressure.

One important limitation is that at this stage of the research, only turbulent flow test conditions have been analyzed and validated. The research group intends to expand the models' validation to include flows approaching laminar conditions, aiming for a more accurate representation, particularly in scenarios such as hydraulic start-up conditions. However, it is important to mention that this condition is not yet incorporated into the library's models.

B. Water pipe

The pipeline is arguably the main component when it comes to the dynamical modeling of DHNs, that's why there are several studies dedicated to finding the most effective way to do so [14]–[16]. For the first validation tests, one pipe model is considered which is the traditional 1D finite volume model. In the 1D finite volume method, the continuous 1D domain is discretized into N control volumes and accounts for mass and energy balances. The mass and energy balance for a single control volume i-th is described in (2) and (3) respectively, while the momentum balance, which could be lumped at the middle or end of the pipe, is described in (4).

$$w_i = w_{i+1} = w \quad (2)$$

$$M_i c_{p,i+1} \frac{d\tilde{T}_i}{dt} = w(h_i - h_{i+1}(\tilde{T}_i)) + Q_{w,i} \quad (3)$$

$$p_{in} - p_{out} = \rho g z + \frac{c_f \omega L}{2\rho A^3} |w| w \quad (4)$$

where i represents the control volume number, w is mass flow rate, M is the mass, c_p is the specific heat capacity, $\tilde{T}$ is the state temperature variable, Q_w is the heat exchanged through the wall pipe, p_{in} and p_{out} are the inlet and outlet pressures of the pipe, ρ is the density, g is gravity, z is the height of the pipe with respect to reference height at the inlet, c_f is the Fanning friction factor, ω is the wet perimeter, L is the pipe length and A is the sectional area.

Authorized licensed use limited to: Politecnico di Milano. Downloaded on August 17,2025 at 07:10:26 UTC from IEEE Xplore. Restrictions apply.

C. Heat exchangers

A counter-current heat exchanger model has been developed by connecting two 1D finite volume conduct models for incompressible fluid with a metal wall component in between, which considers the thermal energy accumulation in the metal wall and is divided with the same number of volumes of the 1D conducts. The heat transfer coefficient U of each 1D conduct is calculated using its nominal value U_{nom}, the actual and nominal mass flow rates w and w_{nom}, and a flow-dependence coefficient α, as described in (5), while the energy balance of the wall volume i is described according to (6), where C_w is the wall heat capacity, T_w is the wall temperature and Q_{int} and Q_{ext} are the heat flow rates at internal side and external side respectively. These last two are computed by multiplying the corresponding equivalent thermal conductance UA by the difference between the wall's temperature T_w and internal or external fluid's temperature T_{int} or T_{ext}. This approach was inspired by a heat exchanger model referenced in [7].

$$U = U_{nom}\left(\frac{w}{w_{nom}}\right)^{\alpha} \tag{5}$$

$$C_{w,i}\frac{dT_{w,i}}{dt} = Q_{int,i} + Q_{ext,i} \tag{6}$$

$$Q_{int,i} = (T_{int,i} - T_{w,i})UA_{int,i} \tag{7}$$

$$Q_{ext,i} = (T_{ext,i} - T_{w,i})UA_{ext,i} \tag{8}$$

D. Thermal generators

Four types of thermal generators are present in the library: gas boiler, electric boiler, combined heat and power (CHP), and heat pumps. Generic models have been considered, utilizing technical information provided by DHTF's suppliers. Basic balance equations describing fluid temperature change (9) and pressure difference (Stevin Law) are employed for modeling.

$$Mc_p\frac{d\tilde{T}}{dt} = w_{in}h_{in} - w_{out}h_{out}(\tilde{T}) + P_h - Q_{amb} \tag{9}$$

An important remark is that these components include an internal ideal outlet temperature control, with the set-point of this variable serving as an input in their respective models. By doing this, the required Heat Power P_h in (9) is calculated by this ideal controller as a manipulated variable.

E. Water pump

Water pumps are modeled based on non-dimensional performance laws, with specific parameters computed from pump curves provided by the supplier. Equations (10) and (11) describe the head and power of the pump respectively, while (12) and (13) describe quadratic functions g_1 and g_2 which depend on the angular velocity and volumetric flow rate [17].

$$H = \left(\frac{\omega}{\omega_n}\right)^2 g_1\left(Q\frac{\omega_n}{\omega}\right) \tag{10}$$

$$W = \left(\frac{\omega}{\omega_n}\right)^3 g_2\left(Q\frac{\omega_n}{\omega}\right) \tag{11}$$

$$g_1 = a_1 + a_2\left(Q\frac{\omega_n}{\omega}\right) + a_3\left(Q\frac{\omega_n}{\omega}\right)^2 \tag{12}$$

$$g_2 = b_1 + b_2\left(Q\frac{\omega_n}{\omega}\right) + b_3\left(Q\frac{\omega_n}{\omega}\right)^2 \tag{13}$$

where H is the head, W is the shaft power, ω and ω_n are the angular velocity and nominal angular velocity of the pump, Q is the volumetric flow rate in m^3/h and a_i and b_i are coefficients dependent on the pump curves.

While most of the described models have undergone experimental validation, some components such as thermal energy storage, CHP system, and heat pumps are currently being assessed. However, their mathematical models have already been incorporated into the library.

IV. District Heating Test Facility Overview

RSE has designed a Distributed Energy Resources Test Facility (DERTF) [18] which enables the interaction between different energy vectors—electric, thermal, and gas networks—allowing the study of MES, as illustrated in Fig. 1. Currently, the electric grid and district heating network are implemented and operational, while the gas network is still in the design phase. This work focuses on the model validation of a DHN library using the DHTF within the DERTF.

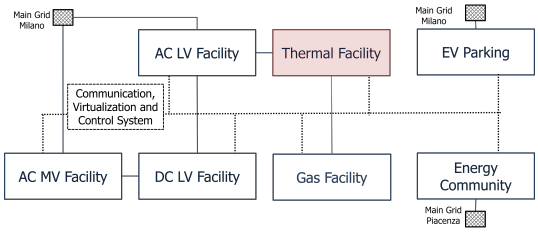


Fig. 1: DERTF Block diagram

RSE's DHTF comprises various types of heat generators connected to a set of loads through a pipeline distribution network. In addition, it features a water-cooling circuit designed to dissipate heat from the loads and/or cool specific components. This DHTF is structured into blocks, each representing a plant subsystem, thanks to their rack and skid structure (see Fig. 2). This modular design allows for operation with specific sets of generators and loads or with all of them simultaneously. Table I provides an overview of the main subsystems present in the facility.

The district heating network has a nominal capacity of approximately 200 kWth, corresponding to the maximum thermal power of the loads. Heat generation can be managed by modulating the different generators according to the operational conditions required by the plant, to integrate

Authorized licensed use limited to: Politecnico di Milano. Downloaded on August 17,2025 at 07:10:26 UTC from IEEE Xplore. Restrictions apply.

TABLE I: Subsystems of the District Heating Test Facility

Code	*Subsystem*	*Main component*
S100	Gas Boiler	147kW$_{th}$ gas boiler
S200	Thermal energy storage	2 water tanks of 10m^3
S300	High-Temp. Heat Pump	49kW$_{th}$ heat pump
S400	Electric Boiler	50kW$_{th}$ electric boiler
S500	Combined Heat and Power	50kW$_e$, 81kW$_{th}$ cogenerator
S600	Low-Temp. Heat Pump	54kW$_{th}$ heat pump
S700	Users	4x50kW$_{th}$ heat exchangers
S900	Rack C/D and Main Pump	2.2 kW$_e$ water pump
A00	Distribution rack	52 electropneumatic valves
R00	Cooling system	207kW$_{th}$ chiller

energy systems. The total thermal power of the generators is approximately 365 kWth.

The maximum system pressure is 5.5 bar, with an operating pressure range of 2-4 bar. The maximum operating temperature is 95°C, while the nominal temperatures for the supply and return lines, in the setup of traditional DHNs, are 80°C and 60°C respectively.

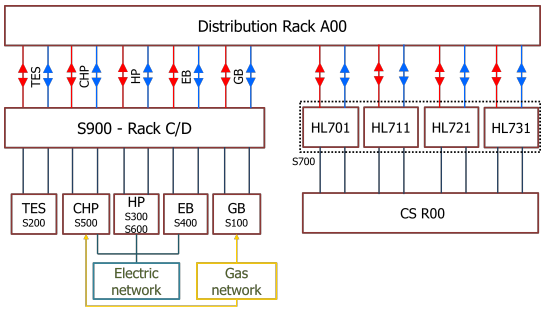


Fig. 2: District Heating Test Facility Block diagram

V. Validation Results

The Modelica library developed for this project is called *MultiEnergySystem* and comprises two main packages. The first one called *DistrictHeatingNetwork* hosts a set of components necessary to model a district heating system. The second important package is called *TestFacility* in which various systems and subsystems representative of the RSE's DHTF are collected. While the library is under constant development, detailed information about its structure will be presented in a future publication. This library has been built using software Dymola, however, most of test cases can be also simulated in OpenModelica. Interested readers can access the developed code for this study on the corresponding GitHub repository [1].

As mention in section II, CVRMSE and NMBE are considered as validation indexes [13]. These metrics are defined in (14) and (15) respectively.

[1]https://github.com/RSE-TGM/multienergysystem

$$CVRMSE(\%) = \frac{\sqrt{\frac{\sum(y_i - \hat{y}_i)^2}{N-1}}}{\bar{y}} * 100\% \quad (14)$$

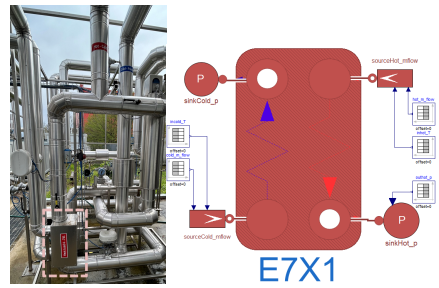
$$NMBE(\%) = \frac{\sum(y_i - \hat{y}_i)}{N\bar{y}} * 100\% \quad (15)$$

where y_i is the individual measured data, $\hat{y}_i$ corresponds to simulation data, $\bar{y}$ is the mean of the measured dataset, and N is the total number of data points. According to [13], acceptable models obtain validation results of CVRMSE $<$ 30% and NMBE $<$ 10%.

For the validation of a component or system, a test model is constructed. This test model includes the component or subsystem to be validated and its boundary conditions, which are defined by data coming from real tests carried out during the operation of the plant. Due to space limitations, all validations are not detailed but some of them are shown in the following sections.

A. Single component - Heat Exchanger

The test model in Fig. 3b has been used for the validation of the single heat exchanger model. The boundary conditions are the inlet temperatures, outlet pressures, and mass flows on both the cold and hot sides; what becomes most interesting in the analysis is the validation of the heat exchanger outlet temperatures.



(a) (b)

Fig. 3: Heat exchanger EX701 (a) Picture of the system. (b) Diagram view of validation model in Modelica

In Fig. 4, the temperature differences between the hot and cold sides of the heat exchanger are depicted. Additionally, Table II presents the corresponding CVRMSE and NMBE values obtained over the 120-minute test period. It is observed that the temperatures on both the hot and cold sides remain within the specified limits.

B. Subsystem - Main circulation pumping system

For the validation of the main pump system, it is important to analyze the hot side, where the circulation pump (P901) is located. In this case, not only the pump but also the flow control valve (FCV901) has been included in the analysis as seen in Fig. 5b. Inlet and outlet pressures and the pump

Authorized licensed use limited to: Politecnico di Milano. Downloaded on August 17,2025 at 07:10:26 UTC from IEEE Xplore. Restrictions apply.

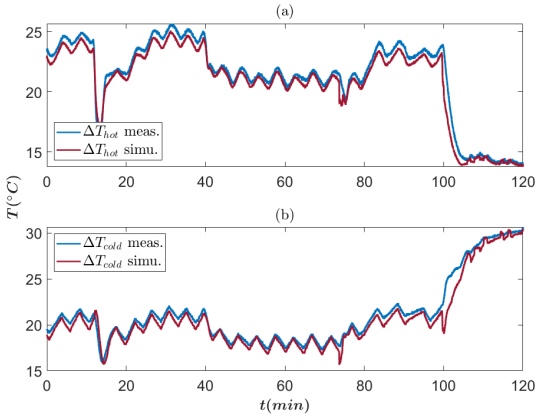
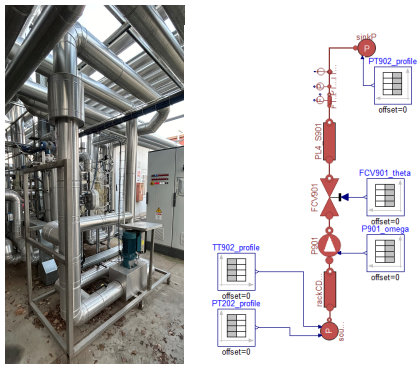


Fig. 4: Measured and simulated temperature differences in heat exchanger. (a) Hot side. (b) Cold side.

frequency have been considered as boundary conditions, while the volumetric flow rate becomes the variable of analysis; the valve remains fully open during the experimentation, and there are no significant heat exchanges, so temperature is neglected during validation.



(a) (b)

Fig. 5: Circulation pumping system (a) Picture of the system. (b) Diagram view of validation model in Modelica.

As depicted in Figure 6, the simulated volumetric flow rate closely mirrors the behavior of the measured data. The CVRMSE is calculated at 1.318%, and NMBE at 0.317% over the 120-minute interval, suggesting that the model demonstrates acceptable accuracy.

C. Configuration 1 - Centralized with parallel users

Up to this point, validation activities have been conducted in an open-loop way, meaning that each component or subsystem was validated independently. In this section, the objective is to validate an initial configuration with at least two energy

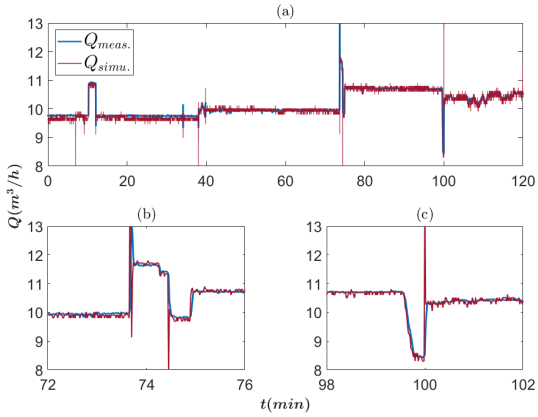


Fig. 6: Measured and simulated volumetric flow rate of the circulation pumping system. (a) Full span. (b) Zoom of the transient between 72 to 76 min. (c) Zoom of the transient between 98 to 102 min.

sources (gas & electric boilers), the main pump, and the cooling system, all connected and operating together.

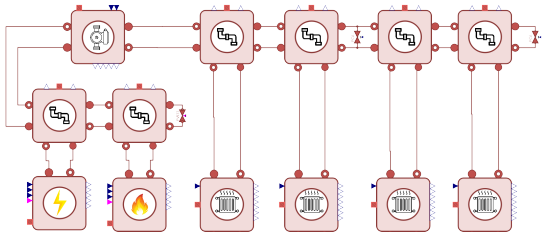


Fig. 7: Modelica diagram of the full centralized plant with gas and electric boilers as heat sources.

In Fig. 7, this configuration in Modelica integrates several key components crucial for the facility's operation. While numerous valves exist within the system $S900$, aimed at creating different possible configurations, only the most pertinent valves necessary to simulate the chosen configuration were considered for modeling this case.

The test starts with the start-up of the boilers which have an outlet set-point temperature of 80°C, while the initial temperatures at the outlet of both subsystems gas and electric boilers are 72.89°C and 69°C respectively. Control valves from systems $S400$ (FCV401) and $S900$ (FCV901) remain with constant opening of 10% and 100% respectively, while control valve opening from system $S100$ (FCV101) changes during the test from 80% to 50%. Pumps frequencies remain constant at 30Hz.

The results of outlet temperatures are illustrated in Fig. 8. Despite minor temperature differences between the simulated and measured results, mainly generated by the ideal internal controller of the thermal generators, the response times of

Authorized licensed use limited to: Politecnico di Milano. Downloaded on August 17,2025 at 07:10:26 UTC from IEEE Xplore. Restrictions apply.

both dynamics are quite similar. Quantitative validation results of the presented case are also shown in Table II, being an acceptable model.

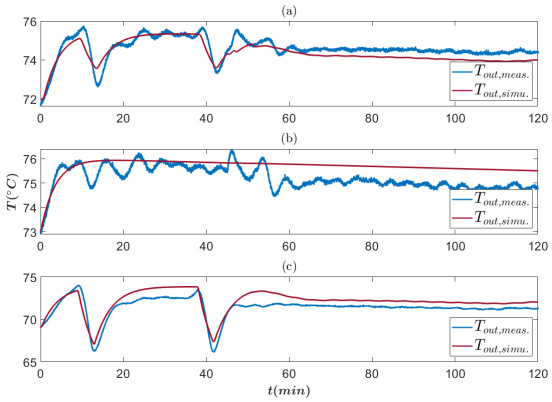


Fig. 8: Measured and simulated outlet temperatures of systems from full centralized plant configuration: (a) S900, (b) S100, (c) S400.

TABLE II: Validation results

Case	*Variable*	*CVRMSE*	*NMBE*
HE	ΔT_{hot}	4.149	3.437
HE	ΔT_{cold}	3.949	3.237
System 900	q	1.318	0.317
Full plant	ΔT_{S900}	13.11	-7.482
Full plant	ΔT_{S100}	16.55	-7.605
Full plant	ΔT_{S400}	17.36	-6.682

VI. Conclusion

This paper has presented the development of a comprehensive Modelica library for the study of novel DHNs using the RSE's DHTF for validation data. The models' accuracy was validated by comparing it with real measured data, encompassing individual components, subsystems, and a centralized system configuration. The models' predictive capabilities extend to forecasting temperatures, pressures, and mass flow rates across the entire system, making them important for evaluating diverse operational and control strategies.

The authors plan to continue with the validation process not only for single components but also for plant models considering distributed and low-temperature configurations. Furthermore, the activity will focus on improving the library by integrating the components necessary to model the interconnection with the electricity grid and the gas network, also considering hydrogen, to create a complete and validated open-source library for the study of MES.

Acknowledgment

This work has been financed by the Research Fund for the Italian Electrical System under the Three-Year Research Plan 2022-2024 between RSE S.p.A. and the Ministry of the Environment and Energy Security (DM MITE n.337, 15.09.2022) - in compliance with the Decree of April 16th, 2018.

References

[1] European Commission, "The European Green Deal," [Online]. Available: https://commission.europa.eu/strategy-and-policy/priorities-2019-2024/european-green-deal_en [Accessed 07-Mar-2024].

[2] European Commission, "State of the Union: Commission raises climate ambition and proposes 55%," [Online]. Available: https://ec.europa.eu/commission/resscorner/detail/en/ip_20_1599. [Accessed 07-Mar-2024].

[3] I. Abbà, A. La Bella, S. P. Corgnati, E. Corsetti, "Assessing flexibility in networked multi-energy systems: A modelling and simulation-based approach", Energy Reports, vol. 11, 2024, pp. 384-393,

[4] A. Vandermeulen, B. van der Heijde, and L. Helsen, "Controlling district heating and cooling networks to unlock flexibility: A review", Energy, vol. 151, pp. 103–115, 2018.

[5] P. Fritzson, and V. Engelson, "Modelica - A Unified Object-Oriented Language for System Modeling and Simulation," Lecture Notes in Computer Science, vol. 1445, 1998.

[6] M. Abugabbara, S. Javed, H. Bagge, and D. Johansson, "Bibliographic analysis of the recent advancements in modeling and co-simulating the fifth-generation district heating and cooling systems," Energy and Buildings, vol. 224, p. 110260, 2020.

[7] F. Casella, A. Leva, "Modelica open library for power plant simulation: design and experimental validation", *3rd International Modelica Conference*, 2003.

[8] L. Giraud, R. Bavière, M. Vallée, and C. Paulus, "Presentation, Validation and Application of the DistrictHeating Modelica Library", 2015.

[9] L. Giraud, R. Bavière, C. Paulus, M. Vallée, and J.-F. Robin, "Dynamic Modelling, Experimental Validation and Simulation of a Virtual District Heating Network", 2015.

[10] M. Wetter, W. Zuo, T. S. Nouidui and X. Pang, "Modelica Buildings library", Journal of Building Performance Simulation, 7(4):253-270, 2014.

[11] Modelica Association, "Modelica Standard Library", [Online]. Available: https://github.com/modelica/ModelicaStandardLibrary. [Accessed: 5-Jan-2024].

[12] L. Maier, D. Jansen, F. Wüllhorst, M. Kremer, A. Kümpel, T. Blacha e D. Müller, "AixLib: an open-source Modelica library for compound building energy systems from component to district level with automated quality management," Journal of Building Performance Simulation, vol. 0, n. 0, 2023, pp. 1-24.

[13] ASHRAE, ASHRAE Guideline 14-2014: Measurement of Energy, Demand, and Water Savings, Tech. rep., Atlanta, 2014.

[14] K. Sartor, D. Thomas, P. Dewallef, "A comparative study for simulating heat transport in large district heating networks," International Journal of Heat and Technology, Vol. 36, No. 1, 2018, pp. 301-308.

[15] T. Oppelt, T. Urbaneck, U. Gross & B. Platzer, "Dynamic thermo-hydraulic model of district cooling networks." *Applied Thermal Engineering*. Vol. 102, pp. 336-345, 2016.

[16] Van der Heijde, B., Fuchs, M., Ribas Tugores, C., Schweiger, G., Sartor, K., Basciotti, D., Müller, D., Nytsch-Geusen, C., Wetter, M. & Helsen, L. "Dynamic equation-based thermo-hydraulic pipe model for district heating and cooling systems." *Energy Conversion And Management*. Vol. 151, 2017, pp. 158-169.

[17] A. J. Steponof, *"Centrifugal and Axial Flow Pumps. Theory, Design and Application"*. 2nd ed., New York: Wiley, 1957.

[18] C. Gandolfi, R. Lazzari, M. Zanoni and D. Palladini, "MISSION Project: Design of MV/LV hybrid AC/DC smart-energy grid," 2022 AEIT International Annual Conference (AEIT), Rome, Italy, 2022, pp. 1-6,

Authorized licensed use limited to: Politecnico di Milano. Downloaded on August 17,2025 at 07:10:26 UTC from IEEE Xplore. Restrictions apply.

I - 4

Experimental Validation of Optimal Regulators and State Estimation for District Heating Network

This Chapter addresses the experimental validation of the control-oriented model introduced previously, Chapter 2. The validation aims to assess the model's capability to optimally manage the network, ensuring model accuracy and cost savings.

- **Conference Article**: *Nigro, L.*, Polimeni, S., Anderis, C., Muro, M., & La Bella, A. (2025). Experimental validation and design of nonlinear predictive control and moving horizon estimation for district heating. IFAC-PapersOnLine, 59(9), 157-162 [51].

4.1 District Heating Network Control

Control-oriented model and Experimental setup

The control-oriented model developed in Chapter 2 is a nonlinear differential algebraic system of equations. The author used this model to design a nonlinear MPC for the RSE test facility network [51]. MPCs are state-feedback controllers; thus, they require the entire system state at each control step, though complete measurement of all states is rarely available. To address this limitation, a Moving Horizon Estimation algorithm was developed and integrated with the nonlinear MPC; both rely on the same modeling framework. The validation assesses the estimator's ability to reconstruct the DHN's state and the regulator's saving potential. The experimental setup is the Test Facility presented above.

Validation results

The validation experiments assessed the performance of the MHE and MPC separately. The moving horizon estimation experiment uses a 900-second sampling time, a 14-step measurement history, and runs for 4 hours. The supply temperature of a load was assumed to be unmeasurable and estimated by the MHE. The estimated states closely matched the measured data, confirming the MHE's ability to reconstruct unmeasured states.

In parallel, the MPC aimed to minimize operational costs while satisfying system constraints under given disturbance and energy price profiles. The minimum user supply temperature enforced was 65°C. Using a simple load profile with a distinct consumption peak, the MPC successfully exploited the network's thermal inertia by preheating the pipelines with the cheaper gas boiler before the demand peak. Economic performance was evaluated across three test cases, comparing the MPC strategy with a benchmark rule-based control where generators operated at constant temperatures. The MPC achieved a 4.27% cost reduction when all three generators (gas boiler, electric boiler, and CHP) are in use.

The work confirmed the proposed control-oriented model's capability to deliver computational efficiency and tangible economic benefits, and offers a readily available solution for optimal control deployment in real DHN applications.

Experimental validation and design of nonlinear predictive control and moving horizon estimation for district heating

Lorenzo Nigro [*], **Simone Polimeni** [**], **Claudio Anderis** [**], **Marcelo Muro** [**], **Alessio La Bella** [*].

[*] *Department of Electronics, Information, and Bioengineering, Politecnico di Milano, Milano, Italy (e-mail: name.surname@polimi.it).*
[**] *Department of Materials and Generation Technologies, Ricerca sul Sistema Energetico SpA, Milano, Italy. (e-mail: name.surname@rse-web.it).*

Abstract: District Heating Networks (DHN) are one of the main infrastructure allowing for the decarbonization of the space heating sector. However, their efficiency is influenced by the control strategy adopted for such networks. This paper presents the design of a model Model Predictive Control (MPC) regulator together with its experimental validation on a real DHN plant. A Moving Horizon Estimation (MHE) algorithm is also designed to estimate, from few output measurements, the full state necessary for the implementation of model-based optimal control strategies. The experimental results show the accuracy of the control-oriented model in predicting the system output, as well as the controller's ability to exploit District Heating Network dynamics to improve performances from the energetic perspective.

Keywords: district heating networks; nonlinear predictive control; moving horizon estimation; smart grids; energy efficiency

1. INTRODUCTION

The space heating sector in the European Union accounts for almost half the total energy consumption, and its demand is met up to 75% by fossil fuels. Decarbonization of space heating is crucial to meet EU 2050 neutrality target European Commission and Directorate-General for Energy et al. (2023). Decarbonization can occur through the use of District Heating Networks, which are one of the main infrastructure that allows the decarbonization of the space heating sector. In fact, DHN enables the efficient integration of large-scale renewable energy sources and the use of various forms of excess heat and cold to achieve decarbonization. District Heating Network can also provide flexibility to powergrids via power to heat converters with either direct electric heating, e.g., electric boilers, or through heat pumps. This flexibility can be use to increase energy efficiency, for example by accommodating renewable electricity production peaks, see European Commission and Directorate-General for Energy et al. (2022); Nigro et al. (2024b).

⋆ The work of Alessio La Bella was carried out within the MICS (Made in Italy - Circular and Sustainable) Extended Partnership and received funding from Next-Generation European Union (EU) (Italian Piano Nazionale di Ripresa e Resilienza (PNRR) - M4 C2, Invest 1.3 - D.D. 1551.11-10-2022, PE00000004). CUP MICS D43C22003120001. The work of C. Anderis, S. Polimeni, M. Muro has been financed by the Research Fund for the Italian Electrical System under the Three Year Research Plan 2025-2027 (MASE, Decree n.388 of November 6th, 2024), in compliance with the Decree of April 12th, 2024

However, District Heating Network energy efficiency is influenced by network control, which is a complex task. The DHN operation involves multiple control actions, nonlinear physical relationships, and the presence of various objectives. Simple rule-based strategies are not efficient in managing such networks and optimal control is beneficial, as discussed in Buffa et al. (2021). Energy networks optimal control can be achieved through the design of state-feedback MPC architectures, see Rathod et al. (2019) and La Bella et al. (2023). Despite its benefits, significant challenges arise when MPC is implemented on DHN. Specifically, to predict the plant future behavior, the MPC requires a system model which is implemented in an optimization problem. For DHN, such model is inherently nonlinear and large-scale and requires a lot of computational effort to be solved. Moreover, the system state knowledge is required at each control iteration, but its full measurement is typically unavailable in practice, and this must be estimated by exploiting few sensors displaced among the DHN.

In the literature, many existing solutions focus on reducing computational complexity by utilizing simplified models. A classic example is the implementation of static thermal power balances without modeling the DHN dynamics, see Taylor et al. (2021) and Farahani et al. (2016). However, these methods do not exploit DHN thermal inertia to increase control performances. Other studies incorporate pipeline dynamical modeling into the model through simplifying assumptions. For example, fixed transport delays and water flow are assumed in Sandou et al. (2005),

whereas solely the dynamics of the return network temperature are modeled in Quaggiotto et al. (2021). Wirtz et al. (2021) neglect thermal losses by assuming a uniform water supply temperature for all loads. On the other hand, detailed models are also proposed, but they end up with computationally intense optimization problems, hardly practical in MPC frameworks. For instance, a complete DHN model is presented in Krug et al. (2021) but the related optimization problem is solved with a prediction horizon of only one step. In the DHN control context, data-driven methods are also proposed, aiming to learn nonlinear dynamics from measurements while maintaining relatively low computational effort, as in Boca de Giuli et al. (2024) and La Bella and Del Corno (2023). The challenge with data-driven models lies in the training dataset, as this must be large and sufficiently exciting system dynamics to achieve high modeling performances.
As previously said, to correctly function, the MPC requires the full state observation of the system, which can be unavailable in practice, e.g., faulty sensors or unmeasurable quantities. The above references rely on exact state knowledge without addressing the issue of measurement availability. Few studies on state estimation for DHN are available in the literature. Some works focus on state estimation based on consumers behavior to assess faults or inefficiencies in the network, e.g., Fang and Lahdelma (2014); Bergsteinsson et al. (2022). Nevertheless, as highlighted in Fang and Lahdelma (2014), the DHN models used for estimation are detailed and may not be scalable for large-scale networks.
A possible solution to address model complexity in control for DHN is discussed in Nigro et al. (2024a), where a control-oriented modeling is proposed. The model features the most influencing physical dynamics in DHN, e.g., transport delays or heat storage, with reduced computational effort, showing high performance from both computational and economic perspectives. However, a state-estimation algorithm is not presented and the results are validated in simulation, which has obvious limitations.

In view of the above discussion, the contributions of this work are:

1. Development of a computationally-efficient MHE algorithm for a District Heating Network (DHN) plant and its integration with a nonlinear MPC regulator exploiting the control-oriented modeling proposed in Nigro et al. (2024a).
2. The experimental assessment of the proposed modeling, control and estimation techniques on real DHN plant located in Milan at Ricerca sul Sistema Energetico SpA (RSE). This is denoted as Thermal Facility (TF) and a picture is available in Figure 1, Anderis et al. (2024).

The experimental results show that the proposed methods are highly effective from the computational and economic perspective, making them easily deployable to real DHN systems.

We present the case study and the model of the system in Section 2. Then, in Section 3, we present the estimation and control strategies, the MHE and the MPC. Finally, we report the results achieved on the real network in Section 4, whereas final conclusions are discussed in Section 5.



Fig. 1. The Thermal Facility

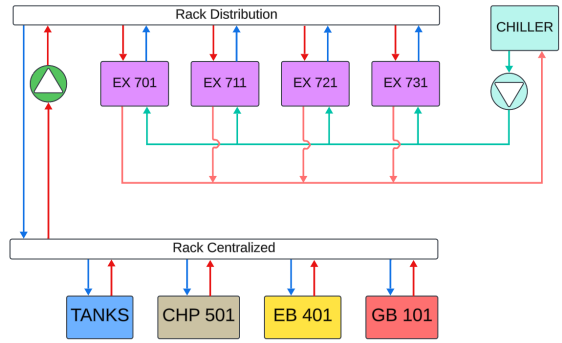


Fig. 2. Topology of the TF

2. SYSTEM MODEL

In this section we describe the physical aspects of the case study, before showing its control oriented model.

2.1 Case study description

The TF is composed of several subsystems, Figure 2. The Gas Boiler (GB) has 147kW$_{th}$ maximum power output and a mass flow driven by a constant speed pump, i.e., a pump whose mass flow will depend on pressure variations. The control variable of the GB is the output supply temperature T_{gb}^{out}. The Electric Boiler (EB) has a maximum power output of 50kW$_{th}$, whereas its mass flow and output temperature T_{eb}^{out} can be controlled. The Combined Heat and Power (CHP) has a maximum of 50kW$_{el}$ electrical power and 81kW$_{th}$ thermal power. The control variables are the mass flow and the output temperature T_{chp}^{out}, Alvarado et al. (2024). The plant also includes a Thermal Energy Storage (TES) composed of two insulated tanks with a total capacity of 20 m^3. In normal operating conditions they are filled at a constant mass, i.e., the mass flow rate input and output are the same. This mass flow is driven by a single pump connected to both TES and is split equally among them. Finally, the subsystems Heat Exchanger (EX) in Fig. 2 are the loads of the network, which are controlled to track prescribed thermal power and return temperature references through local Proportional Integral Differential (PID) controllers, acting on the requested water flow.

These subsystems can operate independently and are connected through the *racks*, i.e., the pipelines. The pipelines

span several hundred meters, feature thick insulation, and are responsible for heat distribution, conveying hot water from the centralized rack to the distribution rack and back. The primary pump, shown in green, generates the water flow and maintains a constant pressure difference at its ports. The heat delivered to the load EX is dissipated through a cooling circuit, specifically the chiller.

2.2 Control oriented model

Below, the control-oriented model of each subsystem is presented by highlighting its main features due to space reasons. In summary, the main assumptions considered to reduce the model consists in:

- fixing water flow direction,
- assuming water incompressibility,
- assuming constant density and specific heat,
- substituting pressure modeling with equivalent algebraic constraints.

These steps enable to obtain a lightway but accurate DHN model prone for control design. More details on the control-oriented modeling approach are presented in Nigro et al. (2024a).

Pipes: The pipelines are collection of pipes and connect the different subsystems. Their physical model employs a one dimensional finite volume discretization. The thermal model of each volume is

$$c_s m_i \dot{T}_i(t) = c_s q(t)(T_{i-1}(t) - T_i(t)) - U(T_i(t) - T^{ext}), \quad (1)$$

where c_s is water specific heat, m_i is the volume water mass, q is the mass flow rate through the pipe, T_i is the i-th volume temperature, T^{ext} is the external temperature, and U is the heat transfer coefficient.

Thermal Energy Storage: The Thermal Energy Storage consists of insulated water tanks where water at different temperature stratifies according to density, creating a temperature gradient along the vertical axis. This axis is discretized using finite volumes and the temperature dynamic at each of them is

$$\begin{aligned} c_s m_i \dot{T}_i(t) = {} & c_s q^s(t)(T_{i-1}(t) - T_i(t)) \\ & - c_s q^r(t)(T_{i+1}(t) - T_i(t)) \\ & + k(T_{i+1}(t) + 2T_i(t) - T_{i-1}(t)) \\ & + U(T_i(t) - T^{ext}). \end{aligned} \quad (2)$$

where q^s is the mass flow from the supply to the return, q_i^r is the mass flow from the return to the supply, k is the thermal conductivity between adjacent layers. The mass flows q_i^s and q_i^r are control inputs that must satisfy their operational limit and they cannot both be different than zero at the same time instant, i.e.,

$$\underline{q}_i^s \le q_i^s(t) \le \bar{q}_i^s \quad (3a)$$

$$\underline{q}_i^r \le q_i^r(t) \le \bar{q}_i^r \quad (3b)$$

$$q_i^s(t) \cdot q_i^r(t) = 0\,. \quad (3c)$$

Generators: A static equation models the heat generators as their transients are negligible with respect to the DHN ones. Consider generation unit $i \in \mathcal{G}$ where $\mathcal{G}$ is the generators set. Then,

$$P_i(t) = \eta_i c_s q_i(t)(T_i^{out}(t) - T_i^{in}(t)) \quad (4)$$

$\forall i \in \mathcal{G}$ subject to power saturation given by machine datasheet

$$\underline{P}_i \le P_i(t) \le \bar{P}_i \quad (5)$$

where T_i^{in}, T_i^{out} are the input and output temperatures, and P_i is the power consumed by the generator.

Loads: It is possible to set the power absorbed and return temperature of consumers. These are also modeled as static as follows

$$P_i(t) = \eta_i c_s q_i(t)(T_i^{in}(t) - \bar{T}_i^{out}(t)) \quad (6)$$

where $i \in \mathcal{L}$ and $\mathcal{L}$ is the load set, $\bar{T}_i^{out}$ is the consumer return temperature, controlled to a known value. Commonly, the network operator and the consumer agrees on a minimum supply temperature

$$T_i^{in}(t) \ge \underline{T}_i^{in} \quad (7)$$

to be maintained over time. In our case study, this value is 65°C.

Overall, the control oriented model of the Thermal Facility is (1) - (7). For the sake of simplicity, omit the time dependency and assume all state, input and disturbance variables rearranged in corresponding x, u, d vectors, respectively. The dynamical equations can be written as

$$\dot{x} = f(x, u, d) \quad (8)$$

where $f(\cdot)$ is a suitable vector function. The algebraic equations, e.g., the power balances, are given by

$$g(x, u, d) = 0, \quad (9)$$

where $g(\cdot)$ is a suitable vector function. Finally, the variables physical constraints are

$$\underline{x} \le x \le \overline{x}, \quad (10a)$$

$$\underline{u} \le u \le \overline{u}. \quad (10b)$$

Note that the input vector u collects the generators output temperatures and the TES mass flow. The disturbances d are the load power consumption. The state variables x includes the temperatures of the finite volumes of each pipe and of the layers of the TES. These values are not easily measurable in practice as they would require numerous invasive sensors, motivating hence the need for a state estimation technique.

3. CONTROL SYSTEM DESIGN

In this section we present the general formulation of the optimal control problem for the MPC and the MHE. Since these two structures typically operate in discrete time, the dynamical equations (8) are discretized using an implicit method, e.g., the Backward Euler method, to allow stability over long time steps.

$$x(k+1) = x(k) + f(x(k+1), u(k), d(k), \tau_s)\,, \quad (11)$$

where τ_s is adopted sampling time.

3.1 Model Predictive Control

Define the current time instant $t = h\tau_s \in \mathbb{R}$ where $h \in \mathbb{N}_{\ge 0}$ and the prediction horizon $\mathcal{T}_h := \{h, \dots, h+N+1\}$, with $N \ge 1$ the number of samples in the horizon.

Then, the controller is designed to minimize the following objective function

$$\sum_{k \in \mathcal{T}_h} \sum_{i \in \mathcal{G}} c_i(k) P_i(k) \quad (12)$$

where c_i is the generator power cost, whether it is gas or electricity.

Therefore, the MPC optimization problem general formulation is

$$\begin{aligned} \underset{u(\cdot)}{\text{minimize}} \quad & (12) \\ \text{subject to} \quad & \forall k \in \mathcal{T}_h, \\ & (9), (10), (11), \\ & x(h) = \hat{x}(h), \end{aligned} \tag{13}$$

where $\hat{x}(h)$ is the state initial value, coming from the MHE algorithm.

3.2 Moving Horizon Estimator

The MPC is a state feedback controller, and as such requires the measure of all the states. Thus, the need for a MHE. We prove the with the same control model proposed in Nigro et al. (2024a), a successful implementation of the MHE is achieved. Define the current time instant $t = h\tau_s \in \mathbb{R}$ where $h \in \mathbb{N}_{\geq 0}$ and the history horizon $\mathcal{T}_h := \{h - N_H, \dots, h\}$, with $N_H \geq 1$ the number of samples in the history.

Reasonably, given the state of DHN are temperatures and directly measurable with sensors, we assume a linear relation between model state and its output

$$y(k) = Cx(k)\,. \tag{14}$$

We can assume measurements availability at the generation units, for safety reasons, and at the consumers, for monitoring purposes. All the remaining states of the networks can not be assumed mensurable in general, e.g., the temperatures of the finite volumes of pipes. Hence, the MHE is of paramount importance and its problem formulation is

$$\min_{x(\cdot)} \quad ||x(h - N_H) - \hat{x}(h - N_H)|| + \sum_{k \in \mathcal{T}_h} ||y_m(k) - Cx(k)|| \tag{15}$$

subject to, $\forall k \in \mathcal{T}_h$, (11)\,,

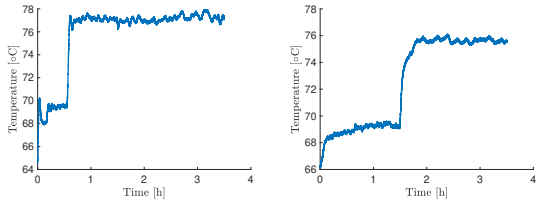
where y_m is the measured output, whereas $\hat{x}(h - N_H)$ is the state estimation at time N_H in the past computed at previous MHE iteration. In particular, the MHE problem returns the state trajectory minimizing the difference between the measured and the model outputs, eventually estimating $\hat{x}(h)$ at each iteration. The first term of cost function in (15) is used as a regularization term, see Rawlings et al. (2017).

4. CASE STUDY

In this section the performances of the proposed control oriented model are evaluated with experimental results from the Thermal Facility. The validation and control are performed on different dataset to verify the model performances across different operative conditions.

4.1 Software tools

The controller is tuned on a simulation environment of the TF, described in Alvarado et al. (2024). The simulation is implemented in Modelica language using Dymola. The controller uses Matlab and the CasADi framework for optimization problem formulation, solved with Ipopt. Finally, Python handles the communication between the developed MPC and the MHE algorithms with the low level controllers present in the plant.



(a) Gas Boiler supply temperature. (b) Electric Boiler supply temperature.

Fig. 3. The validation experiment inputs.

4.2 Model and estimation experimental validation

During the model validation, the plant is warmed up to reach a given steady state. Then, the GB tracks a step reference at T_{gb}^{out}, Figure 3a, the EB tracks a reference change at T_{eb}^{out}, Figure 3b, while the CHP output temperature is kept constant at 65°C. It is worth noting that disturbances, e.g., power absorbed by the load or external temperature, are assumed known by the optimal models. This is possible thanks to historical data from past years operation. The inputs to the GB, EB, and CHP are the same for both model and estimation validation, Figure 3a, Figure 3b.

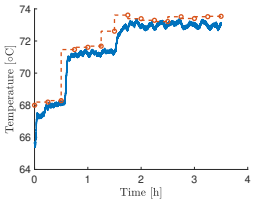
Model validation: The results show the supply temperature of the 4 loads: EX701, EX711, EX721, and EX731, Figure 4. Note that the predicted temperature in red has good accuracy compared to the real measurements in blue. The error is approximately within 0.5°C. The small temperature difference may be due to wrong physical parameters, which can be caused by a mismatch between the plant project and its actual construction.

Estimator Validation: The proposed MHE has a sampling time $\tau_s = 900$s and an horizon of $N_H = 14$ steps. The experiment lasts approximately 4h, for a total of 15 steps. Performance assessment is conducted on the supply temperature of load EX701 denoted as T_{701}^{in}. Although a measure of T_{701}^{in} is available, we assume it to be unmeasurable and use the MHE to estimate it instead. This approach enables the performance evaluation of the designed MHE algorithm by comparing the measured and estimated variables.

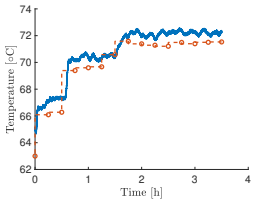
Overall, the MHE validation yields satisfying results shown in Figure 5, where the estimated states appears in red, while the experimental measures are in blue.

4.3 Control experimental results

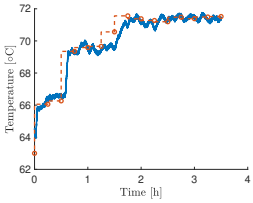
The goal of the controller is to minimize operational cost and respect operational constraints given the disturbances and energy costs shown in Figure 6. Note that the minimum user supply temperature is $\underline{T}_i^{in} = 65$°C. The MPC sampling time is 15 min with a prediction horizon of 2



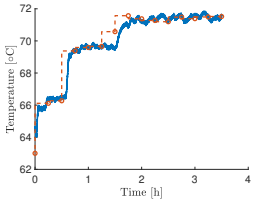
(a) EX701 supply temperature.



(b) EX711 supply temperature.

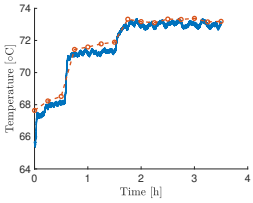


(c) EX721 supply temperature.

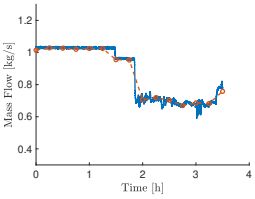


(d) EX731 supply temperature.

Fig. 4. Control oriented model predictions (red) compared with real data (blue).



(a) EX701 supply temperature.



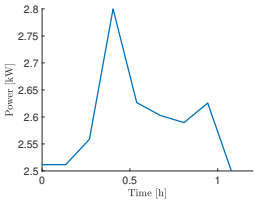
(b) EX701 mass flow rate.

Fig. 5. MHE state estimations (red) compared with real data (blue).

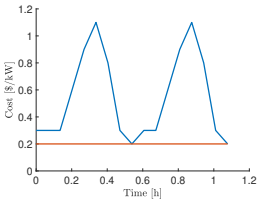
hours. Various tests were performed on the plant; for space reasons, the dynamical transients of only one of them is reported here. The reader is referred to Tognacca (2024) for discussion on the additional tests. However, despite not being discussed in details, the results of the additional tests have been used to evaluate the proposed MPC economic performances as discussed later.

For clarity, a simple load profile is used, which has a large consumption peak around hour 0.4 and constant power afterwards, as reported in Figure 6a. This profile set-point is sent equally to all loads. From Figures 7a and 7b we can see that the MPC attempts to heat the water using the GB, which is cheaper than the EB. The pre-charge of the network is performed to prevent the absorption peak of the load. This behavior, known as packing, involves the exploitation of the thermal inertia of the water in the pipes as a form of storage and is enabled by the proposed control-oriented model.

Hence, from the start of the experiment up to moments before the peak, the supply temperature of the GB increases to prevent the increase in demand and subsequent temperature drop. Nonetheless, mainly due to the short time between the beginning of the experiment and the peak, the temperature drops slightly below the required lower limit, Figure 7c, considering also the presence of

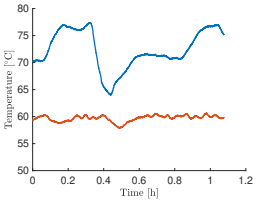


(a) Power absorbed by loads.

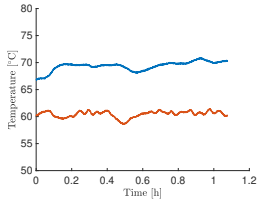


(b) Power costs, electricity (blue) and gas (red).

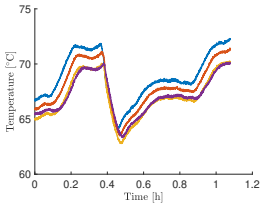
Fig. 6. Disturbance setpoints.



(a) Gas Boiler supply (blue) and return (red) temperature.



(b) Electric Boiler supply (blue) and return (red) temperature.



(c) Load supply temperatures: EX701, 711, 721, 731, blue, red, yellow, and purple.

Fig. 7. Experimental control results.

small, albeit existing, modeling errors discussed earlier. The MPC is able to recover immediately after that and reaches a steady state temperature by hour 0.7. It is worth noting that that the state and output constraints are implemented as soft constraints for feasibility reasons, as typical in MPC frameworks.

Before concluding the experiment, the MPC starts to pack the network again, around time 0.9 h. As the power disturbance is repeated equally over time, the MPC prediction horizon is already expecting the next peak, Figure 6a.

For completeness, three different tests were run on the real plant. The first test, discussed above, features a GB, EB, and a CHP. The second test works without the CHP to restrict the MPC degrees of freedom. Lastly, the third test works with a benchmark rule base strategy where all generators are operated at constant temperature, as common in real DHN plants, see La Bella and Del Corno (2023). The MPC achieves cost savings of 4.27% when three generators are employed and 1.63% when the CHP is off with respect to the rule-based strategy.

5. CONCLUSION

In this work, the authors demonstrate the design and experimental assessment of a nonlinear MPC and a MHE algorithm exploiting the control-oriented modeling approach described Nigro et al. (2024a). This effectively enables the practical implementation of optimal controllers in District Heating Network plants. In particular, the developed MHE algorithm is able to estimate unmeasured state variables by exploiting few system measurements. Moreover, this can be effectively coupled with a nonlinear MPC to achieve high performances from the computational perspective.

Future work may explore how to improve the model online by utilizing real-time measurements to better capture time-variant changes in network components, e.g., consumers behavior and generators degradations. Other potential studies could address generation unit commitment or robustness against disturbances.

ACKNOWLEDGEMENTS

Thanks to Marco Tognacca for its effort in tuning the District Heating Network model and handling the communication set up with the Thermal Facility during his months of internship at RSE.

REFERENCES

Alvarado, M.A.M., Anderis, C., Lazzari, R., Nigro, L., and La Bella, A. (2024). Development and experimental validation of an open-source model library for district heating network simulation. In *2024 Open Source Modelling and Simulation of Energy Systems (OSMSES)*, 1–6. IEEE.

Anderis, C., Alvarado, M.A.M., and Lazzari, R. (2024). Implementation of an experimental facility for district heating networks flexibility assessment. In *2024 AEIT International Annual Conference (AEIT)*, 1–6. IEEE.

Bergsteinsson, H.G., Vetter, P.B., Møller, J.K., and Madsen, H. (2022). Estimating temperatures in a district heating network using smart meter data. *Energy Conversion and Management*, 269, 116113.

Boca de Giuli, L., La Bella, A., and Scattolini, R. (2024). Physics-informed neural network modeling and predictive control of district heating systems. *IEEE Transactions on Control Systems Technology*, 32(4), 1182–1195.

Buffa, S., Fouladfar, M.H., Franchini, G., Lozano Gabarre, I., and Andrés Chicote, M. (2021). Advanced control and fault detection strategies for district heating and cooling systems—a review. *Applied Sciences*, 11(1), 455.

European Commission and Directorate-General for Energy, Bacquet, A., Galindo Fernández, M., Oger, A., Themessl, N., Fallahnejad, M., Kranzl, L., Popovski, E., Steinbach, J., Bürger, V., Köhler, B., Braungardt, S., Billerbeck, A., Breitschopf, B., and Winkler, J. (2022). *District heating and cooling in the European Union – Overview of markets and regulatory frameworks under the revised Renewable Energy Directive*. Publications Office of the European Union.

European Commission and Directorate-General for Energy, Dröscher, T., Ladermann, A., Maurer, C., Tersteegen, B., Willemsen, S., Billerbeck, A., Kiefer, C., Winkler, J., Bernath, C., Sensfuß, F., Kranzl, L., Müller, A., Kotek, P., and Tóth, B. (2023). *Potentials and levels for the electrification of space heating in buildings – Final report*. Publications Office of the European Union.

Fang, T. and Lahdelma, R. (2014). State estimation of district heating network based on customer measurements. *Applied Thermal Engineering*, 73(1), 1211–1221.

Farahani, S.S., Lukszo, Z., Keviczky, T., De Schutter, B., and Murray, R.M. (2016). Robust model predictive control for an uncertain smart thermal grid. In *2016 European Control Conference (ECC)*, 1195–1200. IEEE.

Krug, R., Mehrmann, V., and Schmidt, M. (2021). Nonlinear optimization of district heating networks. *Optimization and Engineering*, 22(2), 783–819.

La Bella, A. and Del Corno, A. (2023). Optimal management and data-based predictive control of district heating systems: The novate milanese experimental case-study. *Control Engineering Practice*, 132, 105429.

La Bella, A., Nigro, L., and Scattolini, R. (2023). Predictive control and benefit sharing in multi-energy systems. *IEEE Transactions on Control Systems Technology*, 32(2), 368–383.

Nigro, L., La Bella, A., Casella, F., and Scattolini, R. (2024a). Control-oriented modeling, simulation, and predictive control of district heating networks. *IEEE Transactions on Automation Science and Engineering*.

Nigro, L., La Bella, A., and Scattolini, R. (2024b). Distributed two-layer predictive control of multi-energy systems. In *2024 European Control Conference (ECC)*, 2429–2434. IEEE.

Quaggiotto, D., Vivian, J., and Zarrella, A. (2021). Management of a district heating network using model predictive control with and without thermal storage. *Optimization and Engineering*, 22(3), 1897–1919.

Rathod, N., La Bella, A., Puleo, G., Scattolini, R., Rossetti, A., and Sandroni, C. (2019). Modelling and predictive control of a solar cooling plant with flexible configuration. *Journal of Process Control*, 76, 74–86.

Rawlings, J.B., Mayne, D.Q., Diehl, M., et al. (2017). *Model predictive control: theory, computation, and design*, volume 2. Nob Hill Publishing Madison, WI.

Sandou, G., Font, S., Tebbani, S., Hiret, A., Mondon, C., Tebbani, S., Hiret, A., and Mondon, C. (2005). Predictive control of a complex district heating network. In *IEEE conference on decision and control*, volume 44, 7372. IEEE; 1998.

Taylor, M., Long, S., Marjanovic, O., and Parisio, A. (2021). Model predictive control of smart districts with fifth generation heating and cooling networks. *IEEE Transactions on Energy Conversion*, 36(4), 2659–2669.

Tognacca, M. (2024). Predictive control and estimation in a real district heating network. *M.Sc. thesis, Politecnico di Milano*.

Wirtz, M., Neumaier, L., Remmen, P., and Müller, D. (2021). Temperature control in 5th generation district heating and cooling networks: An milp-based operation optimization. *Applied Energy*, 288, 116608.

Part II
Multi-Energy Systems

II - 5

Centralized Control for MES Coordination

Coordinating multi-energy systems involves handling coupled dynamics, heterogeneous time scales, and economic objectives under distributed information constraints. This Chapter targets the challange of multi-energy systems optimal coordination and operation. The author [41] introduces a two-level hierarchical control architecture with centralized coordination.

- **Journal Article**: La Bella, A., *Nigro, L.*, & Scattolini, R. (2023). Predictive control and benefit sharing in multi-energy systems. IEEE Transactions on Control Systems Technology, 32(2), 368-383 [41].

5.1 Centralized Control

Hierarchical Framework

Multi-energy systems synergetically integrate subsystems across different energy domains through energy conversion devices such as cogeneration systems and heat pumps. To operate MES synergetically, the author designed a hierarchical model predictive control architecture shown in Figure 5.1. The variables $\mathcal{S}_i, \mathcal{S}_j$, and $\mathcal{S}_k$ represent physical energy carriers.

On top, there are two layers:

- **High-Level MPC (HL-MPC)**: Model energy carriers with a convex linear model independent of the energy domain. The high-level solutions are the optimal power exchanges and storage references for the low-level layer to track. In turn, the HL-MPC receives the current subsystem states.

- **Low-Level MPC (L-MPC)**: The low-layer contains decentralized MPC regulators. Each L-MPC controls a single subsystem with detailed, potentially nonlinear dynamics. Each regulator operates with a sampling period tailored to its subsystem, tracking HL-MPC references while minimizing local operational costs and satisfying constraints.

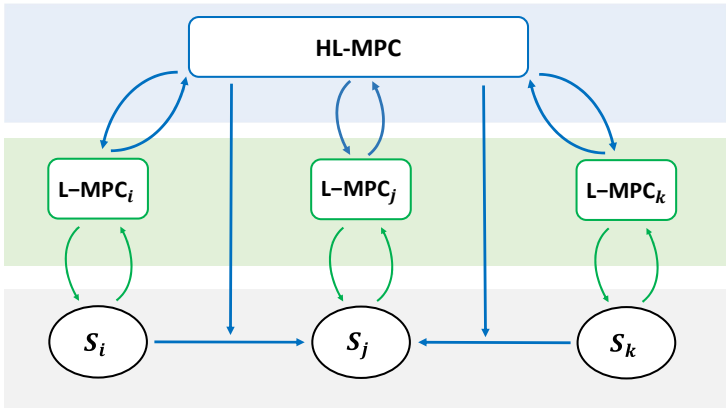


Figure 5.1: Two layer hierarchical control architecture. The High-Level MPC in blue, and the Low-Level MPC in green. In grey the real subsystems.

Benefit Sharing

Despite coordination, MES operation can produce uneven economic benefits across subsystems, potentially imposing additional costs on subsystems that are cheaper to operate and can generate for others. Consequently, to promote participation, all subsystems involved should distribute the profit arising from coordinated operations among themself. The proposed control regulator is integrated with a benefit-sharing mechanism based on cooperative game theory, specifically a bargaining approach, guaranteeing that all subsystems profit from cooperation.

Results

J_i	S_{el} (IEEE 37-bus system)	S_{dhn} (AROMA DHN)	$\sum_{\forall i}(Total)$
J_i^{nc}	−128.4$	6881$	6752.3$
J_i^{c}	1050.2$	1952$	3002.2$
z_i^*	3053.7$	3053.7$	0
$J_i^{c} - z_i^*$	−2003.4$	5005.6$	3002.2$

Table 5.1: Multi-energy system operational costs and Nash Bargaining solutions.

The presented regulator is tested on two case studies. First, a simplified system with three energy carriers demonstrates effective coordination of power flows and storage management while respecting local constraints. Second, a larger case study assesses scalability. It comprises the IEEE 37-bus electrical grid and the AROMA district heating network, i.e., a case study from the literature [36].

Results confirm the architecture's ability to handle large-scale nonlinear systems and demonstrate that the benefit-sharing mechanism successfully resolves initial cost imbalances, as shown in Table 5.1.

Let J_i^{nc} be the non-cooperative cost of subsystem i and J_i^c the cooperative cost. The fair economic allocation computes optimal transfers between subsystems, z_i^*. In the cooperative operation, the electrical subsystem incurs a cost of $J_{el}^c = 1050.2\$$ compared to a standalone profit of 128.4\$. Nonetheless, due to the AROMA network's cooperative savings $J_{dhn}^{nc} - J_{dhn}^c = 4929\$$, the electrical subsystem receives an additional profit of 1875\$, see Table 5.1. The hierarchical strategy's sub-optimality relative to a centralized controller is minimal, approximately -0.6%.

The work contributes to the literature by designing a regulator for MES control in the presence of large-scale subsystems, integrating the benefits of coordination with the advantages of accurate models for optimal control.

Predictive Control and Benefit Sharing in Multi-Energy Systems

Alessio La Bella, *Member, IEEE*, Lorenzo Nigro, Riccardo Scattolini

***Abstract*—This paper proposes the design of a hierarchical control architecture capable of optimally coordinating Multi-Energy Systems (MESs). A MES involves the synergetic operation of subsystems belonging to different energy domains (e.g., thermal, electrical or gas), enhancing their energy efficiency and economic savings, at the price of significant control challenges. In fact, MESs imply an increased model complexity and the interaction of networked subsystems with largely different dynamics. This motivates the design of a multi-layer control architecture where, at the upper level, a Model Predictive Control (MPC) regulator relies on energy models of reduced order to coordinate power exchanges among MES subsystems, while, at the lower layer, decentralized MPC regulators locally control subsystems with different sampling rates, consistently with their local dynamics. On the other hand, the optimal MES regulation may imply additional costs to few subsystems, although the overall operational cost decreases. Thus, benefit sharing algorithms are also proposed, relying on game-theoretical methods, enabling to properly share the achieved economic benefit among subsystems, and guaranteeing that the MES operation is more convenient than the independent regulation for each single subsystem. The designed control strategy is tested on two different MES case-studies, considering also the presence of referenced electrical and thermal networks, showing high versatility and enhanced performances.**

***Index Terms*—Model Predictive Control; Multi-Energy Systems; Hierarchical Control; Bargaining problem.**

I. Introduction

MULTI-ENERGY Systems (MESs) are today gaining much attention, being recognized as a key solution to achieve a reliable, resilient and low-carbon energy system [1]. The MES concept consists in the synergetic operation of subsystems belonging to different energy domains, which can exchange energy through proper conversion devices (e.g., interconnected electrical grids, district heating systems and gas networks). The optimal coordination of these additional degrees of flexibility can significantly increase the efficiency and storage capacity of the energy system, which are crucial aspects to support a large-scale diffusion of intermittent renewable energy sources [2]. For example, a surplus of renewable electrical energy can be stored in other forms, such as in a thermal or a gas storage tank through a proper conversion process, and used when necessary. The growing interest in MESs has been also pushed by the today commercial availability of different conversion devices, such as co-generation systems (gas to electricity and heat), heat pumps (electricity to heat), hydrogen electrolysers (electricity to gas) and fuel cells (gas to electricity).

The benefits given by an integrated control of MESs come however at a price. In fact, MESs can be large-scale systems characterized by very different dynamic behaviours, such as "fast" electricity systems and "slow" thermal ones, and they can be governed by complex nonlinear equations (as for thermal and gas networks [3], [4]). Moreover, since energy systems of different domains may belong to different owners or operators, privacy issues can be of paramount importance. Finally, it is also worth noting that, despite the coordinated control of MESs can lead to consistent economic saving, this benefit could be a priori not equally shared among the involved energy systems or owners. In fact, for each single energy system, it must be ensured that the coordinated MES optimization is more convenient than its autonomous regulation.

A. State of the art

The problem of modelling and control of MESs has recently gained attention, given their inherent complexity and benefits, as discussed in [5]. In [6], the *energy hub* concept is discussed, comprising the interconnection of different MES devices, and showing that applying Model Predictive Control (MPC) strategies can actually lead to enhanced energy savings. A generalised modelling methodology for MESs has been proposed in [7], leading to the formulation of mixed-integer linear models suited for the design of MPC regulators. In [8], a MES is modelled using state-space linear systems and an economic MPC controller is designed for its optimal regulation. Other optimization-based control approaches for MESs consider robust methods [9], [10], data-based approaches [11]–[13], or the presence of time-varying constraints [14]. Nevertheless, all the mentioned contributions concern the design of centralized regulators, which could be an impractical solution for MESs due to computational issues and privacy concerns.

Motivated by this, distributed approaches have been also proposed. The design of a distributed MPC scheme for MESs is described in [15], relying on dual-decomposition techniques. In [16], [17], distributed optimization algorithms for energy systems described by mixed-integer linear models are discussed. A distributed algorithm relying on the Alternating Direction Method of Multipliers (ADMM) is proposed in [18], assuming networked energy systems to be represented by models. Nevertheless, distributed control strategies can be critical in a multi-energy scenario. They often involve iterative optimization processes, which can be slow, and, moreover, are not guaranteed to converge to the optimal solution in

Alessio La Bella, Lorenzo Nigro and Riccardo Scattolini are with the Dipartimento di Elettronica, Informazione e Bioingegneria, Politecnico di Milano, 20133 Milan, Italy (e-mails: *alessio.labella@polimi.it*, *lorenzo.nigro@polimi.it* and *riccardo.scattolini@polimi.it*).

presence of nonconvex and nonlinear problems, typical in MESs. Because of this, a heuristic procedure based on the relaxation of nonlinear constraints is proposed in [19], able to recover at least a feasible solution if the designed distributed algorithm fails in optimizing the MES. Other control approaches for networked energy systems have relied on hierarchical architectures, enabling enhanced scalability and prompt system regulation [20]–[23]. In this context, a two-layer control architecture for large-scale networks is proposed in [24], exploiting a network partitioning procedure to identify the subsystems to control, but however focusing only on on the electrical energy domain.

Concerning the distribution of the benefit achieved by the optimal control of interconnected energy subsystems, most literature has relied on game-theoretical approaches. A well-known technique for this task is the Shapley value method, firstly proposed in [25], where the profit is distributed based on the effective contribution of each agent to the coalition [26]. Profit redistribution via Shapley value is applied to a residential microgrid in [27], however highlighting that it can be intractable from the computational point of view, as each agent needs to know the achievable benefit by any possible coalition of agents [28]. An alternative game-theoretical method to redistribute the benefit in cooperative fashion is the Nash bargaining problem, firstly proposed in [29]. This benefit sharing technique is exploited in [30] and in [31], considering the interconnection of electrical microgrids. Similar methods are applied in [32] and in [33], proposing distributed bargaining algorithms which lead to real-time trading frameworks among energy subsystems.

Nevertheless, note that most of the mentioned references consider simplified system models (e.g., mixed-integer linear), which are not suited to represent dynamical energy networks, such as thermal and gas ones which are inherently nonlinear. On the other hand, the presented approaches use the same sampling period for controlling all devices, which can compromise performances in presence of MESs as they often comprehend subsystems with largely different dynamics and transients. Finally, note that the mentioned references do not investigate benefit sharing strategies applied to different multi-energy domains, which usually belong to distinct owners.

B. Main contribution

The mentioned challenges motivate the design of a novel hierarchical MPC architecture for MESs. In particular, we consider a MES including interconnected subsystems belonging to distinct energy domains (e.g., an electrical grid, a district heating system and a gas network) and that can exchange energy through proper conversion devices (e.g., heat pumps, gas boilers, cogenerators etc.). The proposed control architecture includes, at the high-level, a MPC controller which, exploiting properly energy models of reduced order, computes the optimal amount of energy to be stored in each MES subsystem and the power exchanges among them. The proposed reduced modelling is independent on the specific energy domain and it enables to describe the subsystem energy dynamics at reduced complexity with respect to their detailed modelling, facilitating their multi-energetic coordination. Power exchanges among subsystems computed at the high-level are directly imposed on conversion devices, whereas the computed energy references are sent to a decentralized low-level layer of MPC controllers, each one regulating a subsystem at the minimum cost. Each low-level MPC controller considers the detailed subsystem model, possibly nonlinear, and is executed with a sampling period consistent with the subsystem dynamical behaviour.

Concerning the benefit sharing problem, a cooperative bargaining game is formulated, resulting in an agreement among subsystems on how the profit given by the multi-energy interaction should be shared. In particular, the proposed bargaining game is supposed to be periodically executed, evaluating the benefit achieved by the designed control strategy during the past instants, and then defining the optimal economic transactions among MES subsystems, so that the obtained benefit is properly distributed.

The main advantages and contributions of the proposed control strategy with respect to the literature are:

- at the high-level, the definition of a novel reduced order modelling of MES subsystems, leading to convex energetic models whose structure is independent on the specific energy domain, enabling the computationally-efficient and prompt coordination of power exchanges among MES subsystems and of their stored energy;
- at the low-level, the possibility of controlling each MES subsystem through a local MPC regulator, considering the detailed system modelling, eventually nonlinear, tracking an optimized overall energy profile at the minimum cost. Moreover, each local MPC regulator can regulate its subsystem with a specific sampling period, consistently with the dynamical characteristics of the corresponding energy domain;
- the design of a benefit sharing algorithm which, relying on bargaining games, enables each subsystem (or owner) to benefit from the MES operation. In particular, the proposed formulation guarantees that, for each subsystem, the multi-energy cooperation is always more convenient with respect to the independent regulation. Moreover, the presented approach enables subsystems to preserve their internal information and models, as they must periodically communicate just their total operational cost.

The proposed control strategy is tested on two MES case-studies. The first, more illustrative, has the purpose of clearly showing the validity of the proposed modelling and how the designed architecture actually solves the highlighted control challenges. The second case study is based on a more realistic MES scenario, where two subsystems are interconnected and jointly regulated, i.e., the IEEE 37-bus electrical grid [34] and the AROMA district heating network [3], showing how the designed control architecture is effective also for the coordination of large-scale MES benchmarks.

C. Outline

The paper is organized as follows. Section II introduces the MES modelling, the control objectives, and presents an illustrative example to motivate the addressed control challenges. The proposed two-layer control architecture is described in details in Section III. Section IV illustrates the formulated bargaining game problem. Section V reports the analysis of the designed control architecture tested on two MES case-studies. The final conclusions are gathered in Section VI.

Notation: Let $\mathbb{R}$ denote the set of real numbers, $\mathbb{R}_{\geq 0}$ the set of positive or null real numbers including zero, and $\mathbb{R}_{>0}$ the set of strictly positive real numbers. Moreover, let $\mathbb{N}$ denote the set of natural numbers. Given a matrix A, $A \in \mathbb{R}^{n,m}$ indicates that it has n rows and m columns and all its entries are real numbers. Given a vector v, $v \in \mathbb{R}^n$ indicates that it has n rows and one column, and all its entries are real numbers. Given a matrix A and a vector v, their transpose are denoted with A' and v', respectively. The vector $\mathbb{1}_n$ is used to define a n-dimensional vector where all entries are 1, i.e., $\mathbb{1}_n = [1, \dots, 1]' \in \mathbb{R}^n$. Similarly, the vector $\mathbb{0}_n$ is used to define a n-dimensional vector where all entries are 0, i.e., $\mathbb{0}_n = [0, \dots, 0]' \in \mathbb{R}^n$. Given two vectors of variables $x, y \in \mathbb{R}^n$, the inequalities among the two, e.g., $x > y$, are intended element-wise. For a vector $x \in \mathbb{R}^n$, the vectors of the corresponding upper and lower bounds are $\overline{x} \in \mathbb{R}^n$ and $\underline{x} \in \mathbb{R}^n$, respectively, with $\overline{x} > \underline{x}$. The operators $\max(x)$ and $\min(x)$ express the maximum and the minimum element of vector x, respectively. Considering a real variable $a \in \mathbb{R}_{\geq 0}$, $b = \lfloor a \rfloor$ is the largest integer less than or equal to a, i.e., $b \in \mathbb{N} \cup \{0\}$. Given a sequence of variables $a_1, \dots, a_n$, and the set of their indexes $\mathcal{N} = \{1, \dots, n\}$, the vector $a = [a_1, \dots, a_n]'$ is compactly written as $a = \{a_i\}_{\forall i \in \mathcal{N}}$. Finally, given a set $\mathcal{N}$, its cardinality is denoted with $\text{card}(\mathcal{N})$.

II. Problem statement

Consider a multi-energy system $\mathcal{S}$ [†] composed by a set of M subsystems $\mathcal{S}_1, ..., \mathcal{S}_M$, where each subsystem $\mathcal{S}_i$ belongs to a specific energy domain (electrical, thermal, gas, etc.) and is assumed to be equipped with local generation and load units. Moreover, assume that power can be transmitted among some specific pairs of subsystems to optimize the overall energy behaviour of $\mathcal{S}$ [†]. More formally, this structure can be described by a directed graph $G(\mathcal{N}, \mathcal{E})$, where the nodes $\mathcal{N}$ represent the subsystems, i.e., $\text{card}(\mathcal{N}) = M$, while the edges $\mathcal{E} \subseteq \mathcal{N} \times \mathcal{N}$ model their energetic interconnections, i.e., $(i, j) \in \mathcal{E}$ if power can be transferred from $\mathcal{S}_i$ to $\mathcal{S}_j$. For each $\mathcal{S}_i$, $i \in \mathcal{N}$, consider the sets of output and input nodes $\mathcal{N}_i^{\text{out}}$, $\mathcal{N}_i^{\text{in}} \subseteq \mathcal{N}$, defined as $\mathcal{N}_i^{\text{out}} = \{j \in \mathcal{N} | (i, j) \in \mathcal{E}\}$ and $\mathcal{N}_i^{\text{in}} = \{j \in \mathcal{N} | (j, i) \in \mathcal{E}\}$, respectively, where $\text{card}(\mathcal{N}_i^{\text{out}}) = o_i$ and $\text{card}(\mathcal{N}_i^{\text{in}}) = v_i$.

Each subsystem $\mathcal{S}_i$ is modelled as

$$\dot{x}_i(t) = f_i(x_i(t), u_i(t), \widetilde{d}_i(t)), \tag{1a}$$

where $x_i \in \mathbb{R}^{n_i}$ is the vector of local states and $u_i \in \mathbb{R}^{m_i}$ is the vector of local inputs, both assumed to be bounded as

$$\underline{x}_i \leq x_i(t) \leq \bar{x}_i, \tag{1b}$$

$$\underline{u}_i \leq u_i(t) \leq \bar{u}_i. \tag{1c}$$

Moreover, in (1a), $\widetilde{d}_i$ represents the vector of exogenous signals for $\mathcal{S}_i$, defined as

$$\widetilde{d}_i(t) = [\, d_i(t)' \;\; w_i(t)' \,]', \tag{1d}$$

where $d_i \in \mathbb{R}^{r_i}$ are local disturbances, while w_i includes the power exchanges between $\mathcal{S}_i$ and the other subsystems. In particular, w_i is structured as

$$w_i(t) = [w_i^{\text{out}}(t)' \;\; w_i^{\text{in}}(t)']', \tag{1e}$$

where $w_i^{\text{out}}(t) \in \mathbb{R}^{o_i}$ and $w_i^{\text{in}} \in \mathbb{R}^{v_i}$ include the power transfers sent and received by $\mathcal{S}_i$, respectively. Expressing with $p_{ij} \in \mathbb{R}$ the power produced by $\mathcal{S}_i$ and transferred to $\mathcal{S}_j$ [1], it follows that

$$w_i^{\text{out}}(t) = \{p_{ij}(t)\}_{\forall j \in \mathcal{N}_i^{\text{out}}}, \quad w_i^{\text{in}}(t) = \{\eta_{ji}\, p_{ji}(t)\}_{\forall j \in \mathcal{N}_i^{\text{in}}}. \tag{1f}$$

where the power transfers in w_i^{in} are weighted by the efficiency term $\eta_{ji} \in \mathbb{R}$, taking into account the conversion losses due to the power transfer from $\mathcal{S}_j$ to $\mathcal{S}_i$, with $j \in \mathcal{N}_i^{\text{in}}$.

Now, assume that a set $\mathcal{G}_i$ of controllable sources and a set $\mathcal{L}_i$ of non-dispatchable loads are present in each $\mathcal{S}_i$ and denote with $p_i^g \in \mathbb{R}^{g_i}$ and $p_i^l \in \mathbb{R}^{l_i}$ their power injections and absorptions, respectively. These are described as functions of the local variables, i.e.,

$$p_i^g(t) = \phi_i(x_i(t),\, u_i(t)), \tag{2a}$$

$$p_i^l(t) = \psi_i(x_i(t),\, d_i(t)), \tag{2b}$$

where, in particular, controllable power flows are functions of local inputs, while the non-dispatchable ones depend on local disturbances [2].

Moreover, introduce the variable $e_i \in \mathbb{R}$, representing the total energy stored in $\mathcal{S}_i$. Then, the following modelling assumption can be stated.

Assumption 2.1: Given a generic energy subsystem $\mathcal{S}_i$ described by (1), the total stored energy $e_i \in \mathbb{R}$ can be defined as a function of the local state, i.e.,

$$e_i = \xi_i(x_i), \tag{3}$$

where $\xi_i : \mathbb{R}^{n_i} \to \mathbb{R}$. Moreover, its derivative with respect to time can be stated as

$$\dot{e}_i(t) = \mathbb{1}'_{g_i} p_i^g(t) \,-\, \mathbb{1}'_{l_i} p_i^l(t) \,+\, \mathbb{1}'_{v_i} w_i^{\text{in}}(t) \,-\, \mathbb{1}'_{o_i} w_i^{\text{out}}(t). \tag{4}$$

□

The formulated assumption is straightforward, as local states in an energy system are generally linked to the stored energy (e.g. batteries' state of charges, fluid temperatures, gas pressures, etc.) and the variation of the total energy is dictated by the power balance. As it will be shown, several energy systems of different domains can be represented by (1)-(2) and satisfy Assumption 2.1. However, the addressed multi-energy control problem and the proposed solution are firstly presented.

[1] For the sake of clarity, p_{ij} is modelled as scalar. However, in case p different power interfaces are available to transfer power from $\mathcal{S}_i$ to $\mathcal{S}_j$, it would follow that $p_{ij} \in \mathbb{R}^p$.

[2] The set $\mathcal{L}_i$ can also include non-dispatchable generators, e.g., renewable sources, which are not explicitly mentioned in the following for the sake of clarity.

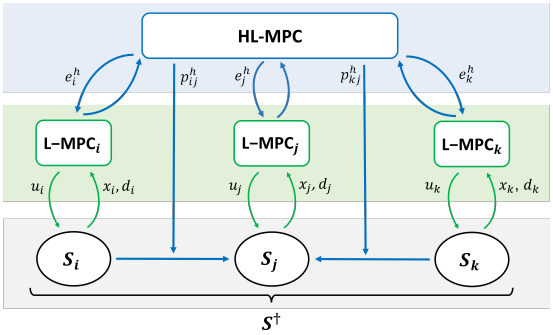


Fig. 1. Schematic of the proposed hierarchical control architecture for multi-energy systems. The variables transmitted along the arrows going from each L-MPC to the HL-MPC are not here depicted for the sake of clarity.

A. Control problem and proposed solution

Considering the presented framework for networked multi-energy systems, the main control objectives can be synthesized as follows:

- Objective 1: locally control each $\mathcal{S}_i$ to maintain its states in prescribed operating bounds, meanwhile minimizing local power production costs;
- Objective 2: coordinate the power exchanges p_{ij} among interconnected subsystems, possibly belonging to distinct energy domains, considering the energy availability and the requirements of each $\mathcal{S}_i$, as well as the minimization of the operational cost of the whole networked multi-energy system $\mathcal{S}^\dagger$.

As discussed in Section I, pure centralized and distributed control approaches are not suited to accomplish these tasks in a multi-energy scenario, given the large-scale dimension of the problem, the different involved time-scales and the modelling complexity. This motivates the design of a novel hierarchical predictive control architecture, depicted in Figure 1. In this structure, a lower layer made by decentralized local MPC controllers (L-MPC), one for each $\mathcal{S}_i$, runs at "small" sampling periods assuming that the energy exchange terms p_{ij} have been set. Each L-MPC$_i$ computes local inputs u_i to satisfy local constraints, minimize internal operational costs, and maintain the total energy stored in $\mathcal{S}_i$ around a given reference, denoted with e_i^h. This reference is computed by a coordination scheme at the higher layer, named High Level MPC (HL-MPC), which, exploiting a reduced energy model for each subsystem and according to an economic criterion, computes the optimal energy to be stored, i.e., e_i^h, and the optimal power exchanges among the interconnected subsystems, denoted with $p_{ij}^h \in \mathbb{R}$, at "large" sampling periods (for the sake of clarity, all variables regulated by the HL-MPC are reported with the superscript h). As shown in the following, the proposed two-layer control architecture enables, on one hand, to locally control each energy subsystem at a specific time rate, separately considering the dynamical model complexity of diverse energy domains, and, on the other hand, to optimally coordinate power exchanges among subsystems taking advantage of a reduced modelling approach. Before describing in detail the formulation of each control layer, an illustrative example of a simple multi-energy system is hereafter reported to better motivate the proposed system modelling and assumptions, as well as the designed control architecture.

B. Illustrative example of a multi-energy system

Consider the multi-energy system $\mathcal{S}^\dagger$ depicted in Figure 2, where three subsystems belonging to different energy domains are interconnected: a gas storage tank (subsystem $\mathcal{S}_1$), a water thermal system (subsystem $\mathcal{S}_2$), and an electrical circuit (subsystem $\mathcal{S}_3$).

The gas storage tank has volume V_g and contains gas at density $\rho_g(t)$. It is subjected to an input mass flow rate $q_g^{in}(t)$, which is locally regulated, and to an output mass flow rate $q_g^{out}(t)$, acting as a disturbance. Moreover, part of the stored gas energy is transferred to the water thermal system through a gas boiler absorbing the primary power $p_g^b(t)$.

The water thermal system includes a water vessel with mass m_w and temperature $T_w(t)$, heated by a temperature-regulated thermal plate of area A and temperature $T_m(t)$. The water contained in the vessel is also heated by a thermal resistance, fed by the external electrical circuit with an electrical power $p_e^r(t)$. A mass flow rate $q_w(t)$ of water is delivered by a pump to an heat exchanger, absorbing an unknown thermal power and returning output water at a temperature $T^r(t)$. In turn, this is heated by the gas boiler and injected again into the tank.

Finally, the electrical circuit is constituted by a locally regulated voltage source $V(t)$ delivering the current $I(t)$, an inductor L, a capacitor C, a time-varying resistor $R(t)$, and a thermal resistance, automatically regulated to absorb the electrical power $p_e^r(t)$. As evident from Figure 2, the capacitor, the time-varying resistor and the thermal resistance are connected in parallel, implying that they are subjected to the same voltage $V_c(t)$.

Hereafter, the presented multi-energy system is modelled as defined in the previous section with $\mathcal{N} = \{\mathcal{S}_1, \mathcal{S}_2, \mathcal{S}_3\}$ and $\mathcal{E} = \{(\mathcal{S}_1, \mathcal{S}_2), (\mathcal{S}_3, \mathcal{S}_2)\}$.

As suggested by [4], the gas temperature dynamics can be neglected given its low thermal capacity. Modelling the mass conservation in subsystem $\mathcal{S}_1$, it follows that

$$\dot{\rho}_g(t) = \frac{1}{V_g}\left(q_g^{in}(t) - q_g^{out}(t) - \frac{p_g^b(t)}{c_g^{lhv}}\right), \tag{5}$$

where c_g^{lhv} is the gas lower heating value. Setting $x_1(t) = \rho_g(t)$, $u_1(t) = q_g^{in}(t)$, $d_1(t) = q_g^{out}(t)$, $w_1^{\text{out}}(t) = p_{12}(t) = p_g^b(t)$ and $w_1^{\text{in}}(t) = 0$, it is clear that (5) belongs to the system class represented by (1). Moreover, the energy stored in the gas tank is

$$e_1(t) = \xi_1(x_1(t)) = c_g^{lhv} V_g \rho_g(t)\,, \tag{6}$$

and, consequently, the energy derivative follows

$$\dot{e}_1(t) = c_g^{lhv} q_g^{in}(t) - c_g^{lhv} q_g^{out}(t) - p_g^b(t)\,. \tag{7}$$

It is apparent that, defining the local injected and absorbed power as $p_1^g(t) = c_g^{lhv} q_g^{in}(t)$ and $p_1^l(t) = c_g^{lhv} q_g^{out}(t)$, respectively, Assumption 2.1 is validated.

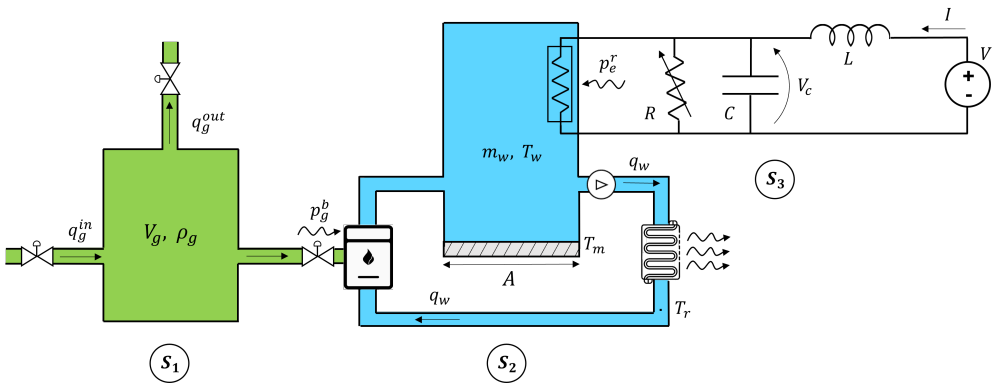


Fig. 2. Schematic of an illustrative example of a multi-energy system $\mathcal{S}^{\dagger}$, composed of a gas storage tank (subsystem $\mathcal{S}_1$), a water thermal system (subsystem $\mathcal{S}_2$), and an electrical circuit (subsystem $\mathcal{S}_3$).

Considering the electrical system $\mathcal{S}_3$, and using the Kirchhoff's circuit laws, it holds that

$$\dot{I}(t) = \frac{1}{L}(V(t) - V_c(t))\,, \tag{8a}$$

$$\dot{V}_c(t) = \frac{1}{C}(I(t) - V_c(t)R(t)^{-1} - p_e^r(t)V_c(t)^{-1})\,. \tag{8b}$$

Define $x_3(t) = [I(t), V_c(t)]'$, $u_3(t) = V(t)$, $d_3(t) = R(t)$, $w_3^{\text{out}}(t) = p_{32}(t) = p_e^r(t)$ and $w_3^{\text{in}}(t) = 0$. Thus, subsystem (8) is represented by a model with the structure of (1). The total energy of the electrical system is stored in the inductor and capacitor, and is defined as

$$e_3(t) = \xi_3(x_3(t)) = \frac{1}{2}L\,I(t)^2 + \frac{1}{2}C\,V_c(t)^2\,, \tag{9}$$

while its derivative is

$$\dot{e}_3(t) = V(t)I(t) - R(t)I(t)^2 - p_e^r(t) \tag{10}$$

Indicating the injected and absorbed power as $p_3^g(t) = V(t)I(t)$ and $p_3^l(t) = R(t)I(t)^2$, respectively, it is evident that Assumption 2.1 holds.

Finally, modelling the thermal dynamics in the water vessel, assuming it to represent the dominant inertia in the water system, it follows that

$$\dot{T}_w(t) = \frac{k_{wm}A}{m_w c_w}\big(T_m(t) - T_w(t)\big) - \frac{q_w(t)}{m_w}\big(T_w(t) - T_r(t)\big) + \\ + \frac{\eta_{gw}p_g^b(t) + \eta_{ew}p_e^r(t)}{m_w c_w}\,, \tag{11}$$

where k_{wm} is the conduction heat transfer coefficient and c_w is the water specific heat capacity. The terms η_{gw} and η_{ew} represent the power conversion efficiencies from the gas and electrical systems to the water system, respectively. Setting $x_2(t) = T_w(t)$, $u_2(t) = T_m(t)$, $d_2(t) = [q_w(t)\ \ T_r(t)]'$, $w_2^{\text{out}}(t) = 0$ and $w_2^{\text{in}}(t) = [\eta_{12}\,p_{12}(t)\ \ \eta_{32}\,p_{32}(t)]' = [\eta_{gw}p_g^b(t)\ \ \eta_{ew}p_e^r(t)]'$, also system (11) is represented by the model structure proposed in (1). Moreover, the total stored energy in the water vessel is

$$e_2(t) = \xi_2(x_2(t)) = c_w m_w T_w(t)\,, \tag{12}$$

its derivative is

$$\dot{e}_2(t) = c_w m_w \dot{T}_w(t) = k_{wm}A(T_m(t) - T_w(t)) + \\ - c_w q(t)(T_w(t) - T_r(t)) + \eta_{gw}p_g^b(t) + \eta_{ew}p_e^r(t)\,. \tag{13}$$

Defining the power injected by the thermal plate as $p_2^g(t) = k_{wm}A(T_m(t) - T_w(t))$ and the one absorbed by the heat exchanger as $p_2^l(t) = c_w q_w(t)(T_w(t) - T_r(t))$, it is apparent that Assumption 2.1 holds.

Many other systems and energy domains can be formulated with the model class (1)-(4) beyond the ones considered in the described example (e.g., mechanical, hydraulic systems, etc), as well as more complex system architectures (e.g., electrical, thermal or gas networks). The formulated example shows which are the possible interactions and control challenges in a multi-energy system, where both local control and coordination of power exchanges must be performed in a cost-effective and scalable manner.

Remark 2.1: It is worth noting that the multi-energy interaction may give many advantages from the energetic and economic point of view, but the achieved benefit could be not a priori equally shared among participating subsystems. In fact, considering the illustrative example in Figure 2, transferring power to the water thermal system implies an additional cost both for the gas and electrical system, which may not want to afford without any revenue. This motivates the necessity of a benefit sharing algorithm, which will be described in Section IV. The formulation of the proposed hierarchical control architecture is described in the following section.

III. Hierarchical predictive control of multi-energy systems

Considering the hierarchical control architecture shown in Figure 1, each L-MPC$_i$ is executed with sampling period τ_i, while the HL-MPC runs with sampling period $\tau_h \geq \tau_i$, $\forall i \in \mathcal{N}$. For the sake of simplicity, τ_h is chosen to be a common multiple of τ_i, $\forall i \in \mathcal{N}$, i.e., $\exists H_i \in \mathbb{N}$ so that $\tau_h = H_i\tau_i$.

A discrete time index $k_i \in \mathbb{N}$ is introduced for each subsystem $\mathcal{S}_i$, defining the time instants $t = k_i\tau_i$ when the L-MPC$_i$ is executed, while $k_h \in \mathbb{N}$ is used for the HL-MPC layer, running at time instants $t = k_h\tau_h$.

A *receding horizon* strategy is adopted for the MPC control design, using N_i prediction steps for L-MPC$_i$ and N_h prediction steps for HL-MPC. This one, providing the optimal energy references to the L-MPC regulators, is designed with a longer prediction horizon with respect to each L-MPC$_i$, precisely setting $N_h\tau_h \geq N_i\tau_i + \tau_h, \forall i \in \mathcal{N}$.

A. High-level coordination of a multi-energy system

The HL-MPC layer considers a reduced energy model for each $\mathcal{S}_i$, formulating a model structure independent on the specific energy domain. Denote with $p_i^{gh}(k_h)$, $p_i^{lh}(k_h) \in \mathbb{R}$ the total generated and absorbed power in $\mathcal{S}_i$ at k_h, respectively. Moreover, use $e_i^h(k_h) \in \mathbb{R}$ to indicate the total energy stored in $\mathcal{S}_i$ at k_h. Thus, equation (4) can be discretized with sampling period τ_h as

$$\begin{aligned} e_i^h(k_h+1) \;=\; & e_i^h(k_h) \;+\; \tau_h \left(p_i^{gh}(k_h) - p_i^{lh}(k_h) + \right. \\ & \left. + \sum_{j \in \mathcal{N}_i^{\text{in}}} \eta_{ji}\, p_{ji}^h(k_h) - \sum_{j \in \mathcal{N}_i^{\text{out}}} p_{ij}^h(k_h) \right), \end{aligned} \tag{14}$$

enabling to obtain a dynamical model representing $\mathcal{S}_i$ from the energetic point of view.

The main objective of HL-MPC is to optimize the energy stored in each $\mathcal{S}_i$ and the power exchanges among $\mathcal{S}_1, \ldots, \mathcal{S}_M$, considering the minimization of an overall production cost. To perform these tasks, the HL-MPC is assumed to have available the following aggregated information for each $\mathcal{S}_i$

- the bounds of the total storable energy $\bar{e}_i^h$, $\underline{e}_i^h \in \mathbb{R}$;
- the required energy nominal level $e_i^{h\,o} \in \mathbb{R}$;
- the bounds of the total generated power $\bar{p}_i^{gh}, \underline{p}_i^{gh} \in \mathbb{R}$;
- the total generation cost function, i.e., $c_i^{gh} : \mathbb{R}^{g_i} \to \mathbb{R}_{\geq 0}$, expressing the total generation cost as a function of p_i^{gh}, i.e., $c_i^{gh}\big(p_i^{gh}\big)$.

Moreover, the HL-MPC receives at time instants $t = k_h\tau_h$ the following variables from each L-MPC$_i$

- the total energy stored at k_h in $\mathcal{S}_i$, denoted as $\widetilde{e}_i^h(k_h) \in \mathbb{R}$;
- the expected total power absorption in $\mathcal{S}_i$, denoted as $\widetilde{p}_i^{lh}(k) \in \mathbb{R}$, with $k \in \mathcal{T}_h = \{k_h, \ldots, k_h + N_h - 1\}$.

For the sake of clarity, the detailed definition of the mentioned variables will be given in the next section, where the L-MPC$_i$ problems are formulated.

Letting the prediction horizon used in HL-MPC defined by $\mathcal{T}_h$, the high-level control problem is formulated as follows

$$\begin{aligned} \min_{\substack{p_i^{gh}(\cdot),\forall i \in \mathcal{N}, \\ p_{ij}^h(\cdot),\forall (i,j) \in \mathcal{E}}} & \sum_{\forall k \in \mathcal{T}_h} \left(\sum_{\forall i \in \mathcal{N}} c_i^{gh}\big(p_i^{gh}(k)\big) + \sum_{\forall (i,j) \in \mathcal{E}} c_{ij}^{ph} \,|\, p_{ij}^h(k) \,| \right) + \\ & + \sum_{\forall i \in \mathcal{N}} \lambda_i \left(e_i^h(k_h + N_h) - e_i^{h\,o} \right)^2 \end{aligned} \tag{15a}$$

subject, $\forall k \in \mathcal{T}_h$, $\forall i \in \mathcal{N}$, to (14) and

$$\underline{e}_i^h \leq e_i^h(k) \leq \bar{e}_i^h, \tag{15b}$$

$$\underline{p}_i^{gh} \leq p_i^{gh}(k) \leq \bar{p}_i^{gh}, \tag{15c}$$

$$e_i^h(k_h) = \widetilde{e}_i^h(k_h), \tag{15d}$$

$$\underline{p}_{ij}^h \leq p_{ij}^h(k) \leq \bar{p}_{ij}^h\,, \qquad \forall (i,j) \in \mathcal{E}. \tag{15e}$$

The cost function (15a) comprises the overall cost for the produced power in each $\mathcal{S}_i$, the one to implement power exchanges among interconnected subsystems, and a terminal cost with coefficient $\lambda_i \in \mathbb{R}_{\geq 0}$ included to prevent excessive variations of e_i^h with respect to the nominal value $e_i^{h\,o}$. The power exchanges cost is expressed using the term $c_{ij}^{ph} \in \mathbb{R}_{\geq 0}$ weighting the absolute value of p_{ij}^h, which is bounded between $\underline{p}_{ij}^h \leq 0$ and $\bar{p}_{ij}^h \geq 0$ in (15e), $\forall (i,j) \in \mathcal{E}$. On the other hand, the variables of each $\mathcal{S}_i$ are constrained by the total power and energy bounds (15b)-(15c), and by the initial energy state (15d).

The solution to (15) is the optimal sequence over $\mathcal{T}_h$ of the total power production in each $\mathcal{S}_i$ and of the power exchanges among $\mathcal{S}_1, \ldots, \mathcal{S}_M$. The optimal energy to be stored in each $\mathcal{S}_i$, indicated with $e_i^{h*}(k \,|\, k_h)$, $k \in \mathcal{T}_h$, can be obtained iterating (14) and is sent as a reference to each L-MPC$_i$. The same holds for the optimal power exchanges computed at k_h, indicated with $p_{ij}^{h*}(k \,|\, k_h)$, $k \in \mathcal{T}_h$, where, in particular, the first step of the sequence is directly imposed by the HL-MPC according to the receding horizon approach, i.e., $p_{ij}(t) = p_{ij}^{h*}(k_h \,|\, k_h)$, for $t \in [k_h\tau_h,\, k_h\tau_h + \tau_h]$. Finally, the power production in each $\mathcal{S}_i$ is re-optimized by the corresponding L-MPC$_i$ with sampling period $\tau_i \leq \tau_h$, considering local constraints, costs and disturbances.

B. Local MPC regulation for single energy subsystem

Each L-MPC$_i$ regulates $\mathcal{S}_i$ considering its discretized dynamics, i.e.,

$$x_i(k_i+1) = \tilde{f}_i^d(x_i(k_i), u_i(k_i), \widetilde{d}_i(k_i))\,, \tag{16}$$

where $\tilde{f}_i^d$ derives from (1) applying a suitable integration method. Letting the prediction horizon used in L-MPC$_i$ be $\mathcal{T}_i = \{k_i, \ldots, k_i + N_i - 1\}$, the local control problem formulation follows

$$\min_{u_i(\cdot),\,\sigma_i(\cdot)} \quad \sum_{\forall k\in\mathcal{T}_i} \Big(c_i^{g\prime}\, p_i^g(k) \,+\, \gamma_i\, \sigma_i(k) \Big) \tag{17a}$$

subject, $\forall k \in \mathcal{T}_i$, to (16) and

$$\underline{x}_i \le x_i(k) \le \bar{x}_i, \tag{17b}$$
$$\underline{u}_i \le u_i(k) \le \bar{u}_i, \tag{17c}$$
$$p_i^g(k) \;=\; \phi_i(x_i(k), u_i(k))\,, \tag{17d}$$
$$\underline{p}_i^{\,g} \le p_i^g(k) \le \bar{p}_i^{\,g}\,, \tag{17e}$$
$$e_i(k) \;=\; \xi_i(x_i(k))\,, \tag{17f}$$
$$e_i(k) \;\le\; e_i^{h*}\left(\left\lfloor \frac{k}{H_i} \right\rfloor | \, k_h \right) + \sigma_i(k)\,, \tag{17g}$$
$$e_i(k) \;\ge\; e_i^{h*}\left(\left\lfloor \frac{k}{H_i} \right\rfloor | \, k_h \right) - \sigma_i(k)\,, \tag{17h}$$
$$\sigma_i(k) \;\ge\; 0\,, \tag{17i}$$
$$p_{ij}(k) \;=\; p_{ij}^{h*}\left(\left\lfloor \frac{k}{H_i} \right\rfloor | \, k_h \right), \qquad \forall j \in \mathcal{N}_i^{\text{out}}\,, \tag{17j}$$
$$p_{ji}(k) \;=\; p_{ji}^{h*}\left(\left\lfloor \frac{k}{H_i} \right\rfloor | \, k_h \right), \qquad \forall j \in \mathcal{N}_i^{\text{in}}\,. \tag{17k}$$

The L-MPC$_i$ cost function (17a) is constituted of two terms. The first term expresses the local power production cost, with $c_i^g \in \mathbb{R}^{g_i}_{\ge 0}$ including the cost of each single power generation in $\mathcal{S}_i$, and the second term minimizing the slack variable $\sigma_i \in \mathbb{R}_{\ge 0}$, weighted by $\gamma \in \mathbb{R}_{>0}$ selected as $\gamma_i \gg \max(c_i^g)$. This slack variable σ_i is introduced to ensure problem feasibility while imposing the HL-MPC energy reference through (17f)-(17i), where it is recalled that, given the definition of τ_h, $k_h = \left\lfloor \frac{k_i}{H_i} \right\rfloor$, $\forall i \in \mathcal{N}$. The optimal power exchanges are included as hard constraints in (17j)-(17k), as these are directly imposed by the HL-MPC. The L-MPC$_i$ regulates $\mathcal{S}_i$ considering its discrete dynamics in (16), and the local states and inputs constraints in (17b)-(17c). Local power injections, defined in (17d), are bounded in (17e). Moreover, it is assumed that a prediction of local disturbances over $\mathcal{T}_i$ is available, otherwise they are considered constant.

Each L-MPC$_i$ enables the fine regulation of $\mathcal{S}_i$, considering local production costs and constraints, while tracking the HL-MPC references of energy and power. Precisely, the first step of the optimal input sequence computed by (17), i.e., $u_i^*(k|k_i)$, $\forall k \in \mathcal{T}_i$, is implemented in $\mathcal{S}_i$, implying that $u_i(t) = u_i^*(k_i|k_i)$ for $t \in [k_i\tau_i,\, k_i\tau_i + \tau_i]$.

Definition of aggregated variables of the energy subsystems: As mentioned in the previous section, the HL-MPC requires some aggregated information regarding each $\mathcal{S}_i$, namely:

- The bounds of the total stored energy in $\mathcal{S}_i$, which are functions of the local state ones. In particular, if the function $\xi_i(\cdot)$ is monotonically increasing (as the ones of the example described in Section II-B), it follows that $\underline{e}_i^h = \xi_i(\underline{x}_i)$ and $\bar{e}_i^h = \xi_i(\bar{x}_i)$;
- The nominal energy level $e_i^{h\,o}$ in $\mathcal{S}_i$ can be defined as a function of state nominal values, denoted as x_i^o, and implying that $e_i^{h\,o} = \xi_i(x_i^o)$;
- The bounds of total generated power in $\mathcal{S}_i$, which can be computed as the sum of the local bounds, i.e., $\bar{p}_i^{gh} = \mathbb{1}'_{g_i} \bar{p}_i^{\,g}$ and $\underline{p}_i^{gh} = \mathbb{1}'_{g_i} \underline{p}_i^{\,g}$;
- The overall cost of the total generated power in $\mathcal{S}_i$, which can be derived through different methods. A simplistic solution is to exploit an average cost, as in [35], i.e., $c_i^{gh}\big(p_i^{gh}\big) = \big(\frac{1}{g_i}\mathbb{1}'_{g_i} c_i^g\big)\, p_i^{gh}$, with g_i representing the number of generators in $\mathcal{S}_i$. On the other hand, a more precise convex quadratic approximation of $c_i^{gh}\big(p_i^{gh}\big)$ can be computed, using the procedure reported [36]. Finally, an alternative method exploiting the structure of problem (17) and leading to a piece-wise definition of $c_i^{gh}\big(p_i^{gh}\big)$ is reported in Appendix A.

On the other hand, the HL-MPC requires also to measure specific variables from each L-MPC$_i$ at each $t = k_h\tau_h$, defining the energy and power conditions of $\mathcal{S}_i$. These are

- The total energy stored, which can be derived from the local state variables as $\widetilde{e}_i^h(k_h) = e_i(k_i) = \xi_i(x_i(k_i))$, with $k_i = k_h H_i$;
- The expected load power absorption in $\mathcal{S}_i$, denoted as $\widetilde{p}_i^{lh}(k)$ with $k \in \mathcal{T}_h$, estimated exploiting (2b) and assuming to have available predictions on the future states, inputs and disturbances in $\mathcal{S}_i$, e.g., given by the optimal solution of (17). Thus, assuming to know future predictions of local load power absorptions in $\mathcal{S}_i$ and indicating it with $\widetilde{p}_i^l(k_i)$, it follows that $\widetilde{p}_i^{lh}(k) = \mathbb{1}'_{l_i} \widetilde{p}_i^l(k\,H_i)$, $\forall k \in \mathcal{T}_h$.

Remark 3.1: The proposed hierarchical control architecture can be implemented with a fully distributed scheme, e.g., similarly to [37], avoiding to share even aggregated information of each $\mathcal{S}_i$ to a central entity. In fact, the HL-MPC control problem (15), exploiting reduced energy models for $\mathcal{S}_1, \ldots, \mathcal{S}_M$, is convex if the overall costs $c_i^{gh}\big(p_i^{gh}\big)$ are defined with convex functions as well (e.g., using the method proposed in [36]). The convexity of (15) would enable its fully distributed computation with guaranteed optimality and convergence, e.g., using the algorithms proposed in [38], [39].

Remark 3.2: The analysis of the recursive feasibility of (15) and (17) is a complex task due to model nonlinearities and disturbance uncertainties. From a practical point of view, the feasibility of (15) can be assumed provided that $\mathcal{S}_1, \ldots, \mathcal{S}_M$ are equipped with sufficient generating power to keep their total energy in the prescribed bounds, considering also the possibility of multi-energy power transfers. In particular, if subsystems are designed such that $\underline{p}_i^{gh} \le \widetilde{p}_i^{lh} \le \bar{p}_i^{gh}$ $\forall i \in \mathcal{N}$, it can be shown that a feasible solution to (15) always exist, because each $\mathcal{S}_i$ can balance its own power absorption without exploiting power exchanges.
The feasibility analysis of (17) is more complex, mainly due to state constraints (17b). However, note that the HL-MPC computes the optimal power transfers considering total energy and power constraints for each $\mathcal{S}_i$, which bounds depend on the

local states and power limits, as previously described. Thus, the feasibility of (17) can be assumed provided that local inputs are sufficiently sized to ensure that (17b) and (17e) are respected. It is also worth noting that, as usual in MPC approaches [40], the recursive feasibility can be guaranteed by the use of additional slack variables in the formulation of constraints (15b) at the high level, and of (17b) and (17e) at the low level.

IV. Benefit sharing in multi-energy systems

The proposed hierarchical control architecture enables the optimized control of a multi-energy system $\mathcal{S}^\dagger$, but it does not consider how the achieved benefit is shared among subsystems $\mathcal{S}_1, \dots, \mathcal{S}_M$. In fact, the multi-energy operation can imply an additional cost to few subsystems and an increased gain to others, even though the overall operational cost of $\mathcal{S}^\dagger$ decreases with respect to the independent regulation of each $\mathcal{S}_i$. This benefit sharing problem is here recast in the framework of cooperative game theory[3], formulating it as a bargaining problem [29].

A bargaining problem, or game, involves a group of players having to reach an agreement about a set of feasible payoff solutions, with the common objective of maximizing their own utility. In particular, it involves M players and a pair (Θ, δ), where $\Theta \subseteq \mathbb{R}^M$ identifies the set of feasible players payoff, whereas $\delta \in \mathbb{R}^M$ corresponds to a given disagreement outcome, i.e., the one that players achieve if they do not cooperate. It is assumed that $\exists \theta \in \Theta$, so that $\theta > \delta$, meaning that there exists at least one cooperative feasible payoff solution exceeding the disagreement outcome for each subsystem. As described in details in [41], there is a unique bargaining solution possessing specific common properties (e.g., the independence of equivalent utility representations).

This is the one maximizing the weighted geometric mean of players utilities[4], i.e.,

$$\begin{aligned} \max_{\theta_1, \dots, \theta_M} \quad & \prod_{i=1}^{M} (\theta_i - \delta_i)^{\alpha_i} \\ \text{subject to} \quad & \\ & \theta \in \Theta\,, \\ & \theta > \delta\,, \end{aligned} \tag{18}$$

where $\alpha_i \in \mathbb{R}_{>0}$ is a parameter denoting the bargaining power of the ith player, defined so that $\sum_{i=1}^{M} \alpha_i = M$. In particular, if $\alpha_i = 1$, $\forall i \in \{1, \dots, M\}$, the solution of (18) is named symmetric Nash bargaining solution, otherwise it is named nonsymmetric Nash bargaining solution [42].

Now, consider our case study and assume that the interaction over multiple energy vectors among subsystems $\mathcal{S}_1, \dots, \mathcal{S}_M$ achieves an overall cost lower than the one achieved by their independent regulation. Moreover, suppose that subsystems agree with a time-period τ_b on how the achieved benefit must be shared. For the sake of simplicity, τ_b is chosen so that $\tau_b = B_i \tau_i$, $\forall i \in \mathcal{N}$, with $B_i \in \mathbb{N}$, and $\tau_b = G_h \tau_h$, with $G_h = B_i / H_i > 1$. Moreover, define with $k_b \in \mathbb{N}$ the discrete time index used in the benefit sharing problem and with $t = k_b \tau_b$ the time instants where agreement must be reached for the time period $[\,(k_b - 1)\tau_b,\ k_b \tau_b\,]$. The cost that each $\mathcal{S}_i$ has effectively afforded over $[(k_b - 1)\tau_b,\ k_b \tau_b\,]$ is

$$\begin{aligned} J_i^{\mathrm{c}}(k_b) = & \sum_{k\,=\,(k_b-1)B_i}^{k_b B_i} \left(c_i^{g\prime}\, p_i^{g*}(k|k) \right) + \\ & + \sum_{k\,=\,(k_b-1)G_h}^{k_b G_h} \left(\sum_{j \in \mathcal{N}_i^{\mathrm{in}}} c_{ji}^{ph}\, |p_{ji}^{h*}(k|k)| \right), \end{aligned} \tag{19}$$

where $p_i^{g*}(k|k)$ is the power generation solution implemented by the L-MPC$_i$, i.e., the first step of the optimal sequence computed at $t = k\tau_i$ by problem (17). On the other hand, as a convention, it is chosen in (19) that the costs to implement power transfers, if present, are applied to the receiving subsystems. It is worth noting that the cost incurred by each $\mathcal{S}_i$ over the period $[(k_b - 1)\tau_b,\ k_b \tau_b\,]$ could be also directly derived from local measurements, e.g., by substituting, in (19), the optimal generated and transferred power with the effectively measured ones.

To evaluate the benefit introduced by the multi-energy operation, assume that each $\mathcal{S}_i$ can be independently regulated, i.e., local input and generation capability are sufficient to satisfy the internal demand without exploiting power exchanges. Thus, the cost that each $\mathcal{S}_i$ would have incurred if independently regulated can be computed by solving, for each $k_i \in [(k_b - 1)B_i,\ k_b B_i]$, the following problem

$$\min_{u_i(\cdot)} \quad \sum_{\forall k \in \mathcal{T}_i} \left(c_i^{g\prime}\, p_i^{g}(k) \right) \tag{20a}$$

subject, $\forall k \in \mathcal{T}_i$, to (16), (17b)-(17e) and

$$p_{ij}(k) \;=\; 0, \qquad \forall j \in \mathcal{N}_i^{\mathrm{out}}\,, \tag{20b}$$

$$p_{ji}(k) \;=\; 0, \qquad \forall j \in \mathcal{N}_i^{\mathrm{in}}\,. \tag{20c}$$

This corresponds to the L-MPC$_i$ problem in case each subsystem $\mathcal{S}_i$ does not exchange energy with the others, aiming solely to the minimization of its internal cost. The optimal power generation computed by (20) is denoted with $p_i^{g**}(k|k)$. Therefore, the cost that each $\mathcal{S}_i$ would have afforded over $[\,(k_b - 1)\tau_b,\ k_b \tau_b\,]$, if independently regulated, is

$$J_i^{\mathrm{nc}}(k_b) = \sum_{k\,=\,(k_b-1)B_i}^{k_b B_i} c_i^{g\prime}\, p_i^{g**}(k|k)\,. \tag{21}$$

It is possible now to define the effective benefit that each $\mathcal{S}_i$ has achieved thanks to the multi-energy interaction over the time period $[\,(k_b - 1)\tau_b,\ k_b \tau_b\,]$, i.e.,

$$\Delta J_i(k_b) = J_i^{\mathrm{nc}}(k_b) - J_i^{\mathrm{c}}(k_b)\,, \tag{22}$$

which is positive in case subsystem $\mathcal{S}_i$ achieves a lower cost while exchanging energy with the others. A positive benefit

[3]For the sake of simplicity, it is here assumed that all subsystems in $\mathcal{S}^\dagger$ take part in the multi-energy cooperation and share the achieved benefit. The scenario where some subsystems decide to not join the coalition $\mathcal{S}^\dagger$ is not here addressed, being the overall cooperation the most convenient scenario (for coalitional approaches, the reader is referred to [26], [28]).

[4]For notational simplicity, the Mth power of the weighted geometric average is used in (18), since this is maximized by the same point of the weighted geometric average [41].

is not guaranteed for each $\mathcal{S}_i$, while a total positive benefit is assumed to be achieved in $\mathcal{S}^\dagger$, i.e.,

$$\Delta J^{\text{tot}}(k_b) = \sum_{i=1}^{M} \Delta J_i(k_b) \geq 0\,. \tag{23}$$

Thus, the total benefit $\Delta J^{\text{tot}}(k_b)$ must now be properly shared among $\mathcal{S}_1, \dots \mathcal{S}_M$, so that all players take advantage from the multi-energy interaction. To do that, introduce $\pi_{ij}(k_b) \in \mathbb{R}$, $\forall (i,j) \in \mathcal{E}$, expressing a payment transfer from $\mathcal{S}_i$ to $\mathcal{S}_j$. Then, the following problem is solved at each $t = k_b \tau_b$

$$\max_{\substack{\pi_{ij} \\ \forall (i,j) \in \mathcal{E}}} \quad \prod_{i=1}^{M} (z_i + \Delta J_i)^{\alpha_i} \tag{24a}$$

$$\text{subject to, } \forall i \in \mathcal{N}, \tag{24b}$$

$$z_i = \sum_{j \in \mathcal{N}_i^{\text{in}}} \pi_{ji} - \sum_{j \in \mathcal{N}_i^{\text{out}}} \pi_{ij}\,, \tag{24c}$$

$$z_i > -\Delta J_i\,, \tag{24d}$$

where, for the sake of clarity, the dependency on k_b has been removed. The variable z_i represents the net payment transfer of each $\mathcal{S}_i$, defined as the difference between the incoming and outgoing payment transfers from, or to, its neighbours, as dictated by (24c). Equation (24d) states that the sum of net payment z_i and of the benefit ΔJ_i must be positive for each $\mathcal{S}_i$, otherwise players would be not incentivized to cooperate. It is worth noting that (24c) implies that

$$\sum_{\forall i \in \mathcal{N}} z_i = \sum_{\forall i \in \mathcal{N}} \sum_{j \in \mathcal{N}_i^{\text{in}}} \pi_{ji} - \sum_{\forall i \in \mathcal{N}} \sum_{j \in \mathcal{N}_i^{\text{out}}} \pi_{ij} = \\ = \sum_{\forall (i,j) \in \mathcal{E}} \pi_{ij} - \sum_{\forall (i,j) \in \mathcal{E}} \pi_{ij} = 0\,,$$

meaning that the sum of the net payments of $\mathcal{S}_1, \dots \mathcal{S}_M$ is balanced, being these used to redistribute the achieved cooperation benefit among subsystems, i.e., $z \in \mathcal{Z} = \{z \in \mathbb{R}^M : \mathbb{1}_M{}' z = 0\}$. Considering the bargaining problem formulation in (18), $\theta_i = z_i$ represents the payoff of each player $\mathcal{S}_i$, while $\delta_i = -\Delta J_i$ identifies its disagreement outcome, i.e., the cost loss (or gain) achieved if subsystems $\mathcal{S}_1, \dots \mathcal{S}_M$ do not cooperate (see (22)).

As mentioned before, α_i in (24a) is a parameter expressing the bargaining power of each $\mathcal{S}_i$. If $\alpha_i = 1$, $\forall i \in \mathcal{N}$, the bargaining problem is symmetric, meaning that the optimal solution of (24) will provide all players the same utility, i.e., $z_1^* + \Delta J_1 = z_2^* + \Delta J_2 = \dots = z_M^* + \Delta J_M$. Note that maximizing the utility of each $\mathcal{S}_i$ in (24) actually corresponds to maximizing the cost reduction achieved by each subsystem with respect to its independent regulation. In fact, it holds that $z_i^* + \Delta J_i = J_i^{\text{nc}} - (J_i^{\text{c}} - z_i^*)$, where the effective final incurred cost of each $\mathcal{S}_i$ is $(J_i^{\text{c}} - z_i^*)$. On the other hand, the total cooperation benefit could be shared according to different strategies exploiting the bargaining power parameters α_i. For instance, α_i can be defined proportionally to the operational cost of each $\mathcal{S}_i$, thus providing a higher cost reduction to subsystems characterized by higher expenses.

Remark 4.1: The benefit sharing problem (24) is assumed to be solved by a central entity, e.g., by an additional control layer or by the HL-MPC itself, as it requires as inputs the benefit achieved by each subsystem $\mathcal{S}_i$, i.e., ΔJ_i. On the other hand, the operations (19)-(22) are separately solved by each $\mathcal{S}_i$, e.g., by the L-MPC$_i$ themselves. It is worth noting that the bargaining problem can be solved in a very reduced computational time and with a large sampling period, being a static problem, as it will be evident in Section V.

Remark 4.2: A different strategy that can be exploited for the benefit sharing problem relies on the Shapley value method [26]. First of all, consider the set of all players $\mathcal{S}^\dagger = \{\mathcal{S}_1, \dots, \mathcal{S}_M\}$ and the achieved benefit by their joint regulation $\Delta J^{\text{tot}}(\mathcal{S}^\dagger) = \sum_{i=1}^{M} \Delta J_i > 0$, defined in (23) (in the following, the time index k_b is removed for notation clarity). The idea of this technique is to redistribute the total achieved benefit $\Delta J^{\text{tot}}(\mathcal{S}^\dagger)$ among all subsystems $\mathcal{S}_1, \dots, \mathcal{S}_M$ based on their effective contribution to the coalition. To do that, consider any possible coalition $\mathcal{C}_l \subseteq \mathcal{S}^\dagger$, with $l \in \{1, \dots, 2^M - 1\}$, and denote with $\Delta J^{\text{tot}}(\mathcal{C}_l)$ the benefit achieved by the joint regulation of $\mathcal{C}_l$. In particular, given a generic coalition $\mathcal{C}_l$, $\Delta J^{\text{tot}}(\mathcal{C}_l)$ can be computed as in (23) by applying the proposed control strategy to the overall $\mathcal{S}^\dagger$ while adding the constraint $p_{ij}^h(k) = 0$, $\forall \mathcal{S}_i, \mathcal{S}_j \notin \mathcal{C}_l$ to (15), i.e., imposing that power exchanges can occur just within $\mathcal{C}_l$. Now, suppose to have computed $\Delta J^{\text{tot}}(\mathcal{C}_l)$ for any $l \in \{1, \dots, 2^M - 1\}$. Then, the Shapley value assigns the final utility to each $\mathcal{S}_i$, denoted as χ_i^*, through the following formula

$$\chi_i^* = \sum_{l=1}^{2^M - 1} \zeta(\mathcal{C}_l, M) \cdot \left(\Delta J^{\text{tot}}(\mathcal{C}_l) - \Delta J^{\text{tot}}(\mathcal{C}_l \setminus S_i) \right)\,, \tag{25a}$$

where

$$\zeta(\mathcal{C}_l, M) = \frac{(M - \text{card}(\mathcal{C}_l))!\,(\text{card}(\mathcal{C}_l) - 1)!}{M!}\,. \tag{25b}$$

The final utility assigned to each $\mathcal{S}_i$ through the Shapley value method is a fraction of the total benefit, implying that $\sum_{i=1}^{M} \chi_i^* = \Delta J^{\text{tot}}(\mathcal{S}^\dagger)$. Considering the formulation of the final utility adopted in the bargaining problem, i.e., $z_i^* + \Delta J_i$, the final net payment transfer for each $\mathcal{S}_i$ using the Shapley value is $z_i^* = \chi_i^* - \Delta J_i$, with ΔJ_i defined by (22).

Conversely to the solution of the bargaining problem (24) with $\alpha_i = 1$ $\forall i \in \mathcal{N}$, now the benefit will be not distributed equally but based on the effective contribution of $\mathcal{S}_i$ to the coalition, i.e., $z_1^* + \Delta J_1 \neq z_2^* + \Delta J_2 \neq \dots \neq z_M^* + \Delta J_M$. Moreover, while the proposed bargaining method implies to just solve (24), the Shapley method requires to solve $2^M - 1$ optimization problems to compute (25), as $\Delta J^{\text{tot}}(\mathcal{C}_l)$ for any possible coalition of subsystems is necessary, making this method often computationally intractable [27].

V. Case studies

The described hierarchical control architecture and benefit sharing algorithm have been tested on two MES case-studies. Firstly, the illustrative example described in Section II-B is considered, showing how the highlighted challenges are solved by the proposed control strategy. Then, a realistic

MES benchmark is considered, where two energy networks referenced in the literature, i.e., an electrical and a thermal one, are effectively regulated by the proposed control architecture.

A. Control of the MES illustrative example

The MES illustrative example, depicted in Figure 2, has been simulated in MATLAB numerically integrating the dynamical equations described in Section II-B, and using the physical parameters reported in Table I. The system has been tested under the regulation of the proposed hierarchical control architecture, implementing a L-MPC regulator for each subsystem, i.e., L-MPC$_1$ for the gas storage tank (subsystem $\mathcal{S}_1$), L-MPC$_2$ for the water thermal system (subsystem $\mathcal{S}_2$) and L-MPC$_3$ for the electrical circuit (subsystem $\mathcal{S}_3$). The HL-MPC, placed at the upper layer, provides the energy set-points to the L-MPC regulators and optimizes the power exchanges among the different subsystems, thus regulating the gas boiler (power transfer from $\mathcal{S}_1$ to $\mathcal{S}_2$) and the thermal resistance (power transfer from $\mathcal{S}_3$ to $\mathcal{S}_2$). The control problems (15) and (17) have been implemented in MATLAB and solved using CasAdi and the IPOPT solver, which are particularly suited for optimizing nonlinear dynamical systems [43]. The main control parameters are reported in Table II (please refer to Section II-B for the physical meaning of the subsystems variables). Please note that $\gamma_i = 10^3$ and $\lambda_i = 10^3$, $\forall i \in \mathcal{N}$. Moreover, note from the Table II that each L-MPC$_i$ regulator runs with a specific sampling period and prediction horizon, chosen consistently with the local requirements of each subsystem. On the other hand, the HL-MPC layer is designed to operate with τ_h = 15 min and $N_h = 16$, optimizing the MES over a prediction horizon larger than the L-MPC regulators ones. The generation costs for each subsystem are depicted in Figure 3(a), where c_1^g is the cost for power injected in the gas tank, c_2^g is the cost for the power generated by the thermal plate and c_3^g is the cost for the electrical power generated by the voltage source. The costs of power interfaces are $c_{12}^{ph} = 0.1$ \$/kW for the gas boiler and $c_{31}^{ph} = 0.01$ \$/kW for the thermal resistance. Moreover, the total costs c_i^{gh} have been derived using the procedure described in Appendix A. The MES example benchmark is tested with time-varying disturbances, which normalized profiles are depicted in Figure 3(b) since they are characterised by different units of measure.

Figure 4 reports a 24-hour simulation of the considered case study, whose numerical results are reported as normalized with respect to their maximum bounds for the sake of clarity. It is evident from Figure 4(a) that the HL-MPC optimal coordination involves a continuous power transfer to $\mathcal{S}_2$, principally from $\mathcal{S}_1$ in the first half of the simulation and from $\mathcal{S}_3$ in the second half. This is mainly due to the generation costs, being $\mathcal{S}_2$ characterized always by the higher one (see Figure 3(a)). While optimally coordinating power transfers among subsystems, the hierarchical control architecture ensures that all local constraints are respected. As an example, consider the time period between 16:00 and 20:00, characterized by an increase of the load water flow q_w in $\mathcal{S}_2$ (dashed-dotted red line in Figure 3(b)). This implies an increment of the power transfer from $\mathcal{S}_3$ and $\mathcal{S}_1$ to $\mathcal{S}_2$ in the same time period

TABLE I
PHYSICAL PARAMETERS OF THE MES EXAMPLE

V_g	0.08 m^3	A	0.049 m^2
c^{lhv}	52.3 MJ/kg	m_w	19.6 kg
L	1 H	c_w	4.186 kJ/(K kg)
C	1 μF	η_{gw}	0.8
k_{wm}	10.5 kW/(K m^2)	η_{ew}	0.9

TABLE II
CONTROL PARAMETERS FOR THE MES EXAMPLE

$\mathcal{S}_i$	$\mathcal{S}_1$ (gas)	$\mathcal{S}_2$ (thermal)	$\mathcal{S}_3$ (electrical)
τ_i	5 min	15 min	1 min
N_i	6	4	12
$(\underline{x}_i, \bar{x}_i)$	$(3, 10)$ kg/m^3	$(75, 90)$ °C	$(2.5, 30)$ A $(5, 20)$ kV
$(\underline{u}_i, \bar{u}_i)$	$(0, 1.5)$ g/s	$(75, 150)$ °C	$(14.4, 22)$ kV
$(\underline{p}_i^g, \bar{p}_i^g)$	$(0, 78.45)$ kW	$(0, 31)$ kW	$(36, 1000)$ kW
e_i^{ho}	21.15 kWh	6.75 kWh	0.3 kWh
$(\underline{p}_{i1}^h, \bar{p}_{i1}^h)$	–	–	–
$(\underline{p}_{i2}^h, \bar{p}_{i2}^h)$	$(0, 42)$ kW	–	$(0, 25)$ kW
$(\underline{p}_{i3}^h, \bar{p}_{i3}^h)$	–	–	–

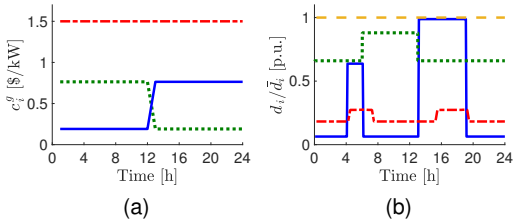


Fig. 3. (a) Power generation costs: c_1^g (solid blue), c_2^g (dotted-dashed red) and c_3^g (dotted green).
(b) Normalized disturbances: d_1, output gas flowrate $q_g^{out}/\bar{q}_g^{out}$, with $\bar{q}_g^{out} = 1.5$ g/s, (solid blue); d_2, output water flowrate $q_w/\bar{q}_w$, with $\bar{q}_w = 1.5$ m^3/s, (dotted-dashed red) and load output water temperature $T^r/\overline{T}^r$, with $\overline{T}^r = 65$°C (dashed yellow); d_3, time-varying load resistance $R/\bar{R}$, with $\bar{R} = 2000\,\Omega$ (dotted green).

(see Figure 4(a)), being local generation in $\mathcal{S}_2$ still too costly. Nevertheless, $\mathcal{S}_1$ is also characterized by a high output gas flowrate q_g, and an extra power transfer to $\mathcal{S}_2$ may cause to violate local state constraints in $\mathcal{S}_1$. Thus, the HL-MPC requires to increase the stored energy in $\mathcal{S}_1$ between 12:00 and 16:00, as evident from Figure 4(b), so that it can support $\mathcal{S}_2$ by transferring the necessary power between 16:00 and 20:00 without violating the local states bounds. The regulation of the L-MPC controllers is depicted in Figure 4(c), ensuring that local inputs and states are optimally controlled at their specific time rates and maintained within the desired bounds. Please note that there is a clear correspondence between the HL-MPC energy references and the local states, e.g., the variation of stored energy in $\mathcal{S}_1$ directly implies a variation of the stored gas density (see Figure 4(b) and (d)).

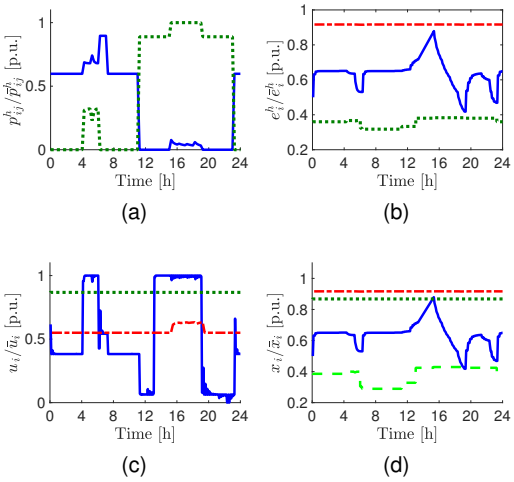


Fig. 4. (a) Power exchanges: $p_{12}/\overline{p}^h_{12}$ (solid blue) and $p_{32}/\overline{p}^h_{32}$ (dotted green).
(b) Energy references: $e_1/\overline{e}^h_1$ (solid blue), $e_2/\overline{e}^h_2$ (dashed-dotted red), $e_3/\overline{e}^h_3$ (dotted green).
(c) Control inputs: q^{in}_g (solid blue), T_m (dashed-dotted red), V (dotted green).
(d) Subsystems states: ρ_g (solid blue), T_w (dashed-dotted red), V_c (dotted green), I (dashed light green).

TABLE III
BARGAINING RESULTS FOR THE MES EXAMPLE

J_i [\$]	$\mathcal{S}_1$ (gas)	$\mathcal{S}_2$ (thermal)	$\mathcal{S}_3$ (electrical)	$\sum_{\forall i}$ (total)
J_i^{nc}	406.5	824.9	2299.4	3530.8
J_i^c	475.2	36	2367.1	2878.3
z_i^*	286.2	−571.4	285.2	0
$J_i^c - z_i^*$	189	607.4	2081.9	2878.3

The benefit sharing problem discussed in Section IV has been solved through the bargaining method at the end of the overall simulation, i.e., using $\tau_b = 24$ h, and considering a symmetric bargaining, i.e., $\alpha_i = 1$, $\forall i \in \mathcal{N}$. The value of the cost functions (19) and (21) are reported Table III. As evident, the optimal MES coordination is economically convenient for the total MES $\mathcal{S}^\dagger$, but it could be not convenient for each single subsystem. As evident, the water thermal system $\mathcal{S}_2$ is the only one achieving a cost reduction with respect to its independent regulation ($J_2^c < J_2^{nc}$), being it supported with the extra power produced by the other subsystems. In fact, solving the benefit sharing problem (24), its optimal solution implies a payment transfer z_i^* from $\mathcal{S}_2$ to $\mathcal{S}_1$ and $\mathcal{S}_3$, eventually resulting in a MES interaction economically convenient for all subsystems. As clear from Table III, the effective final cost, i.e., $J_i^c - z_i^*$, is lower than the one achieved by the independent regulation, i.e., J_i^{nc}, for each subsystem belonging to $\mathcal{S}^\dagger$. For the sake of comparison, the benefit sharing problem is solved also through the Shapley value method, described in Remark 4.2. In particular, calculating the achieved benefit by each possible coalition (see Remark 4.2), it is obtained that: $\Delta J^{\text{tot}}(\{\mathcal{S}_i\}) = 0\$$, $\forall i \in \mathcal{N}$, $\Delta J^{\text{tot}}(\{\mathcal{S}_1, \mathcal{S}_3\}) = 0\$$, $\Delta J^{\text{tot}}(\{\mathcal{S}_1, \mathcal{S}_2\}) = 391.2\$$, $\Delta J^{\text{tot}}(\{\mathcal{S}_2, \mathcal{S}_3\}) = 483.4\$$, $\Delta J^{\text{tot}}(\{\mathcal{S}_1, \mathcal{S}_2, \mathcal{S}_3\}) = 652.4\$$. First of all, these results witness that the cooperation among all subsystems is the scenario that achieves the maximum total benefit. Applying the Shapley value method discussed in Remark 4.2, the final outcome is $z_1^* = 190.48$, $z_2^* = -426.95$, $z_3^* = 235.57$, leading to the following effective final cost for each subsystem: $J_1^c - z_1^* = 284.8$, $J_2^c - z_2^* = 462.2$, $J_2^c - z_3^* = 2131.5$. Comparing these results with the one reported in Table III, it is evident that Shapley method assigns to the water thermal system $\mathcal{S}_2$ a lower final effective cost with respect to the bargaining method. This is motivated by the fact that Shapley method redistributes the benefit based on the contribution of each $\mathcal{S}_i$ to the coalition, and $\mathcal{S}_2$ is the element that actually enables the power exchanges among the different subsystems and, consequently, leads to cost saving. Note that, given the benefit problem formulation, also the Shapley value method ensures that the final cost of each $\mathcal{S}_i$, i.e., $J_i^c - z_i^*$, is lower than the one achieved by the independent regulation, i.e., J_i^{nc}.

Finally, the performances achieved from a centralized controller running with $\tau_{centr} = 15$ min are also reported, computed as described in Appendix B. The obtained optimal cost functions are $J_1^{centr} = 473.14$, $J_2^{centr} = 30.59$, and $J_3^{centr} = 2356.6$, whereas the total cost is $\sum_{\forall i} J_i^{centr} = 2860.3$. Comparing these values with J_i^c in Table III, it is evident that the sub-optimality introduced by the proposed hierarchical strategy is quite limited, i.e., $(\sum_{\forall i} J_i^{centr} - J_i^c)/(\sum_{\forall i} J_i^{centr}) = -0.6\%$.

B. Control of a realistic networked MES benchmark

The proposed hierarchical control architecture has been also tested considering the realistic multi-energy scenario depicted in Figure 5, where two energy networks are jointly coordinated, i.e., the AROMA District Heating Network (DHN) [3] and the IEEE 37-bus electrical network [44]. According to the modelling framework presented in Section II, we denote the IEEE 37-bus electrical subsystem as $\mathcal{S}_1$ and the AROMA DHN subsystem as $\mathcal{S}_2$. The two subsystems are energetically connected through a heat pump, which converts electrical power into thermal one, transferring energy from $\mathcal{S}_1$ to $\mathcal{S}_2$, as clear from Figure 5. As a consequence, $\mathcal{S}^\dagger$ can be represented by a graph G$(\mathcal{N}, \mathcal{E})$ with $\mathcal{N} = \{\mathcal{S}_1, \mathcal{S}_2\}$ and $\mathcal{E} = (\mathcal{S}_1, \mathcal{S}_2)$.

The detailed models of $\mathcal{S}_1$ and $\mathcal{S}_2$ are not here reported in details for the sake of compactness, being them relying on well-known physical equations for electrical and thermo-hydraulics network systems [3], [18]. Nevertheless, the reader is referred to [18] and [45, Chapter 1] for the detailed modelling of $\mathcal{S}_1$ and $\mathcal{S}_2$. Hereafter, a general description of each $\mathcal{S}_i$ in $\mathcal{S}^\dagger$ and of the involved main variables is given.

The IEEE 37-bus electrical subsystem $\mathcal{S}_1$ is equipped with three storage batteries (nodes E5, E21, and E30), two photovoltaic generators (nodes E15 and E32), twelve loads (nodes E6-9, E16-19, and E33-36), and a converter-interfaced connection with the main utility (node E26), as depicted in Figure 5. The vector of local states $x_1(t)$ comprises the state of charges of batteries, which dynamics is described through the

battery integrator model [46]. The local control inputs are the active power absorbed (delivered) from (to) the main utility, i.e., $p_1^g(t) = u_1(t)$ (defined to be positive if absorbed from the main utility), and the active power output of batteries in nodes E5 and E30, i.e., $p_2^g(t) = u_2(t)$ and $p_3^g(t) = u_3(t)$ (defined to be positive if injected into the grid). In fact, the battery in node E21 is not power-controlled, but it is regulated to maintain a fixed voltage at its node (similarly to [46]), implying that its output power automatically ensures the overall power balance. The load power absorption and the photovoltaic power production are local disturbances, and so compacted in $d_1(t)$. The electrical power absorbed by the heat pump (node E11) is $w_1(t) = p_{12}(t)$, whereas the total energy in $\mathcal{S}_1$ is the sum of the ones stored in the batteries, implying that $e_1(t)$ linearly depends on $x_1(t)$. On the other hand, the electrical model of $\mathcal{S}_1$ is nonlinear, being it based on the power-flow equations [18].

The AROMA DHN subsystem $\mathcal{S}_2$ is equipped with a thermal boiler, a thermal storage (with a constant water mass), and eight thermal loads (see Figure 5). In particular, the district heating network is constituted of two parallel layers: an upper network which supplies hot water to the loads, and a lower returning layer where the output load water flows back towards the heating stages. The district heating network and the thermal storage are modelled through the finite-volume method, where thermal pipes and the thermal storage are partitioned in finite-volume sections parallel to the water flow direction, and each finite-volume section is described by a local lumped temperature model [3], [47]. On the other hand, the thermal boiler and loads are described through static models, given their smaller time constants with respect to the thermal network ones [48]. Considering the model of $\mathcal{S}_2$, the local state $x_2(t) = [x_{21}(t)' \; x_{22}(t)']'$ comprehends the water temperature in the sections of the heating supply network, included in $x_{21}(t)$, and in the ones of the thermal storage, included in $x_{22}(t)$. Moreover, as common in practice [48], the thermal boiler is temperature-regulated, and the inlet/outlet water flowrate of the thermal storage is regulated through a local pump. Thus, the local inputs $u_2(t) = [u_{21}(t) \; u_{22}(t)]'$ are the output temperature of the thermal boiler, denoted with $u_{21}(t)$, and the water flowrate for the thermal storage, denoted as $u_{22}(t)$ (defined as positive if hot water from the upper network layer is injected in the thermal storage). The local power generation $p_2^g(t)$ includes the power injected by the thermal boiler, whereas the vector of disturbances $d_2(t)$ are the power absorptions of thermal loads. The energy $e_2(t)$ stored in $\mathcal{S}_2$ is a linear function of $x_2(t)$, i.e., of the temperatures of pipes and storage sections, as in (12) for the MES illustrative example. Nevertheless, the model of $\mathcal{S}_2$ is nonlinear, mainly due to transport dynamics in thermo-hydraulic networks and their nonlinear dependence on the water flowrate.

The physical parameters of the IEEE 37-bus electrical network and of the AROMA district heating network, as well as their topologies, are reported in details in [3], [44], whereas additional parameters regarding generation and storage units are available in Table IV. The power profiles of the electric loads and of the photovoltaic generators are depicted in Figure 6(a) and (b), respectively, whereas the power absorbed by thermal loads is reported in Figure 6(c). The cost of the electrical power exchanged with the main utility and the one of the gas power consumed by the thermal boiler are reported in Figure 6(d). The main control design parameters adopted for the numerical tests are reported in Table V, considering also that $\gamma_i = 10^3$ and $\lambda_i = 10$, $\forall i \in \mathcal{N}$. As clear from Table V, also in this case the L-MPC regulators operate with different sampling periods and prediction horizons, given the different involved time constants in electrical and thermal systems. On the other hand, the HL-MPC layer is executed at a slower time rate, having a sampling period of $\tau_h = 1$ h and a prediction horizon of $N_h = 24$ steps. Also for the considered case study, control problems have been implemented and solved using CasAdi and the IPOPT solver in MATLAB. The overall MES benchmark is simulated using Simscape, a MATLAB library which enables the co-simulation of different physical domains (e.g., electrical, thermal liquid, etc.).

Figure 7 reports the numerical results obtained by running the proposed hierarchical architecture on the considered MES benchmark for one day. Taking into account the electrical energy cost depicted in Figure 6(d), it is clear from Figure 7(b) that the HL-MPC coordinates $\mathcal{S}_1$ and $\mathcal{S}_2$ so as to increase the stored energy when the cost is lower (i.e., before 7:00 and between 9:00 and 16:00), and to use the stored energy when the cost is higher (i.e., around 8:00 and 19:00). Coherently, the HL-MPC also regulates the heat pump so that its maximum power is transferred from $\mathcal{S}_1$ to $\mathcal{S}_2$ when the electrical energy cost is lower, as shown in Figure 7(a). In turn, the L-MPC controllers regulate their own subsystems to track the energy

TABLE IV
ADDITIONAL PHYSICAL PARAMETERS FOR THE MES REALISTIC BENCHMARK

Batteries energy capacity	33.3 kWh
Thermal storage volume	99.5 m^3
Thermal storage heat transfer coefficient	0.00121 W/(m^2 K)
Thermal boiler efficiency	0.8
Heat pump Coefficient of Performance	2.5
Heat pump water flow-rate	5 kg/s
Thermal loads return temperature	65 °C

TABLE V
CONTROL DESIGN PARAMETERS FOR THE MES REALISTIC BENCHMARK

$\mathcal{S}_i$	$\mathcal{S}_1$ (IEEE 37-bus system)	$\mathcal{S}_2$ (AROMA DHN)
τ_i	1 min	30 min
N_i	30	48
$(\underline{x}_i, \bar{x}_i)$	(10, 90) %	x_{21} : (75, 85) °C x_{22} : (65, 85) °C
$(\underline{u}_i, \bar{u}_i)$	$(-250, 250)$ kW	u_{21} : (75, 85) °C u_{22} : (-6, 6) kg/s
$(\underline{p}_i^g, \bar{p}_i^g)$	$(-250, 250)$ kW	$(0, 500)$ kW
e_i^{ho}	50 kWh	10.5 MWh
$(\underline{p}_{i2}^h, \bar{p}_{i2}^h)$	$(0, 200)$ kW	–

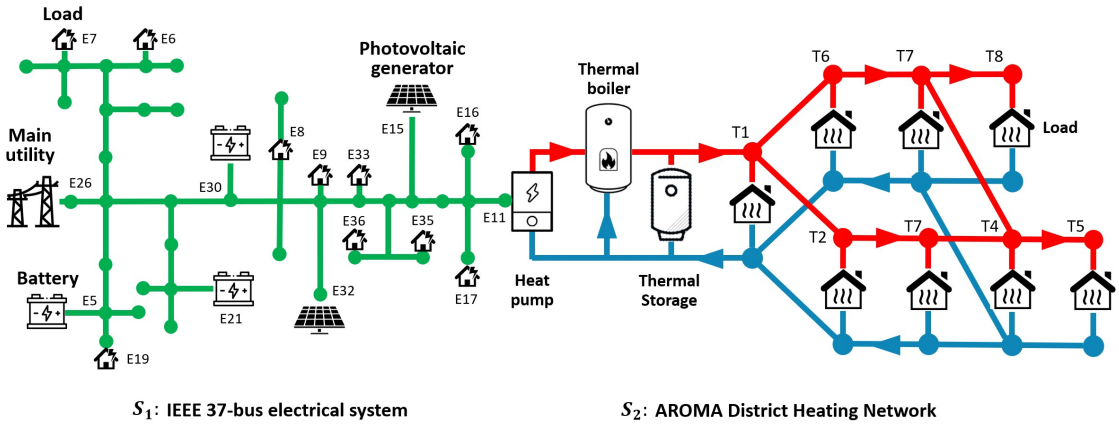


Fig. 5. MES realistic case study: IEEE 37-bus electrical network [44] (subsystem $\mathcal{S}_1$) and AROMA district heating network [3] (subsystem $\mathcal{S}_2$).

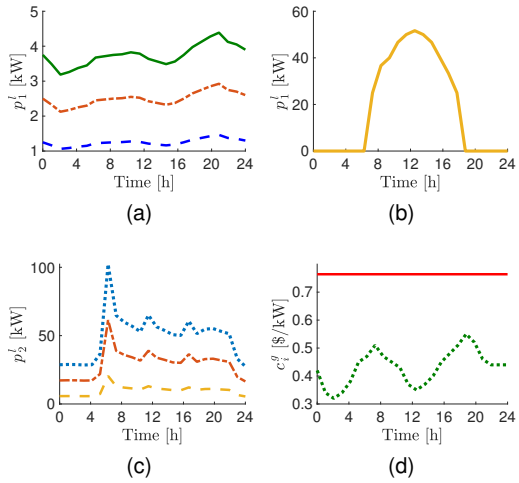


Fig. 6. (a) Active power absorbed by loads in nodes E6-E9 (dashed blue), load in nodes E16-E19 (dashed-dot red), load in nodes E33-E36 (solid green). (b) Active power produced by photovoltaic generators in nodes E15 and E32. (c) Thermal power absorbed by loads in nodes T1, T2, T6 (dotted blue), by loads in nodes T3, T4 and T7 (dashed-dotted red) and by loads in nodes T5 and T8 (dashed yellow).
(d) Cost of consumed gas power by the thermal boiler (solid red) and cost of exchanged electrical energy with the main utility (dotted green).

TABLE VI
BARGAINING RESULTS FOR THE MES REALISTIC EXAMPLE

J_i [$]	$\mathcal{S}_1$ (IEEE 37-bus system)	$\mathcal{S}_2$ (AROMA DHN)	$\sum_{\forall i}$ (total)
J_i^{nc}	-128.4	6881	6752.3
J_i^c	1050.2	1952	3002.2
z_i^*	3053.7	-3053.7	0
$J_i^c - z_i^*$	-2003.4	5005.6	3002.2

references defined by the HL-MPC, while optimizing their local resources. In particular, L-MPC$_1$ modulates the power exchanged with the main utility, depicted in Figure 7(c), so that the total energy stored in batteries in $\mathcal{S}_1$ tracks the HL-MPC reference, as evident from the states of charge profiles depicted in Figure 7(d), while ensuring the optimal electrical power supply to the heat pump. The L-MPC$_2$ regulates the output temperature of the thermal boiler, depicted in Figure 7(e), and the water flowrate of the thermal storage, depicted in Figure 7(g), so as to store the energy transferred from the electrical system, tracking the energy reference dictated at the HL-MPC layer. In particular, it is worth noticing that most power produced by the photovoltaic generators is not sold to the main utility by $\mathcal{S}_1$, but it is transferred to $\mathcal{S}_2$ between 8:00 and 16:00, whereas L-MPC$_2$, in turn, acts on the local inputs so as to increase the water temperature at each node of the heating supply network (see Figure 7(f)) and at the different sections of the thermal storage (see Figure 7(h)). The stored thermal energy is later used, i.e., between 16:00 and 20:00, while keeping the output temperature of the thermal boiler at its lower bound so as to minimize the local gas consumption.

The benefit sharing problem discussed in Section IV is solved for the considered scenario at the end of the day, using $\tau_b = 24$ h, and considering a symmetric bargaining, i.e., $\alpha_i = 1$, $\forall i \in \mathcal{N}$. The obtained results are reported in Table VI. It is evident that the total operative cost of $\mathcal{S}^\dagger$ significant decreases when the proposed hierarchical control architecture is applied (i.e., $\sum_{\forall i} J_i^c < \sum_{\forall i} J_i^{nc}$). This operation is in principle not convenient for all subsystems, as the operative cost of $\mathcal{S}_1$ increases (it delivers additional energy to $\mathcal{S}_2$ instead of selling it to the main utility), whereas the operative cost of $\mathcal{S}_2$ significantly decreases. This issue is solved by running the benefit sharing problem formulated in (18), achieving an effective final cost for each subsystem, i.e., $(J_i^c - z_i^*)$, much lower than the one achievable by their independent regulation. The described case study witnesses that the designed control strategy is effective in enabling the optimal and efficient opera-

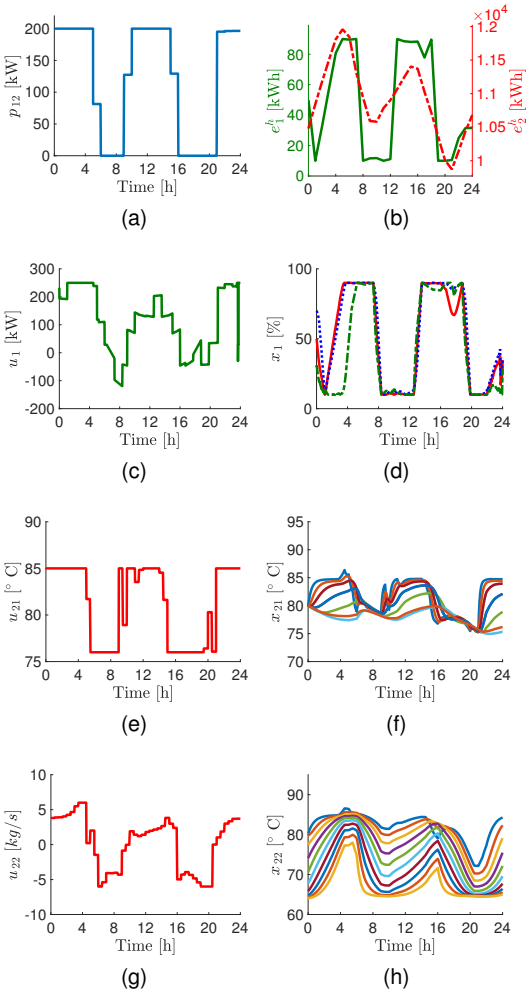


Fig. 7. (a) Electrical power absorbed by the heat pump;
(b) Energy references for $\mathcal{S}_1$ and $\mathcal{S}_2$ defined by the HL-MPC;
(c) Electrical power exchanged with the main utility in $\mathcal{S}_1$;
(d) States of charge of batteries in $\mathcal{S}_1$: node E5 (solid red), node E21 (dotted blue), and node E30 (dashed green);
(e) Output temperature of the thermal boiler in $\mathcal{S}_2$;
(f) Temperature at each node of the supply network in $\mathcal{S}_2$;
(g) Water flowrate of the thermal storage in $\mathcal{S}_2$;
(h) Temperature at each layer of the thermal storage in $\mathcal{S}_2$.

tion of MES, also when applied to large-scale energy networks. The control problem has been solved on a laptop with an Intel i7-11850H processor, recording an average computational time of 0.03 s for solving the HL-MPC coordination problem, 3.7 s for solving the L-MPC$_1$ control problem and 0.35 s for solving the L-MPC$_2$ one. On the other hand, the computational time for solving the benefit sharing problem in (18) is 0.37 s, whereas the one to solve (20) is, for each subsystem, similar to the one of the corresponding L-MPC regulator.

VI. Conclusions

The paper describes the design of a novel hierarchical predictive control architecture for the coordination of multi-energy systems (MESs), i.e., interconnected energy systems of different energy domains (e.g., thermal, electrical or gas). The proposed control strategy involves, at the high level, an energy modelling of reduced order for each MES subsystem, which enables the computational-effective and optimal coordination of power exchanges among MES subsystems. Moreover, at the high level, an energy reference for each MES subsystem is computed, which is then tracked by a low-level MPC regulator regulating local subsystem inputs. On the other hand, a benefit sharing algorithm is designed, with the goal of properly sharing the economic saving achieved by the multi-energy interaction among MES subsystems. As witnessed by the numerical results, the formulated control framework can be easily applied to different MES benchmarks, being capable of dealing with nonlinear large-scale systems, as most model complexity is addressed by the local low-level regulators and not by the high-level one. The approach described in the paper allows for many extensions, currently underway. Among them: *(i)* the design of a distributed control algorithm for the high-level coordination, *(ii)* the formulation of robust and/or stochastic MPC algorithms to deal with possible uncertainties in the prediction of disturbances, *(iii)* the investigation of a more structured game-theoretical framework for the benefit sharing, where MES subsystems may directly compute the optimal energy exchanges through negotiation strategies, and *(iv)* the investigation of more advanced coordination strategies among multi-energy subsystems, e.g., involving demand-response services.

Appendix A
Piece-wise definition of total generation cost

It is here presented an alternative method, other than the ones discussed in Section III-B, to approximate the total produced power cost $c_i^{gh}(p_i^{gh})$, used by HL-MPC in (15), using the local generation costs c_i^g exploited by L-MPC$_i$ in (17a). For the sake of readability and without any loss of generality, this procedure is here described considering $\underline{p}_i^g = \mathbb{0}_{g_i}$. First of all, number power generators in $\mathcal{S}_i$ in increasing order with respect to their costs, assumed to be different among each other, i.e., $c_{i1}^g < c_{i2}^g < \ldots < c_{i\,g_i}^g$. Then, assuming local state and input constraints (17b)-(17c) to be respected, each L-MPC$_i$ will use local power generators in increasing order with respect to their index, until their power bounds are reached, minimizing the operational cost. Thus, the overall cost of the total generation in each $\mathcal{S}_i$ can be modelled at the HL-MPC level as

$$c_i^{gh}(p_i^{gh}) = \begin{cases} c_{i1}^g\, p_i^{gh} & \text{if} \quad \mathbb{0}_{g_i} \le p_i^{gh} \le \bar{p}_{i1}^g, \\ c_{ij}^g\, p_i^{gh} + \sum_{l=1}^{j-1} \bar{p}_{il}^g (c_{il}^g - c_{ij}^g) & \text{if} \quad \sum_{l=1}^{j-1} \bar{p}_{il}^g \le p_i^{gh} \le \sum_{l=1}^{j} \bar{p}_{il}^g, \\ & \forall j \in \{2, \ldots, g_i\}. \end{cases}$$

The idea behind this cost formulation can be better appreciated considering Figure 8, where the function $c_i^{gh}(p_i^{gh})$ is depicted for a system with $g_i = 3$ power sources. As evident, the overall cost represents, at the HL-MPC level, the fact that generators in $\mathcal{S}_i$ would be exploited by the L-MPC$_i$ regulator in sequence with respect to their cost.

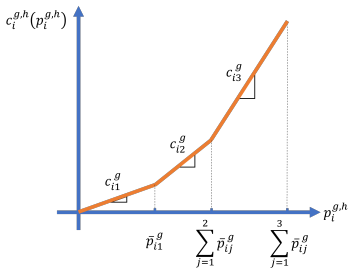


Fig. 8. Cost of total produced power in $\mathcal{S}_i$ with $g_i = 3$ local power sources.

APPENDIX B
CENTRALIZED CONTROL PROBLEM

Hereafter, the centralized control problem for the coordination of $\mathcal{S}^\dagger$ is formulated. Consider a sampling period τ_{centr} and a prediction horizon $\mathcal{T}_{centr} = \{k, \dots, k + N_{centr} - 1\}$, with $N_{centr} > 0$. Thus, at each k, a centralized predictive regulator should solve the following problem

$$\begin{aligned} &\min_{u_{\forall i}(\cdot)} \sum_{\forall k \in \mathcal{T}_i} \left(\sum_{\forall i=1,\dots,M} c_i^{g\prime} p_i^g(k) + \sum_{\forall (i,j)\in\mathcal{E}} c_{ij}^{ph} |p_{ij}(k)| \right) \\ &\text{subject, } \forall k \in \mathcal{T}_i, \text{ to} \\ &\qquad (16),\ (17b) - (17e), \quad \forall\, i = 1, \dots, M\,, \\ &\qquad \underline{p}_{ij} \le p_{ij}(k) \le \bar{p}_{ij}\,, \quad \forall (i,j) \in \mathcal{E}. \end{aligned} \tag{26}$$

Denote the optimal power production and exchanges computed by (26) with $p_i^{g***}(k|k)$ and $p_{ij}^{g***}(k|k)$, respectively. Similarly to Section IV, considering a sampling period $\tau_b > 0$ and the generic time instant $t = k_b \tau_b$, with $k_b \in \mathbb{N}$, the operational cost of each $\mathcal{S}_i$ over $[\,(k_b - 1)\tau_b,\ k_b \tau_b\,]$ is

$$J_i^{\text{centr}}(k_b) = \sum_{k=(k_b-1)B_i}^{k_b B_i} \left(c_i^{g\prime} p_i^{g***}(k|k) + \sum_{j \in \mathcal{N}_i^{\text{in}}} c_{ji}^{ph} |p_{ji}^{h***}(k|k)| \right),$$

where, as a convention, the cost of power exchanges are applied to the receiving subsystems (as in (19)).

ACKNOWLEDGEMENT

The research activity of Lorenzo Nigro has been financed by the Research Fund for the Italian Electrical System under the Contract Agreement between RSE S.p.A. and the Ministry of Economic Development - General Directorate for the Electricity Market, Renewable Energy and Energy Efficiency, Nuclear Energy in compliance with the Decree of April 16th, 2018. The work of Riccardo Scattolini is carried out within the MICS (Made in Italy – Circular and Sustainable) Extended Partnership and received funding from Next-Generation EU (Italian PNRR – M4 C2, Invest 1.3 – D.D. 1551.11-10-2022, PE00000004). CUP MICS D43C22003120001

REFERENCES

[1] G. Chicco, S. Riaz, A. Mazza, and P. Mancarella, "Flexibility from distributed multienergy systems," *Proceedings of the IEEE*, vol. 108, no. 9, pp. 1496–1517, 2020.

[2] E. Dall'Anese, P. Mancarella, and A. Monti, "Unlocking flexibility: Integrated optimization and control of multienergy systems," *IEEE Power and Energy Magazine*, vol. 15, no. 1, pp. 43–52, 2017.

[3] R. Krug, V. Mehrmann, and M. Schmidt, "Nonlinear optimization of district heating networks," *Optimization and Engineering*, vol. 22, no. 2, pp. 783–819, 2021.

[4] K. Liu, L. T. Biegler, B. Zhang, and Q. Chen, "Dynamic optimization of natural gas pipeline networks with demand and composition uncertainty," *Chemical Engineering Science*, vol. 215, p. 115449, 2020.

[5] C. Klemm and P. Vennemann, "Modeling and optimization of multi-energy systems in mixed-use districts: A review of existing methods and approaches," *Renewable and Sustainable Energy Reviews*, vol. 135, p. 110206, 2021.

[6] M. Arnold, R. R. Negenborn, G. Andersson, and B. De Schutter, "Model-based predictive control applied to multi-carrier energy systems," in *2009 IEEE power & energy society general meeting*. IEEE, 2009, pp. 1–8.

[7] S. Long, O. Marjanovic, and A. Parisio, "Generalised control-oriented modelling framework for multi-energy systems," *Applied Energy*, vol. 235, pp. 320–331, 2019.

[8] P. C. Blaud, P. Haurant, F. Claveau, B. Lacarrière, P. Chevrel, and A. Mouraud, "Modelling and control of multi-energy systems through multi-prosumer node and economic model predictive control," *International Journal of Electrical Power & Energy Systems*, vol. 118, p. 105778, 2020.

[9] R. Carli, G. Cavone, T. Pippia, B. De Schutter, and M. Dotoli, "Robust optimal control for demand side management of multi-carrier microgrids," *IEEE Transactions on Automation Science and Engineering*, 2022.

[10] E. A. M. Ceseña and P. Mancarella, "Energy systems integration in smart districts: robust optimisation of multi-energy flows in integrated electricity, heat and gas networks," *IEEE Transactions on Smart Grid*, vol. 10, no. 1, pp. 1122–1131, 2018.

[11] D. Bilgic, A. Koch, G. Pan, and T. Faulwasser, "Toward data-driven predictive control of multi-energy distribution systems," *Electric Power Systems Research*, vol. 212, p. 108311, 2022.

[12] A. La Bella, A. Del Corno, and A. Scaburri, "Data-driven modelling and optimal management of district heating networks," in *2021 AEIT International Annual Conference (AEIT)*. IEEE, 2021, pp. 1–6.

[13] G. Ceusters, R. C. Rodríguez, A. B. García, R. Franke, G. Deconinck, L. Helsen, A. Nowé, M. Messagie, and L. R. Camargo, "Model-predictive control and reinforcement learning in multi-energy system case studies," *Applied Energy*, vol. 303, p. 117634, 2021.

[14] A. Lesage-Landry, H. Wang, I. Shames, P. Mancarella, and J. A. Taylor, "Online convex optimization of multi-energy building-to-grid ancillary services," *IEEE Transactions on Control Systems Technology*, vol. 28, no. 6, pp. 2416–2431, 2019.

[15] M. Arnold, R. R. Negenborn, G. Andersson, and B. D. Schutter, "Distributed predictive control for energy hub coordination in coupled electricity and gas networks," in *Intelligent Infrastructures*. Springer, 2010, pp. 235–273.

[16] M. Taylor, O. Marjanovic, and A. Parisio, "Decentralised predictive control of multi-energy resources in buildings," in *2021 29th Mediterranean Conference on Control and Automation (MED)*. IEEE, 2021, pp. 39–44.

[17] A. La Bella, A. Falsone, D. Ioli, M. Prandini, and R. Scattolini, "A mixed-integer distributed approach to prosumers aggregation for providing balancing services," *International Journal of Electrical Power & Energy Systems*, vol. 133, p. 107228, 2021.

[18] A. La Bella, M. Farina, C. Sandroni, and R. Scattolini, "Design of aggregators for the day-ahead management of microgrids providing active and reactive power services," *IEEE Transactions on control systems technology*, vol. 28, no. 6, pp. 2616–2624, 2019.

[19] D. Xu, Q. Wu, B. Zhou, C. Li, L. Bai, and S. Huang, "Distributed multi-energy operation of coupled electricity, heating, and natural gas networks," *IEEE Transactions on Sustainable Energy*, vol. 11, no. 4, pp. 2457–2469, 2019.

[20] Y. Xu, A. Parisio, and Z. Ding, "Hierarchical model predictive control for energy efficient buildings with multi-energy storage systems," in *2020 IEEE Power & Energy Society General Meeting (PESGM)*. IEEE, 2020, pp. 1–5.

[21] A. La Bella, F. Bonassi, M. Farina, and R. Scattolini, "Two-layer model predictive control of systems with independent dynamics and shared control resources," *IFAC-PapersOnLine*, vol. 52, no. 3, pp. 96–101, 2019.
[22] O. Kaya, E. Van Der Roest, D. Vries, and T. Keviczky, "Hierarchical model predictive control for energy management of power-to-x systems," in *2020 IEEE PES Innovative Smart Grid Technologies Europe (ISGT-Europe)*. IEEE, 2020, pp. 1094–1098.
[23] F. Bonassi, A. La Bella, R. Lazzari, C. Sandroni, and R. Scattolini, "Supervised control of hybrid ac-dc grids for power balance restoration," *Electric Power Systems Research*, vol. 196, p. 107107, 2021.
[24] A. La Bella, P. Klaus, G. Ferrari-Trecate, and R. Scattolini, "Supervised model predictive control of large-scale electricity networks via clustering methods," *Optimal Control Applications and Methods*, vol. 43, no. 1, pp. 44–64, 2022.
[25] L. S. Shapley *et al.*, "A value for n-person games," *Contributions to the Theory of Games*, vol. 2, no. 28, pp. 307–317, 1953.
[26] F. J. Muros, J. M. Maestre, E. Algaba, T. Alamo, and E. F. Camacho, "Networked control design for coalitional schemes using game-theoretic methods," *Automatica*, vol. 78, pp. 320–332, 2017.
[27] W. Cai, A. B. Kordabad, and S. Gros, "Energy management in residential microgrid using model predictive control-based reinforcement learning and shapley value," *Engineering Applications of Artificial Intelligence*, vol. 119, p. 105793, 2023.
[28] A. A. Raja and S. Grammatico, "Payoff distribution in robust coalitional games on time-varying networks," *IEEE Transactions on Control of Network Systems*, vol. 9, no. 1, pp. 511–520, 2022.
[29] J. F. Nash Jr, "The bargaining problem," *Econometrica: Journal of the econometric society*, pp. 155–162, 1950.
[30] H. Kim, J. Lee, S. Bahrami, and V. W. Wong, "Direct energy trading of microgrids in distribution energy market," *IEEE Transactions on Power Systems*, vol. 35, no. 1, pp. 639–651, 2019.
[31] H. Wang and J. Huang, "Incentivizing energy trading for interconnected microgrids," *IEEE Transactions on Smart Grid*, vol. 9, no. 4, pp. 2647–2657, 2016.
[32] M. Amirfattahi and M. Haeri, "A real-time bargaining-based algorithm for energy trading market in smart grid," in *2019 11th International Conference on Electrical and Electronics Engineering (ELECO)*. IEEE, 2019, pp. 17–21.
[33] G. Belgioioso, W. Ananduta, S. Grammatico, and C. Ocampo-Martinez, "Operationally-safe peer-to-peer energy trading in distribution grids: A game-theoretic market-clearing mechanism," *IEEE Transactions on Smart Grid*, vol. 13, no. 4, pp. 2897–2907, 2022.
[34] W. H. Kersting, "Radial distribution test feeders," *IEEE Transactions on Power Systems*, vol. 6, no. 3, pp. 975–985, 1991.
[35] S. R. Cominesi, A. La Bella, M. Farina, and R. Scattolini, "A multi-layer control scheme for microgrid energy management," *IFAC-PapersOnLine*, vol. 49, no. 27, pp. 256–261, 2016.
[36] A. La Bella, F. Bonassi, C. Sandroni, L. Fagiano, and R. Scattolini, "A hierarchical approach for balancing service provision by microgrids aggregators," *IFAC-PapersOnLine*, vol. 53, no. 2, pp. 12 930–12 935, 2020.
[37] A. La Bella, F. Bonassi, P. Klaus, and R. Scattolini, "A fully distributed control scheme for power balancing in distribution networks," *IFAC-PapersOnLine*, vol. 53, no. 2, pp. 13 178–13 183, 2020.
[38] A. Falsone, I. Notarnicola, G. Notarstefano, and M. Prandini, "Tracking-ADMM for distributed constraint-coupled optimization," *Automatica*, vol. 117, p. 108962, 2020.
[39] T.-H. Chang, M. Hong, and X. Wang, "Multi-agent distributed optimization via inexact consensus ADMM," *IEEE Transactions on Signal Processing*, vol. 63, no. 2, pp. 482–497, 2014.
[40] J. M. Maciejowski, *Predictive control: with constraints*. Pearson education, 2002.
[41] A. E. Roth, *Axiomatic models of bargaining*. Springer Science & Business Media, 2012, vol. 170.
[42] E. Kalai, "Nonsymmetric nash solutions and replications of 2-person bargaining," *International Journal of Game Theory*, vol. 6, no. 3, pp. 129–133, 1977.
[43] J. Andersson, J. Åkesson, and M. Diehl, "Casadi: A symbolic package for automatic differentiation and optimal control," in *Recent advances in algorithmic differentiation*. Springer, 2012, pp. 297–307.
[44] W. H. Kersting, "Radial distribution test feeders," in *2001 IEEE Power Engineering Society Winter Meeting. Conference Proceedings (Cat. No. 01CH37194)*, vol. 2. IEEE, 2001, pp. 908–912.
[45] L. Nigro, "Hierarchical predictive control of networked multi-energy systems," https://www.politesi.polimi.it/handle/10589/186416, 2022, [Online; accessed 04-February-2023].
[46] A. La Bella, S. Negri, R. Scattolini, and E. Tironi, "A two-layer control architecture for islanded ac microgrids with storage devices," in *2018 IEEE conference on control technology and applications (CCTA)*. IEEE, 2018, pp. 1421–1426.
[47] H. Bastida, C. E. Ugalde-Loo, M. Abeysekera, M. Qadrdan, J. Wu, and N. Jenkins, "Dynamic modelling and control of thermal energy storage," *Energy Procedia*, vol. 158, pp. 2890–2895, 2019.
[48] A. La Bella and A. Del Corno, "Optimal management and data-based predictive control of district heating systems: The novate milanese experimental case-study," *Control Engineering Practice*, vol. 132, p. 105429, 2023.



Alessio La Bella received the B.Sc. and M.Sc. in Automation Engineering cum laude from Politecnico di Milano in 2013 and 2015, respectively. In 2016, he received the Alta Scuola Politecnica Diploma, together with the M.Sc. in Mechatronics Engineering cum laude at Politecnico di Torino. He received the Ph.D. Degree cum laude in Information Technology at Politecnico di Milano in 2020. In 2018, he was visiting researcher at the Automatic Control Lab of the École Polytechnique Fédérale de Lausanne, Switzerland. From 2020 to 2022, he worked as Research Engineer at Ricerca sul Sistema Energetico - RSE SpA, designing and implementing advanced predictive control systems for district heating networks and large-scale battery plants, in collaboration with industrial companies and energy utilities. In 2022, he joined Politecnico di Milano as Assistant Professor at Dipartimento di Elettronica, Informazione e Bioingegneria. He is Associate Editor of the International Journal of Adaptive Control and Signal Processing and of EUCA Conference Editorial Board. His research interests concern the theory and design of predictive, multi-agent and learning-based control systems, with particular emphasis on practical challenges arising from the upcoming energy transition. He was recipient of the Dimitris N. Chorafas Prize in 2020.



Lorenzo Nigro received the M.Sc. in Automation and Control Engineering from Politecnico di Milano, Italy, in 2022. In 2021, he was visiting student at RWTH Aachen University in Aachen, Germany. In 2022, he worked as Research Assistant at Politecnico di Milano, collaborating with the research center Ricerca Sul Sistema Energetico - RSE SpA. Currently, he is working towards the Ph.D. Degree in Information Technology at Politecnico di Milano. His research focuses on the areas of model predictive control, optimization, and the modelling of energy systems, with a particular interest in multi-energy systems and district heating networks.



Riccardo Scattolini is Full Professor of Automatic Control at Politecnico di Milano, Italy. He was awarded Heaviside Premium of the Institution of Electrical Engineers, United Kingdom, and was Associate Editor of the IFAC journal Automatica. His main research interests include modelling, identification, simulation, diagnosis, and control of industrial plants and energy systems, with emphasis on theory and applications of Model Predictive Control and fault detection methods to large-scale and networked systems.

II - 6

Distributed Control for MES Coordination

This Chapter extend the previous by addressing privacy and scalability concern arising from the centralized coordination layer. The author work [50] extends this by implementing a fully distributed high-level layer, improving scalability and privacy preservation.

- **Conference Article**: *Nigro, L.*, La Bella, A., & Scattolini, R. (2024, June). Distributed two-layer predictive control of multi-energy systems. In 2024 European Control Conference (ECC) (pp. 2429-2434). IEEE [50].

6.1 Distributed Control

Building on hierarchical MES control, further development is required to address the inherent limitations of centralized coordination. Although local MPC regulators effectively handle subsystem dynamics, the high-level optimizer remains centralized, creating scalability bottlenecks and raising privacy concerns due to the need for global information exchange.

Control Framework

To overcome these issues, the work [50] proposes a distributed two-layer predictive control architecture shown in Figure 6.1, that enables fully decentralized coordination. The framework consists of:

(i) Low-Level MPC (L-MPC), identical to the previous design, providing local tracking of high-level references; and

(ii) High-Level MPC (HL-MPC) implemented in a distributed fashion, where each subsystem exchanges information only with its neighbors. Coordination is achieved through the Dual Consensus ADMM algorithm, enabled by the convex energy-model abstraction of the high-level.

The distributed control framework was evaluated on an extended MES composed of three interconnected energy domains:

- IEEE 37-bus electrical grid (S_1).
- AROMA district heating network, (S_2).
- Hydrogen energy system, (S_3).

Results

Simulation results demonstrate that the distributed HL-MPC achieves effective coordination among the subsystems. The controllers exploit cross-domain energy storage by converting surplus electricity into hydrogen or thermal energy during low-cost periods (e.g., high renewable generation) and releasing it when electricity prices rise.

Overall, the proposed distributed architecture preserves the benefits of centralized MPC while enhancing scalability and ensuring privacy.

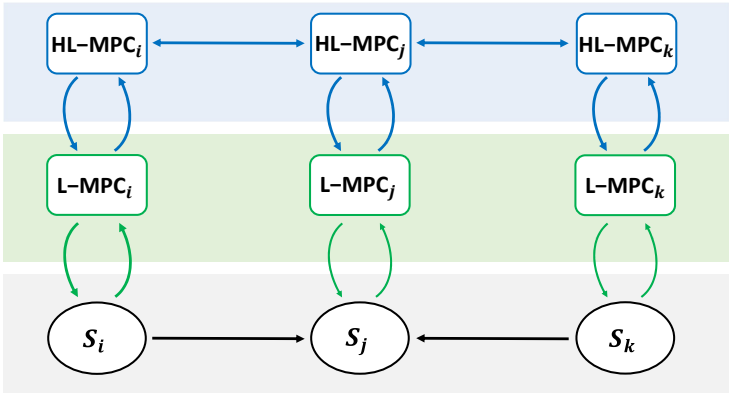


Figure 6.1: Hierarchical control architecture with distributed HL-MPC.

Distributed two-layer predictive control of multi-energy systems

Lorenzo Nigro[1,2], Alessio La Bella[1] and Riccardo Scattolini[1].

***Abstract*— Multi-energy systems (MESs) involve the synergetic operation of different energy vectors, unlocking higher system flexibility and efficiency. Nonetheless, they suffer from high model complexity, large-scale dimension, and different dynamical transient time constants. Moreover, each energy vector may have its own stakeholder, raising privacy concerns. In this framework, this article proposes a distributed two-layer predictive control architecture enabling to solve the mentioned issues. The lower level consists of decentralized Model Predictive Control (MPC) regulators considering detailed models, possibly nonlinear, while the high level exploits a convex and unified energy modelling of each energy vector using a fully distributed algorithm named Dual Consensus ADMM (DC-ADMM). The proposed control architecture is tested on an extended case study composed of three interconnected energy vectors i.e., a hydrogen energy system, a district heating network from the literature, and the IEEE 37-bus power system, showing promising results.**

I. Introduction

Multi-energy systems (MESs) are a possible solution for the decarbonization of energy system. MES consists of the synergetic operation of different energy vectors together, unlocking higher system flexibility and efficiency [1]. They achieve these benefits through meaningful energy exchange among different energy vectors, e.g., electrical, gas, or district heating networks. The energy exchanges is enabled by interface devices availability e.g., heat pumps (electrical-to-thermal energy), fuel cells (gas-to-electrical energy) or boilers (gas-to-thermal energy). Nonetheless, the control of MES is not an easy task due to the model complexity, the large-scale dimension, and the time constants diversity, e.g., fast electrical dynamics and slow thermal ones. Also, the control approach should deal with privacy concerns as the subsystems may belong to different system operators.

Recently, the literature worked on finding appropriate control architectures for multi-energy systems [2]. A common reference model is the *energy hub* (EH), a linear and lumped-element framework to develop new control techniques for MES [3], e.g., optimal control through model predictive control (MPC) [4]. Increasing control complexity, mixed-integer linear models [5], time-varying constraints [6] or data-driven methods [7], [8] are present in the literature. Unfortunately, these solutions are based on centralized controls which suffer from scalability issues (i.e., computational problems related to agents number or complexity growth) due to energy vector models' complexity, and they do not preserve local confidential information. This complexity led others to test hierarchical control strategies [9], [10] pushing the complexity to lower levels trying to achieve lightweight centralized high level optimization problems. Nonetheless, scalability issues also affects pure hierarchical approaches. Distributed control approaches may solve scalability and privacy issues, but their optimality, convergence and feasibility are guaranteed only in the presence of convexity [11]. Though, MES are typically characterized by nonconvex and nonlinear models. Thus, some distributed approaches present in the literature exploit either linear problems or MILP formulations resulting in simplified models that are less optimal in energy vector management, e.g., due to the inability to utilize networks effects [12], [13].

Given the above discussion, the main goal of this work is to propose a control architecture that solves scalability and privacy concerns and exploits the benefits of distributed algorithms in the presence of nonlinear models to optimally coordinate MES. This is possible thanks to a novel modelling technique that exploits low level data to create a high level problem that is convex and unified across all energy vectors.

The proposed control strategy is based on a distributed two-layer architecture. The lower level consists of several local decentralized MPC, each one controlling an energy vector with a suitable time-rate and nonlinear model. The local MPC minimizes the local operational costs, while tracking references on the total energy to be stored and on the power exchanges among different vectors imposed by the high-level layer. The latter is based on a distributed framework of supervising MPC regulators, exploiting the Dual Consensus ADMM algorithm [11], a fully distributed scheme with enhanced scalability properties [14]. Additionally, we guarantee the distributed algorithm convergence by exploiting the generalized energy formulation previously developed in [10]. This modelling technique unlocks a unified convex representation of different energy vectors and ensures distributed control strategies convergency.

We analyze the proposed control architecture performances on an extended MES example composed of three energy vectors: a gas network, a district heating network, the AROMA [15], and a power system, the IEEE 37bus. The collected data support the proposed control optimality and scalability. The work is an evolution of [10], surpassing its shortcomings in two ways: getting rid of the high-level centralized layer and its scalability and privacy-related issues, and ensuring that power exchanges among multi-energy subsystems are locally imposed by the local regulators instead of being imposed by a supervisory layer.

[1]Alessio La Bella, Lorenzo Nigro and Riccardo Scattolini are with the Dipartimento di Elettronica, Informazione e Bioingegneria, Politecnico di Milano, 20133 Milan, Italy (alessio.labella@polimi.it, lorenzo.nigro@polimi.it and riccardo.scattolini@polimi.it)

[2]Lorenzo Nigro with RSE S.p.A. - Research on Energy System, Milan 20134, MI, Italy.

Notation: We denote the set of real numbers as $\mathbb{R}$. Moreover, given a matrix A, $A \in \mathbb{R}^{n,m}$ represents a real-valued matrix with n rows and m columns. Considering the same matrix, we indicate as A' its transpose. The operator $blkdiag(\{A\}_n)$ defines a block-diagonal matrix with n-times matrix A as blocks. The same holds for vectors. We denote as $\mathbb{1}$ a 1D vector of suitable dimensions which entries are all 1, e.g., $[1, \ldots, 1]'$. The same holds for the vector $\mathbb{0}$ which entries equal to 0. Furthermore, the lower and upper bounds of a vector $x \in \mathbb{R}^n$ are $\underline{x} \in \mathbb{R}^n$ and $\bar{x} \in \mathbb{R}^n$ respectively, it holds $\underline{x} < \bar{x}$. Finally, given a set of indexes $\mathcal{N} = \{1, \ldots, n\}$ with cardinality $card(\mathcal{N})$ and a related sequence of variables $s_1, \ldots, s_n$, the vectors $s^\dagger = [s_1, \ldots, s_n]'$ is written element-wise as $s^\dagger = \{s_i\}_{\forall i \in \mathcal{N}}$.

II. Problem statement

Define a multi-energy system $\mathcal{S}^\dagger$ including M subsystems $\mathcal{S}_1, \ldots, \mathcal{S}_M$. The generic $\mathcal{S}_i$ consists of a specific energy vector with its own generators, loads and storage units, e.g., a subsystem $\mathcal{S}_i$ can represent an electrical grid or a district heating network. Subsystems may be able to exchange power among each other through power interfaces which allow the overall MES $\mathcal{S}^\dagger$ management optimization. Example of these interfaces are fuel cells for gas-to-electrical or heat pumps for electrical-to-thermal energy. It is possible to formalize MES structure using a directed graph $\mathcal{G} = (\mathcal{N}, \mathcal{E})$, where $\mathcal{N} = \{1, \ldots, M\}$ identifies the set of subsystems, while $\mathcal{E}$ denotes the edges' set modelling the interconnections among subsystems, i.e., $(i, j) \in \mathcal{E}$ if the power p_{ij}^{tr} can be transferred between $\mathcal{S}_i$ and $\mathcal{S}_j$. As a convention, in the following assume the transferred power p_{ij}^{tr} positive if flowing according to the edge's orientation, i.e., if transferred from $\mathcal{S}_i$ to $\mathcal{S}_j$ with $(i, j) \in \mathcal{E}$. For each node $i \in \mathcal{N}$, the connected nodes set is $\mathcal{N}_i = \{j \in \mathcal{N} | (i, j) \vee (j, i) \in \mathcal{E}\}$ regardless of the edge orientation, with $n_i = card(\mathcal{N}_i)$.

Each subsystem $\mathcal{S}_i$ can be modelled as a nonlinear system

$$\dot{x}_i(t) = f_i^s(x_i(t), u_i(t), \tilde{d}_i(t)), \tag{1a}$$

where $x_i \in \mathbb{R}^{x_i}$ represents the local states vector and $u_i \in \mathbb{R}^{m_i}$ is the input vector, locally bounded as

$$\underline{x}_i \leq x_i(t) \leq \bar{x}_i, \tag{1b}$$

$$\underline{u}_i \leq u_i(t) \leq \bar{u}_i. \tag{1c}$$

Furthermore, the exogenous signal vector $\tilde{d}_i(t)$ in (1a) is

$$\tilde{d}_i(t) = [d_i(t)'\, w_i(t)']', \tag{1d}$$

where $d_i(t) \in \mathbb{R}^{r_i}$ are the local disturbances of $\mathcal{S}_i$, while w_i is the vector of power exchanges of $\mathcal{S}_i$ with other connected subsystems. Specifically,

$$w_i(t) = \{p_{ij}^{tr}(t)\}_{j \in \mathcal{N}_i} \tag{1e}$$

where $w_i(t) \in \mathbb{R}^{n_i}$. Additionally, each subsystem $\mathcal{S}_i$ includes g_i controllable sources and l_i nondispatchable units. Hence, each $\mathcal{S}_i$ controllable power generation is $p_i^g \in \mathbb{R}^{g_i}$ and the nondispatchable power is $p_i^l \in \mathbb{R}^{l_i}$, and they have the following expressions

$$p_i^g(t) = \phi_i(x_i(t),\, u_i(t)), \tag{1f}$$

$$p_i^l(t) = \psi_i(x_i(t),\, d_i(t)). \tag{1g}$$

Specifically, the power produced by controllable sources depends on local states and inputs, whereas the noncontrollable power depends on local states and external disturbances. For the sake of clarity, nondispatchable units relate to either loads or nondispatchable generators, e.g., renewable energy sources.

The subsystems' models (1) can be nonlinear, nonconvex, and large-scale dimension (e.g., if $\mathcal{S}_i$ is a thermal energy network). Thus, it is not suited for efficient MES optimization as its implementation in centralized control approaches would suffer from computational and scalability issues, while fully distributed architectures would present convergence and feasibility problems. Hence, a high-level subsystem's reduced energy modelling is introduced and discussed in details in [10]. This model enables the design of a novel distributed multi-layer control architecture. The formulation represents each $\mathcal{S}_i$ with an energy based model independent of the specific energy vector.

Assumption 1: Consider the i-th subsystem represented as (1), its total stored energy is

$$e_i = \xi_i(x_i), \tag{2}$$

where $e_i \in \mathbb{R}$ and $\xi_i : \mathbb{R}^{n_i} \to \mathbb{R}$. Also, the stored energy dynamic is

$$\dot{e}_i(t) = \mathbb{1}_{g_i}' p_i^g(t) - \mathbb{1}_{l_i}' p_i^l(t) - \mathbb{1}_{n_i}' w_i(t). \tag{3}$$

The presented assumption states that the total energy stored in $\mathcal{S}_i$ is equal to a function of the local states and its variation over time depends on $\mathcal{S}_i$'s power balance. This assumption is commonly valid in energy systems, as shown in [10]. For instance, the energy stored in a district heating network is a function of the water temperature, while in a power system it depends on the batteries' states of charge. For the sake of clarity, efficiencies related to power exchanges among different energy vectors are not considered in (3), but they can be easily included.

III. Control problem formulation

As discussed in Section I, the control of MES has to satisfy multiple specifications, i.e., optimize the overall MES $\mathcal{S}^\dagger$, optimize each subsystems $\mathcal{S}_i$, $\forall i \in \mathcal{N}$, and satisfy operative constraints. An effective MESs' control scheme must also deal with three main challenges: control architecture scalability, control actions at different time rates given the energy dynamics diversity, and involved energy distributors' privacy concerns. The proposed solution involves a two-layer control architecture, with a distributed coordination scheme at the high-level and a decentralized predictive control architecture at the low level. This distributed multi-layer control architecture main functioning is described hereafter with reference to Figure 1.

The subsystems' set $\mathcal{S}^\dagger$ is highlighted in grey. Each $\mathcal{S}_i$ has its own local low-level controller named Local-MPC$_i$ highlighted in green in Figure 1. Each L-MPC$_i$ runs at a time rate that suits $\mathcal{S}_i$'s dynamical behaviour and considers the nonlinear model (1). The local controller optimizes its

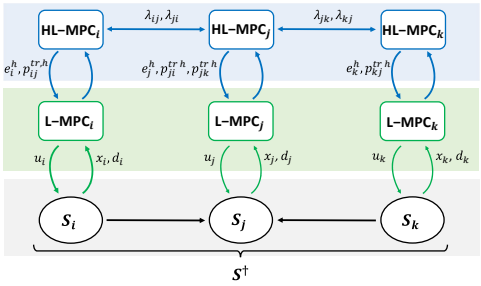


Fig. 1: Schematic of the MES distributed hierarchical control.

subsystem with two main goals: operational costs minimization and optimal references tracking of the total energy stored e_i^{h*} and power exchanges $p_{ij}^{tr\,h*}$ coming from the high-level layer, highlighted in blue in Figure 1. This layer consists of distributed predictive regulators named High-Level MPC$_i$ (HL-MPC$_i$) which optimize $\mathcal{S}_i$'s energy stored and power exchanges. Additionally, the HL-MPC$_i$ implements the reduced energy model (3) for its convexity that guarantees distributed algorithms' convergence and feasibility. Specifically, the high-level exploits the Dual Consensus ADMM (DC-ADMM) algorithm [11] for its enhance scalability and optimality performances.

Before describing the presented control architecture, define the L-MPC$_i$ sampling time as τ_i, its prediction horizon as $\mathcal{T}_i = \{k_i, \dots, k_i + N_i - 1\}$, where N_i are the prediction steps, while the current step is $k_i \in \mathbb{N}$, so $t = k_i \tau_i$. Furthermore, the sampling time of each HL-MPC$_i$ is τ_h, its prediction horizon is $\mathcal{T}_h = \{k_h, \dots, k_h + N_h - 1\}$, where N_h are the prediction steps, while the current step is $k_h \in \mathbb{N}$, hence $t = k_h \tau_h$. To simplify the notation, assume τ_h and τ_i to be multiples with $\tau_h = H_i \tau_i$ and $\tau_h \geq \tau_i \ \forall i \in \mathcal{N}$. Finally, assuming a suitable integration method, the nonlinear model (1a) becomes

$$\dot{x}_i(k+1) = \tilde{f}_i^s(x_i(k), u_i(k), \tilde{d}_i(k)), \tag{4}$$

where $\tilde{f}_i^s$ derives from the discretization of the continuous time state function f_i^s. In the same way, the discretized reduced energy model (3) is

$$e_i^h(k+1) = e_i^h(k) + \tau_h \left(p_i^{gh}(k) - p_i^{lh}(k) - \sum_{j \in \mathcal{N}_i} p_{ij}^{tr\,h}(k) \right). \tag{5}$$

A. Local MPC problem formulation

The general L-MPC$_i$ optimization problem is

$$\min_{u_i(\cdot), \sigma_i(\cdot)} \sum_{\forall k \in \mathcal{T}_i} \left(c_i^g p_i^g(k) + \alpha_i \sigma_i(k) \right) \tag{6a}$$

subject $\forall k \in \mathcal{T}_i$, to(4) and

$$\underline{x}_i \leq x_i(k) \leq \bar{x}_i, \tag{6b}$$
$$\underline{u}_i \leq u_i(k) \leq \bar{u}_i, \tag{6c}$$
$$p_i^g(k) = \phi_i(x_i(k), u_i(k)), \tag{6d}$$
$$\underline{p}_i^g \leq p_i^g(k) \leq \bar{p}_i^g, \tag{6e}$$
$$e_i(k) = \xi_i(x_i(k)), \tag{6f}$$
$$e_i(k) \leq e_i^{h*}\left(\left\lfloor \frac{k}{H_i} \right\rfloor | k_h \right) + \sigma_i(k) \tag{6g}$$
$$e_i(k) \geq e_i^{h*}\left(\left\lfloor \frac{k}{H_i} \right\rfloor | k_h \right) - \sigma_i(k) \tag{6h}$$
$$p_{ij}^{tr}(k) = p_{ij}^{tr\,h*}\left(\left\lfloor \frac{k}{H_i} \right\rfloor | k_h \right) \quad \forall j \in \mathcal{N}_i \tag{6i}$$
$$\sigma_i(k) \geq 0 \tag{6j}$$

The two terms of the L-MPC$_i$ cost function (6a) are the local power production cost $c_i^g \in \mathbb{R}_{\geq 0}^{g_i}$ and the minimization of the slack variable $\sigma_i \in \mathbb{R}_{\geq 0}$, where α_i is an arbitrary weight and $\alpha_i \gg max(c_i^g)$. The slack variable ensures the optimal high-level energy reference tracking feasibility. Energy and power reference tracking are enforced by constraints (6f) - (6i), where given the time rate of the high-level τ_h, $k_h = \lfloor (k_i / H_i) \rfloor$, $\forall i \in \mathcal{N}$. Recall that the optimal references e_i^{h*} and $p_{ij}^{tr\,h*}$ comes from the HL-MPC$_i$.

B. High level MPC problem formulation and distributed resolution

For the sake of clarity, we firstly present the centralized optimization problem and distribute it afterwards. Denote with $p_i^{gh}(k_h)$, $p_i^{lh}(k_h) \in \mathbb{R}$ the the high level generated and absorbed power at time k_h respectively. Hence, the centralized high level problem is

$$\min_{p_i^{gh}(\cdot), p_{ij}^{tr\,h}(\cdot)} \sum_{\forall i \in \mathcal{N}} \sum_{\forall k \in \mathcal{T}_h} \left(c_i^{gh} p_i^{gh}(k) + \sum_{j \in \mathcal{N}_i} \gamma_i^{tr} p_{ij}^{tr\,h}(k)^2 \right) + \sum_{\forall i \in \mathcal{N}} \beta_i (e_i^h(k_h + N_h) - e_i^{h0})^2 \tag{7a}$$

subject $\forall i \in \mathcal{N}$, $\forall k \in \mathcal{T}_h$, to (5),

$$\underline{e}_i^h \leq e_i^h(k) \leq \bar{e}_i^h, \tag{7b}$$
$$\underline{p}_i^{gh} \leq p_i^{gh}(k) \leq \bar{p}_i^{gh}, \tag{7c}$$
$$\underline{p}_i^{lh} \leq p_i^{lh}(k) \leq \bar{p}_i^{lh}, \tag{7d}$$
$$\underline{p}_{ij}^{tr\,h} \leq p_{ij}^{tr\,h}(k) \leq \bar{p}_{ij}^{tr\,h} \quad \forall j \in \mathcal{N}_i, \tag{7e}$$
$$e_i^h(k_h) = \tilde{e}_i^h(k_h), \tag{7f}$$
$$p_{ij}^{tr\,h}(k) + p_{ji}^{tr\,h}(k) = 0 \quad \forall j \in \mathcal{N}_i. \tag{7g}$$

In the centralized problem (7), upper and lower bounds (7b)-(7e) on the states and the generation cost c_i^{gh} in the cost function (7a) come from a proper aggregation of lower-level local variables, more details in [10]. Constraints (7f) initialize the total energy stored to the i-th subsystems' current energy state, where $\tilde{e}_i^h(k_h)$ is the total stored energy computed by the L-MPC at time instant k_h. Finally, we guarantee the power exchanges feasibility imposing the reciprocity constraints (7g). Concerning the cost function (7a), the first term is the local generation cost, the second one is the trading interface's usage cost, and the third is a terminal cost to avoid unnecessary usage of internal energy. Also, notice that thanks to the energy model, the resulting centralized problem (7) is convex. Although the presented formulation (7) is complete, a more compact representation is introduced to better describe its distributed resolution. For each $\mathcal{S}_i$, define the time step trading variable vector as $\boldsymbol{p}_i^{tr\,h}(k) = \{p_{ij}^{tr\,h}(k)\}_{\forall j \in \mathcal{N}_i}$ where $\boldsymbol{p}_i^{tr\,h}(k) \in \mathbb{R}^{M-1}$. Then, collect them in a single vector $\boldsymbol{p}_i^{tr\,h} = \{\boldsymbol{p}_i^{tr\,h}(k)\}_{k=k_h,\dots,k_h+N_h-1} \in \mathbb{R}^{(M-1)N_h}$. In analogy, define $\boldsymbol{e}_i^h = \{e_i^h(k)\}_{k=k_h,\dots,k_h+N_h} \in \mathbb{R}^{N_h+1}$ and

$\boldsymbol{p}_i^{gh} = \{p_i^{gh}(k)\}_{k=k_h,\dots,k_h+N_h-1} \in \mathbb{R}^{N_h}$ collecting variables influencing only subsystem i. The subsystems' optimization variables vector becomes

$$\boldsymbol{x}_i^h = \begin{bmatrix} \boldsymbol{e}_i^h \\ \boldsymbol{p}_i^{gh} \\ \boldsymbol{p}_i^{tr\,h} \end{bmatrix} \in \mathbb{R}^{x_i^h}. \tag{8}$$

Also, define the cost function of each agent $f_i(\boldsymbol{x}_i^h)$ as

$$f_i(\boldsymbol{x}_i^h) = \sum_{\forall k \in \mathcal{T}_h} \left(c_i^{gh}\, p_i^{gh}(k) + \sum_{j \in \mathcal{N}_i} \gamma_i^{tr} p_{ij}^h(k)^2 \right) + \beta_i (e_i^h(k_h + N_h) - e_i^{h0})^2.$$

Therefore, the centralized cost function (7a) becomes

$$\sum_{\forall i \in \mathcal{N}} f_i(\boldsymbol{x}_i^h). \tag{9}$$

Similarly, define the local constraint set $\mathcal{X}_i$ containing (5)-(7f), they are compactly written as

$$\boldsymbol{x}_i^h \in \mathcal{X}_i. \tag{10}$$

The reciprocity constraints (7g) can be compactly written as

$$\sum_{\forall i \in \mathcal{N}} \tilde{E}_i\, \boldsymbol{x}_i^h = \mathbb{0} \tag{11}$$

where the matrix $\tilde{E}_i = [\mathbb{0}\, blkdiag(\{E_i\}_{N_h})] \in \mathbb{R}^{(M-1)N_h,\, x_i^h}$ and each $E_i \in \mathbb{R}^{M-1,M-1}$ is defined as

$$[E_i]_{j,j} = \begin{cases} 1 & \text{if } \begin{array}{l}(j \in \mathcal{N}_i \wedge j < i) \vee \\ (j+1 \in \mathcal{N}_i \wedge j+1 > i)\end{array} \\ 0 & \text{otherwise.} \end{cases}, \tag{12}$$

for $j \in \{1, \dots, M-1\}$. Despite the definition of E_i in (12) is not intuitive, it enables the reciprocity constraint expression simplification from (7g) to (11) selecting the exchanged powers between subsystem $\mathcal{S}_i$ and its neighbours in $\mathcal{N}_i$.

In conclusion, the compact form of the centralized problem (13) is

$$\min_{\boldsymbol{x}_i^h(\cdot)} \sum_{\forall i \in \mathcal{N}} f_i(\boldsymbol{x}_i^h) \tag{13a}$$

s.t.

$$\boldsymbol{x}_i^h \in \mathcal{X}_i,\ \forall i \in \mathcal{N} \tag{13b}$$

$$\sum_{\forall i \in \mathcal{N}} \tilde{E}_i\, \boldsymbol{x}_i^h = \mathbb{0} \tag{13c}$$

We denote as *primal problem* this optimization problem, noting that it is convex. The DC-ADMM algorithm allows direct communication among agents and relies on iterative solutions that asymptotically converge to the centralized optimal value [13], [11], [16] in case of connected communication and convex problem. As problem (13) is already convex, to guarantee connected communications assume that each agent is able to communicate with at least one other agent. This assumption is reasonable as no isolated system would participate in a MES. The first step to implement the DC-ADMM algorithm is the construction of the Lagrangian function of problem (13) as

$$L(\boldsymbol{x}_1^h, \dots, \boldsymbol{x}_M^h) = \sum_{\forall i \in \mathcal{N}} \left(f_i(\boldsymbol{x}_i^h) + \boldsymbol{\lambda}\, \tilde{E}_i\, \boldsymbol{x}_i^h \right) \tag{14}$$

which is the relaxation of the reciprocity constraints (13c) with the introduction of the global dual variable $\boldsymbol{\lambda} \in \mathbb{R}^{(M-1)N_h}$. Based on the Lagrangian, we can define the *dual problem* as

$$\min_{\boldsymbol{\lambda}} \sum_{\forall i \in \mathcal{N}} \left(- \min_{\boldsymbol{x}_i^h \in \mathcal{X}_i} \left(f_i(\boldsymbol{x}_i^h) + \boldsymbol{\lambda}'\, \tilde{E}_i\, \boldsymbol{x}_i^h \right) \right) = \min_{\boldsymbol{\lambda}} \sum_{\forall i \in \mathcal{N}} \phi_i(\boldsymbol{\lambda}). \tag{15}$$

With the given assumptions, define $\boldsymbol{\lambda}_i$ the dual variable local copy for each subsystem i. It holds the equivalence between (15) and

$$\min_{\boldsymbol{\lambda}_1, \dots, \boldsymbol{\lambda}_M} \sum_{\forall i \in \mathcal{N}} \phi_i(\boldsymbol{\lambda}_i) \tag{16a}$$

$$\text{subject to } \boldsymbol{\lambda}_i = \boldsymbol{\lambda}_j \quad \forall i \in \mathcal{N},\ \forall j \in \mathcal{N}_i. \tag{16b}$$

Finally, the dual problem formulation (16) is separable and we can apply a standard consensus ADMM to solve it. The DC-ADMM algorithm implementation is reported for clarity in the following, where the superscript (k) indicates the ADMM iteration.

Algorithm 1 DC-ADMM

1: **Choose** $c > 0$. ▷ *Tuning parameter*
2: **Set** $\boldsymbol{x}_i^{h,0}$, $\boldsymbol{\lambda} i^0 = 0$, $\boldsymbol{\mu}_i^0 = 0 \quad \forall i \in \mathcal{N}$.
3: $k \leftarrow 1$. ▷ *ADMM Iteration counter*
4: **repeat**
5: **for all** $i \in \mathcal{N}$ **do** ▷ *Each agent in parallel*
6: $\boldsymbol{\mu}_i^{(k)} = \boldsymbol{\mu}_i^{(k-1)} + c \sum_{j \in \mathcal{N}_i} \left(\boldsymbol{\lambda}_i^{(k-1)} - \boldsymbol{\lambda}_j^{(k-1)} \right)$,
7: $\boldsymbol{x}_i^{h,(k+1)} = \underset{\boldsymbol{x}_i^h \in \mathcal{X}_i}{\operatorname{argmin}} \left(f_i(\boldsymbol{x}_i^h) + \right.$
$\left. + \frac{c}{4n_i} \left\| \frac{\tilde{E}_i \boldsymbol{x}_i^h - \boldsymbol{\mu}_i^{(k)}}{c} + \sum_{j \in \mathcal{N}_i} \left(\boldsymbol{\lambda}_i^{(k-1)} - \boldsymbol{\lambda}_j^{(k-1)} \right) \right\|^2 \right)$,
8: $\boldsymbol{\lambda}_i^{(k)} = \frac{1}{2n_i} \left(\sum_{j \in \mathcal{N}_i} \left(\boldsymbol{\lambda}_i^{(k-1)} - \boldsymbol{\lambda}_j^{(k-1)} \right) - \boldsymbol{\mu}_i^{(k)}/c + \tilde{E}_i \boldsymbol{x}_i^{h(k+1)}/c \right)$.
9: Share $\boldsymbol{\lambda}_i^k$ with $\forall j \in \mathcal{N}_i$
10: $k \leftarrow k+1$
11: **until** Tolerances are met

In Algorithm 1, we can see the computational effort, Steps 6-9, is pushed down to the agents and the solution is parallelized. Moreover, the goal of distribution is reached thanks to the communication Step 9, where agents interact with neighbours and exchange dual informations. At each iteration, the agents locally update $\boldsymbol{\lambda}_i$ (Step 8), their optimal solution (Step 7) and the dual variable $\boldsymbol{\mu}_i$ (Step 6). The dual variables $\boldsymbol{\mu}$ guarantee the convergence of the variables $\boldsymbol{\lambda}$ to the same value. In turn, $\boldsymbol{\lambda}$'s convergence ensures the dual problem solution feasibility.

IV. Numerical example

In this section, we investigate the performance of the distributed two-layer control architecture applied to a multi-

energy case study reported in Figure 2 and composed of three interconnected energy subsystems of different domains: a H_2 energy system (depicted in dark blue), a thermal network (with supply pipelines depicted in red and return ones in light blue), and a electricity grid (depicted in green). The electricity grid is based on the IEEE 37-bus system [17] and the district heating network on the AROMA network described in [15]. The main parameters of the energy subsystems and their units are reported in Table I. The results relate to a 24h MES optimization where the control parameters are also in Table I, and the nondispatchable profiles are reported in Figure 3 together with power costs. The IEEE 37-bus systems uses the power flow model to simulate the behaviour of its elements, while the gas system equations are presented in [10]. Lastly, the AROMA network simulation runs in Simscape and its models are based on standard nonlinear thermo-hydraulic equations as in [15]. The HL-MPC layer is implemented with a prediction horizon of 24 hours and a time-rate of $\tau_h = 30$ min. This is solved relying on the DC-ADMM procedure reported in Algorithm 1, where parameter $c = 1e^{-2}$. The convergence tolerance of the dual variables is $1e^{-4}$, and the ADMM cycle takes, on average, $127\,s$ when executed sequentially. The parallelization of the computation would significantly drop the ADMM cycle computational time. In this paper, to keep the explanation concise, only one dual variable appears.

We use the hierarchical control structure of Figure 1 to optimize one day of operation and obtained the results reported in Figure 4. Some results are normalized with respect to their maximum value to display different energy vectors jointly. The cost of electricity varies during the day. Since it is the pivotal driver of the HL-MPC economical optimization, the subsystems' total energy stored references and power generation profiles reflect the cost variation, as in Figure 4. In particular, the MES HL-MPC profiles proves the effectiveness of the coordination in Figures 4a-4c. The three subsystems work together to indirectly store electricity as hydrogen or heat when most convenient and deliver it back later when energy prices rise. Moreover, we can notice the limitation of different forms of energy in Figure 4a. The battery profile (green) is the fastest-changing as batteries are fast to charge and discharge, whereas the thermal energy (red) has the slowest delivery time. Additionally, consider the energy trading between $\mathcal{S}_1$ and $\mathcal{S}_2$ in Figure 4b. Since the heat pump is more efficient than the gas boiler, it runs all day according to electrical energy availability, specifically at night and in the afternoon, when loads absorb the least and solar production is highest, respectively. Now, consider the energy trading between $\mathcal{S}_1$ and $\mathcal{S}_3$ in Figure 4c. The hydrogen energy system can store and produce electricity thanks to an electrolyzer and a fuel cell. These components activate during one day of operation. Specifically, hydrogen is produced during electricity low-cost hours, i.e., early in the morning and at midday, and consumed to produce electricity at peak cost hours.

Figure 4a reports the profiles of the normalized energy references dictated by the high-level layer, where energy is stored when most convenient. The L-MPC regulators track the energy references as shown in Figures 4d-4f. Specifically, the $\mathcal{S}_1$ batteries' states of charge are depicted in Figure 4d, the $\mathcal{S}_3$ gas density is shown in Figure 4f, whereas Figure 4e illustrates the $\mathcal{S}_2$ pipe temperatures. The latter shows how the L-MPC$_2$ regulator allows to store energy in pipelines, a strategy known as packing [18] in thermal energy control.

$\mathcal{S}_i$	$\mathcal{S}_1$	$\mathcal{S}_2$	$\mathcal{S}_3$
τ_i min	1	30	5
$\mathcal{T}_i$ hours	24	24	24
$(\underline{e}_i^{h0}, \bar{e}_i^{h})$ kWh	50	$10.4e^3$	25.4
$(\underline{e}_i^{h}, \bar{e}_i^{h})$ kWh	(10, 90)	$(9.4, 12)e^3$	(3.5, 50.2)
$(\underline{p}_i^{gh}, \bar{p}_i^{gh})$ kW	$(-500, 500)$	$(0, 700)$	$(0, 78.5)$
$(\underline{p}_{i1}^{tr\,h}, \bar{p}_{i1}^{tr\,h})$ kW	–	$(-200, 0)$	$(-250, 250)$
$(\underline{p}_{i2}^{tr\,h}, \bar{p}_{i2}^{tr\,h})$ kW	$(0, 200)$	–	–
$(\underline{p}_{i3}^{tr\,h}, \bar{p}_{i3}^{tr\,h})$ kW	$(-250, 250)$	–	–

TABLE I: Control parameters of the case study.

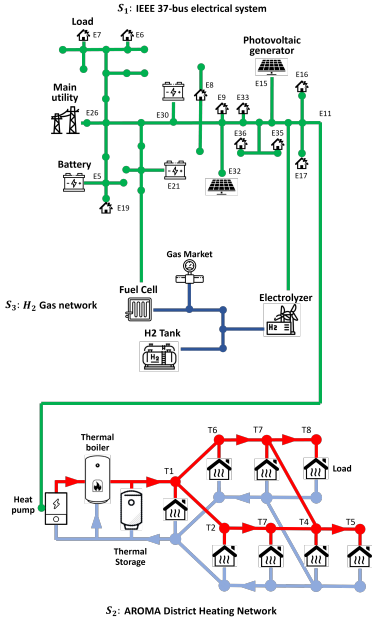


Fig. 2: Topology of the numerical example network.

V. CONCLUSIONS

In conclusion, the proposed two-layer distributed control architecture for MES systems solves the issues of scalability and time rates diversity. This results are possible through a decentralized framework of MPC regulators at the low level, locally controlling each energy vector with its detailed modelling, and a high-level layer of distributed MPC systems, coordinating MES subsystems. The application of a distributed algorithm is made possible thanks to a novel convex unified energy modelling. The results showed promising performances when tested on the large networks presented in

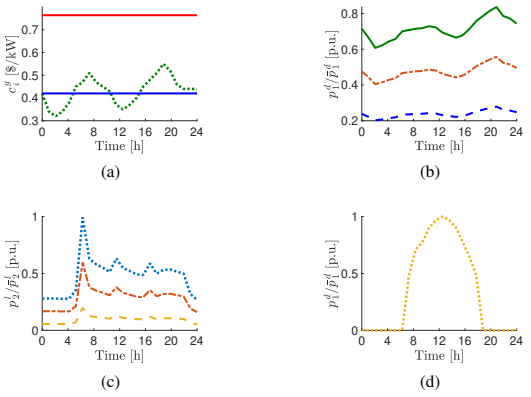


Fig. 3: (a) Power generation costs: c_1^g in green, c_2^g in red, c_3^g in blue. (b) Normalized electrical loads. (c) Normalized thermal loads. (d) Normalized solar panel production.

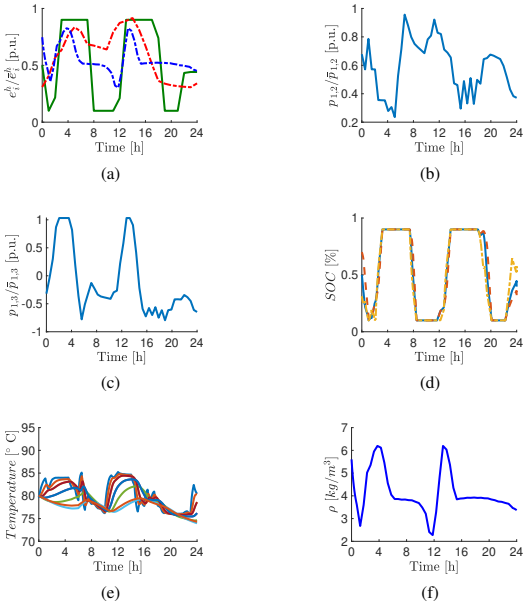


Fig. 4: (a) Normalized energy storage of systems $\mathcal{S}_1$ (green), $\mathcal{S}_2$ (red), and $\mathcal{S}_3$ (blue). (b) Normalized energy exchange between $\mathcal{S}_1$ and $\mathcal{S}_2$. (c) Normalized energy exchange between $\mathcal{S}_1$ and $\mathcal{S}_3$. (d) Batteries' state of charge. (e) Temperature of the water in pipes. (f) Gas density inside the H_2 storage.

the case study. Future work will focus on the development of game-theoretical coordination schemes for multi-energy systems, enabling negotiation mechanisms among operators of different energy vectors, so as to agree the optimal multi-energy power exchanges.

ACKNOWLEDGMENT

The research activity of Lorenzo Nigro has been financed by the Research Fund for the Italian Electrical System under the Contract Agreement between RSE S.p.A. and the Ministry of Economic Development - General Directorate for the Electricity Market, Renewable Energy and Energy Efficiency, Nuclear Energy in compliance with the Decree of April 16th, 2018. The work of Riccardo Scattolini is carried out within the MICS (Made in Italy – Circular and Sustainable) Extended Partnership and received funding from Next-Generation EU (Italian PNRR – M4 C2, Invest 1.3 – D.D. 1551.11-10-2022, PE00000004). CUP MICS D43C22003120001.

REFERENCES

[1] G. Chicco, S. Riaz, A. Mazza, and P. Mancarella, "Flexibility from distributed multienergy systems," *Proceedings of the IEEE*, vol. 108, no. 9, pp. 1496–1517, 2020.

[2] C. Klemm and P. Vennemann, "Modeling and optimization of multi-energy systems in mixed-use districts: A review of existing methods and approaches," *Renewable and Sustainable Energy Reviews*, vol. 135, p. 110206, 2021.

[3] P. Mancarella, "Mes (multi-energy systems): An overview of concepts and evaluation models," *Energy*, vol. 65, pp. 1–17, 2014.

[4] M. Arnold, R. R. Negenborn, G. Andersson, and B. De Schutter, "Model-based predictive control applied to multi-carrier energy systems," in *2009 IEEE power & energy society general meeting*. IEEE, 2009, pp. 1–8.

[5] S. Long, O. Marjanovic, and A. Parisio, "Generalised control-oriented modelling framework for multi-energy systems," *Applied Energy*, vol. 235, pp. 320–331, 2019.

[6] A. Lesage-Landry, H. Wang, I. Shames, P. Mancarella, and J. A. Taylor, "Online convex optimization of multi-energy building-to-grid ancillary services," *IEEE Transactions on Control Systems Technology*, vol. 28, no. 6, pp. 2416–2431, 2019.

[7] A. La Bella, A. Del Corno, and A. Scaburri, "Data-driven modelling and optimal management of district heating networks," in *2021 AEIT International Annual Conference (AEIT)*. IEEE, 2021, pp. 1–6.

[8] G. Ceusters, R. C. Rodríguez, A. B. García, R. Franke, G. Deconinck, L. Helsen, A. Nowé, M. Messagie, and L. R. Camargo, "Model-predictive control and reinforcement learning in multi-energy system case studies," *Applied Energy*, vol. 303, p. 117634, 2021.

[9] A. La Bella, F. Bonassi, M. Farina, and R. Scattolini, "Two-layer model predictive control of systems with independent dynamics and shared control resources," *IFAC-PapersOnLine*, vol. 52, no. 3, pp. 96–101, 2019.

[10] A. La Bella, L. Nigro, and R. Scattolini, "Predictive control and benefit sharing in multi-energy systems," *IEEE Transactions on Control Systems Technology*, 2023.

[11] T.-H. Chang, M. Hong, and X. Wang, "Multi-agent distributed optimization via inexact consensus admm," *IEEE Transactions on Signal Processing*, vol. 63, no. 2, pp. 482–497, 2014.

[12] A. La Bella, A. Falsone, D. Ioli, M. Prandini, and R. Scattolini, "A mixed-integer distributed approach to prosumers aggregation for providing balancing services," *International Journal of Electrical Power & Energy Systems*, vol. 133, p. 107228, 2021.

[13] V. N. Behrunani, A. Irvine, G. Belgioioso, P. Heer, J. Lygeros, and F. Dörfler, "Designing fairness in autonomous peer-to-peer energy trading," *IFAC-PapersOnLine*, vol. 56, no. 2, pp. 3751–3756, 2023.

[14] A. La Bella, P. Klaus, G. Ferrari-Trecate, and R. Scattolini, "Supervised model predictive control of large-scale electricity networks via clustering methods," *Optimal Control Applications and Methods*, vol. 43, no. 1, pp. 44–64, 2022.

[15] R. Krug, V. Mehrmann, and M. Schmidt, "Nonlinear optimization of district heating networks," *Optimization and Engineering*, vol. 22, pp. 783–819, 2021.

[16] G. Banjac, F. Rey, P. Goulart, and J. Lygeros, "Decentralized resource allocation via dual consensus admm," in *2019 American Control Conference (ACC)*. IEEE, 2019, pp. 2789–2794.

[17] W. H. Kersting, "Radial distribution test feeders," in *2001 IEEE Power Engineering Society Winter Meeting. Conference Proceedings (Cat. No. 01CH37194)*, vol. 2. IEEE, 2001, pp. 908–912.

[18] L. Saarinen, "Modelling and control of a district heating system," 2008.

II - 7

Design and experimental validation of MES control architectures

This chapter presents the experimental validation of the multi-layer control framework for the coordinated operation of multi-energy systems presented in Chapter 5, addressing the challenges posed by heterogeneous dynamics, nonlinear models, large-scale optimization, and the presence of multiple independent stakeholders.

- *Nigro, L.*, Polimeni, S., & La Bella, A. (2025). Experimental Assessment of Multi-Layer Control Framework for Multi-Energy Systems control with Multiple Coordination Mechanics. To Be Submitted. [52]

7.1 Experimental Validation of MES control

Coordination mechanism

The proposed methodology adopts a hierarchical design. At the lower layer, local Model Predictive Controllers regulate the detailed nonlinear dynamics of each subsystem, exploiting multi-rate sampling to accommodate diverse time constants across electrical and thermal systems. At the upper layer, three coordination mechanisms are implemented:

(i) a centralized MPC that optimizes the global MES cost,

(ii) a distributed MPC based on Dual Consensus ADMM that preserves privacy by requiring only neighbor-to-neighbor communication,

(iii) a non-cooperative game-theoretic strategy formulated as a Generalized Nash Equilibrium Problem capturing rational self-interested agent behavior.

Validation Results

The framework is experimentally validated on the RSE Distributed Energy Resources Test Facility introduced in the introduction 1, comprising an electrical microgrid, a district heating network, and a multi-energy hub with local conversion and storage assets. Experiments incorporate real energy price data and dynamic disturbances over multi-hour

operating windows. Results show that all coordination strategies satisfy operational constraints and successfully manage cross-domain interactions. Centralized control delivers the lowest overall operating cost but requires full information sharing 7.1. Distributed MPC achieves comparable performance. The game-theoretic architecture, although yielding higher system-level cost, ensures incentive compatibility and fair economic exchanges, encouraging participation from self-interested agents. All coordination strategies ensure feasible computational times even for the distributed and game-theoretic architectures, as shown in Table 7.2. As expected, the computational times of the lower level does not depend on the adopted coordination strategy, is within the sampling time and is independent of the number of agents and their sampling time. On the other hand, the time for the upper level depends on the number of agents especially the centralized approach. The distributed and game-theoretic architectures pay a higher computational cost than the centralized one, due to the additional communication overhead to preserve privacy, which may turn advantageous increasing the number of agents.

Test	**Agent Cost [€]**			**Cost [€]**	
	TF	**EF**	**EH**	[%]	
Bench.	46.6	18.1	0	(Ref.)	64.7
Central.	48.4	5.7	0	(-16.5)	54.1
Dist.	48.0	14.0	0	(-4.1)	62.0
G.T.	23.7	11.5	23.1	(-9.8)	58.3

Table 7.1: KPIs achieved in the tests. In order: Benchmark, Centralized, Distributed, and Game theory. The table reports also each subsystem cost: thermal facility (TF), electric facility (EF), and energy hub (EH). Finally, the MES operational cost and its percentage variation with respect to the benchmark.

Level	**Strategy/Agent**	**Time [s]**	τ **[s]**
Top	Centralized	≈ 5	900
	Distributed	≈ 90	900
	Game Theory	≈ 180	1800
Low	TF	≈ 60	900
	EF	≈ 1	60
	EH	≈ 2	300

Table 7.2: Approximate computational times for control elements against their sampling time.

Overall, the article demonstrates that the proposed multi-layer control framework effectively unifies advanced control and coordination mechanisms, enabling scalable, privacy-preserving, and economically rational operation of complex MESs. The experimental evidence confirms its practical viability and highlights its potential for real-world deployment in future low-carbon, integrated energy networks.

Hierarchical control of Multi-Energy Systems under cooperative and non-cooperative coordination mechanisms: design and experiments

Lorenzo Nigro[a,b], Alessio La Bella[a], Simone Polimeni[b], Riccardo Scattolini[a]

[a]*Department of Electronics, Information, and Bioengineering, Politecnico di Milano, Milano, Italy,*
[b]*Ricerca sul Sistema Energetico, R.S.E. spa, Milano, Italy,*

Abstract

Europe's REPowerEU plan highlights the need for innovative solutions to improve energy system flexibility and efficiency. Multi-energy systems (MESs) represent a promising solution as they involve the synergetic operation of different energy carriers, (e.g., interconnected electrical grids, heating systems, and gas networks), facilitating the integration of renewable energy sources. However, the deployment of MES poses significant challenges, including the need to model complex physical interactions, optimally manage heterogeneous dynamics (e.g., fast electrical and slow thermal transients), and address privacy and competition among independent stakeholders. To overcome these issues, this work proposes a multi-layer control architecture that enables both optimal cross-domain coordination and local energy systems control. This multi-layer control framework enables the design of three coordination strategies, i.e., centralized, distributed, and game-theoretic. The proposed control strategies are experimentally tested on a multi-energy test facility plant, located at Ricerca sul Sistema Energetico S.p.A. (RSE) in Milan, including a thermal network, an electrical grid, and a multi-energy hub. Results show that, despite system complexity and heterogeneity, the proposed control framework optimally satisfies load demands and operative constraints, paving the way to large-scale MES control.

Keywords: Multi-energy systems (MES), energy hubs, model predictive control (MPC), hierarchical control, distributed optimization, game-theory, experimental validation

1. Introduction

The global commitment to decarbonization and energy transition is driving a profound transformation in energy generation, distribution, and consumption. In this context, the European Union (EU) REPowerEU plan and the European Green Deal define ambitious targets: eliminating fossil fuel dependency, increasing renewable integration, and achieving climate neutrality by 2050, [1]. Given that the energy sector accounts for 75% of Europe's total greenhouse gas emissions (GHG), its transformation is imperative, [2]. The mentioned european policies mandate an accelerated transition from fossil fuels to renewables, improved energy efficiency, and enhanced network interconnection for a more resilient infrastructure.

Multi-Energy Systems emerged as a key solution of this transition. By coupling multiple energy carriers, such as electricity, heat, and gas, MES enhance overall efficiency and improve operational resilience. Through coordinated power conversion (e.g., electricity-to-heat with heat pumps or electricity-to-gas with electrolyzers) and storage devices, MES mitigate renewable intermittency and support the decarbonization of heating and cooling sectors, directly contributing to the objectives of the EU's policy frameworks, [3]. Despite their relevance for the energy transition, multi-energy systems are hindered by a series of technical challenges inherent to their scale, interconnected nature, and different ownership:

- *Model complexity and heterogeneity:* MES often

involve nonlinear dynamics (e.g., thermo-hydraulic transport) evolving at different time scales (e.g., fast electrical and slow thermal transients).

- *Computational scalability*: MES are typically large-scale and complex systems. Employing their dynamical models for optimization or control purposes could be unfeasible in real-time.

- *Privacy*: MES often involves the presence of multiple independent stakeholders (e.g., operators, prosumers, etc), restricting possibility of data sharing and cooperative coordination.

- *Economic rationality*: individual profit objectives may conflict with global efficiency, requiring incentive-compatible or nonoperative coordination strategies.

Related work

Centralized control schemes have been widely investigated for MES coordination, employing nonlinear [4], linearized [5], mixed-integer [6], or robust optimization approaches [7]. However, centralized approaches are often impractical for large-scale and complex MES, given possible computational issues and privacy concerns. Moreover, centralized approaches are not suited for regulating systems with hetereogeneous dynamics, given that a unique sampling time is commonly chosen.

To alleviate these issues, distributed optimization techniques, e.g., based on dual decomposition [8, 9, 10, 11], have been proposed. These frameworks improve scalability, but frequently rely on simplified models and iterative mechanisms, which have limited convergence and feasibility guarantees under nonconvex dynamics, which is a quite common framework in MES.

Because of this, hierarchical control structures have gained traction for handling complexity in large-scale systems through layered decision-making [12, 13, 14]. However, existing approaches focus on single energy domains (e.g., electricity) or employ simplified subsystem representations, limiting their applicability for large-scale MES. In this contexts, a hierarchical control approach for MES was proposed in [15], employing high-level energy reduced models for cross-vector coordination, and detailed nonlinear models for local control. Despite the enhanced computational efficiency, the approach still relies on a centralized coordination scheme, not considering local objectives or privacy concerns of individual energy stakeholders.

In fact, all mentioned control methods implement coordination schemes where MES subsystems cooperate to achieve global welfare and not by pursuing local objectives and interests, which a more realistic scenario in the energy system [16]. Such aspects can be solved within game theoretical methods, addressing incentives design and providing rigorous frameworks to manage cooperation profit among interconnected systems. Classical cooperative approaches such as the Shapley value or Nash bargaining offer fairness guarantees but either become computationally intractable for large coalitions [17, 18] or rely on simplified models [19]. In contrast, non-cooperative game theory can model the behavior of self-interested agents where collaboration cannot be assumed [20]. Each subsystem optimizes its local objective while accounting for coupling constraints, leading to equilibrium-based coordination rather than centralized optimization. Stackelberg formulations are often used with success, but may lack convergence guarantees [21]. More recently, Generalized Nash Equilibrium Problems (GNEPs) better represent coupling among agents, with distributed algorithms ensuring convergence, scalability, and privacy preservation [22]. In this context, a game-theoretical control framework for interconnected electricity and gas networks was presented in [23], relying on model approximation procedures to guarantee convergent and feasible coordination, without considering network dynamics.

Contribution

This work proposed a novel hierarchical control approach for MES that overcomes the limitations of previous methods and is experimentally validated on a real benchmark.

The proposed control architecture consists on the following features:

1. It separates decision-making across layers: decentralized low-level model predictive controllers (L-MPCs) regulate individual subsystems, or clusters of subsystems, while a high-level coordinator optimizes exchanges among different subsystems across different energy domains. Each L-MPC operates with a

control rate compatible to the subsystem dynamics, allowing multi-rate scalable control of large-scale complex systems.

2. An energetic modeling framework is employed at the high-level coordination layer, supporting multiple coordination paradigms:
   - Centralized coordination, achieving globally optimal operation.
   - Distributed coordination, achieving globally optimal operation while preserving privacy.
   - Game-theoretic coordination, considering local objectives and interests, while preserving privacy and guaranteeing fair economic outcomes.
3. The control architecture is validated experimentally on a real multi-energy test facility in Milan, located at Ricerca sul Sistema Energetico - RSE, comprising interconnected thermal and electrical networks, as well as a multi-energy hub.

Experimental results confirm the efficiency, flexibility, and scalability of the proposed control paradigm and its ability to operate according to different coordination frameworks. This provides practical tools for the optimal and secure operation of large-scale MESs.

Outline

The paper is structured as follows. Section 2 state the MES problem and associated challenges. Section 3 formulates the regulator's architecture and coordination algorithms. Section 4 presents the experimental setup and case study. Section 5 discusses the results and performance comparison.

2. Problem Statement

2.1. High-level and detailed MES modelling

Consider a multi-energy system $S^\dagger$ comprising M interconnected subsystems $S_1, \dots, S_M$. The interconnections can be described by a directed graph $G(\mathcal{N}, \mathcal{E})$, where nodes $\mathcal{N}$ denote subsystems and edges $\mathcal{E}$ represent their power transfer links. Each edge $(i, j) \in \mathcal{E}$ implies the ability to transfer power p_{ij} from S_i to S_j, subject to an efficiency $\eta_{ij} \in (0, 1]$ representing transfer losses. Moreover, we define the set of inlet and outlet nodes of S_i as $N_i^{\text{in}} = \{j \in \mathcal{N} | (j, i) \in \mathcal{E}\}$ and $N_i^{\text{out}} = \{j \in \mathcal{N} | (i, j) \in \mathcal{E}\}$, respectively. Each ith subsystem can be characterized by a unique energy domain (e.g., a district heating network) or by different energy domains regulated by a unique control unit (e.g., a multi-energy hub or building). The subsystems within $S^\dagger$ can exchange power through multi-energy power interfaces such as heat pumps (from electrical to thermal), fuel cells (from gas to electrical), or co-generators (from gas to electrical and thermal), all characterized by defined efficiencies. Hence, a MES $S^\dagger$ can be representative of a multi-energy district, e.g., an island or a campus, where electrical grids, district heating networks, and multi-energy buildings are interconnected and can exchange energy through conversion interfaces.

Each subsystem S_i within $S^\dagger$ can be generically described as a nonlinear dynamical model

$$\dot{x}_i(t) = f_i(x_i(t), u_i(t), d_i(t), p_i^t(t)), \tag{1}$$

where x_i denotes local states, u_i local control inputs, d_i exogenous disturbances, whereas p_i^t, defined as

$$p_i^t(t) = [\{p_{ij}(t)\}_{\forall j \in \mathcal{N}_i^{\text{out}}}, \{\eta_{ji} p_{ji}(t)\}_{\forall j \in \mathcal{N}_i^{\text{in}}}], \tag{2}$$

collects the outgoing and ingoing power transfers of S_i with its neighboring subsystems, with η_{ji} being the efficiency for the power transfer from S_j to S_i. Note that bidirectional power flows are treated with two opposite edges.

Nonetheless, MES models, being inherently complex and large-scale and involving multi-domain dynamics, can be unsuitable for optimization-based control algorithms. A possible solution to this issue relies on a high-level energetic subsystem modeling, involving just energy dynamics and cross-domain power flows, resulting in a linear model suitable for control design (more details in [15]). In particular, the energy stored in each subsystem S_i can be expressed as a generic function of its internal states

$$e_i(t) = \xi_i(x_i(t)), \tag{3}$$

whereas its time variation is given by the overall power balance, i.e.,

$$\dot{e}_i(t) = p_i^g(t) - p_i^l(t) - \sum_{\forall j \in \mathcal{N}_i^{\text{out}}} p_{ij}(t) + \sum_{\forall j \in \mathcal{N}_i^{\text{in}}} \eta_{ji} p_{ji}(t). \tag{4}$$

where p_i^g and p_i^l denote the net local power generation and absorption in a given subsystem S_i, whereas the sums in (4) represent all ingoing/outgoing power transfers. The generated and absorbed powers in a subsystem S_i are function of local states, inputs, and disturbances [15]. As later clarified, this compact energy-based model in (4), being linear, shows to be suitable for large-scale coordination, whereas the detailed model (1) can be exploited for local control to ensure feasibility and cost-effective regulation.

2.1.1. Modelling example

To provide a clearer physical interpretation of the differences between the detailed dynamical model (1) and the high-level energetic model (4) of thermo-hydraulic subsystem S_i, consider the example of a heat pump which receives a water flow to be heated which is then injected in a pipe connected in series. The input flow to the heat pump has a temperature T_{in}^{hp} and a mass flow q^{hp}. The heat pump heats the fluid by receiving an electrical power input P_{el}^{hp} and an electrical-to-thermal power efficiency η^{hp}, resulting in an output temperature T_{out}^{hp}:

$$T_{out}^{hp}(t) = T_{in}^{hp}(t) + \frac{\eta^{hp} P_{el}^{hp}(t)}{q^{hp}(t) c_p}, \tag{5a}$$

where c_p is the specific heat. The fluid leaves the heat pump and enters the pipe at the same water flow-rate. Following the finite-volume modeling method [24], the pipe is spatially discretized into n segments, each with temperature T_i and uniform mass m. The dynamic behavior of each ith pipe segment, with $i \in \{1, \dots, n\}$, is

$$c_p\, m\, \dot{T}_i^p(t) = c_p\, q^{hp}(T_{i-1}^p(t) - T_i^p(t)) + k\,(T_{ext}(t) - T_i^p(t)), \tag{5b}$$

where T_{ext} represents the external ambient temperature, while $T_0^p = T_{out}^{hp}$ and $T_{out}^p = T_n^p$ are the input and output temperatures of the pipe, respectively. Defining the state $x = [T_1^p, \dots, T_n^p]$, the manipulable input $u = [T_{in}^{hp},\ q^{hp}]$, the power exchange with the electricity domain $p^t = \eta^{hp} P_{el}^{hp}$, and the disturbance $d = T_{ext}$, the formulation in (5) recovers the detailed nonlinear dynamical model (1).

Additionally, consider the total energy of the system, i.e., the one stored in the pipe volumes, which is defined as $e(t) = \sum_i^n c_p m T_i^p(t)$. The total energy dynamics can be obtained by summing (5b) across all pipe sections, including (5a), i.e.,

$$\begin{aligned}
\dot{e}(t) &= c_p q^{hp}(t)(T_{out}^{hp}(t) - T_{out}^p(t)) + k \sum_i^n (T_{ext}(t) - T_i^p(t)) \\
&= c_p q^{hp}(t) T_{in}^{hp}(t) + \eta^{hp} P_{el}^{hp}(t) - c_p q^{hp}(t) T_{out}^p(t) \\
&\quad + k \sum_i^n (T_{ext}(t) - T_i^p(t)), \qquad (6) \\
&= p^g(t) + p^t(t) + p^l(t), \qquad (7)
\end{aligned}$$

where $p^g(t) = c_p q^{hp}(t) T_{in}^{hp}(t)$ is the local power injection, $p^t(t) = \eta^{hp} P_{el}^{hp}(t)$ represents the power exchanged with the electrical domain, and $p^l(t) = -c_p q^{hp}(t) T_{out}^p(t) + k \sum_i^n (T_{ext} - T_i^p(t))$ is the net local power absorption. Introducing these power variables, it is possible to express the total energy dynamics as in (4), yielding to a linear model prone for high-level coordination.

2.2. Control objectives

Controlling an interconnected and heterogeneous MES $S^\dagger$ involves multiple objectives:

1. *Large-scale and multi-domain coordination*: Cross-vector power exchanges among subsystems $S_1, \dots, S_M$ within $S^\dagger$ must be optimally managed in scalable fashion, despite its dimension, complexity, and heterogeneous dynamics.
2. *Self-interests and confidentiality*: Subsystems S_i may belong to diverse operators or final users, characterized by different local conflicting objectives and subject to privacy concerns.
3. *Local control and feasibility*: Each subsystem S_i must be locally regulated at a time rate compatible to the local dynamics, guaranteeing cost-effective and feasible operation of local resources.

Given the necessity of addressing both coordination-oriented and local objectives, a multi-layer control approach is proposed in the following, enabling different coordination schemes.

3. Multi-Layer Control Framework

The proposed multi-layer control framework addresses MES challenges highlighted in Section 1 by distributing

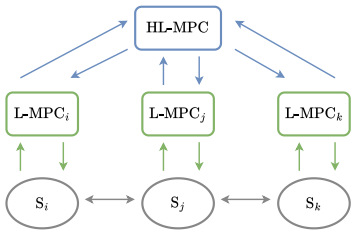


Figure 1: Multi-layer regulator with centralized coordination.

decision-making across two control layers, as schematically presented in Figure 1. The framework separates local regulation from global coordination, addressed by the low and high control layer, respectively. The low-level layer employs a local Model Predictive Controller for each subsystem S_i, denoted as L-MPC$_i$, which leverage the detailed subsystem model (1). Each L-MPC operates with a prediction horizon $N_i > 0$ and sampling period $\tau_i > 0$, designed for the local dynamical behavior. This control layer is designed to ensure cost-effective operation and local feasibility, addressing Objective 3 in Section 2.2, while tracking references provided by a high-level coordination layer.

The High-Level Model Predictive Control (HL-MPC) layer is designed to optimize power exchanges among all subsystems within $S^\dagger$, as well as their overall stored energy, exploiting the energy-based model (4) of each subsystem. This control layer, based on linear energetic models, enables scalable coordination of power exchanges in $S^\dagger$. The high layer supports centralized, distributed, or game-theoretic approaches depending on the degree of cooperation and data-sharing permitted, as it will be detailed in Section 3.2. Such architectures will enable to achieve Objectives 1 and 2 in Section 2.2.

The HL-MPC layer operates with a larger sampling time with respect to the each L-MPC$_i$, i.e., $\tau_h \geq \tau_i$ $\forall i \in \mathcal{N}$, and its optimization horizon $N_h\tau_h$ must cover the entire local prediction windows of each local regulator, i.e., $N_h\tau_h \geq N_i\tau_i + \tau_h$. For simplicity, τ_h is chosen as a multiple of τ_i, i.e., $\exists H_i \in \mathbb{N} \mid \tau_h = H_i\tau_i$. For the sake of clarity, a discrete time index $k_i \in \mathbb{N}$ is introduced for the local regulation of each subsystem S_i, defining the time instants $t = k_i\tau_i$ when the L-MPC$_i$ is executed, while $k_h \in \mathbb{N}$ is used for the HL-MPC layer, which is executed at time instants $t = k_h\tau_h$.

3.1. Low-Level Model Predictive Control

Each L-MPC$_i$ regulates a subsystem S_i considering a prediction horizon $\mathcal{T}_i = \{k_i, \dots, k_i + N_i - 1\}$, $\forall i \in \mathcal{N}$. It is designed to minimize a local generic cost function $\mathcal{F}(x_i(k), u_i(k))$, while tracking high-level references computed by the HL-MPC. These are the total energy stored $e_i^*(k)$ and power exchanged with all neighboring subsystems, included in $p_i^{t*}(k)$. The L-MPC$_i$ problem is

$$\min_{\substack{u_i(\cdot), p_i^t(\cdot) \\ \epsilon_i^e(\cdot),\, \epsilon_i^e(\cdot)}} \sum_{k\in\mathcal{T}_i} \left(\mathcal{F}(x_i(k), u_i(k)) + \gamma_i^e \epsilon_i^e(k)^2 + \gamma_i^p \epsilon_i^p(k)^2 \right) \quad (8a)$$

$$\text{s.t.} \quad \forall k \in \mathcal{T}_i,$$

$$x_i(k+1) = \tilde{f}_i(x_i(k), u_i(k), d_i(k), p_i^t(k)), \quad (8b)$$

$$x_i(k_i) = x_i^m(k_i), \quad (8c)$$

$$\underline{x} \leq x_i(k) \leq \bar{x}, \quad (8d)$$

$$\underline{u} \leq u_i(k) \leq \bar{u}, \quad (8e)$$

$$e_i^*\left(\left\lfloor \frac{k}{H_i} \right\rfloor\right) = \xi(x_i(k)) + \epsilon_i^e(k), \quad (8f)$$

$$p_i^{t*}\left(\left\lfloor \frac{k}{H_i} \right\rfloor\right) = p_i^t(k) + \epsilon_i^p(k), \quad (8g)$$

where (8b) is a discretized version of (1) using a suitable integration method, (8c) sets the initial state to the measure x_i^m, and (8d)-(8d) express local bounds. Morever, (8f)-(8g) express the tracking of the high-level references, and step index $\left(\left\lfloor \frac{k_i}{H_i} \right\rfloor\right)$ returns the corresponding high level step index $k_h \in \mathcal{T}_h$. $\epsilon_i^e, \epsilon_i^p$ are slack variables included for feasibility reasons, highly penalized in the cost function through the weights $\gamma_i^e, \gamma_i^p > 0$.

3.2. High-Level Coordination Layer

The coordination layer, i.e., the HL-MPC, employs the high-level energy model (4), discretized as

$$e_i(k_h+1) = e_i(k_h) + \tau_h \Bigg(p_i^g(k_h) - p_i^l(k_h) - \sum_{\forall j \in \mathcal{N}_i^{\text{out}}} p_{ij}(k_h) + \sum_{\forall j \in \mathcal{N}_i^{\text{in}}} \eta_{ji} p_{ji}(k_h) \Bigg). \quad (9)$$

The HL-MPC assumed to receive the following information from the low-level regulators:

- The total energy stored in each subsystem S_i at time k_h, i.e., $e_i(k_h) = \xi_i(x_i^m(k_h H_i))$.
- The maximum and minimum storable energy in each subsystem S_i, denoted as $\bar{e}_i$ and $\underline{e}_i$ respectively, which can be derived exploiting the local states bounds and (3).
- The maximum and minimum power that can be generated within each subsystem S_i, denoted as $\bar{p}_i^g$ and $\underline{p}_i^g$ respectively.
- A convex function expressing the local produced power cost in each subsystem S_i, denoted as $c_i^g(p_i^g)$.

The L-MPC regulators can compute such information from local variables. They can also provide conservative estimates to the high-level coordination layer, preserving some energy and power margins for local management.

The goal of the HL-MPC layer is to define the energy stored e_i^* reference for each subsystem S_i and the power exchanges p_{ij}^{*} among all subsystems within S [†]. For this purpose, three different control architectures are formulated and then tested, having different characteristics. The first and the second are a centralized and a fully-distributed HL-MPC formulation, respectively, both coordinating the overall MES using a cooperative approach where the overall MES cost is minimized. Moreover, the fully-distributed HL-MPC ensures privacy preservation and enhanced scalability with computational complexity does not increase with the MES size. The third formulation is a distributed game-theoretical HL-MPC formulation, where each subsystem negotiates with the others to minimize its own cost function. Note that the design of these different coordination strategies is enabled by the proposed two-layer control approach, managing coordination-oriented strategies at the high-level through energetic linear modeling, while local model complexity is addressed at the low-level layer.

3.2.1. Centralized cooperative coordination

In the centralized scenario, all subsystems share their operational data and agree to optimize the overall MES as a single entity. The high-level controller therefore solves one centralized MPC problem that encompasses all subsystems and their interconnections. Thanks to the linear energy-based model (9), the overall optimization remains computationally tractable also for systems with large-scale dimension and complexity.

The centralized optimal coordination problem is

$$\min_{\substack{e_i(\cdot),p_i^g(\cdot),p_{ij}(\cdot)\\ \forall i\in\mathcal{N},\forall j\in\mathcal{N}_i^{\text{out}}}} \quad \sum_{i\in\mathcal{N}}\sum_{k\in\mathcal{T}_h} c_i^g(p_i^g(k)) \tag{10a}$$

$$\text{s.t.} \quad \forall\, k \in \mathcal{T}_h, \forall\, i \in \mathcal{N},$$

$$e_i(k+1) = e_i(k) + \tau_h\Big(p_i^g(k) - p_i^l(k) - \sum_{\forall\, j\in\mathcal{N}_i^{\text{out}}} p_{ij}(k) + \sum_{\forall\, j\in\mathcal{N}_i^{\text{in}}} \eta_{ji} p_{ji}(k)\Big) \tag{10b}$$

$$e_i(k_h) = \xi_i(x_i^m(k_h H_i)), \tag{10c}$$

$$\underline{e}_i \le e_i(k) \le \bar{e}_i, \tag{10d}$$

$$\underline{p}_i^g \le p_i^g(k) \le \bar{p}_i^g, \tag{10e}$$

$$\underline{p}_{ij} \le p_{ij}(k) \le \bar{p}_{ij}, \quad \forall\, j \in \mathcal{N}_i^{\text{out}}, \tag{10f}$$

where (10c) expresses the state initialization, whereas (10d)-(10f) impose the bounds of the energy, power generation, and power exchanges.

The cost function (10a) minimizes the overall MES operational cost, i.e., aiming to the social welfare of the cooperation. Solving (10) enables to achieve Objective 1 and 3 in Section 2.2, but requires complete data sharing and full cooperation among all agents, not satisfying Objective 2. In fact, stakeholders may be unwilling to disclose operational details or accept solutions different from a self-interested strategy. These limitations motivate the transition toward distributed coordination, where privacy concerns are addressed by decomposing the centralized problem while preserving optimality.

3.2.2. Distributed coordination

To overcome the scalability and privacy limitations of centralized control, the coordination layer can be decomposed into local optimization problems solved by individual subsystem controllers (see Figure 2). This distributed approach is well-suited for systems with independent stakeholders, as it inherently restricts the exchange of private information among neighboring agents, thus fulfilling Objective 2 (Section 2.2). As mentioned, two different distributed strategies are proposed based either on

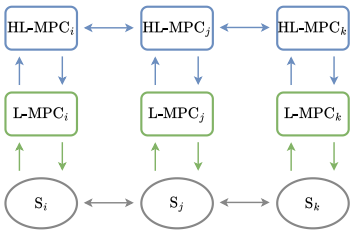


Figure 2: Multi-layer regulator with distributed coordination.

cooperative or non-cooperative coordination frameworks. These are formulated in the following.

Cooperative coordination via distributed optimization

Cooperative coordination can be achieved using dual decomposition algorithms like Dual Consensus ADMM. This requires reformulating the centralized problem (10) into a separable form [25, 26]. The subproblem of each subsystem S_i is then solved by a distributed high-level regulator, denoted as HL-MPC$_i$. Each HL-MPC$_i$ is here formulated to optimize its own local variables in (10), i.e., e_i and p_i^g, as well as the power that S_i receives from the neighbouring subsystems S_j, i.e., p_{ji} with $j \in \mathcal{N}_i^{\text{in}}$. To couple all subsystems optimization problems, each HL-MPC$_i$ optimizes a local copy of the power transferred from S_i to the neighbouring subsystems, denoted as $\tilde{p}_{ij}$ with $j \in \mathcal{N}_i^{\text{out}}$. This enables to rewrite (10) as

$$\min_{\substack{e_i(\cdot),p_i^g(\cdot),\\ \tilde{p}_{ij}(\cdot),p_{ji}(\cdot)\\ \forall i\in\mathcal{N},\forall j\in\mathcal{N}_i^{\text{out}}}} \quad \sum_{i\in\mathcal{N}}\sum_{k\in\mathcal{T}_h} c_i^g(p_i^g(k)) \tag{11a}$$

$$\text{s.t.} \quad \forall k \in \mathcal{T}_h, \forall i \in \mathcal{N},$$

(10c)-(10e),

$$e_i(k+1) = e_i(k) + \tau_h\Big(p_i^g(k) - p_i^l(k) - \sum_{\forall j\in\mathcal{N}_i^{\text{out}}} \tilde{p}_{ij}(k) + \sum_{\forall j\in\mathcal{N}_i^{\text{in}}} \eta_{ji} p_{ji}(k)\Big) \tag{11b}$$

$$\underline{p}_{ij} \le \tilde{p}_{ij}(k) \le \bar{p}_{ij}, \quad \forall j \in \mathcal{N}_i^{\text{out}}, \tag{11c}$$

$$\underline{p}_{ji} \le p_{ji}(k) \le \bar{p}_{ji}, \quad \forall j \in \mathcal{N}_i^{\text{in}}, \tag{11d}$$

$$\tilde{p}_{ij}(k) = p_{ij}(k), \quad \forall j \in \mathcal{N}_i^{\text{out}}. \tag{11e}$$

For the sake of clarity, the local decision variables of each subsystem S_i are included in the following vector

$$x_i^c = [e_i,\ p_i^g, \{\tilde{p}_{ij}\}_{\forall j\in\mathcal{N}_i^{\text{out}}}, \{p_{ji}\}_{\forall j\in\mathcal{N}_i^{\text{in}}}]^\top, \tag{12}$$

enabling to compactly write problem (11) as

$$\min_{\substack{x_i^c(\cdot)\\ \forall i\in\mathcal{N}}} \quad \sum_{i\in\mathcal{N}}\sum_{k\in\mathcal{T}_h} \mathcal{J}_i^c(x_i^c(k)) \tag{13a}$$

$$\text{s.t.} \quad \forall k \in \mathcal{T}_h, \tag{13b}$$

$$x_i^c(k) \in \mathcal{X}_i^c, \quad \forall i \in \mathcal{N}, \tag{13c}$$

$$\sum_{i\in\mathcal{N}} E_i^c x_i^c(k) = 0, \tag{13d}$$

where $\mathcal{J}_i^c(\cdot)$ generically represents the convex cost in (11a), $\mathcal{X}_i^c$ includes the local constraints (10c)-(10e), (11b)-(11d), whereas (13d) represents the coupling constraint (11e) through a suitable definition of the matrix E_i^c. This formulation, including a cost function (13a) separable among subsystem problems and local constraints (13c) decomposed from the coupling ones (13d), is suited for the design of distributed control algorithms, such as the Dual Consensus ADMM (DC-ADMM). In DC-ADMM, agents retain privacy as they solve problems optimizing local variables, costs, and constraints, while converging iteratively on coupling constraints (e.g., interconnecting powers) through dual variable updates. The mathematical details of the algorithm for the distributed solution of (13) is not reported here for the sake of compactness, but the interested reader is referred to [26]. This approach employs an iterative exchange of specific variables, named dual variables, among each couple of distributed regulators HL-MPC$_i$ and HL-MPC$_j$ such that $(i, j) \in \mathcal{E}$, each of them solving local optimization problems. Under mild assumptions, respected in our framework (e.g., problem convexity and connected communication graph), the algorithms convergences to the optimal solution of the centralized problem [13].

This distributed approach also offer scalability benefits over the centralized approach as computational burden does not grow with the number of subsystems. In fact, local problems are solved in parallel by the corresponding HL-MPC distributed regulators. This method however still relies on full cooperation among agents and aims to achieve the social welfare for the overall community, which may not be individually beneficial. A possible so-

lution are benefit allocation algorithms, such as Nash Bargaining, which a-posteriori compute optimal economical transactions among peers to fairly allocate the profit of a collaboration [15]. Nevertheless, non-cooperative coordination frameworks may be necessary, in case agents want to pursue their own objectives.

Non-cooperative coordination via Game Theory

In realistic multi-owner MES scenarios, subsystems may behave strategically and prioritize their own interests. This is here modeled through the introduction of transaction costs c_{ij}, representing the selling price set by S_i for transferring power to S_j, denoted as p_{ij} with $j \in \mathcal{N}_i^{\text{out}}$. Specifically, for each edge $(i, j) \in \mathcal{E}$, we denote S_i as *selling subsystem*, locally optimizing the selling price c_{ij}, and S_j as *buying subsystem*, locally optimizing the received power p_{ij}. This enables to establish a negotiation framework among subsystems HL-MPC regulators, each aiming to maximize its local profit. Hence, selling prices must be added as decision variables for each subsystem S_i

$$x_i^{nc} = [x_i^{c\top} \quad \{c_{ij}\}_{\forall j \in \mathcal{N}_i^{\text{out}}}]^\top,$$

with x_i^c in (12). For the sake of clarity, we define the set of neighbouring subsystems of S_i as $\mathcal{N}_{-i} = \mathcal{N}_i^{\text{in}} \cup \mathcal{N}_i^{\text{out}}$, and the vector containing all their local decision variables as $\boldsymbol{x}_{-i}^{nc} = \{x_j^{nc}\}_{\forall j \in \mathcal{N}_{-i}}$. The non-cooperative coordination problem involves each HL-MPC$_i$ to minimize the following local cost function H_i at each time instant

$$H_i(x_i^{nc}(k), \boldsymbol{x}_{-i}^{nc}(k)) = \mathcal{J}_i^{nc}(x_i^{nc}(k)) + \mathcal{G}_i^{nc}(x_i^{nc}(k), \boldsymbol{x}_{-i}^{nc}(k)) = \mathcal{J}_i^{nc}(x_i^{nc}(k)) - \sum_{\forall j \in \mathcal{N}_i^{\text{out}}} c_{ij}(k) p_{ij}(k) + \sum_{\forall j \in \mathcal{N}_i^{\text{in}}} c_{ji}(k) p_{ji}(k), \quad (14)$$

where $\mathcal{J}_i^{nc}(x_i^{nc}(k))$ is the convex local cost (11a), whereas $\mathcal{G}_i^{nc}(x_i^{nc}(k), \boldsymbol{x}_{-i}^{nc}(k))$ includes the trading costs, i.e., the gain and the cost related to the power exchange with the outlet and inlet neighbouring subsystems of S_i, respectively. Specifically, $\mathcal{G}_i^{nc}(x_i^{nc}(k), \boldsymbol{x}_{-i}^{nc}(k))$ depends on local variables in x_i^{nc}, i.e., the selling price $\{c_{ij}\}_{\forall j \in \mathcal{N}_i^{\text{out}}}$ and the inlet power transfers $\{p_{ji}\}_{\forall j \in \mathcal{N}_i^{\text{in}}}$, and on external variables in $\boldsymbol{x}_{-i}^{nc}$ decided by the neighboring subsystems, i.e., the buying price $\{c_{ji}\}_{\forall j \in \mathcal{N}_i^{\text{in}}}$ and the outlet power transfers $\{p_{ij}\}_{\forall j \in \mathcal{N}_i^{\text{out}}}$.

Before formulating the noncooperative problem, an additional constraint must be introduced to regulate negotiations among subsystems. In fact, being selling subsystems aiming to maximize their local gain, they may indefinitely increase selling prices. However, if this occurs, buying subsystems may stop requesting energy since power transfers may not be convenient with respect to local production. To overcome this scenario, a constraint implementing an "economy of scale" framework is introduced for each selling subsystem S_i, i.e.,

$$c_{ij}(k) \leq -m p_{ij}(k) + q, \quad \forall j \in \mathcal{N}_i^{\text{out}} \quad (15)$$

with $m > 0$ and $q > 0$ being design parameters. The idea of (15) is to upper bound the selling price based on the transferred power, i.e., the higher the transferred power, the lower the selling price. For instance, setting $q = \overline{c}_{ij}$ and $m = \frac{\Delta c_{ij}}{\overline{p}_{ij}}$, with $\overline{c}_{ij} > 0$ and $0 < \Delta c_{ij} < \overline{c}_{ij}$, we obtain a selling price ranging from $\overline{c}_{ij} - \Delta c_{ij}$ (when $p_{ij} = \overline{p}_{ij}$) to $\overline{c}_{ij}$ (when $p_{ij} = 0$). This inherently bounds the selling prices and establishes a regulation framework for multi-energy transactions among subsystems.

Therefore, each HL-MPC$_i$ regulator must solve the following local problem

$$\begin{aligned}
\min_{x_i^{nc}(\cdot)} \quad & \sum_{k \in \mathcal{T}_h} H_i(x_i^{nc}(k), \boldsymbol{x}_{-i}^{nc}(k)) && \text{(16a)}\\
\text{s.t.} \quad & \forall k \in \mathcal{T}_h, && \text{(16b)}\\
& x_i^{nc}(k) \in \mathcal{X}_i^{nc}, && \text{(16c)}\\
& \sum_{i \in \mathcal{N}} E_i^{nc} x_i^{nc}(k) = 0, && \text{(16d)}
\end{aligned}$$

where (16c) includes local constraints (10c)-(10e), (11b)-(11d), and (15), whereas (16d) include the coupling constraint (11e) through a suitable definition of the matrix E_i^{nc}. Unlike the distributed coordination problem in (13), which decomposes the centralized problem while preserving its global objective, (16) focuses on individual subsystem objectives, maximizing a local profit given by internal costs and external trading.

Under mild assumptions, e.g., convexity, this problem can be casted in the framework of Generalized Nash Equilibrium Problem (GNEP) in game-theoretical control, where each agent solves a local optimization problem with costs and constraints depending on other agents' variables [27]. In this framework, iterative algorithms are usually exploited to find a Generalized Nash Equilibrium. Specifically, the Forward-Reflected-Backward Algorithm (FoRB) [22] is exploited to solve (16) in a dis-

tributed manner, ensuring convergence using local information without revealing internal models, as shown in Section 5. Also in this case, the explicit algorithm is not here reported, but its mathematical details are available in [22].

4. Experimental Facility Description

The capabilities of the proposed multi-layer control framework are rigorously evaluated through experimental validation on the Distributed Energy Resources Test Facility (DER-TF) [28, 29], located at Ricerca sul Sistema Energetico in Milan. This test facility is explicitly designed to represent a real-world Multi-Energy System (MES), comprising M=3 interconnected subsystems, S_1, S_2, S_3, which correspond to the Thermal Facility (TF), the Electrical Facility (EF), and the Multi-Energy Hub (EH), respectively. Figure 3 provides a schematic overview of this topology, while Figure 4 shows a photograph of the RSE's Thermal Facility. The interconnection structure is modeled by a directed graph $\mathcal{G}(\mathcal{N}, \mathcal{E})$, where $\mathcal{N} = \{S_1, S_2, S_3\}$ represents the nodes (subsystems) and $\mathcal{E}$ represents the power transfer (p_{ij}) links between them. As illustrated in Figure 3, the physical coupling allows for energy exchange between these domains, subject to associated transfer efficiencies (η_{ji}). Specifically:

- the Thermal Facility (S_1) and the Electrical Facility (S_2) are linked via the Combined Heat and Power (CHP) unit, allowing coupled thermal and power production creating the exchange p_{12}.
- The Energy Hub (S_3) acts as an interface, receiving both electrical power p_{23} and thermal power p_{13} from the Electrical Facility (S_2) and Thermal Facility (S_1), respectively. This hub utilizes internal resources like an electric boiler and a Li-Ion battery to satisfy its dual-carrier load demands.

The topology confirms the complexity of the MES, where multiple domains with heterogeneous dynamics (fast electrical vs. slow thermal) must be optimally coordinated via the defined control framework. The subsequent subsections detail the specific components and operational parameters of each subsystem that constitute the graph nodes.

4.1. Thermal Facility

The Thermal Facility (TF), S_1, reported in Figure 3, integrates multiple heat generation units interfaced with thermal loads via an extensive pipeline distribution infrastructure. Table 1 summarizes the power limits of the main components.

TF component	Data
Gas Boiler	147 kW_{th}
CHP	50 kW_e, 81 kW_{th}
Heat Loads	50 kW_{th}

Table 1: Thermal facility components: power limits.

The subsystem includes two generation units, i.e., a gas boiler and a CHP unit with an thermal-to-electrical efficiency $\eta_{12} = 0.58$, as well as a Thermal Energy Storage (TES) of 10 m^3. These are connected to three internal heat loads (HL1, HL2, HL3) and one external load (HL4, belonging to the Energy Hub) through a pipeline network. The interconnections with the Energy Hub (p_{13}) is represented by HL4, and the one with the EF (p_{12}) represents the electrical power output of the CHP. The TF maximum load capacity is 200 kW_{th}, while the total generation capacity is 365 kW_{th}. The nominal pressure ranges between 2-4 bar, whereas the temperature can vary in range $60 - 80°C$ [30, 24].

The TF subsystem is modelled using the method described in [24], experimentally validated in [29]. The TF's states, included in x_1, encapsulate variables related the thermal dynamics, i.e., (8b), including the water temperature in each piping segment (to capture transport delay and thermal inertia according to finite-volume modelling) and the water temperature of each TES layer. The local controllable inputs u_1 for the TF L-MPC_1 are:

- Gas boiler output temperature setpoint.
- TES charge/discharge flow rate setpoint.

4.2. Electric Facility

The electric facility (EF), S_2, is a low-voltage AC microgrid including an asynchronous generator, a storage system (ESS4) and an electric load. The main components are listed in Table 2, more details in [31].

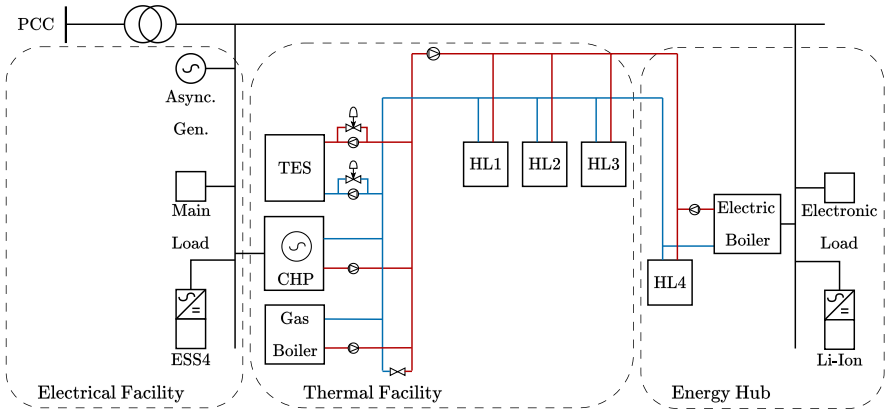


Figure 3: Topology of the entire MES and its connection points to the other subsystems.



Figure 4: Photo of the RSE's Thermal Facility in Milan. The TES tanks on the right side, heat loads and pipline in the center, and the heat load dissipating unit on the left hand side (a chiller).

EF component	**Data**
Async. Generator	6 kW_e
ESS4	57 kWh_e, 15 kW_e
Main Load	60 kW_e

Table 2: Electrical Facility components: power and energy limits.

The total controllable active power genertion capability is 6kW_e from the generator and up to 15kW_e from the ESS4. Loads include the Main Load and power exchganges with the EH (p_{23}). The exchange with the TF is only through the CHP unit. The network topology, shown in Figure 3 is modeled as a single bus.

The electrical subsystem state vector x_2 is defined by the system's electrical state variables primarily including the State of Charge of the battery ESS4, which uses an inner logic and a power meter to keep track of the SOC.

The controllable inputs, u_2, for the EF L-MPC$_2$ are:

- Power setpoint for the asynchronous generator.
- Power setpoint for the ESS4 battery.

4.3. Multi-Energy Hub

The Energy Hub (EH), S_3, interfaces with both the TF (S_1) and the EF (S_2), consuming both thermal and electrical energy. The interdependence stems from the heat load 4 (p_{13}) and from the consumption of electricity (p_{23}) by the electric boiler (EB). Internally, the EH manages its demand using the EB, a Lithium-Ion Battery. The components are detailed in Table 3.

The state vector for the EH, x_3, comprises the state variables necessary to model its dynamics, like the state of charge of the lithium battery. The controllable inputs, u_3, for the L-MPC to manage temperatures and electric demand are:

- Power setpoint for the electric boiler,
- Power setpoint for the Li-Ion battery.

EH component	Data
Electronic Load	10.5 kW_e
Li-Ion	30 kWh_e, 25 kW_e
Electric Boiler	45 kW_{th}
Heat Load 4	50 kW_{th}

Table 3: Energy Hub components: power and energy limits.

5. Results

The proposed control framework, integrating both centralized and distributed high-level regulators within a hierarchical structure, is rigorously tested on the physical Multi-Energy System test facility at RSE in Milan.

Communication between high- and low-level controllers is handled via the MQTT protocol, which enables scalable and asynchronous data exchange for distributed agents. The same protocol is also utilized to share dual variables within high-level distributed optimization algorithms. Local controllers interface with physical assets through standard industrial protocols (OPC UA and Modbus). To accurately reflect the behavior of a real-world distributed algorithm, each controller is deployed on a dedicated virtual machine on a central server, enabling the realistic simulation of inter-agent communication delays and computational constraints. The optimization problems for all scenarios are formulated with CasADi [32] coupled with the large-scale nonlinear solver Interior Point OPTimizer (IPOPT) [33]. Each experimental run lasts approximately six hours, as required for safe on-site operation.

The framework's performance is evaluated by testing the three distinct coordination strategies in the high-level layer, each configured with suitable parameters:

- **Centralized Coordination:** This scenario solves the centralized optimization problem (10). The sampling period for the high-level layer is set to $\tau_h = 15$ min, with a prediction horizon of $N = 24$ samples.
- **Distributed Coordination (ADMM):** The Dual Consensus ADMM [26, 13] is applied to problem (13), suitable for distributed optimization as previously discussed, with sampling time $\tau_h = 15$ min and prediction horizon $N = 24$.
- **Game-Theoretic Coordination (GNEP):** To model self-interested agents, the FoRB [22] algorithm is employed to solve the resulting Generalized Nash Equilibrium Problem (16). Due to the potentially longer time required to find a non-cooperative equilibrium, a larger sampling time of $\tau_h = 30$ min is employed for the HL-MPC, with a horizon of $N = 12$ steps.

The low-level Model Predictive Controllers (L-MPCs) maintain subsystem-specific settings across the scenarios to suit the heterogeneous dynamics. The Thermal Facility local regulator is designed with $\tau_1 = 15$ min with $N_1 = 24$ steps, the Electrical Facility one with $\tau_2 = 1$ min with $N_2 = 60$, whereas the Energy Hub one with $\tau_3 = 5$ min with $N_3 = 36$. As evident, the proposed hierarchical control architecture enables to set different sampling times for each energy domain, consistently with the local time constants.

Finally, electrical and gas energy prices for local production are sourced from the Italian day-ahead energy market data from May 1st, 2025 [34]. The applied external disturbances (prices, electrical loads, and thermal loads) are detailed in Figures 5. Grid electrical prices are shown in Figure 5a, the electric power absorbed by the EF and the EH in Figure 5b, and the thermal loads of the TF and the EH in Figure 5c.

In the following, the results of the experimental tests of the three control strategies are firstly presented. Then, a KPI analysis comparing the achieved costs are discussed.

5.1. Centralized cooperative coordination

First, the centralized control framework has been tested on the multi-energy plant, i.e., solving (10) at high level. The following plots illustrate the power dispatch under centralized coordination for the thermal facility (Figure 6), the energy hub (Figures 7a, 7b), and the electrical facility (Figure 7c).

The dispatch problem for the thermal facility (Figure 6a) shows the consistent use of the CHP (purple) for its capability of producing both thermal and electrical power. The gas boiler (orange) is used as baseline generation to satisfy the load demand. The TES charged/discharged power (cyan) in Figure 6a is represented with the generator convention: power is positive when injected in the TF, and negative when absorbed by the TES for charging. Storage

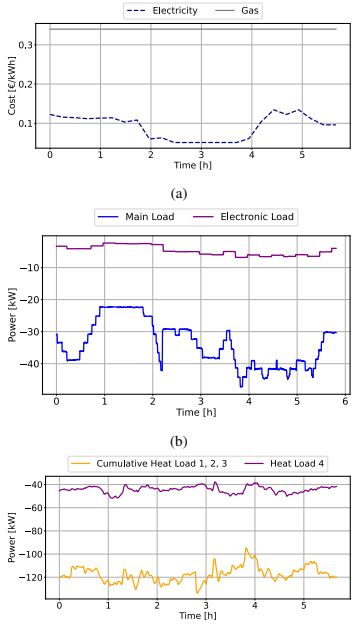


Figure 5: Disturbances used in the tests: (a) Electrical and gas price. (b) Consumption of electrical loads. (c) Consumption of thermal loads.

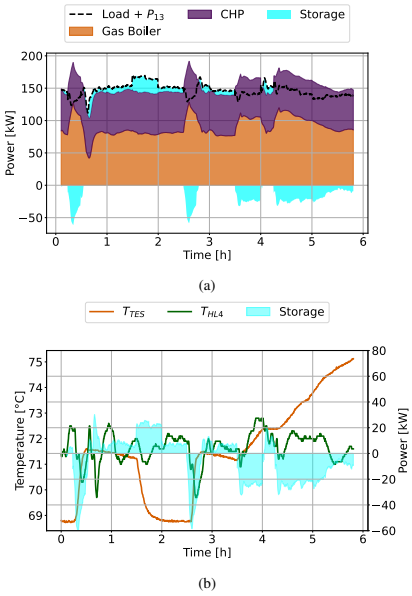


Figure 6: Centralized hierarchical coordination: (a) Energy dispatch for the thermal facility. (b) Relation between internal energy variation and supply pipe of heat load 4, TES top and bottom layer temperatures.

compensates for demand fluctuations. In fact, the storage is discharged when HL1-3 thermal demand peaks, e.g., 1:00-2:00, and charged when it drops, e.g., between 2:30 and 3:00. In the thermal subsystem, energy can be stored either in the TES or in the pipes, as shown in Figure 6b. For example, between 4:00 and 6:00, the TF subsystem is required to store energy, being the storage power negative. This implies the TES temperature to rise, while the pipe temperature varies based on the requested power demand. The Energy hub has two energy carriers, thermal and electrical. The electrical dispatch for the EH, Figure 7a, shows the power exchange with the electrical facility (blue) satisfying the load demand plus the electric boiler consumption (dotted black line). The Storage (cyan) is charged when the electrical prices are low, e.g., from 2:00 to 4:00, and discharged otherwise. On the other hand, the energy hub thermal demand, depicted in Figure 7b, is met by the electric boiler generation (dark blue) and the thermal exchange with the thermal facility (orange).

Finally, Figure 7c shows the Electrical Facility dispatch plot. The black dotted line represent the local electric load plus the energy exchanged with the energy hub. Since the local generation from the asynchronous motor (grey) is limited to 6 kW_{el}, the main sources of energy are the power exchange with the thermal system CHP (purple) and the power bought from the grid (yellow), represented with the generators convention. The EF also sells energy to the grid when prices are high, e.g., around 05:00. Moreover, the EF operates the storage (cyan) accordingly to electrical prices, charging it when prices are low and discharging it when they raise.

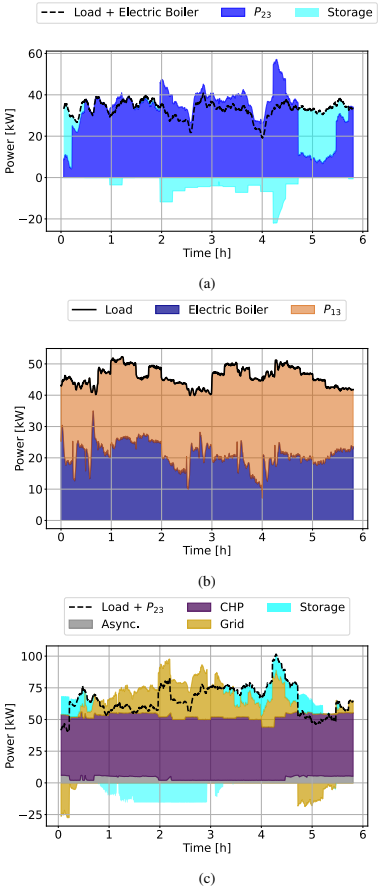


Figure 7: Centralized hierarchical coordination: (a) Electrical dispatch for the energy hub. (b) Thermal dispatch for the energy hub. (c) Electrical facility power dispatch.

5.2. *Distributed cooperative coordination*

The same scenario is tested using the distributed DC-ADMM coordination scheme. As expected, the results in Figures 8 and 9 are close to those of the centralized coordination problem. The differences are due to small variations in disturbance profiles and initial conditions with respect to the centralized tests, impossible to being exactly replicated in the experimental settings. As later discussed in Section 5.4, the centralized and decentralized cooperative coordination achieve similar overall cost.

Notably, the thermal facility L-MPC causes larger variations for loads temperatures with respect to the centralized solution, as evident in Figure 8b. For example, HL 4 supply temperature drops and rises from 4:00 to 4:30, while the TES temperatures remain almost constant. Moreover, looking at the energy hub dispatch shown in Figures 9a and 9b there is an increased use of the electric boiler, leading to a larger exchange with the electric facility. In turn, the EF no longer sells energy to the grid (Figure 9c). Still, the ESS4 charge and discharge cycles in the EF are dictated by the electricity price variations, storing energy when electrical prices are low and discharging when they increase.

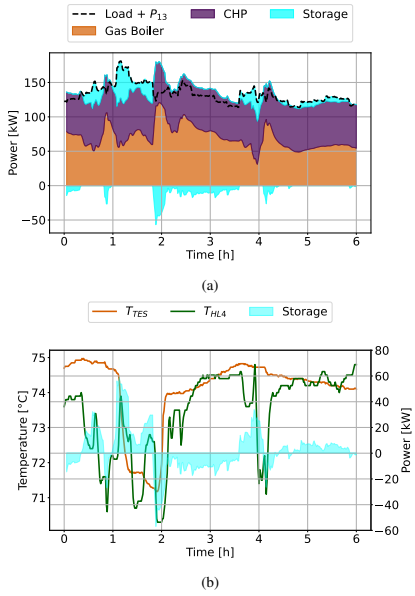


Figure 8: Distributed coordination: (a) Energy dispatch for the thermal facility. (b) Relation between internal energy variation and pipe-TES temperatures.

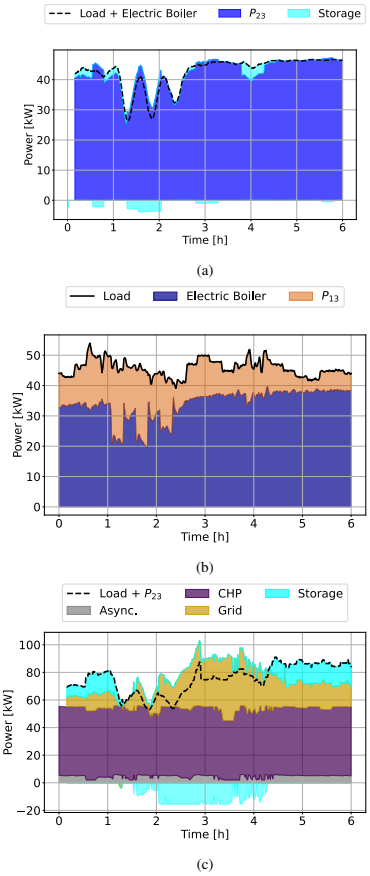


Figure 9: Distributed coordination: (a) Electrical dispatch for the energy hub. (b) Thermal dispatch for the energy hub. (c) Energy dispatch for the electrical facility.

5.3. *Game-Theoretical non-cooperative coordination*

Lastly, the experimental assessment of the noncooperative coordination mechanism is reported. The control strategy computes at each time instant the Nash Equilibrium for the power exchange and the transaction energy prices at once. Such prices are shown in Figure 10a. Because of (15), transaction prices at equilibrium do not indefinitely increase but their trends are related to the energy prices in Figure 5a, remaining competitive with respect to them to incentivize power trading. The outcome aligns with economic principles, as agents are incentivized to purchase from peers when prices are competitive with respect to national energy rates.

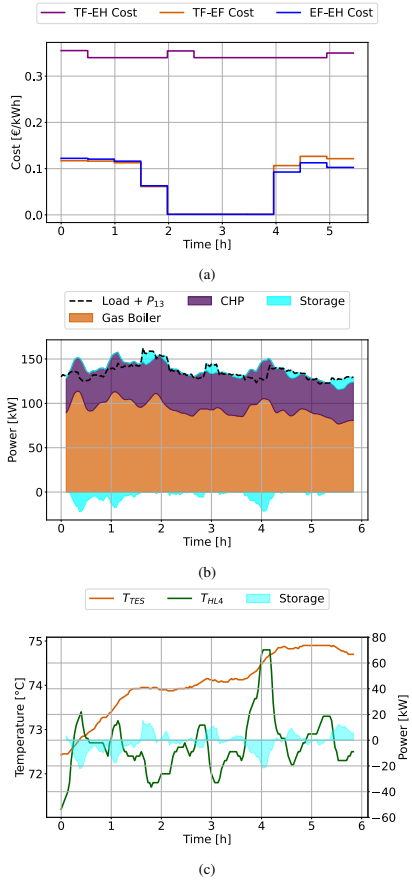


Figure 10: Game theoretical coordination: (a) Equilibrium prices for the power exchanges. (b) Energy dispatch for the thermal facility. (c) Relation between internal energy variation and pipe-TES temperatures.

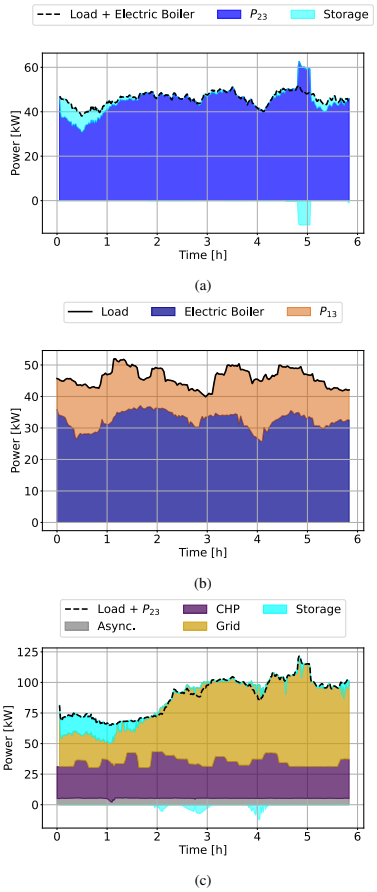


Figure 11: Game theoretical coordination: (a) Electrical dispatch for the energy hub. (b) Thermal dispatch for the energy hub. (c) Electrical Facility power dispatch.

Figure 10b shows the thermal facility dispatch, which operates the CHP around 25 kW, relying more on the gas boiler with respect to the cooperative framework. This is mainly due to the higher efficiency of the gas boiler, implying lower cost for the Thermal facility with respect to fully using the CHP.

Interestingly, more than in previously discussed results, the noncooperative framework exploits more the thermal energy stored in pipes, raising and dropping temperature based on the local HL-MPC requests (Figure 10c).

Moreover, Figure 11a illustrates that exchanges between the energy hub and the electrical facility increase, primarily to meet the EH electric boiler requirements.

Finally, the electrical facility uses its battery when prices are high, 0:00 to 1:30, and charges otherwise, to minimize energy costs, as apparent from Figure 11c. Overall, as CHP inputs are lower than in previous case studies, the energy bought from the grid compensates the difference. Nevertheless, the noncooperative algorithm maintains the ability to satisfy load demands across all agents and energy vectors.

5.4. KPIs Analysis

The evaluation of the proposed regulators is based on Key Performance Indicators (KPIs), which offer both an operational and an economic assessment of the coordination strategies. Specifically, the cost incurred by each subsystem for the cooperative cases (Centralized and DC-ADMM) is evaluated summing the $\mathcal{J}_i^c(\cdot)$ function in (11) for the whole 6-hour experiment. On the other hand, for the non-cooperative case, the cost function $H_i(\cdot,\cdot)$ is evaluated for each agent for the whole experiment, including not only the local costs but also the trading profit/gain.

The achieved results are compared against a benchmark control strategy, relying solely on local control strategies without high-level coordination. Specifically, the TF and EF exchange energy with the power grid only, whereas the energy hub buys from the TF. Table 4 reports the KPIs achieved by the different regulation strategies in the respective experiment. The four 6-hour experiments were conducted over two weeks to ensure consistent boundary conditions, i.e., external temperatures. Unfortunately, due to weather variations, it was not possible to guarantee stable conditions. To account for weather variation, a statistical analysis over multiple experiments is required. Nonetheless, insights are given below.

Centralized coordination achieves the lowest MES cost, with a 16.5% reduction with respect to the benchmark strategy, where power exchanges are not optimized. Although the overall reduced cost, the TF incurs the highest cost due to the lack of profit allocation. In fact, the energy hub does not pay its fair share for the energy consumed in

a fully cooperative scenario. Analogously, the distributed cooperative MES regulation achieves a 13.3% cost reduction compared to the benchmark strategy.
On the other hand, the noncooperative strategy guarantees each agent a profit from the game. The overall MES cost is lower than the benchmark one (9.8% saving) but higher than the cooperative centralized and distributed approaches. This result is expected, as the game theory minimizes players' selfish cost function rather than the common operation. Despite the higher MES cost, subsystems trade the energy exchanges by setting transaction prices. Compared to the benchmark case, the TF and EF are paid by the EH for the transferred energy, incurring lower management costs with respect to the cooperative solutions. As a result, now the EH management implies some operational costs, even if this subsystem is not equipped with local generation.

In conclusion, we report the analysis of controllers' computational times. All coordination strategies ensure feasible computational times even for the distributed and game-theoretic architectures, as shown in Table 5. As expected, the computational times of the lower level does not depend on the adopted coordination strategy, is within the sampling time and is independent of the number of agents and their sampling time. On the other hand, the computational time for the high-level depends on the number of agents, especially the centralized approach. The distributed and game-theoretic architectures employ higher computational time than the centralized one, due to the iterative algorithms able to preserve privacy, which may turn advantageous increasing the number of agents.

Test	**Agent Cost [€]**			**Cost [€]**	
	TF	**EF**	**EH**	[%]	
Bench.	46.6	18.1	0	(Ref.)	64.7
Central.	48.4	5.7	0	(−16.5)	54.1
Dist.	46.3	9.8	0	(−13.3)	56.1
G.T.	23.7	11.5	23.1	(−9.8)	58.3

Table 4: KPIs achieved in the tests. In order: Benchmark, Centralized, Distributed, and Game theory. The table reports also each subsystem cost: thermal facility (TF), electric facility (EF), and energy hub (EH). Finally, the MES operational cost and its percentage variation with respect to the benchmark.

Level	**Strategy/Agent**	**Time [s]**	τ **[s]**
Top	Centralized	≈ 5	900
	Distributed	≈ 90	900
	Game Theory	≈ 180	1800
Low	TF	≈ 60	900
	EF	≈ 1	60
	EH	≈ 2	300

Table 5: Approximate computational times for control elements against their sampling time.

6. Conclusions

The research successfully validated a multi-layer control framework designed for optimal MES management. A significant advantage of this architecture is the interchangeable coordination layer, facilitating the integration of a wide range of coordination mechanisms based on system specifications. This flexibility allows the framework to address complex challenges arising from diverse time constants, model complexity, multiple ownership, and conflicting objectives inherent in MES.

Empirical validation proved that the proposed control framework satisfies the necessary operational constraints of the MES facility. The centralized and distributed coordination strategies effectively manage the network, minimizing the overall operational cost. The non-cooperative coordination, which seeks a Generalized Nash Equilibrium, also maintained the capability to satisfy load demands across all subsystems and energy vectors while computing the optimal economic exchanges.

Future research will focus on improving the robustness and applicability of the proposed framework. Key priorities include developing online learning models to handle time-varying parameters in MES operations, and exploring data-driven methods for direct control or model identification in the low-level MPC layer, reducing reliance on complex model-based regulators.

References

[1] E. Commission, Repowereu plan, https://eur-lex.europa.eu/legal-content/EN/TXT/?uri=COM:2022:230:FIN, accessed: 2025-09-29 (2022).

[2] E. Commission, D.-G. for Communication, European green deal – Delivering on our targets, Publications Office of the European Union, 2021. doi:doi/10.2775/373022.

[3] D.-G. f. E. European Commission, Powering a climate-neutral economy: An eu strategy for energy system integration, https://eur-lex.europa.eu/legal-content/EN/ALL/?uri=COM:2020:299:FIN, accessed: 2025-09-30 (2020).

[4] M. Geidl, G. Andersson, A modeling and optimization approach for multiple energy carrier power flow, in: 2005 IEEE Russia power tech, IEEE, 2005, pp. 1–7.

[5] M. Geidl, G. Andersson, Optimal power flow of multiple energy carriers, IEEE Transactions on power systems 22 (1) (2007) 145–155.

[6] A. Garg, K. Niazi, S. Tiwari, S. Sharma, T. Rawat, Optimal energy management of multi-carrier energy system considering uncertainty in renewable generation, Scientific Reports 15 (1) (2025) 25936.

[7] R. Carli, G. Cavone, T. Pippia, B. De Schutter, M. Dotoli, Robust optimal control for demand side management of multi-carrier microgrids, IEEE Transactions on Automation Science and Engineering 19 (3) (2022) 1338–1351.

[8] A. La Bella, M. Farina, C. Sandroni, R. Scattolini, Design of aggregators for the day-ahead management of microgrids providing active and reactive power services, IEEE Transactions on control systems technology 28 (6) (2019) 2616–2624.

[9] M. Taylor, O. Marjanovic, A. Parisio, Decentralized supervisory control of networked multienergy buildings, IEEE Transactions on Control Systems Technology 32 (3) (2024) 945–959.

[10] V. N. Behrunani, H. Cai, P. Heer, R. S. Smith, J. Lygeros, Distributed multi-horizon model predictive control for network of energy hubs, Control Engineering Practice 147 (2024) 105922.

[11] A. La Bella, A. Falsone, D. Ioli, M. Prandini, R. Scattolini, A mixed-integer distributed approach to prosumers aggregation for providing balancing services, International Journal of Electrical Power & Energy Systems 133 (2021) 107228.

[12] Y. Xu, A. Parisio, Z. Ding, Hierarchical model predictive control for energy efficient buildings with multi-energy storage systems, in: 2020 IEEE Power & Energy Society General Meeting (PESGM), IEEE, 2020, pp. 1–5.

[13] A. La Bella, P. Klaus, G. Ferrari-Trecate, R. Scattolini, Supervised model predictive control of large-scale electricity networks via clustering methods, Optimal Control Applications and Methods 43 (1) (2022) 44–64.

[14] O. Kaya, E. Van Der Roest, D. Vries, T. Keviczky, Hierarchical model predictive control for energy management of power-to-x systems, in: 2020 IEEE PES Innovative Smart Grid Technologies Europe (ISGT-Europe), IEEE, 2020, pp. 1094–1098.

[15] A. La Bella, L. Nigro, R. Scattolini, Predictive control and benefit sharing in multi-energy systems, IEEE Transactions on Control Systems Technology 32 (2) (2023) 368–383.

[16] G. Belgioioso, W. Ananduta, S. Grammatico, C. Ocampo-Martinez, Operationally-safe peer-to-peer energy trading in distribution grids: A game-theoretic market-clearing mechanism, IEEE Transactions on Smart Grid 13 (4) (2022) 2897–2907.

[17] W. Cai, A. B. Kordabad, S. Gros, Energy management in residential microgrid using model predictive control-based reinforcement learning and shapley value, Engineering Applications of Artificial Intelligence 119 (2023) 105793.

[18] A. A. Raja, S. Grammatico, Payoff distribution in robust coalitional games on time-varying networks, IEEE Transactions on Control of Network Systems 9 (1) (2021) 511–520.

[19] M. Xu, Y. Yang, Q. Xu, L. Fang, R. Tang, H. Ji, Asymmetric nash bargaining for cooperative operation of shared energy storage with multi-type users engagement, Frontiers in Energy Research 12 (2024) 1420393.

[20] C.-S. Karavas, K. Arvanitis, G. Papadakis, A game theory approach to multi-agent decentralized energy management of autonomous polygeneration microgrids, Energies 10 (11) (2017) 1756.

[21] T. Guo, P. Li, Z. Wang, R. Shi, Z. Han, H. Xia, J. Li, Integrated modelling and optimal operation analysis of multienergy systems based on stackelberg game theory, Energy 236 (2021) 121472.

[22] G. Belgioioso, S. Grammatico, Semi-decentralized generalized nash equilibrium seeking in monotone aggregative games, IEEE Transactions on Automatic Control 68 (1) (2021) 140–155.

[23] W. Ananduta, S. Grammatico, A two-stage approach for a mixed-integer economic dispatch game in integrated electrical and gas distribution systems, IEEE Transactions on Control Systems Technology 32 (1) (2023) 86–98.

[24] L. Nigro, A. La Bella, F. Casella, R. Scattolini, Control-oriented modeling, simulation, and predictive control of district heating networks, IEEE Transactions on Automation Science and Engineering (2024).

[25] L. Nigro, A. La Bella, R. Scattolini, Distributed two-layer predictive control of multi-energy systems, in: 2024 European Control Conference (ECC), IEEE, 2024, pp. 2429–2434.

[26] T.-H. Chang, M. Hong, X. Wang, Multi-agent distributed optimization via inexact consensus admm, IEEE Transactions on Signal Processing 63 (2) (2014) 482–497.

[27] G. Belgioioso, P. Yi, S. Grammatico, L. Pavel, Distributed generalized nash equilibrium seeking: An operator-theoretic perspective, IEEE Control Systems Magazine 42 (4) (2022) 87–102.

[28] C. Gandolfi, R. Lazzari, M. Zanoni, D. Palladini, Mission project: Design of mv/lv hybrid ac/dc smart-energy grid, in: 2022 AEIT International Annual Conference (AEIT), IEEE, 2022, pp. 1–6.

[29] L. Nigro, S. Polimeni, C. Anderis, M. Muro, A. La Bella, Experimental validation and design of nonlinear predictive control and moving horizon estimation for district heating, IFAC-PapersOnLine 59 (9) (2025) 157–162.

[30] C. Anderis, M. A. M. Alvarado, R. Lazzari, Implementation of an experimental facility for district heating networks flexibility assessment, in: 2024 AEIT International Annual Conference (AEIT), IEEE, 2024, pp. 1–6.

[31] R. Lazzari, A. La Bella, Distributed multi-layer control of hybrid ac/dc grids: Design and experimental validation, IET Renewable Power Generation 18 (2024) 4414–4425.

[32] J. A. Andersson, J. Gillis, G. Horn, J. B. Rawlings, M. Diehl, Casadi: a software framework for nonlinear optimization and optimal control, Mathematical Programming Computation 11 (1) (2019) 1–36.

[33] A. Waechter, Ipopt documentation, `https://coin-or.github.io/Ipopt/AUTHORS.html` (2025).

[34] G. M. Energetici, Database of italian energy prices, `https://www.mercatoelettrico.org/` (2025).

8

Conclusion

This dissertation has addressed the design of scalable and optimal control architectures for networked multi-energy systems, focusing on achieving efficient, coordinated, and sustainable operation across interconnected energy domains. The research was structured around two central questions: how to model and control district heating networks for optimal and reliable performance, and how to coordinate large-scale MES while respecting scalability, privacy, and stakeholder rationality. Through this dual focus, the work has provided both methodological advancements and experimentally validated results that bridge the gap between theoretical control frameworks and their deployment in real-world energy infrastructures.

Scientific Contribution

The first part of the dissertation developed a unified control-oriented modeling framework for district heating networks. A detailed simulation model and a reduced-order control model were proposed to enable, respectively, accurate dynamic studies and real-time model predictive control implementation. The simulation model, implemented in Modelica and validated experimentally at the RSE Test Facility, demonstrated strong agreement with measured data, thereby ensuring physical fidelity. The reduced-order model enabled the formulation of a nonlinear MPC that exploits network thermal inertia and achieves up to 15% cost reductions compared with rule-based control. These results provide an effective trade-off between model complexity and computational feasibility, establishing a rigorous foundation for control of thermohydraulic systems within larger energy networks.

The second part advanced control and coordination strategies for multi-energy systems. One hierarchical framework was developed to balance complexity and allow coordination. The proposed framework supports different coordination mechanisms to answer specific needs of the MES. Specifically, three coordination mechanisms were proposed. Two solutions assume agents' cooperation: a centralized MPC and a distributed two-layer predictive control framework ensuring scalability and privacy. The third, a distributed game theory algorithm, assumes non-cooperation while guaranteeing privacy and agents' selfish interests. The cooperative strategies were coupled with a cooperative bargaining mechanism to ensure fair economic benefit sharing among subsystems, addressing rationality and incentivization factors for real-world MES adoption. The architectures were validated on experimental MES configurations. Results confirmed the regulator's capabilities, maintaining operation and reducing costs.

Final Remarks

This work contributes to the field of MES coordination by unifying advanced control design, game-theoretic coordination, and experimental validation within a single, scalable framework. It extends existing literature by demonstrating that nonlinear, cross-domain energy interactions can be managed optimally without compromising local autonomy or privacy. The findings have implications for both theory and practice: they reinforce the role of control-oriented modeling in energy systems integration, establish MPC as a viable tool for future smart energy infrastructures, and provide concrete mechanisms to align technical optimality with stakeholder incentives.

Ultimately, this dissertation demonstrates that scalable and optimal control architectures are not only theoretically attainable but also practically realizable. By integrating physical modeling, optimal control, and coordination in privacy-aware frameworks, the research supports the transition toward more resilient, efficient, and decarbonized energy networks. These contributions hold enduring value for both the academic and industrial control communities, offering a pathway toward the next generation of intelligent, cooperative, and sustainable multi-energy systems.

Future Work

While this dissertation advances the state-of-the-art in control for multi-energy systems, several limitations remain. First, the framework assumes perfect knowledge of the plant structure and static operation conditions (e.g., water flow directions) over the prediction horizon. Thus, neglecting potential dynamical changes in plant topology or operation. Second, nonlinearities and mapping of components efficiency are not detailed, which could lead to suboptimal control decisions. Third, while renewable energy sources are key features of MES, the proposed case studies do not account for the stochasticity intrisic of RES. Finally, the computational complexity of the lower level optimization for large-scale networks could lead to intractable optimization problems. Addressing these limitations is an opportunity for future research.

Plant reconfiguration and changing operating condition.

Over the controller's prediction horizon, the plant may experience changes in operating conditions, including flow directions reversal, power grid switching actions, or network topology changes. Neglecting these dynamics can lead to structurally inconsistent models, leading to suboptimal or even infeasible control decisions.

To address this, future work could integrate mixed-integer decision variables into the optimal control formulation, enabling the controller to actively reconfigure the network (e.g., adjust valve settings or switchs) while optimizing continuous inputs [47]. Another promising direction is the fusion of model-based control and online learning, where data-driven components update model parameters and logic to account for slowly varying conditions and unmodeled configuration changes [11].

Efficiency and nonlinear behaviors.

To further reduce energy consumption, the economic MPC should explicitly model the nonlinear efficiency behaviors of key devices, such as pumps, boilers, and heat pumps, where efficiency varies nonlinearly with operating conditions (e.g., speed, power, temperature). These nonlinearities are critical for accurate energy optimization.

Achieving this requires augmenting the lower-level model with mixed-integer variables to accurately capture mode switches, start-up/shut-down trajectories, minimum power thresholds, and piecewise efficiency approximations. This approach will enable the controller to more accurately minimize energy consumption [26].

Stochastic models and robus MPC.
The inherent stochasticity of renewable energy sources, such as wind and photovoltaic generation, introduces operational uncertainty directly affecting the feasibility and economic performance of control strategies.

To address these challanges, future work could explore stochastic and robust MPC formulations. Stochastic methods focus on minimizing expected cost under uncertainty, whereas robust optimization guarantees constraint satisfaction in uncertain conditions. Possible research directions include: (i) design of robust MPC using scenario-based approaches [9], and (ii) experimental validation of robust MPC with stochastic components [58].

Computational complexity at the lower level.
The computational complexity introduced by nonlinearities and possible mixed-integer variables in the lower-level optimization can make real-time economic MPC intractable for large-scale energy systems.

To address this challange, hierarchical control structures, such as those proposed in the author's work [41], could be considered. This approach would distribute the optimization burden, enabling more scalable and efficient real-time control.

By pursuing these directions, future research can overcome the current limitations and enable the deployment of scalable, robust, and efficient control architectures for next-generation multi-energy systems.

Bibliography

References

[1] M. A. M. Alvarado, C. Anderis, R. Lazzari, L. Nigro, and A. La Bella. Development and experimental validation of an open-source model library for district heating network simulation. In *2024 Open Source Modelling and Simulation of Energy Systems (OSMSES)*, pages 1–6. IEEE, 2024.

[2] M. Arnold, R. R. Negenborn, G. Andersson, and B. De Schutter. Model-based predictive control applied to multi-carrier energy systems. In *2009 IEEE power & energy society general meeting*, pages 1–8. IEEE, 2009.

[3] V. N. Behrunani, A. Irvine, G. Belgioioso, P. Heer, J. Lygeros, and F. Dörfler. Designing fairness in autonomous peer-to-peer energy trading. *IFAC-PapersOnLine*, 56(2):3751–3756, 2023.

[4] G. Belgioioso and S. Grammatico. Semi-decentralized generalized nash equilibrium seeking in monotone aggregative games. *IEEE Transactions on Automatic Control*, 68 (1):140–155, 2021.

[5] G. Belgioioso, W. Ananduta, S. Grammatico, and C. Ocampo-Martinez. Operationally-safe peer-to-peer energy trading in distribution grids: A game-theoretic market-clearing mechanism. *IEEE Transactions on Smart Grid*, 13(4):2897–2907, 2022.

[6] D. Bilgic, A. Koch, G. Pan, and T. Faulwasser. Toward data-driven predictive control of multi-energy distribution systems. *Electric Power Systems Research*, 212:108311, 2022.

[7] P. C. Blaud, P. Haurant, F. Claveau, B. Lacarrière, P. Chevrel, and A. Mouraud. Modelling and control of multi-energy systems through multi-prosumer node and economic model predictive control. *International Journal of Electrical Power & Energy Systems*, 118:105778, 2020.

[8] F. Bonassi, A. La Bella, R. Lazzari, C. Sandroni, and R. Scattolini. Supervised control of hybrid ac-dc grids for power balance restoration. *Electric Power Systems Research*, 196:107107, 2021.

[9] M. C. Campi, S. Garatti, and M. Prandini. The scenario approach for systems and control design. *Annual Reviews in Control*, 33(2):149–157, 2009.

[10] R. Carli, G. Cavone, T. Pippia, B. De Schutter, and M. Dotoli. Robust optimal control for demand side management of multi-carrier microgrids. *IEEE Transactions on Automation Science and Engineering*, 19(3):1338–1351, 2022.

[11] V. Casagrande, M. Ferianc, M. Rodrigues, and F. Boem. An online learning method for microgrid energy management control. In *2023 31st Mediterranean Conference on Control and Automation (MED)*, pages 263–268. IEEE, 2023.

[12] F. Casella and A. Leva. Modelling of thermo-hydraulic power generation processes using modelica. *Mathematical and Computer Modelling of Dynamical Systems*, 12(1): 19–33, 2006.

[13] E. A. M. Ceseña and P. Mancarella. Energy systems integration in smart districts: Robust optimisation of multi-energy flows in integrated electricity, heat and gas networks. *IEEE Transactions on Smart Grid*, 10(1):1122–1131, 2018.

[14] G. Ceusters, R. C. Rodríguez, A. B. García, R. Franke, G. Deconinck, L. Helsen, A. Nowé, M. Messagie, and L. R. Camargo. Model-predictive control and reinforcement learning in multi-energy system case studies. *Applied Energy*, 303:117634, 2021.

[15] T.-H. Chang, M. Hong, and X. Wang. Multi-agent distributed optimization via inexact consensus admm. *IEEE Transactions on Signal Processing*, 63(2):482–497, 2014.

[16] G. Chicco, S. Riaz, A. Mazza, and P. Mancarella. Flexibility from distributed multi-energy systems. *Proceedings of the IEEE*, 108(9):1496–1517, 2020.

[17] E. Commission. Communication from the commission to the european parliment, the european council, the council, the european economic and social commitee and the committee of the regions repowereu plan. `https://eur-lex.europa.eu/legal-content/EN/TXT/?uri=COM:2022:230:FIN`, 2022. Accessed: 2025-09-29.

[18] E. Commission. Energy performance of buildings directive. `https://energy.ec.europa.eu/topics/energy-efficiency/energy-performance-buildings/energy-performance-buildings-directive_en`, 2023. Accessed: 2025-08-18.

[19] E. Commission and D.-G. for Communication. *European green deal – Delivering on our targets*. Publications Office of the European Union, 2021. doi: doi/10.2775/373022.

[20] E. Commission, D.-G. for Energy, F. I. for Systems, I. R. ISI, Guidehouse, M. . C. Inc, TNO, Trinomics, U. University, O. Hoogland, V. Fluri, C. Kost, M. Klobasa, M. Kühnbach, M. Khanra, M. Antretter, J. Koornneef, H. v. d. Weijde, A. Satish, E. Battistutta, K. Veum, J. Gorenstein Dedecca, A. Doorman, L. Van Nuffel, B. Breitschopf, A. Herbst, and O. Cerny. *Study on energy storage*. Publications Office of the European Union, 2023. doi: doi/10.2833/333409.

[21] A. Dahash, S. Mieck, F. Ochs, and H. J. Krautz. A comparative study of two simulation tools for the technical feasibility in terms of modeling district heating systems: An optimization case study. *Simulation Modelling Practice and Theory*, 91:48–68, 2019.

[22] E. Dall'Anese, P. Mancarella, and A. Monti. Unlocking flexibility: Integrated optimization and control of multienergy systems. *IEEE Power and Energy Magazine*, 15(1): 43–52, 2017.

[23] A. J. del Real, A. Arce, and C. Bordons. Combined environmental and economic dispatch of smart grids using distributed model predictive control. *International Journal of Electrical Power & Energy Systems*, 54:65–76, 2014.

[24] C. o. t. E. U. European Parliament. *Directive (EU) 2023/1791 of the European Parliament and of the Council of 13 September 2023 on energy efficiency and amending Regulation (EU) 2023/955 (recast)*. Official Journal of the European Union, 2023. doi: http://data.europa.eu/eli/dir/2023/1791/oj.

[25] Eurostat. Eurostat database. `https://ec.europa.eu/eurostat/web/main/data/database`, 2024.

[26] M. Fallmann, L. Stanger, M. Fischer, M. Kureck, A. Schirrer, R. Hofmann, S. Jakubek, and M. Kozek. Experimental validation of mixed-integer model predictive control for energy management in an industrial food processing plant. *Case Studies in Thermal Engineering*, page 106988, 2025.

[27] S. S. Farahani, Z. Lukszo, T. Keviczky, B. De Schutter, and R. M. Murray. Robust model predictive control for an uncertain smart thermal grid. In *2016 European Control Conference (ECC)*, pages 1195–1200. IEEE, 2016.

[28] C. Francesco. Thermopower library. `https://github.com/casella/ThermoPower`, 2002. Accessed: Sep. 20, 2024.

[29] S. Frank and S. Rebennack. An introduction to optimal power flow: Theory, formulation, and examples. *IIE transactions*, 48(12):1172–1197, 2016.

[30] C. Gandolfi, R. Lazzari, M. Zanoni, and D. Palladini. Mission project: Design of mv/lv hybrid ac/dc smart-energy grid. In *2022 AEIT International Annual Conference (AEIT)*, pages 1–6. IEEE, 2022.

[31] A. Gopalakrishnan and L. T. Biegler. Economic nonlinear model predictive control for periodic optimal operation of gas pipeline networks. *Computers & Chemical Engineering*, 52:90–99, 2013.

[32] T. Guo, P. Li, Z. Wang, R. Shi, Z. Han, H. Xia, and J. Li. Integrated modelling and optimal operation analysis of multienergy systems based on stackelberg game theory. *Energy*, 236:121472, 2021.

[33] S.-A. Hauschild, N. Marheineke, V. Mehrmann, J. Mohring, A. M. Badlyan, M. Rein, and M. Schmidt. Port-hamiltonian modeling of district heating networks. In *Progress in differential-algebraic equations II*, pages 333–355. Springer, 2020.

[34] J. He, Y. Li, H. Li, H. Tong, Z. Yuan, X. Yang, and W. Huang. Application of game theory in integrated energy system systems: A review. *Ieee Access*, 8:93380–93397, 2020.

[35] C.-S. Karavas, K. Arvanitis, and G. Papadakis. A game theory approach to multi-agent decentralized energy management of autonomous polygeneration microgrids. *Energies*, 10(11):1756, 2017.

[36] R. Krug, V. Mehrmann, and M. Schmidt. Nonlinear optimization of district heating networks. *Optimization and Engineering*, 22(2):783–819, 2021.

[37] A. La Bella and A. Del Corno. Optimal management and data-based predictive control of district heating systems: The novate milanese experimental case-study. *Control Engineering Practice*, 132:105429, 2023.

[38] A. La Bella, F. Bonassi, M. Farina, and R. Scattolini. Two-layer model predictive control of systems with independent dynamics and shared control resources. *IFAC-PapersOnLine*, 52(3):96–101, 2019.

[39] A. La Bella, A. Del Corno, and A. Scaburri. Data-driven modelling and optimal management of district heating networks. In *2021 AEIT International Annual Conference (AEIT)*, pages 1–6. IEEE, 2021.

[40] A. La Bella, A. Falsone, D. Ioli, M. Prandini, and R. Scattolini. A mixed-integer distributed approach to prosumers aggregation for providing balancing services. *International Journal of Electrical Power & Energy Systems*, 133:107228, 2021.

[41] A. La Bella, L. Nigro, and R. Scattolini. Predictive control and benefit sharing in multi-energy systems. *IEEE Transactions on Control Systems Technology*, 32(2):368–383, 2023.

[42] R. Lazzari and A. La Bella. Distributed multi-layer control of hybrid ac/dc grids: Design and experimental validation. *IET Renewable Power Generation*, 18:4414–4425, 2024.

[43] Y. Li, Y. Rezgui, and H. Zhu. Dynamic simulation of heat losses in a district heating system: A case study in wales. In *2016 IEEE Smart Energy Grid Engineering (SEGE)*, pages 273–277. IEEE, 2016.

[44] Z. Liao and A. Parisio. Reliability optimization of multi-energy system considering energy storage devices effects under weather uncertainties. *Energies*, 15(3):696, 2022.

[45] S. Long, O. Marjanovic, and A. Parisio. Generalised control-oriented modelling framework for multi-energy systems. *Applied Energy*, 235:320–331, 2019.

[46] J. E. Machado, M. Cucuzzella, and J. M. Scherpen. Modeling and passivity properties of multi-producer district heating systems. *Automatica*, 142:110397, 2022.

[47] O. Montoya, W. Gil-González, J. C. Hernández, D. A. Giral-Ramírez, and A. Medina-Quesada. A mixed-integer nonlinear programming model for optimal reconfiguration of dc distribution feeders. *Energies*, 13(17):4440, 2020.

[48] F. J. Muros, J. M. Maestre, E. Algaba, T. Alamo, and E. F. Camacho. Networked control design for coalitional schemes using game-theoretic methods. *Automatica*, 78:320–332, 2017.

[49] L. Nigro, A. La Bella, F. Casella, and R. Scattolini. Control-oriented modeling, simulation, and predictive control of district heating networks. *IEEE Transactions on Automation Science and Engineering*, 2024.

[50] L. Nigro, A. La Bella, and R. Scattolini. Distributed two-layer predictive control of multi-energy systems. In *2024 European Control Conference (ECC)*, pages 2429–2434. IEEE, 2024.

[51] L. Nigro, S. Polimeni, C. Anderis, M. Muro, and A. La Bella. Experimental validation and design of nonlinear predictive control and moving horizon estimation for district heating. *IFAC-PapersOnLine*, 59(9):157–162, 2025.

[52] L. Nigro, S. Polimeni, and A. La Bella. Experimental assessment of multi-layer control framework for multi-energy systems control with multiple coordination mechanics. -, -:–, 2025.

[53] E. Press. State of the union: Commission raises climate ambition and proposes 55 Press release, 2020.

[54] D. Quaggiotto, J. Vivian, and A. Zarrella. Management of a district heating network using model predictive control with and without thermal storage. *Optimization and Engineering*, 22(3):1897–1919, 2021.

[55] G. Sandou, S. Font, S. Tebbani, A. Hiret, C. Mondon, S. Tebbani, A. Hiret, and C. Mondon. Predictive control of a complex district heating network. In *IEEE conference on decision and control*, page 7372. IEEE; 1998, 2005.

[56] M. Taylor, S. Long, O. Marjanovic, and A. Parisio. Model predictive control of smart districts with fifth generation heating and cooling networks. *IEEE Transactions on Energy Conversion*, 36(4):2659–2669, 2021.

[57] F. Verrilli, A. Parisio, and L. Glielmo. Stochastic model predictive control for optimal energy management of district heating power plants. In *2016 IEEE 55th Conference on Decision and Control (CDC)*, pages 807–812. IEEE, 2016.

[58] S. Wang, H. Gangammanavar, S. D. Ekşioğlu, and S. J. Mason. Stochastic optimization for energy management in power systems with multiple microgrids. *IEEE Transactions on Smart Grid*, 10(1):1068–1079, 2017.

[59] M. Wirtz, L. Neumaier, P. Remmen, and D. Müller. Temperature control in 5th generation district heating and cooling networks: An milp-based operation optimization. *Applied Energy*, 288:116608, 2021.

[60] Y. Xu, A. Parisio, and Z. Ding. Hierarchical model predictive control for energy efficient buildings with multi-energy storage systems. In *2020 IEEE Power & Energy Society General Meeting (PESGM)*, pages 1–5. IEEE, 2020.

Acronyms

ADMM alternating direction method of multipliers.

BES battery energy storage.

CHP combined heat and power.

CVRMSE Coefficient of Variation of the Root Mean Square Error.

DAE Differential Algebraic Equations.

DC-ADMM Dual Consensus ADMM.

DHN district heating network.

EB electric boiler.

EH energy hub.

EU European Union.

EX Heat Exchangers.

FoRB forward-reflected-backward.

GB gas boiler.

GHG greenhouse gas.

GNEP generalized Nash equilibrium problem.

HL-MPC High-Level MPC.

L-MPC Low-Level MPC.

MES multi-energy system.

MHE moving horizon estimation.

MILP mixed-integer linear programming.

MPC model predictive control.

NMBE Normalized Mean Bias Error.

RES renewable energy sources.

RSE Ricerca sul Sistema Energetico s.p.a..

TES thermal energy storage.

TF thermal facility.

Ringraziamenti

Questa tesi presenta i risultati della ricerca condotta tra il 2022 e il 2025 presso il Dipartimento di Elettronica, Informazione e Bioingegneria del Politecnico di Milano. La ricerca è stata finanziata principalmente da Ricerca sul Sistema Energetico s.p.a. (RSE).

Questo lavoro non sarebbe stato possibile senza la guida e il sostegno del mio relatore, il Professor Riccardo Scattolini, e del mio co-relatore, il Professor Alessio La Bella. La loro incrollabile fiducia nelle mie capacità, la loro competenza tecnica e il sostegno personale sono stati fondamentali per accompagnarmi lungo tutto il progetto. Sono grato per le innumerevoli ore trascorse in riunioni, discussioni e revisioni, che hanno plasmato questo lavoro e la mia crescita come ricercatore.

Desidero ringraziare il Professor Sergio Grammatico per i suoi consigli e per avermi accolto come parte del suo team durante il mio soggiorno di ricerca presso la TU Delft. Questa esperienza mi ha offerto una nuova prospettiva sul mondo della ricerca, arricchendo la mia crescita accademica. Ringrazio inoltre la Professoressa Alessandra Parisio per aver accettato di far parte della commissione di dottorato e per aver valutato la mia tesi.

Ringrazio RSE per il sostegno finanziario e per l'opportunità di lavorare a questo progetto. Un grazie speciale ai miei colleghi del team RSE: Simone Polimeni, Marcelo Andre Muro Alvarado, Claudio Anderis e Riccardo Lazzari per l'impegno profuso nel rendere possibile questo progetto. In particolare, grazie per le ore trascorse a condurre i test sperimentali, senza i quali questo lavoro non sarebbe stato realizzabile. Un ringraziamento speciale a Francesco Casella per la sua competenza e i consigli nelle fasi iniziali del progetto.

Sono grato ai miei colleghi e amici del Politecnico di Milano per le pause tanto necessarie tra le lunghe sessioni di lavoro. Questi momenti hanno mantenuto alto il mio spirito durante le sfide. Un grazie speciale al team della "chocolaterie": Alessandro Del Duca, Andres Filipe Córdoba, Araavind Sridhar, Fabio Bonassi, Isabella Lanzani, Jing Xie, Laura Boca de Giuli, Samuel Mallik, Sergio Milo e gli altri per i bei momenti e il cibo delizioso.

Infine, un sentito ringraziamento ai miei genitori, Marco e Virna, e ai miei fratelli, Maurizio ed Eleonora, per essere stati presenti nei momenti di bisogno e per avermi accompagnato in questo percorso intrapreso per evitare quello che chiamate "lavoro vero". Un sincero grazie anche a Giulia per la sua comprensione lungo tutto il cammino e a tutti gli altri che sono stati al mio fianco. Avete reso possibile e piacevole il raggiungimento di questo traguardo; ora è il momento per me di trovare una nuova direzione.

Lorenzo
Milano, Marzo 2026